

# **Combining X-ray and optical/NIR data to study GRBs and their host galaxies**

**Dissertation  
zur Erlangung des akademischen Grades  
Dr. rer. nat.**

vorgelegt dem Rat der Physikalisch-Astronomischen Fakultät  
der Friedrich-Schiller-Universität Jena

**eingereicht von Dottore Magistrale Andrea Rossi  
geboren am 28.03.1977 in Cividale del Friuli (Italien)**

**Gutachter**

Prof. Dr. Artie Hatzes, TLS Tautenburg

Prof. Dr. Ulrich Heber, University of Bamberg

Prof. Dr. Giampaolo Piotto, University of Padova

**Tag der Disputation:** 15.03.2012

# Zusammenfassung

Diese Arbeit widmet sich dem Thema der Gammastrahlen-Bursts (GRBs), einem der z.Z. faszinierendsten Forschungsfelder in der Astrophysik. Gammastrahlen-Bursts sind Blitze energiereicher Strahlung, die am Himmel aus zufälligen Richtungen zu zufälligen Zeiten kommen. Während ihres Auftretens überstrahlen sie für einen Zeitraum von einigen Millisekunden bis zu einigen Minuten jede andere Quelle am Gammastrahlen-Himmel, bevor sie wieder verblassen.

Das gegenwärtige Modell zur Erklärung der während eines GRBs freigesetzten großen Energiemenge ist das *fireball model*. Demgemäß wird die Energie beim Kollaps des Kerns eines massereichen Sterns oder beim Verschmelzen zweier kompakter stellarer Objekte freigesetzt. Der Kollaps führt zur Emission von sich mit relativistischer Geschwindigkeit ausbreitenden polaren Jets. Die interne Dissipation von Energie innerhalb der Jets führt zu nichtthermischer energiereicher Strahlung, dem eigentlichen GRB. Verbunden mit dem Abbremsen des relativistischen Ausflusses im interstellaren Medium ist das Auftreten eines langlebigen Aufleuchtens, sichtbar vom Röntgen- bis zum Radioband, der sog. *Afterglow*.

In dieser Arbeit konzentriere ich mich auf Beobachtungsaspekte der GRB-Forschung basierend auf einer Kombination von Gammastrahlen-Daten mit Beobachtungen im Optischen und im Röntgenband. Das Ziel umfaßt drei wichtige Aspekte: (i) die Analyse der Eigenschaften der Strahlung in der *GRB prompt phase*, (ii) Arbeiten über die *Afterglow*-Phase und (iii) die Untersuchung der Eigenschaften der Muttergalaxien einer bestimmten Untergruppe von GRBs.

Nach einer Einleitung in das Forschungsfeld in den Kapiteln 1 und 2 widmet sich Kapitel 3 der *GRB prompt phase*, d.h. dem eigentlichen Burst. Hier konzentriere ich mich auf GRB 080928. Unter Verwendung von Daten, die mit verschiedenen Instrumenten erhalten wurden, zeige ich, dass die spektrale Energieverteilung vom Optischen bis zum Gammaband in Einklang ist mit der Natur von Synchrotronstrahlung. Meines Wissens konnte dies erst hierbei zum ersten Mal für einen GRB eindeutig demonstriert werden. Es bestätigt, dass grundlegende Annahmen des Standard GRB-Modells korrekt sind. Zusätzlich zeige ich, dass die zeitliche und spektrale Entwicklung der sog. *tail emission* des mit dem Burst verbundenen starken Röntgen-Flares durch das Modell der *large angle emission* erklärt werden kann. Zudem konnte ich der zeitlichen Entwicklung der spektralen Energieverteilung des Flares folgen.

Kapitel 4 umfaßt eine Studie der *Afterglows* von GRB 080514B und 080928. Ersterer Burst ist relevant, weil er der erste sehr energiereiche GRB war, bei dem ein optischer/NIR *Afterglow* gefunden wurde. Ich bestimme seine photometrische Rotverschiebung und ich finde, dass die Eigenschaften des *Afterglows* von GRB 080514B sich nicht vom Haupt-Ensemble der langen Bursts unterscheiden, obgleich der Burst hinsichtlich seiner Emission bei sehr hohen Energien ungewöhnlich war. Dies macht deutlich, dass eine energiereiche Emission im Gammaband offenbar nicht mit speziellen Eigenschaften des zugehörigen *Afterglows* korreliert ist. Sehr verschieden von GRB 080514B ist der *Afterglow* von GRB 080928, welcher durch seine ungewöhnliche Lichtkurve auffällt, in der sich eine Reihe sog. *re-brightenings* zeigen. Interessanterweise konnte hier keine GRB-Muttergalaxie gefunden werden, ich kann nur tiefe obere Schranken an ihre Helligkeit setzen.

Kapitel 5 beschäftigt sich mit den Muttergalaxien von sog. optisch schwachen GRBs, die jedoch einen Röntgen*afterglow* aufwiesen, die sog. *dark GRBs*. Ich schließe auf die Eigenschaften der Muttergalaxien und verwende diese Resultate um zu verstehen, warum konkret diese Bursts im

Optischen schwache Afterglows gehabt haben mögen. Ich zeige, dass Extinktion durch kosmischen Staub in den Muttergalaxien die plausibelste Erklärung dafür ist. Der sog. *Lyman drop out* im Optischen, d.h. eine Rotverschiebung  $z \gtrsim 4.5$ , ist in den meisten Fällen zur Erklärung der Beobachtungen nicht vonnöten. Eine der hauptsächlichen Schlussfolgerungen hier ist, dass die *dark bursts* zu einer Untergruppe sehr verröteter, global in Staub eingehüllter Galaxien führen, welche sich deutlich von der Hauptpopulation der GRB-Muttergalaxien unterscheidet, nämlich den blauen, leuchtkraftarmen, kompakten Galaxien.

Kapitel 6 fasst die Resultate und die hauptsächlichen Schlussfolgerungen dieser Arbeit zusammen.

# Abstract

This thesis focuses on the topic of Gamma-Ray Bursts (GRBs), which is currently one of the most fascinating research fields in Astrophysics. Gamma-Ray Bursts are flashes of high-energy radiation which appear in the sky at random times from random directions. Briefly, from a few milliseconds to a few minutes, they outshine every other source of gamma-rays in the sky, and then they fade away.

The current model to explain the large amount of energy released during a GRB is the fireball model. Within this framework, the energy is released in a short period of time by the collapse of the core of a massive star or the merger of two compact stellar objects. The collapse of this compact object ejects ultra-relativistic polar jets. The internal dissipation of energy within the jets leads to non-thermal high-energy emission, the GRB itself. The shock created from the deceleration of the relativistic outflow in the interstellar medium leads to a long-lasting transient, visible from X-rays to the radio band, called *afterglow*.

In this thesis I concentrate on observational aspects of GRB research based on a combination of gamma-ray data with optical and X-ray observations. The goal is threefold: (i) reveal the radiation properties of the *prompt GRB phase*, (ii) learn more about the GRB afterglow phase and (iii) investigate the nature of the host galaxy population of a certain subfraction of GRBs.

After an introduction into the research field in Chapters 1 and 2, Chapter 3 is devoted to the GRB prompt phase. Here I focused on the prompt emission phase of GRB 080928. Using data obtained with several facilities, I was able to show that the spectral energy distribution (SED) of the proper burst from the optical to the gamma-ray band is in agreement with synchrotron radiation. To the best of my knowledge, this was the first time that this could be unambiguously demonstrated for a GRB, confirming that the basic assumptions of the standard GRB model are correct. In addition, I showed that the evolution of the tail emission of the strong X-ray flare during the prompt phase of this GRB can be explained by the large angle emission (LAE) model. Furthermore, I followed the time evolution of spectral energy distribution during evolution of the flare.

Chapter 4 includes the study of the afterglows of GRB 080514B and GRB 080928. The former is the first very high-energy burst with a detected optical/NIR afterglow. I derived the photometric redshift and I found that the afterglow properties of GRB 080514B did not differ from those exhibited by the global sample of long bursts, even if this burst was special because of its high-energy emission properties. This suggests that high-energy emission in the gamma-ray band does not correlate with the occurrence of special features in the corresponding afterglow light. Very different to GRB 080514B is the case of the afterglow of GRB 080928, which was remarkable for its peculiar light curve, marked by several re-brightening episodes. Interestingly, no host galaxy could be associated with GRB 080928 down to deep upper limits.

Chapter 5 deals with the host galaxies of optically faint GRBs with X-ray afterglows, the so-called *dark GRBs*. I derived conclusions on the host galaxy properties and I used these results to find explanations for the faintness of their corresponding afterglows. I showed that extinction by dust in the host galaxies is the most obvious explanation for dark GRBs. Lyman dropout in the optical bands, i.e. a redshift  $z \gtrsim 4.5$ , was in most cases not required. I concluded that dark bursts trace a subpopulation of extremely red, globally dust-enshrouded galaxies, markedly different from the main body of the GRB host galaxy population, namely the blue, subluminal, compact galaxies.

Chapter 6 summarizes the results and the main conclusions of this thesis.



# Contents

<b>Zusammenfassung</b>	<b>I</b>
<b>Abstract</b>	<b>III</b>
<b>1 Gamma-Ray Bursts: introduction</b>	<b>1</b>
1.1 The 1990s: A decade of revolutionary results . . . . .	2
1.2 Unveiling the GRB progenitors . . . . .	4
1.3 The <i>Swift</i> satellite era . . . . .	6
1.4 Rapid ground follow-up and multi-band imaging . . . . .	6
1.5 GROND: the 7-channel imager . . . . .	7
<b>2 Gamma-Ray Bursts: physical background and observations</b>	<b>9</b>
2.1 The gamma-ray emission . . . . .	9
2.1.1 Long and short bursts . . . . .	10
2.2 The physics behind GRBs and afterglows . . . . .	11
2.2.1 The compactness problem in the gamma-ray band . . . . .	11
2.2.2 The fireball model . . . . .	12
2.2.3 Spectral energy distribution (SED) and light curve . . . . .	13
2.3 Afterglow phenomenology . . . . .	16
2.3.1 Is there a canonical optical X-ray and optical light curve ? . . . . .	16
2.3.2 Jets: collimated outflows . . . . .	17
2.3.3 X-ray flares and large-angle emission . . . . .	18
2.3.4 Optically dark GRBs with X-ray afterglows . . . . .	19
2.4 GRB host galaxies . . . . .	23
2.4.1 The main GRB host galaxy population . . . . .	24
2.4.2 Dark GRB host galaxies . . . . .	24
<b>3 The prompt phase of GRB 080928 from optical to gamma-rays</b>	<b>27</b>
3.1 Data and analysis . . . . .	27
3.1.1 <i>Swift</i> /BAT and <i>Fermi</i> /GBM data . . . . .	27
3.1.2 <i>Swift</i> /XRT data . . . . .	28
3.1.3 Optical/NIR data . . . . .	29
3.2 The prompt phase . . . . .	31
3.2.1 From gamma-rays to X-rays . . . . .	31
3.2.2 From gamma-rays to optical bands . . . . .	32
3.2.3 Evidence for large-angle emission from X-rays to the optical band . . . . .	35

3.2.4	The isotropic equivalent energy and gamma-ray peak luminosity . . . . .	38
3.2.5	Constraints on the initial Lorentz factor of the outflow . . . . .	38
3.3	Summary of the GRB 080928 prompt emission . . . . .	39
<b>4</b>	<b>Afterglow studies from near-infrared to X-rays</b>	<b>41</b>
4.1	Follow-up observations of the AGILE high-energy burst GRB 080514B . . . . .	41
4.1.1	Data gathering: optical/NIR and X-ray observations . . . . .	42
4.1.2	The Optical/NIR and X-ray afterglow: detection and light curve . . . . .	43
4.1.3	The SED and the photometric redshift . . . . .	45
4.1.4	Optical/NIR to X-ray SED from GROND and <i>Swift</i> . . . . .	46
4.1.5	The host galaxy of GRB 080514B . . . . .	48
4.2	The afterglow of the long GRB 080928 . . . . .	49
4.2.1	The X-ray and optical/NIR light curve . . . . .	49
4.2.2	GROND and <i>Swift</i> optical/NIR to X-ray SED . . . . .	52
4.2.3	Theoretical interpretation of the light curve . . . . .	53
4.2.4	The search for the host galaxy of GRB 080928 . . . . .	55
4.3	Summary of the afterglow and host observations . . . . .	58
<b>5</b>	<b>Host galaxies of dark GRBs</b>	<b>59</b>
5.1	The GRB sample . . . . .	60
5.1.1	Optical/NIR data analysis of ESO/VLT and GROND observations . . . . .	61
5.1.2	Optical and X-ray data to define a golden dark burst subsample . . . . .	61
5.2	Detailed overview of the ESO/VLT and GROND observations . . . . .	65
5.2.1	Notes for individual targets . . . . .	65
5.3	The properties of the host galaxy population . . . . .	80
5.3.1	The magnitude-probability criterion . . . . .	80
5.3.2	Dust extinction and edge-on galaxies . . . . .	82
5.3.3	Extremely red objects (EROs) . . . . .	82
5.3.4	Lyman-dropout candidates . . . . .	83
5.3.5	Interacting pairs of galaxies as host galaxy candidates . . . . .	84
5.3.6	Redshift estimates . . . . .	84
5.3.7	Burst locations close to very bright galaxies and groups or clusters of galaxies . . . . .	84
5.3.8	Host galaxy candidates of the golden dark burst sample . . . . .	85
5.3.9	What makes dark bursts: it is not high redshift . . . . .	85
5.3.10	EROs as an important subpopulation of GRB host galaxies of dark GRBs . . . . .	86
5.4	Summary of the host galaxies of dark GRBs . . . . .	87
<b>6</b>	<b>Summary</b>	<b>89</b>
	<b>Bibliography</b>	<b>92</b>
	<b>Appendix</b>	<b>I</b>
<b>A</b>	<b>The optical/NIR data set of GRB 080928 and its afterglow</b>	<b>I</b>
<b>B</b>	<b>The optical/NIR data set of the afterglow of GRB 080514B</b>	<b>V</b>



<b>C</b>	<b>Notes, tables and figures on the host galaxy search</b>	<b>VII</b>
C.1	Additional notes on individual targets for the host galaxy search: observations by Swift and other facilities . . . . .	VII
	<b>Additional references (Appendix only)</b>	<b>XIII</b>
	<b>Acknowledgements</b>	<b>XXIII</b>



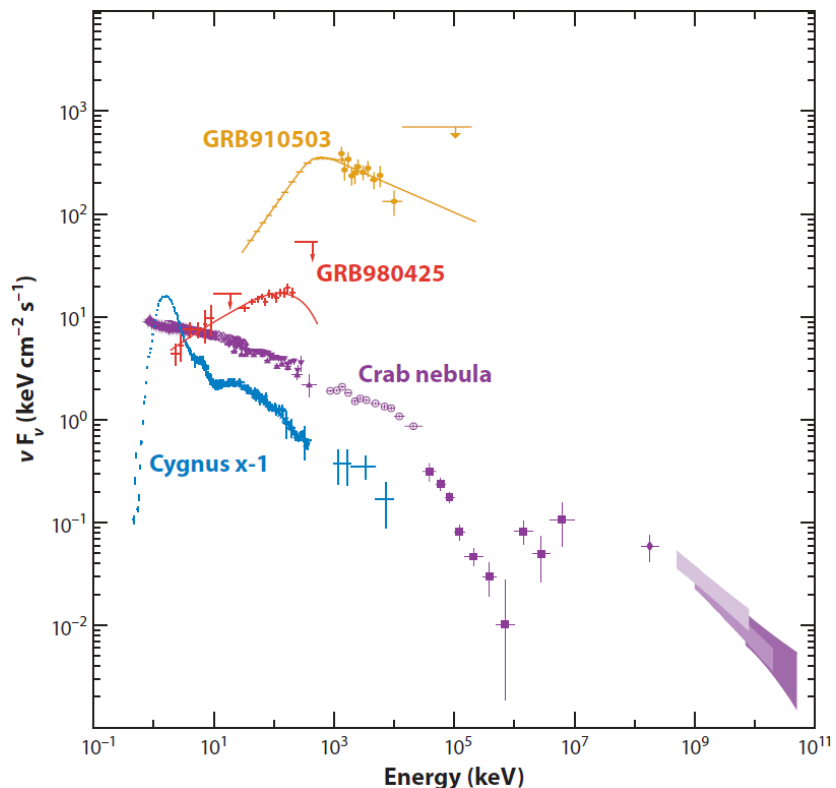
# Chapter 1

## Gamma-Ray Bursts: introduction

Klebesadel et al. (1973) reported the discovery of gamma-ray bursts (GRBs), bright flashes of gamma radiation of not terrestrial or solar origin. This discovery was covered by military secret since 1967, because was made by the Vela satellites, used to detect gamma-rays emitted from nuclear weapon tests and originally built to ensure the compliance with the Limited Nuclear Test Ban Treaty signed between the USA and the USSR in 1963. However, after this discovery no significant step forwards were done in unveiling the physical origin of these events. The burst was detected by several other high-energy instruments, but no systematic and dedicated approach was attempt.

In this chapter I will summarize the main results achieved since the first GRBs discovered in the 1960s.

Figure 1.1: *Gamma-ray bursts are the most energetic phenomena in nature, and for few seconds outshine the most bright gamma-ray sources in the sky. Shown here are representative spectra of GRBs 910503 and 980425 along with the Crab nebula and the galactic black hole candidate Cygnus X-1. Adapted from Gehrels et al. (2009). Note: the nomenclature for GRBs is GRB YYMMDD, where YY=year, MM=month, DD=day. An additional letter is added if there are more than one GRB on a certain day.*



## 1.1 The 1990s: A decade of revolutionary results

A big step forward to reveal the physical origin of GRBs was made with the launch of the Compton Gamma-Ray Observatory (CGRO) in 1991. Its *Burst and Transient Source Experiment* (BATSE; Fishman et al. 1985), a sensitive gamma-ray detector, provided crucial data indicating that the distribution of GRBs on the sky is isotropic, not biased toward any particular direction, and therefore that the bursts are cosmological in origin (Fig. 1.2). But these data did not reveal what kind of progenitors were responsible for the GRBs. Also, the localization accuracy provided by BATSE (some degrees) was still not good enough to allow prompt follow-up observations from X-ray, optical, near-infrared (NIR) or radio telescopes. Theoretical considerations had led to the conclusion, however, that a fading emission should have been visible at longer wavelengths after the gamma ray detection.

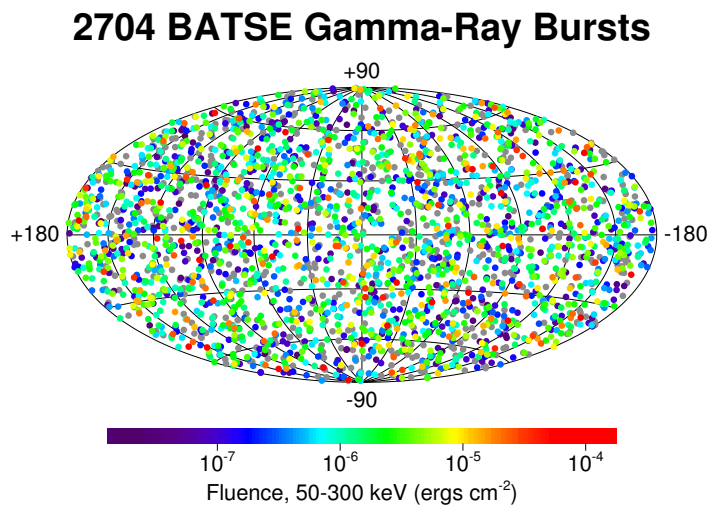


Figure 1.2: Sky map of the 2704 GRBs detected by BATSE during its 10 years mission. The projection is in galactic coordinates. The different colors refer to the fluence released during the GRB duration, increasing from red to blue. Source: [www.batse.msfc.nasa.gov/batse/grb/](http://www.batse.msfc.nasa.gov/batse/grb/).

And indeed the watershed was made by a mission capable of performing simultaneous observations over more than 3 decades of energy, from 0.1 up to 700 keV, thanks to the several instruments on board. The mission was the Italian-Dutch *BeppoSAX* (Boella et al. 1997a), in operation between 1996 and 2003, named "Beppo" after the Italian physicist Giuseppe Occhialini (1907-1993). The winning philosophy of *BeppoSAX* was the combination of a almost all-sky view Gamma-Ray Burst Monitor (GRBM; Frontera et al. 1997), capable to detect nearly all GRBs in the 40-700 keV range and roughly determine its coordinates, a set of Wide Field Cameras (WFC; 2-28 keV; Jager et al. 1997) made possible to constrain the localization down to about 5 arcmin. After repointing the satellite on this position the four Narrow Field Instruments (NFIs; 0.1-300 keV; Boella et al. 1997b; Frontera et al. 1997; Manzo et al. 1997; Parmar et al. 1997) could be used to refine the error box to 1 arcmin accuracy.

This complex configuration was perfect to provide precise and rapid localizations, and therefore to begin the follow-up with ground-based telescopes to search for optical/NIR or radio counterparts.

On 28 February 1997 the WFCs detected the X-ray counterpart of GRB 970228 (Costa et al. 1997b; Fig. 1.3, top panel). Thanks to the prompt communication of this discovery and a small error box, the first optical counterpart of a GRB was observed some hours later by van Paradijs et al. (1997) with the *William Herschel* Telescope (WHT). Later, the afterglow was followed up by the *Hubble Space Telescope* (Fig. 1.3). The optical and soft X-ray light curve indicated that the counterparts were fading following a steep power-law  $t^{-1.1}$ . This fact pointed out that the search for

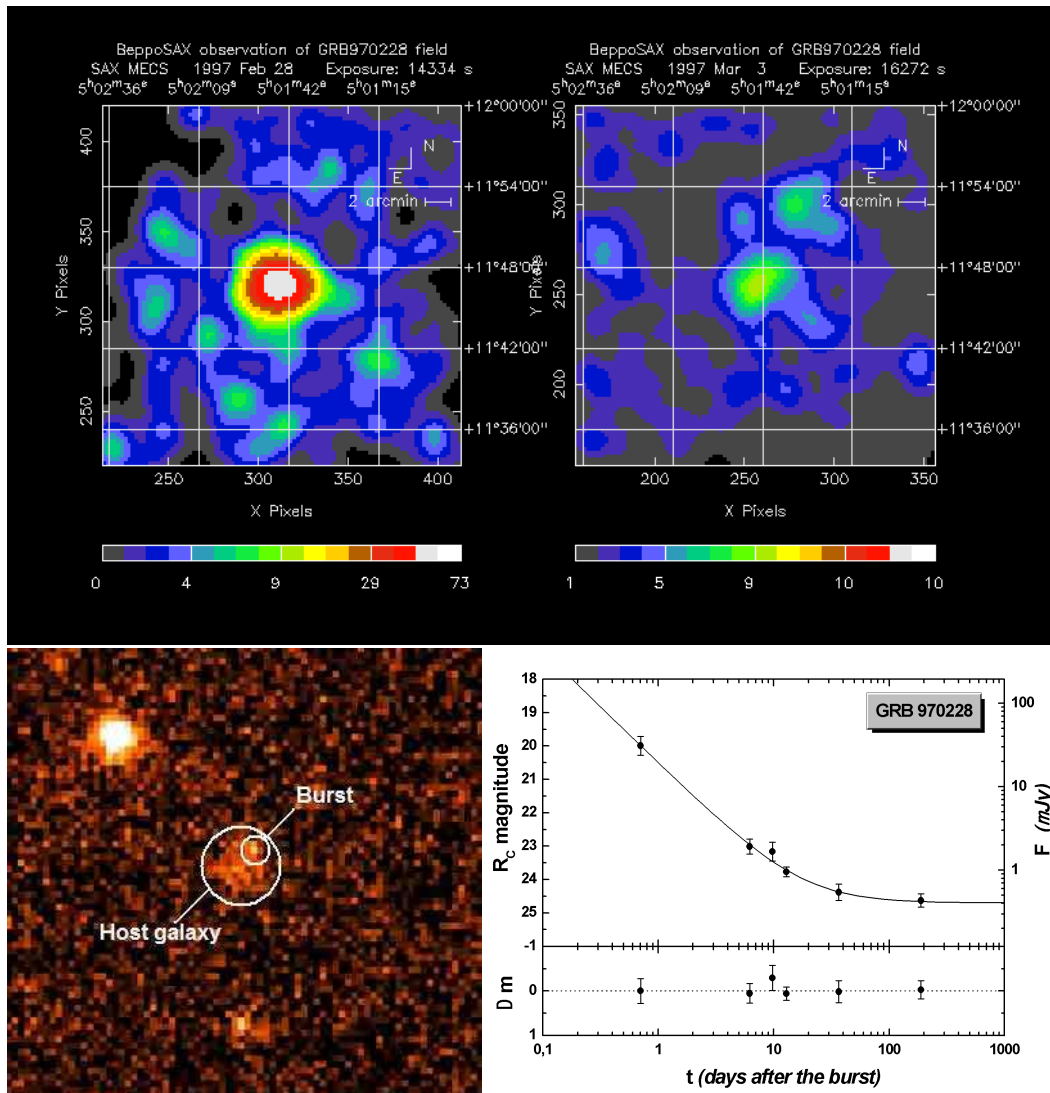


Figure 1.3: **Top:** X-ray counterpart of GRB 970228 detected by WFC/BeppoSAX (Costa et al. 1997a). **Bottom Left:** Observation of the optical counterpart from the Hubble Space Telescope. The position of the host galaxy and the optical afterglow are indicated (adapted from <http://imgsrc.hubblesite.org/hu/db/images/hs-1997-30-a-pdf.pdf>). **Bottom Right:** The first optical light-curve of an afterglow was obtained for GRB 970228 (adapted from Zeh et al. 2006).  $Dm$  indicates the residuals from the fit in magnitudes.

GRB afterglows required a quick response from all the observing facilities.

The final confirmation that GRBs have a cosmological origin came with GRB 970508. Thanks to the prompt localization by *BeppoSAX*, several research teams started observing much sooner than in case of any previous burst. This made possible to observe the afterglow of GRB 970508 when it was still bright enough to perform spectroscopic observations with one of the Keck telescopes, obtaining a redshift of 0.835 (Metzger et al. 1997a,b). Few months later the discovery of the host galaxy of GRB 970228 at  $z = 0.695$  proved that GRBs occur in high distance galaxies (Djorgovski et al. 1999).

After placing the GRBs in galaxies at cosmological distances, it was clear that GRBs are the most powerful explosions in the Universe, releasing as much energy in a few seconds as the Sun will emit during its entire 10 billion years lifetime. Still, the progenitors of the GRBs were a matter of debate.

## 1.2 Unveiling the GRB progenitors

The biggest hint on the nature of the GRB progenitors came with GRB 980425. The burst was discovered by *BeppoSAX* but not seen by CGRO/BATSE. An X-ray afterglow was detected by *BeppoSAX* and its 8 arcmin error circle was found to include a rather bright spiral galaxy. No optical counterpart of the afterglow was detected, however. Within days after the GRB, an unusual supernova emerged from this galaxy (SN 1998bw; Galama et al. 1998; Fig. 1.4). Spectroscopic observations classified it as a Type Ic SN (core collapse and deficient in hydrogen and helium). Broad spectral lines indicated that the ejecta was moving at  $0.1c$ . It was soon labeled "hypernova" (Iwamoto et al. 1998). GRB 980425 was the first link between long GRBs and the death of massive stars.



Figure 1.4: *Optical color composite obtained with the ESO NTT Telescope on La Silla on May 4, 1998. The SN 1998bw, indicated with an arrow, is located in a spiral of its host galaxy (source <http://www.eso.org/public/images/eso9847a/>).*

A further milestone in the identification of the progenitors of long GRBs came 5 years later. In October 2000 the *High Energy Transient Explorer (HETE II)* (Vanderspek et al. 1999) was launched. The satellite was not able to slew like *BeppoSAX*, but thanks to its Soft X-ray camera it was able to localize a GRB with an accuracy of some arcmin within less than a minute. On March 29, 2003, *HETE II* discovered the very bright GRB 030329 (Ricker 2003). Its bright afterglow was followed up by several research teams and this provided the largest amount of data for a single event. Spectroscopic observations unveiled the features characteristic of a supernova, later designated SN2003dh (Hjorth et al. 2003; Stanek et al. 2003). The early spectra showed a power law continuum with narrow emission lines originating from H II regions in the host galaxy at low redshift ( $z = 0.1687$ ; Greiner et al. 2003). The late spectra obtained after April 5, however, showed broad lines characteristic of a supernova. After correcting for the afterglow component, the spectra were remarkably similar to the type Ic event SN 1998bw associated to GRB 980425. This gave clear evidence that the core-collapse of massive stars can give rise to GRBs. The imprint of the supernova became lately slightly visible also in the afterglow light curve (Zeh et al. 2005; Fig. 1.5).

Already in the 1960s, shortly before the discovery of GRBs at all, it was speculated that SNe could give rise to signals in the gamma-ray band (see Klebesadel et al. 1973). About 25 years later Woosley (1993) proposed the "collapsar" model, in which the core of a massive star in the final stages of its evolution collapse into a black hole. This turned out to be the most successful model to explain

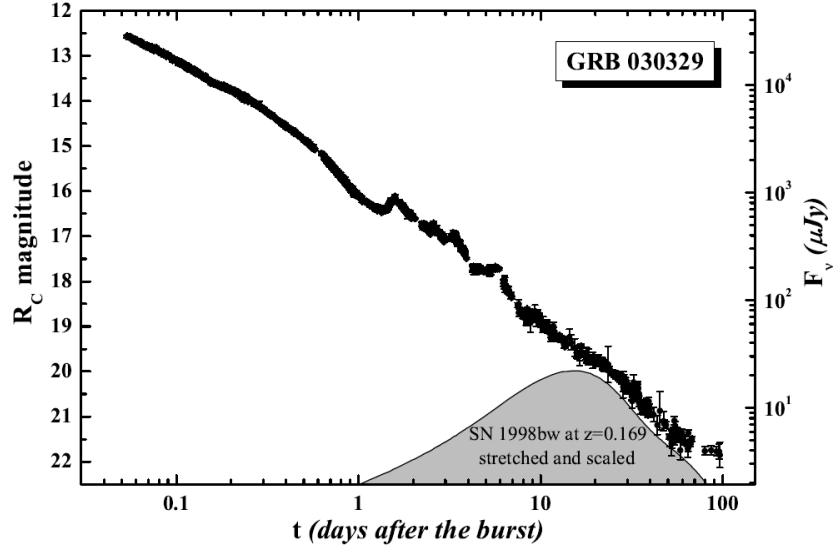


Figure 1.5: *The light curve of the GRB 030329 afterglow. While the SN contribution is difficult to discern from the afterglow light curve, the comparison with spectroscopic observation confirmed that the SN is dominating during late times (adapted from Zeh et al. 2005).*

the central engine that finally drives a GRB. Within this context, an accretion disk is formed around a black hole that is fed by the falling matter and provides the energy to launch a jet and a counter-jet along the rotational axis of the collapsing star. A highly magnetized accretion disk in combination with a rapidly rotating black hole could be a key ingredient of this model Lee et al. (2000). Within this scenario, energy is extracted electromagnetically with a mechanism first proposed by Blandford & Znajek (1977). In case of black hole of mass  $M$  rotating at maximum velocity, the Blandford-Znajek mechanism can extract up to  $1.6 \times 10^{53} (M/M_{\odot})$  erg (Lee et al. 2000). Within this context, the observed collimated outflows (jets) are created within the collapsing star. Therefore, they have to pass through the outer layers of the star, where they lose part of their energy. If the stellar envelope is too extended, the jets will be completely absorbed inside the star. Thus, a collapsing Wolf-Rayet star is a good progenitor candidate, because it has lost its outer hydrogen and sometimes even helium layers, due to a strong stellar wind ( $\sim 2000$  km/s). Indeed, the association of long GRBs with type Ic SNe strongly supports this picture (e.g., Galama et al. 1998; Hjorth et al. 2003; Pian et al. 2006; Chornock et al. 2010). The latest of these events with well-observed SN light in their spectrum is GRB 100316B, which we in detail discuss in Olivares E. et al. (2011).

The situation is different for short-hard bursts, however, which constitute  $\sim 30\%$  of the BATSE sample (Kouveliotou et al. 1993). These events are not associated with supernovae. Also, to explain the shorter time scale during which the GRB emission takes place ( $< 2$  s), it is necessary that the time interval when the jet evolves and the lifetime of the accretion disk are smaller than what is possible within the collapsar scenario (Woosley & Bloom 2006). The most favoured alternative is the merger of two compact objects, like NS-NS or NS-BH (NS stands for neutron star, BH for black hole; for a review see Nakar 2007; Lee & Ramirez-Ruiz 2007; Ruffert & Janka 2001, 2010).

GRB 050509B was the first case where an X-ray afterglow has been observed associated to a short GRB (Gehrels et al. 2005). This and the following observations of optical and X-ray afterglows of short GRBs finally allowed observers to associate short GRBs to galaxies with an old stellar population, in particular also to elliptical galaxies (e.g., Gehrels et al. 2005; Berger 2009), consistent with the model of compact mergers (Nakar 2007). Meanwhile about 20 short bursts have been localized with high angular precision but in no case has ever been found an underlying SN component (for a review, see Kann et al. 2011).



### 1.3 The *Swift* satellite era

In November 2004, the NASA *Swift* satellite was launched and it is still operative to date (June 2011). The mission is dedicated to the rapid localization of GRBs in gamma and X-rays, and capable of detecting optical afterglows. This thanks to three co-aligned instruments (Gehrels et al. 2004): the *Burst Alert Telescope* (BAT) observing in the 15-150 keV range; the *X-Ray Telescope* (XRT) observing in the 0.3-10 keV range and the *Ultra-Violet/Optical Telescope* (UVOT, 170-650 nm). While BAT is already capable to offer localization in the order of  $< 3$  arcmin, *Swift* can slew within 60-120 seconds allowing the narrow field instruments XRT and UVOT to follow-up the afterglow. *Swift* detects about 100 GRBs per year and the great sensitivity of XRT make possible to detect  $\sim 75\%$ <sup>1</sup> of X-ray afterglows within a few arcseconds accuracy, while in the other cases observations were not immediately possible only due to observability constraints (e.g., the field was close the Sun) opening the way to the extensive study of the afterglows at these energies. In addition, about once a month the INTEGRAL gamma-ray satellite, localizes a GRB with similar position accuracy (see Vianello et al. 2009). Thanks to *Swift*'s rapid and autonomous slewing capabilities, in combination with its highly sensitive X-ray telescope (XRT; Burrows et al. 2005a) as well as its optical/UV telescope (UVOT; Roming et al. 2005), about 50 to 70 GRB optical afterglows can be localized annually, with 30 to 40 having redshifts determined.

While not dedicated to GRBs, other missions extend the study of GRB phenomena to very high energies. Roughly four years after *Swift*'s launch the *Fermi* Gamma-Ray Space Telescope was launched into orbit (June 2008). Its Gamma-Ray Burst Monitor (GBM; Meegan et al. 2009) and Large Area Telescope (LAT; Atwood et al. 2009) cover an unprecedentedly wide energy range from 8 keV to 300 GeV. Up to the end of May 2011, LAT had localized roughly 20 GRBs to positions of less than a degree in error, of these, eight have optical afterglows and redshifts<sup>2</sup>. Furthermore, a larger number of *Swift* GRBs have also been detected by *Fermi*/GBM, allowing a more thorough investigation of the prompt emission above 150 keV. Also the Italian AGILE high-energy satellite (Tavani et al. 2009) contributes about a handful of burst detections and localizations per year (e.g., Giuliani et al. 2008b; Rossi et al. 2008b).

*Swift* led to many discoveries, maybe the most fascinating is the discovery of the redshift record GRB 090423 at  $z \sim 8.2$  (Salvaterra et al. 2009; Tanvir et al. 2009) the second most distant source spectroscopically confirmed to date. The second more distant is GRB 080913 ( $z \sim 6.7$ ; Rossi et al. 2008c; Greiner et al. 2009b) record holder for 6 months, for which I discovered the optical/NIR afterglow. Having in mind the high-redshift to which one can observe GRBs and the connection with the death of massive stars, these discoveries made GRBs new observational tools to investigate the early stages of the evolution of the Universe.

### 1.4 Rapid ground follow-up and multi-band imaging

A important step over for coordinating the several research teams and instrumentations involved in studies the GRB phenomena from gamma to radio bands is the set up of the Gamma-ray bursts Coordinates Network<sup>3</sup> (GCN) to distribute locations of GRBs detected by spacecraft most in real-time while the burst is still bursting. The system provides notices, named GCN.

<sup>1</sup>See Jochen Greiner webpage at <http://www.mpe.mpg.de/~jcg/grbgen.html>.

<sup>2</sup>See *Fermi*/LAT GRB table at [http://fermi.gsfc.nasa.gov/ssc/observations/types/grbs/grb\\_table](http://fermi.gsfc.nasa.gov/ssc/observations/types/grbs/grb_table).

<sup>3</sup>See GCN webpage at [http://gcn.gsfc.nasa.gov/gcn\\_main.html](http://gcn.gsfc.nasa.gov/gcn_main.html).



To perform rapid optical/near-infrared (NIR) follow-up several facilities have been developed in the last years. The approaches are several. Usually small ( $< 1$  m) robotic telescopes are used together with commercial cameras and are placed in different locations on the Earth to follow *Swift* observations (e.g. ROTSE III Akerlof et al. 2003, BOOTES Castro-Tirado et al. 1999). Or there are programs with telescope and instruments which have part of the time dedicated to GRB studies and are automatically activated to follow-up GRBs after receiving the GRB coordinates (e.g., REM Zerbi et al. 2001, PAIRITEL Bloom et al. 2006, P60 Cenko et al. 2006). These instruments have often the capability to offer multi-band imaging, which is important to study the color evolution of an optical/NIR afterglow. This observations can also be compared with the X-ray observations performed by *Swift*, and therefore the possibility of performing a spectral analysis which span from NIR to X-rays and even gamma-rays, if the GRB is still active and the target is observable.

## 1.5 GROND: the 7-channel imager

The most productive of these instruments is GROND, mounted at the 2.2m MPG/ESO<sup>4</sup> telescope on La Silla in Chile (Greiner et al. 2007, 2008). GROND was build with the aim of having the possibility to collect not only information about the light curve behavior, but also about the spectral properties of the afterglow. Therefore this instrument can image in seven photometric bands simultaneously ( $g'r'i'z'JHK$ ), making it an ideal tool to observe GRB afterglows (Fig. 1.6). It operates in semi-robotic mode, because the telescope itself and the analysis of the acquired data require assistance before spreading the results to the scientific community and before activating further photometric and spectroscopic observations on larger telescopes. Before GROND had first light, simultaneous multi-band capabilities were possible for three bands at best (like for REM and PAIRITEL, see above), and the telescope aperture was often too small to detect the afterglow. Therefore, multi-band observations required a lot of observational and organizational effort from different facilities in the world, which were not always possible to achieve. Allowing us to study the spectral properties of GRB afterglows with just one shot on target, GROND offers also the possibility to a first estimate of the GRB photometric redshift, if this is  $z > 3.5$ . Lyman- $\alpha$  absorption due to hydrogen on the line of sight suppresses all light at wavelength  $\lambda < 1216(1 + z)$  Å, the so called *Lyman dropout*. Therefore, if a dimming becomes visible in the  $g'$  band ( $\sim 4500$  Å), the redshift must be at least  $\sim 3.5$ , or higher, if the light is suppressed at higher wavelengths, too. This approach is possible due to the fact that the spectral energy distribution (SED) of an afterglow is a simple power law, without emission lines. Of course, the extinction on the line of sight (Galactic and in the GRB environment) can complicate this approach, but it can be taken into account, and actually it also plays a role in understanding the extinction properties of the host galaxies of GRBs.

Among the several results we have obtained with GROND, one deserves to be mentioned in particular. On 13 Semptember 2008, during one on my stays on La Silla, I was able to discover the afterglow of GRB 080913 in  $z$  band, while nothing was visible in bluer bands (Rossi et al. 2008c). Further analysis, demonstrate that the afterglow was visible in infrared, and my group was able to estimate the photometric redshift of  $z = 6.4 \pm 0.3$ , (Fig. 2.10; see Greiner et al. 2008b), later confirmed spectroscopically to be  $z = 6.695 \pm 0.025$  (Greiner et al. 2009b).

While this discussion gained a lot of scientific attention (Greiner et al. 2009b; Zhang et al. 2009;

---

<sup>4</sup>MPG stays for *Max-Planck-Gesellschaft*; ESO stays for *European Southern Observatory*.

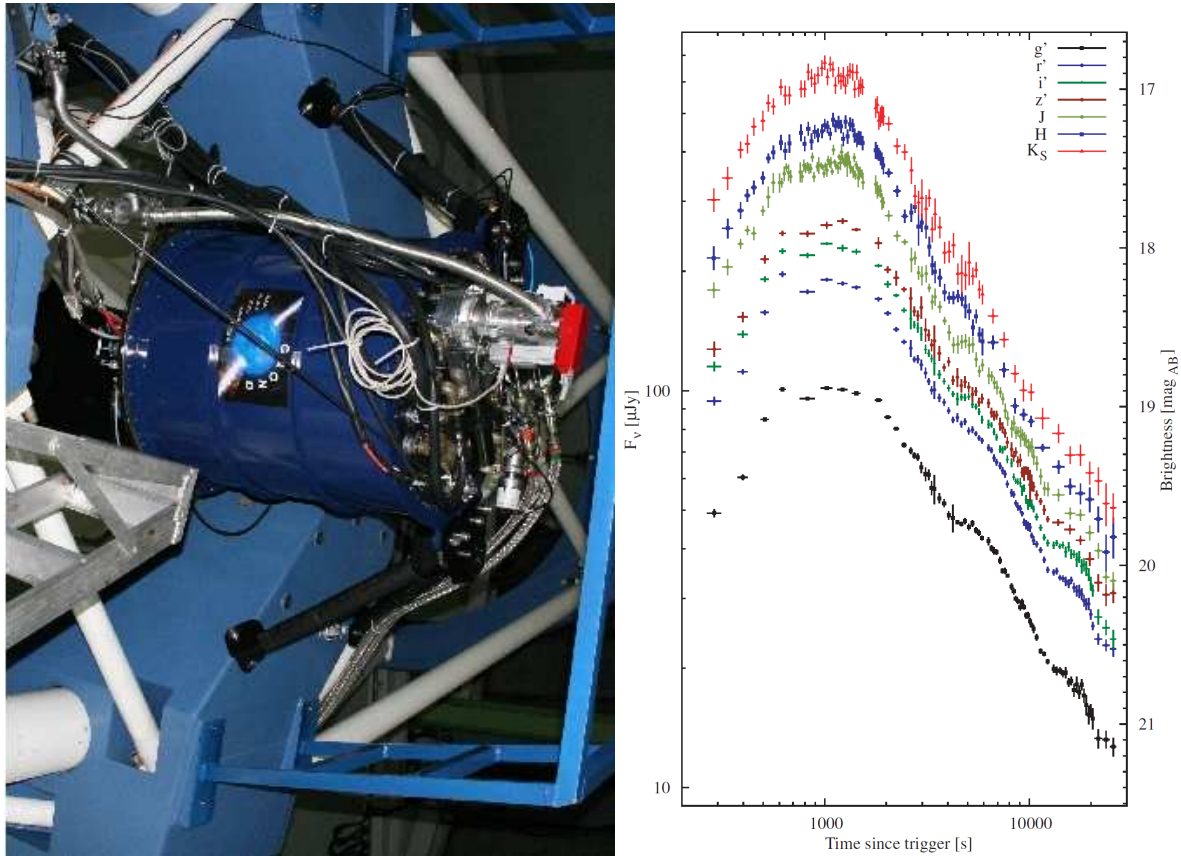


Figure 1.6: **Left:** *GROND*, the instrument operated by our group at the 2.2m telescope on La Silla, Chile. **Right:** *GROND* optical and NIR light curve of the afterglow of XRF 071031 taken between  $\sim 4$  minutes and 7 hr after the trigger. The data-set consist of a total of  $\sim 1000$  observations in the  $g'r'i'z'JHK_S$  bands, useful to well sample the lightcurve. Adapted from Krühler et al. (2009).

Pérez-Ramírez et al. 2010; see also ESO press release from 28 April 2009<sup>5</sup>), in this thesis I will not discuss its discovery in more detail. It should just be stressed that at that time it was the most distant GRB, and the second most distant object, ever observed.

I will present further results along the next chapter, after a overview of the main aspects in the GRB field.

<sup>5</sup><http://www.eso.org/public/news/eso0917/>

## Chapter 2

# Gamma-Ray Bursts: physical background and observations

In this chapter I give an overview of the observational features of the GRB phenomenon. Also, I present the main physical interpretation of GRBs. However, the aim of this thesis is not to describe the theory but to discuss observational data. Therefore, in this chapter I will include only the theoretical aspects I will use later. A detailed description of the GRB physics and their observations are described in several reviews; e.g., Zhang & Mészáros (2004); Piran (2005); Woosley & Bloom (2006); Zhang (2007); Gehrels et al. (2009).

Along all the thesis, for the flux density of the afterglow I use the usual convention  $F_{\nu}(t) \propto t^{-\alpha} \nu^{-\beta}$ . Here  $\alpha$  is the temporal decay index and  $\beta$  is the spectral slope. Note that a positive  $\alpha$  implies a fading light curve, and a positive  $\beta$  implies that the flux density is increasing with wavelength.

### 2.1 The gamma-ray emission

The first phase of a GRB is the prompt phase. Most of the energy is released in gamma-rays, although some GRBs have luminous optical counterparts as well. GRB 080319B, for example, was accompanied by an optical flash that peaked at a visible magnitude of 5.3 (Racusin et al. 2008), comparable to that of the dimmest naked-eye stars despite the burst's redshift of  $z = 0.937$ . However, this is the only phase where gamma-rays are emitted and its characteristics are different from the later afterglow phase.

The light curves of the GRB-prompt events show a wide variety of structure, ranging from smooth, fast-rise and quasi-exponential decay, through curves with several peaks to highly variable curves (Fig. 2.1).

The duration of a gamma-ray burst is usually given as  $T_{90}$ , which is the time in which a burst emits from 5% to 95% of its total measured counts, accumulating 90% of the counts. Following this definition, their duration has been found to last from  $10^{-3}$  s to about  $10^3$  s.

The gamma-ray spectra of GRBs are non-thermal (Fig. 2.1, right), with photons observed at energies ranging from a few keV up to several GeV (e.g., GRB 080916C, Greiner et al. 2009b; GRB 090510, De Pasquale et al. 2010). The spectra are well fitted with an empirical function consisting of two power-laws, smoothly connected by a broken power-law, the so-called *Band* function, with a spectral break usually in the 0.1 – 2 MeV range (Band et al. 1993).

A measure of the  $\gamma$ -ray spectral properties is given by the GRB hardness, usually designated as

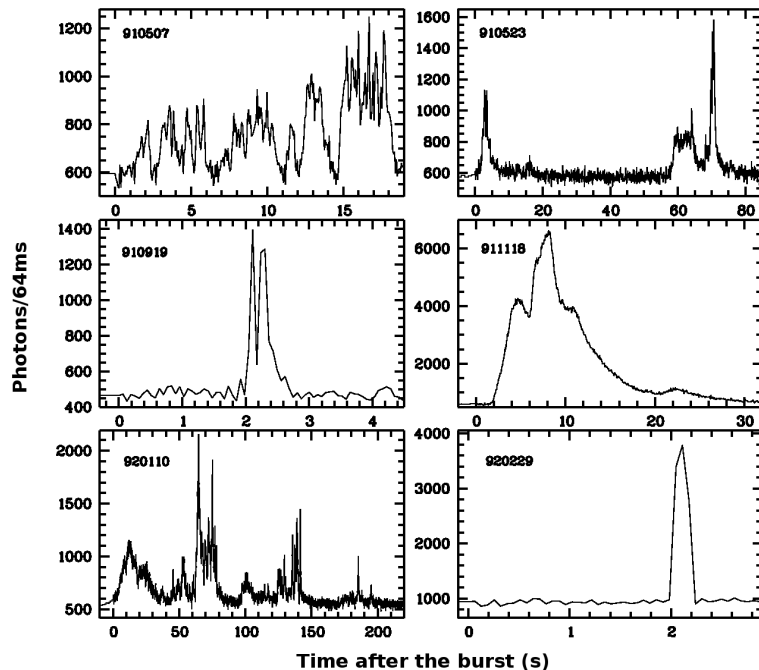


Figure 2.1: **Left:** A sample of BATSE GRB light curves (adapted from Fishman et al. 1994).

HR, that is for BATSE bursts defined as the ratio between the total counts in energy ranges 100 – 300 keV and 50 – 100 keV. Therefore, the harder is a burst, the larger is the portion of energy emitted at high frequencies. This also means that the slope of the spectral energy distribution (SED) would be flatter at higher energies.

### 2.1.1 Long and short bursts

During the first years of its operation, BATSE discovered that GRBs can be classified in two different types, a fact that turned out to be crucial in the debate on the nature of the GRB progenitors. In fact, KONUS data showed that the duration distribution of GRBs is bimodal (Mazets et al. 1981). This result was then confirmed and improved by BATSE (Kouveliotou et al. 1993), which showed that the GRBs are grouped not only according to their duration  $T_{90}$  but to their hardness ratio  $HR$ , too. This approach divides the GRBs in two classes (Fig. 2.2): • **Short-Hard GRBs**, with a  $T_{90}$  duration shorter than 2 seconds, a higher peak energy in their spectrum and an average duration of  $\sim 0.3$  s. • **Long-Soft GRBs**, with a  $T_{90}$  duration longer than 2 seconds, a lower peak energy in their spectrum and an average duration of  $\sim 25$  s<sup>1</sup>. Based on the duration distribution, a possible third class of GRBs of intermediate duration, between 2 and 10 s, has been proposed (Horváth 1998; Mukherjee et al. 1998; Horváth et al. 2006), but it is still under debate (de Ugarte Postigo et al. 2011).

Amati et al. (2002) found for a small sample of *BeppoSAX* long GRBs that the peak energy  $E_p$ , obtained from fitting the data with a Band function, correlates with the isotropic energy  $E_{iso}$  released in the rest-frame 1 keV - 10 MeV bandpass (Bloom et al. 2001). Later this relation was confirmed with a larger sample but with an increased scatter (Amati 2006). However, further updates showed that the relation is still valid, even when different instruments are used, and even at the higher energies for which *Fermi*/LAT is sensitive (Amati et al. 2009; McBreen et al. 2010). Still, even when the it was possible to determine the redshift, short bursts proved to not fit the relation for long GRBs.

<sup>1</sup>Donaghy et al. (2006) suggest 5 seconds as a more realistic dividing line.

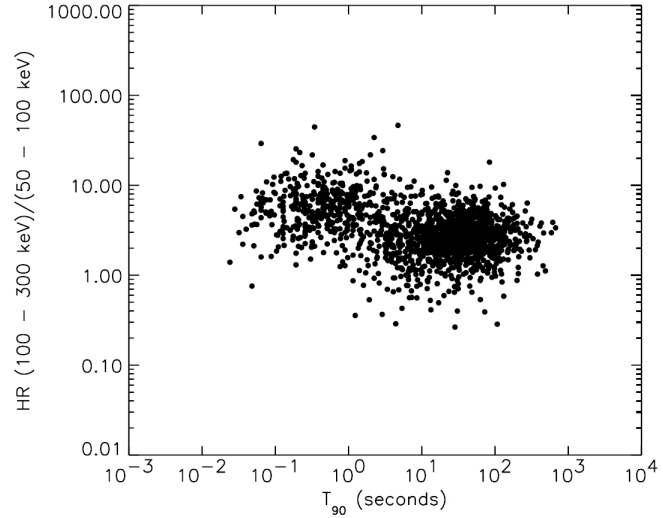


Figure 2.2: The bimodality in hardness ratio  $HR$  and  $T_{90}$  (Kouveliotou et al. 1993) suggests the presence of two classes of GRBs. Adapted from G.J. Fishman (1999).

Kouveliotou et al. (1993) also showed that both classes have an isotropic sky distribution, but their different temporal and spectral properties could indicate that they have different progenitors (Sect. 1.2; see also Veres et al. 2010). In this thesis I will mainly focus on long GRBs.

## 2.2 The physics behind GRBs and afterglows

### 2.2.1 The compactness problem in the gamma-ray band

The discovery in the early 1990s that GRBs have a cosmological origin pointed to the problem about how to release in few seconds an enormous energy up to  $\sim 10^{54}$  erg. Moreover, prompt emission light curves showed millisecond time variability down of  $dt = 200 \mu\text{s}$  (Schaefer 2007), constraining the emitting region to  $R \leq cdt \sim 100$  km (Fig. 2.1). This implied the release of a large amount of energy in a small volume of space and led to the *compactness problem*.

The large amount of energy and the small size of the emitting engine imply that the source should be optically thick and emit blackbody radiation due to the formation of a large number of electron-positron pairs via photon-photon interaction ( $\gamma + \gamma \leftrightarrow e^+ + e^-$ ), with values of the optical depth in the order of  $\tau_{\gamma\gamma} \sim 10^{13}$  (e.g., Piran 1997). But the observations revealed that the prompt emission spectra are non-thermal, often well fitted by a smoothly broken power-law.

This problem was solved by assuming that the emitting source is moving towards us at a relativistic speed, with a Lorentz factor  $\Gamma = 1/\sqrt{1 - v^2/c^2} \gg 1$ . Firstly, this affects the size of the observed source. In the emitter frame an electron radiates isotropically. However, if the electron is moving close to the speed of light towards the observer, due to relativistic aberration the photons emitted in the hemisphere facing the observer will all lie within a cone with a half opening angle  $\theta_{rel} = 1/\Gamma$ , with  $\Gamma \gg 1$  (Fig. 2.3; e.g., Longair 1994; Granot & Ramirez-Ruiz 2010). Hence, for a shell of radiating electrons expanding with a Lorentz factor  $\Gamma$ , all electrons emit radiation within a cone of angle  $\theta_{rel}$ , so that the observer will observe light coming only from the region of the shell within the angle  $\theta_{rel} = 1/\Gamma$ . Assuming a spherical relativistic expansion, it can be shown that  $R \leq 2\Gamma^2 cdt$  (Fig. 2.4; Rybicki & Lightman 1979). It follows that the spatial dimension of the source can be larger by a factor  $2\Gamma^2$  compared to the classical result. Secondly, since the emitting region is moving towards us with relativistic speed, the energy of the photons is blueshifted and, therefore, in the emitter frame it

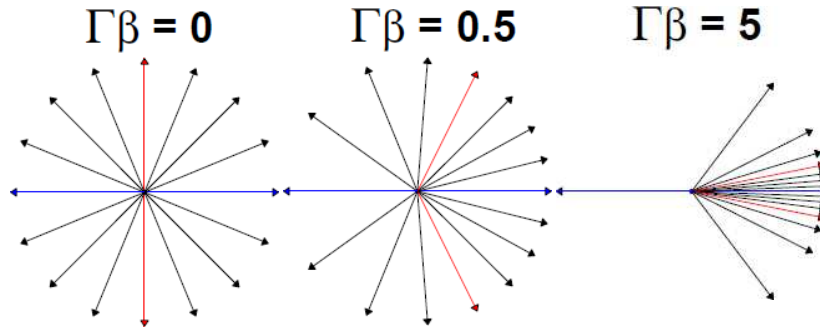


Figure 2.3: *Relativistic aberration: the arrows show the directions of photons in the lab-frame for a source that emits isotropically moving with speed  $\Gamma\beta = \Gamma v/c$ . The red arrows show the photons emitted within the angle  $\theta_{rel}$ . In the left image the source is at rest with respect to the lab-frame and  $\theta_{rel} = \pi/2$ ; in the center the source travels with half light speed and on the right close the speed of light. The faster is the source speed, the more are the photons skewed to the forward direction (adapted from Granot & Ramirez-Ruiz 2010).*

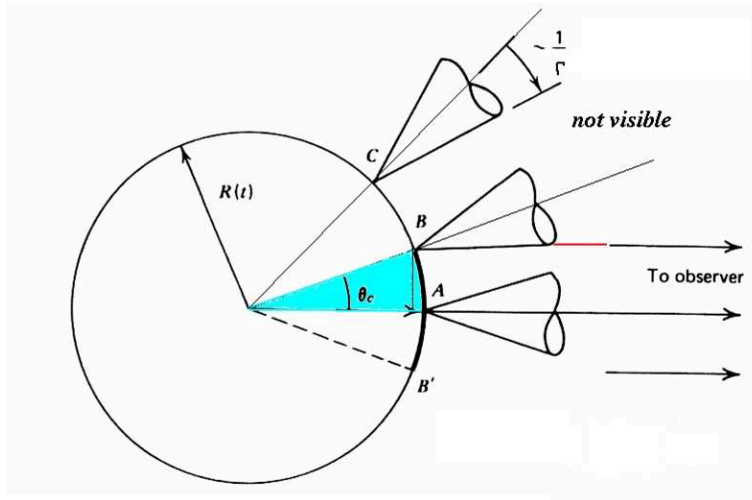


Figure 2.4: *Scheme of the emission cones for electrons in a relativistic expanding shell with bulk Lorentz factor  $\Gamma$ . The cones have a relativistic angle  $\theta_{rel} = 1/\Gamma$ . Photons emitted from an electron at position A will reach the observer. The same at increasing angles  $\theta_c$  till photons emitted from electron B, situated at an angle  $\theta_c = \theta_{rel} = 1/\Gamma$ . Photons emitted from electrons at higher angles, like electron C, will not be visible for the observer. Adapted from Rybicki & Lightman (1979).*

is lower by a factor  $\Gamma$ .

If the observed spectrum is written as  $F(\nu)d\nu \sim \nu^{-\beta}d\nu$ , Lithwick & Sari (2001) showed that in relativistic regime the optical depth becomes smaller by a factor  $\Gamma^{-2(\beta+2)}$ . These arguments together imply that for a spectrum with a typical low-energy spectral index of  $\beta = 1$ , the opacity  $\tau_{\gamma\gamma}$  has to be corrected by a factor  $\Gamma^{-6}$ . Since we observe a non-thermal spectrum, which implies  $\tau_{\gamma\gamma} \leq 1$ , it follows that  $\tau_{\gamma\gamma}$  has to be reduced by a factor in the order of  $10^{13}$ , which requires  $\Gamma > 100$  to make the emitting region optically thin. Therefore, relativistic motion is required to solve the compactness problem.

## 2.2.2 The fireball model

The leading model to explain the creation of a GRB was developed by Rees & Mészáros (1992). The model describes the formation of a GRB by the collisions of mini-shells intermittently emitted by a central engine with different Lorentz factors, therefore it is called internal shock model. These collisions happens at a typical distance from the source of  $2\Gamma^2 cdt \sim 10^{13}$  cm, where  $\Gamma$  is the Lorentz factor of the slower shell (e.g., Rees & Mészáros 1992; Zhang & Mészáros 2004).

When the fireball expands, it collects inter-stellar matter (ISM). Once the relativistic energy of

the collected matter becomes comparable to the relativistic energy of the shell itself, the fireball is decelerated. For typical values of the fireball parameters (total energy  $E_{iso} \sim 10^{52}$  erg,  $\Gamma \sim 100$ ) this happens at a distance of  $\sim 10^{16}$  cm from the explosion center (e.g., Zhang & Mészáros 2004). Therefore, this is called deceleration radius. A forward shock is produced, which propagates in the interstellar medium, the so-called external shock.

The collision of two mini-shells (internal shock) and of the ejected shells with the ISM (external shock), heats and accelerates the matter (protons and electrons<sup>2</sup>). It is usually assumed that they are subject to *Fermi* acceleration, being repeatedly reflected by interaction with random magnetic fields in the fireball, resulting in a power-law distribution  $N(E_e)dE_e \propto E_e^{-p}dE_e$ , where  $p$  is called electron index (e.g., Sari et al. 1998). Electrons are accelerated and emit synchrotron radiation, the most natural mechanism for non-thermal emission. Synchrotron radiation becomes visible when the fireball becomes optically thin. This happens at the so-called photospheric radius. The electrons accelerated in the internal shock emit the photons responsible for the GRB emission, to date observed from visible to gamma-rays. The emission coming from the electrons in the external shock produces the slowly fading transient visible for hours or even months from radio-band to X-rays, the afterglow.

The confirmation of this picture came in case of GRB 970508 at redshift  $z = 0.836$  (Metzger et al. 1997a,b), which afterglow was the first one observed in the radio band (Frail et al. 1997). Fluctuations observed in the radio light curve could be explained as caused by Galactic interstellar scintillation, due to irregularities in the interstellar medium, which diffracts the light coming from a source with a very small angular size, and results in the twinkling of the radio source (Frail et al. 1997; Goodman 1997). These fluctuations became less strong about one month later, implying that the angular size of the source increased to a value that the interstellar scintillation was not visible anymore. The increment in size within one month allowed to derive the explosion speed of the shell, which allowed Frail et al. (1997) to conclude that the emitting shell was expanding at relativistic speed.

### 2.2.3 Spectral energy distribution (SED) and light curve

I will explain here the basics of the synchrotron radiation from an electron in the shock with energy  $E_e = \gamma_e m_e c^2$ , where  $\gamma_e \gg 1$  is the Lorentz factor of the electron. It is known from the theory of synchrotron radiation that an electron accelerated in a magnetic field radiates energy with a spectral power  $P_\nu$  (power per unit frequency, in units of erg Hz<sup>-1</sup> s<sup>-1</sup>), which varies as  $\nu^{1/3}$  until it breaks with an exponential cut off for frequencies higher than  $\nu = \nu(\gamma_e) \propto \gamma_e^2$ .

In astrophysical situations, however, and in particular in the case of a GRB fireball, the radiating electron ensemble, if not continuously fed with energy, loses energy and in this way it cools down. If the energy loss by cooling cannot be neglected, the Lorentz factor of the electron decreases and this affects its emitted SED. This defines a critical Lorentz factor of the electron, called  $\gamma_c$  (where  $c$  stands for cooling). An electron with an initial  $\gamma_e > \gamma_c$  will cool to a Lorentz factor  $\gamma_c$ , while all other electrons will not. This leads to the concept of the so-called *cooling frequency*, which is related to  $\gamma_c$  via the aforementioned equation  $\nu(\gamma_e) \propto \gamma_e^2$ , and which represents a 2nd break in the SED of the cooling electron (Sari et al. 1998). In summary, the theory of synchrotron radiation shows that for an electron the spectrum has three segments: for  $\nu < \nu_c$  it goes like  $P_\nu \propto \nu^{1/3}$ ; for  $\nu_c < \nu < \nu(\gamma_e)$  it goes like  $P_\nu \propto \nu^{-1/2}$ , and for  $\nu > \nu(\gamma_e)$  there is an exponential cutoff.

---

<sup>2</sup>Since a proton has a mass of  $\sim 1836$  times the electron mass, the mass of the shell depends mainly on the number of protons. However, since the radiation power (energy per unit time) scales as  $1/m^2$  (e.g., Longair 1994), the contribution of protons to the radiated energy is negligible.

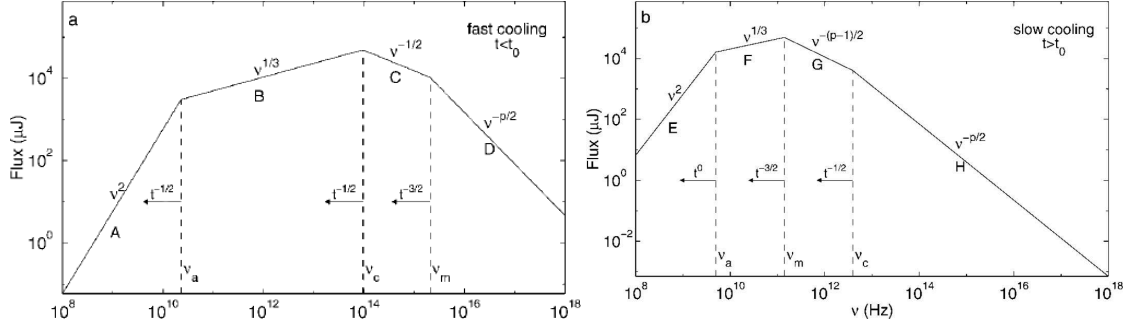


Figure 2.5: Synchrotron spectrum of a relativistic shock with a power-law electron distribution. In addition to the various power-law regimes described in the text, here it is shown also the behavior below the self-absorption break  $\nu_a$ , which however has an effect only at low frequencies not considered in this work. See, for example, Rybicki & Lightman (1979) for details. Sari et al. (1998) described the evolution with time of the more characteristic frequencies  $\nu_m$  and  $\nu_c$ , indicated above the arrows. **Left:** In case of fast cooling, the spectrum consists of four segments, identified as A, B, C, and D. **Right:** In case of slow cooling the four segments are identified as E, F, G, and H. Adapted from Sari et al. (1998).

Sari et al. (1998) applied these basics to the case of electrons in a shocked fluid with a bulk Lorentz factor  $\Gamma$  propagating through a uniform cold medium (i.e., with a density profile  $\eta(r) = \text{constant}$ , where  $r$  is the distance from the progenitor) and assumed that electrons have a power-law distribution of energy resulting from the Fermi acceleration (Sect. 2.2.2). Since  $E_e = \gamma_e mc^2$ , it is  $N(\gamma_e)d\gamma_e \propto \gamma_e^{-p}d\gamma_e$ , with a minimum Lorentz factor  $\gamma_m$ . Considering all electrons, Sari et al. (1998) recognized two cases: *fast cooling*, when  $\gamma_m > \gamma_c$ , and therefore all electrons cool down to the energy  $\gamma_c$  within a time  $t$ ; *slow cooling* which happens when  $\gamma_c > \gamma_m$ , thus only electrons with  $\gamma_e > \gamma_c$  cool. Figure 2.5 shows the synchrotron spectrum of a power-law distribution of electrons in a relativistic shock in both cases. It is characterized by four main features in the flux density  $F_\nu$  measured by the observer: 1) the spectrum peaks at  $\nu_c$  in case of fast cooling, and at the *injection frequency*  $\nu_m$  in case of slow cooling; 2) at lower energies the spectrum follows  $F_\nu \propto \nu^{1/3}$ ; 3) the frequencies  $\nu_m$  and  $\nu_c$  exchange position between the two possible regimes, with different spectral slopes in between (see Fig. 2.5); 4) at very high energies the observed flux density follows the law  $F_\nu \propto \nu^{-p/2}$ . The different nature of the peaks and the different evolution between  $\nu_m$  and  $\nu_c$  allow us to distinguish between the two regimes. At early times the electrons have more energy, therefore they are expected to have  $\gamma_m > \gamma_c$ , thus the fast cooling is favored during the early phase, while the slow cooling is valid thereafter. Also, while the evolution might be different, the description of the synchrotron emission in the fast-cooling scenario might be appropriate for the prompt-GRB phase, too (Zhang & Mészáros 2004). This is also clear when comparing the different evolution of the characteristic frequencies  $\nu_m$  and  $\nu_c$ :  $\nu_m$  moves to lower frequencies faster than  $\nu_c$  (which can even not decrease, if some assumptions on the model changes; see later in this Section and Chevalier & Li 2000), thus at some point there is a transition from fast to slow-cooling regime.

The original theory was developed based on the assumption that the shells expand in an interstellar medium with a constant density profile. However, this might not always be true. If the progenitor is a *Wolf-Rayet* star, the strong wind will change the density profile into a wind profile  $\eta(r) = r^{-2}$ . This affects the way the characteristic frequencies  $\nu_m$  and  $\nu_c$  evolve with time and, therefore, the shape of the light curve (Chevalier & Li 2000; Zhang & Mészáros 2004).

A further development of the theory was the inclusion of a non-spherical explosion (Sari et al. 1999). Indeed several studies (e.g., Rhoads 1999) have shown that the isotropic assumption is likely



Table 2.1: *Closure relations valid for a power-law index of the electron distribution function with  $p > 2$  and for the slow-cooling regime, i.e. during the afterglow phase.*

Model	$\alpha(\beta)$	$\beta(p)$
Isotropic case		
ISM, $\nu < \nu_c$	$3/2\beta$	$(p - 1)/2$
ISM, $\nu > \nu_c$	$3/2\beta - 1/2$	$p/2$
Wind, $\nu < \nu_c$	$3/2\beta + 1/2$	$(p - 1)/2$
Wind, $\nu > \nu_c$	$3/2\beta - 1/2$	$p/2$
Jet		
$\nu < \nu_c$	$2\beta + 1$	$(p - 1)/2$
$\nu > \nu_c$	$2\beta$	$p/2$

unrealistic<sup>3</sup>. When one assumes that the fireball is collimated in a jet, there are some consequences to take into account.

For spherical expansion as well as for a jet, an observer receives only the light emitted within the relativistic angle  $\theta_{rel} = 1/\Gamma$ , due to relativistic aberration. Therefore, the observer has no knowledge about whether outside this cone the emitter is radiating or not, and he cannot distinguish between the isotropic and the jet case. However, since the fireball decelerates, i.e.,  $\Gamma$  decreases, there is a time when  $\theta_{rel}$  becomes bigger than the intrinsic jet-opening angle  $\theta_j$ . After this time the observer starts to see a deficit of photons compared to the isotropic case, because the emitting surface within the angle  $\theta_j$  does not increase together with  $\theta_{rel}$  anymore (Piran 1997). After this transition the afterglow is in the jet regime. An important aspect which derives from the jet model is that the cooling frequency  $\nu_c$  is constant in time in the case of a jet (Sari et al. 1999). This is valid also in case of wind density profile (Chevalier & Li 2000).

The results obtained from several authors, who studied the spectral and light curve behavior, showed that the electron index  $p$  determines both the light curve decay index and the spectral slope. For example, Figure 2.5 shows that the synchrotron spectrum of a relativistic shock depends at high frequencies from the electron index. Therefore, it is possible to obtain a relation between the temporal decay index  $\alpha$  and the spectral index  $\beta$ , the so-called *closure relations*, summarized in Table 2.1 (Zhang & Mészáros 2004; Piran 2005).

An important aspect of the afterglow theory is that during the early phase, i.e. the pre-jet phase, both the injection frequency  $\nu_m$  and the cooling frequency  $\nu_c$  are a function of time and usually  $\nu_m$  has passed the optical bands ( $\nu_{opt}$ ) towards lower frequencies already at very early times, i.e.,  $\nu_m < \nu_{opt} < \nu_c$ , while  $\nu_c$  can stay above or below the X-ray band  $\nu_X$ . Hence, even later during the jet-phase when  $\nu_c$  is constant, there are only two possibilities: either the optical and the X-ray band are in the same spectral branch, i.e., for the spectral slopes one has  $\beta_X = \beta_{opt}$ , or the cooling frequency  $\nu_c$  is in between the optical branch (spectral index  $(p - 1)/2$ ) and the X-ray branch (spectral index  $p/2$ ). Therefore, in the last case it is  $\beta_X = \beta_{opt} + 0.5$  (e.g., see Sari et al. 1998). A good observational demonstration of this is given by Zafar et al. (2011).

Even though the theoretical picture explained above is very successful to explain the observations, there are still some open tasks to do, among which are the following: (i) It has to be demonstrated observationally that during the prompt phase the shape of the SED from the optical to the gamma-ray band is in agreement with synchrotron radiation. (ii) It has to be shown that the evolution of the SED during the prompt emission phase follows the expected behavior of an ensemble of cooling elec-

<sup>3</sup>The main reason is the enormous amount of energy that results from the isotropic assumption. Also other astronomical sources, e.g., quasars and AGN, have proved to have collimated afterglows.

trons. These tasks will be performed in Chapter 3. Furthermore, the internal-external shock scenario predicts that the emission during the prompt and during the afterglow phase should be decoupled, i.e., the prompt emission should not affect the properties of the afterglow. This could be tested best in case of an event with a high energy peak in the prompt gamma-ray emission, i.e., a high-energy GRB with photons detected above several MeV. Unfortunately, GRBs are rarely detected in the MeV domain. Moreover, until recently a high-energy burst with an optical afterglow, well sampled in time and frequency, has never been detected. This raises the following question: (iii) In case of a high-energy GRB, do the physical properties of its afterglow stand out from the corresponding properties of the afterglows of the main GRB population? I will show in Chapter 4 that in fact the *AGILE* GRB 080514B was well suited to tackle this question.

## 2.3 Afterglow phenomenology

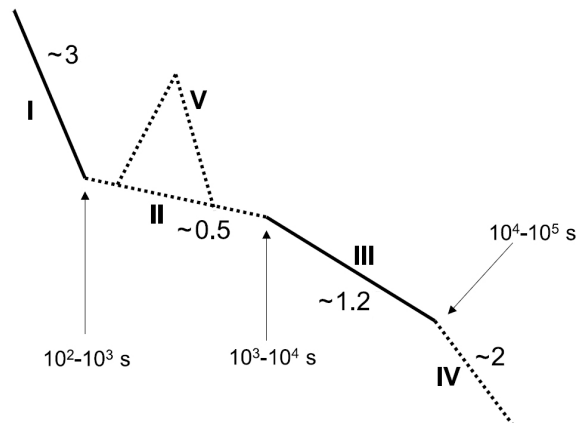
The most serious observational problem since the discovery of GRBs was the apparent absence of a counterpart at any other wavelength than at gamma-rays. As described before (see Sect. 1.1), the big breakthrough then came with the discovery of the afterglow of GRB 970228 thanks to the *BeppoSAX* satellite.

### 2.3.1 Is there a canonical optical X-ray and optical light curve ?

The light curves of long GRB afterglows are observed in a wide range of wavelengths, from radio to X-rays. Since 2004, thanks to the capabilities of *Swift*, afterglows are usually discovered at first in the X-ray band, a few seconds after the burst. One of the early results that emerged from the first 27 X-ray afterglows collected by *Swift* in the years 2004-2005 was the suggested existence of a *canonical* X-ray light curve (Fig. 2.6) structured in four segments (Nousek et al. 2006). At early times,  $t \lesssim 100$  s, the X-ray afterglow is often still hidden by the prompt-GRB light curve, which often has a low-energy tail in the X-ray band, too. At this stage it is decaying very rapidly, with decay indexes  $\alpha > 3$ , as it is also observed in gamma-rays. When the afterglow becomes dominant, the light curve flattens to a shallow decay phase ( $0 < \alpha < 1$ ; Liang et al. 2007), which is then followed by a slightly steeper decay ( $1 < \alpha < 1.5$ ). Finally, usually after 10 ks the light curve breaks to a more steep decay  $\alpha > 1.5$ , which is usually explained as the signature of the transition to the jet-phase (Sect. 2.2.3). This segment is called post-jet-break phase, while the segment before is the pre-jet-brake phase (e.g., Zhang & Mészáros 2004; Racusin et al. 2009). However, in a much bigger sample of 327 *Swift*/XRT light curves, this canonical behavior has been observed only in less than half of the cases, calling into question this model (e.g., Evans et al. 2009; de Pasquale et al. 2009).

The behavior of the afterglow emerging in the optical/NIR bands is similar to that in X-rays (e.g., Kann et al. 2010; Oates et al. 2009), even if sometimes the breaks do not occur simultaneously in both regions of the electromagnetic spectrum. These deviations have not been satisfactorily explained yet. Zeh et al. (2006) found that in almost all cases where the light curve was well-sampled, the observations were deep enough and not contaminated by underlying bright host galaxies, an achromatic break was found within the optical/NIR regime. This can be shown also for  $> 60\%$  of X-ray afterglows in the *Swift* era, while for the remaining 40% the break can be hidden in other features, even though this is still matter of debate (e.g., Panaitescu 2007; Liang et al. 2008; de Pasquale et al. 2009).

Figure 2.6: Originally proposed canonical X-ray light curve based on the observational data from the Swift X-ray Telescope (Nousek et al. 2006; Zhang et al. 2006). In the afterglow light curve it is possible to identify four power-law segments, with the average values for temporal indexes indicated. Segments III (normal decay phase) and IV (jet break phase) were already observed in the pre-Swift era, while the other segments have been observed thanks to Swift. The majority of X-ray light curves are observed during phases I and III, while the other components are observed only for a fraction of bursts. In some cases, a flare (V) is observed, too. Adapted from Zhang et al. (2006).



### 2.3.2 Jets: collimated outflows

As explained in Sect. 2.2, after the transition to the jet phase, the observer starts to see a deficit of photons compared to the isotropic case. This implies a break in the light curve, the so called *jet-break*, usually at a *break-time* of  $\sim 10^4 - 10^5$  s, followed by a steep decay with  $\alpha > 1.5$ , typical for the post-jet-break phase (Sect. 2.3.1). For example, the relations in Table 2.1 show that for a typical value of the optical spectral slope  $\beta_{\text{opt}} = 0.7$ , after the break the decay index  $\alpha_{\text{opt}}$  changes from 1.05 to 2.4 (for an ISM environment). An important characteristic of the jet-break is that it must be achromatic, i.e. the break-time must be the same at all observed frequencies. This is because the break is just a geometric effect.

In Nicuesa Guelbenzu et al. (2011) we discuss the case of the short GRB 090426 (Antonelli et al. 2009). By combining GROND data with observations from other facilities we found an achromatic jet-break (Fig. 2.7). The jet-break time (34500 s) and the post jet decay index ( $2.43 \pm 0.19$ ) well match with the values measured in case of long GRBs. GROND multi-band observations allowed us to test the afterglow model, too. For a post-jet phase, we find a slope for the optical/NIR SED of  $\beta_{\text{opt}} = 0.76 \pm 0.14$ , which implies for the post-break a decay index of  $\alpha = 2.50 \pm 0.28$  if the cooling frequency  $\nu_c$  is above the optical/NIR bands (Sect. 2.2.3), well in agreement with the measured value.

Jets in GRBs were first suggested for GRB 970508 (Waxman et al. 1998), and were claimed for GRB 990123 (e.g., Fruchter et al. 1999) to explain its enormous energy release. Later, Frail et al. (2001), after correcting for collimation<sup>4</sup>, argued that the released beamed energy  $E_\gamma$  seems to group around a quasi-standard value of  $5 \times 10^{50}$  ergs for a sample of long GRBs.

Several recent studies showed that for many events it is difficult to reconcile the observed light curve with a single-jet model (e.g., Panaitescu 2007; Evans et al. 2009; de Pasquale et al. 2009) and that different effects may come into play here. In Nardini et al. (2011), we give a summary of the possible models that can be applied to explain the observed light curve of an afterglow, when it shows a complicated behavior, like in the case of GRB 080928 (Sect. 4.2).

<sup>4</sup>Sari et al. (1999) showed that  $\theta_j \propto t_b^{3/8}$  and that the jet corrected energy is  $E_j = E_{\text{iso}} \theta_j^2 / 2$  (Sect. 2.2.3), where  $\theta_j$  is the half-opening angle of the jet (Sect. 2.2.3) and  $t_b$  is the break time. Zeh et al. (2006) found for  $\theta_j$  and for the beaming factor  $2/\theta_j^2$  typical values of about 0.1 rad and 100, respectively.

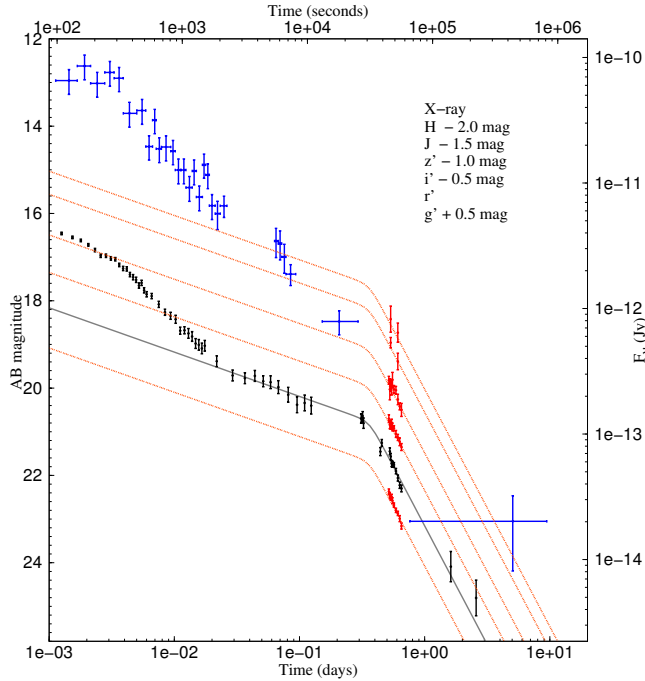


Figure 2.7: *Rc-band light curve of the GRB 090426 afterglow and best fit with a single broken power law after host galaxy subtraction and correction for Galactic extinction. The fit starts at 0.05 days. For comparison the g'i'z'JH bands (in red; left y-axis) and the X-ray light curve from Swift/XRT (in blue, Evans et al. 2010b; right y-axis) are also shown. Adapted from our work published in Nicuesa Guelbenzu et al. (2011).*

### 2.3.3 X-ray flares and large-angle emission

Some X-ray light curves show flares, which are a sudden increase in flux, with a very steep rise and followed by a similar steep decay, which cannot be explained within the framework of the standard afterglow model (Chincarini et al. 2010). X-ray flares are commonly observed in GRB afterglows, with the most known example being GRB 050502B (e.g., Burrows et al. 2005b; Chincarini et al. 2007, 2010; Fig. 2.8). Even stronger flares have been observed in other cases (GRBs 060124, Romano et al. 2006; 061121, Page et al. 2007). On the basis of a big sample of 33 bursts showing flaring activity in their light curves, Chincarini et al. (2007), Falcone et al. (2007) and Chincarini et al. (2010) showed that flares present common features. In particular, they showed that most flares cannot be related to the external shock mechanism responsible for the afterglow. Instead, the observed behavior is very similar to the one of prompt emission pulses. The energy emitted during a bright flare is in some cases of the order of the prompt emission. To explain these properties, those authors advocate for a long-lasting activity for the central engine, responsible of the proper GRB emission. In an updated study, Chincarini et al. (2010) confirmed their previous results.

The most promising and simple interpretation of the fast decay observed in X-ray flares is the large-angle emission (LAE) model (Fenimore & Sumner 1997; Kumar & Panaitescu 2000). Within the standard LAE model, there is a one-to-one correspondence between the photon arrival time  $t$  and the location of the emitting fluid:  $t = (1 + z)R\theta^2/c$ , where  $R$  is the source radius and  $\theta$  the direction of fluid motion relative to the center-observer line. According to the model, the observer receives emission from fluid regions moving at progressively larger angles  $\theta$ . Thus, at different times the observer receives emission from different regions and from different electrons. Thereby, the following assumptions are made: (1) the electron population is the same at all angles  $\theta$  and (2) the surface brightness of the emitting shell is uniform in angle. From these assumptions it follows that the flux decreases as  $t^{-(2+\beta)}$  (Fenimore & Sumner 1997; Kumar & Panaitescu 2000). This raises the question: Does the measurement of the spectral slope from optical to X-rays, together with the monitoring of the light curve, confirms the LAE model? In Sect. 3.2.3 I apply the LAE model to explain the complicate

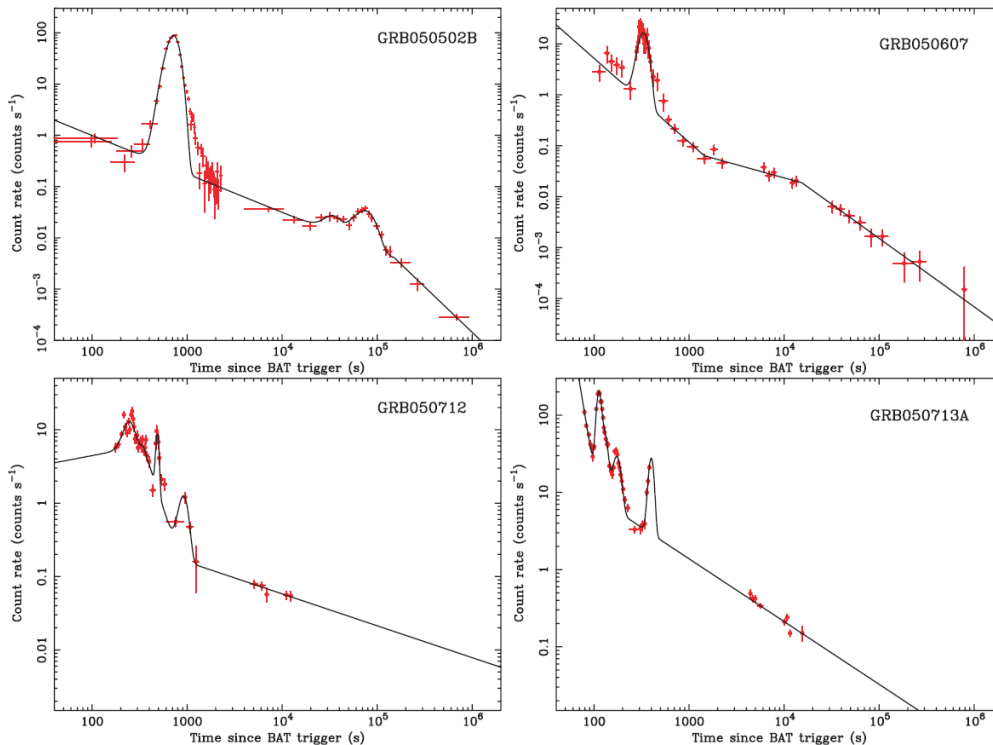


Figure 2.8: Flares in X-ray light curves of afterglows observed with Swift/XRT. The thick line is the best fit to the XRT data (filled circles). The flares are fitted with a Gaussian. Adapted from Chincarini et al. (2007).

early X-ray light curve of GRB 080928, and I will show that in fact there is observational evidence for the need of a more general LAE model.

### 2.3.4 Optically dark GRBs with X-ray afterglows

Among the  $\sim 700$  GRBs localized since the detection of the first X-ray/optical transient (GRB 970228), about 75% have a detected X-ray afterglow. In the late 1990s there was some hope that all afterglows would be detectable within the magnitude range of  $R = 19$  to 21 within 1 day after the burst, allowing for a precise localization of the bursts, redshift measurements and the identification of the GRB host galaxies. However, just  $\sim 60\%$  have been observed in the optical and near infrared (NIR) bands, too (e.g., Evans et al. 2007; Roming et al. 2009; Kann et al. 2010; see also J. Greiner’s page<sup>5</sup>). Their brightness distribution in the optical bands is broad and time-dependent, spanning at least 14 magnitudes within the first hour after the corresponding burst, and still spanning at least 10 magnitudes at around 1 day (Kann et al. 2010, 2011). While most of these optical non-detections are simply due to observing constraints resulting in no optical follow-up observations at all or observations performed only many hours after a burst, or with telescopes having too small aperture, some events (after correction for Galactic extinction) were truly faint if compared with the sample of the optical/NIR detected afterglows. Sometimes they were even fainter than what one expects after extrapolating the observed X-ray flux to longer wavelengths. After the non-detection of the optical afterglow of GRB 970828 down to  $R \sim 24$  in a 30 arcsec X-ray error circle on optical images taken 4 hours after the burst (Groot et al. 1998), the term *dark GRB* was created to describe these optically faint events.

<sup>5</sup><http://www.mpe.mpg.de/~jcg/grbgen.html>

Basically, there are three possible explanations for dark GRBs<sup>6</sup> (e.g., Fynbo et al. 2001): (I) a reduced observed flux due to extinction by dust in the interstellar medium (ISM) of the GRB host galaxy (e.g., Lazzati et al. 2002); (II) an optical dropout due to very high-redshift when Lyman absorption moves into the optical bands; (III) since the optical and X-ray emission of an afterglow is bound by the SED (Sect. 2.2.3), a faint X-ray afterglow, still detectable from the *Swift*/XRT, could have a faint optical counterpart that escapes optical detection; or a mixture of any of these three scenarios.

In case of extinction by dust along the line of sight, however, it affects all bands and it is more visible in the bluer filters. In case of a high-redshift GRB the light coming from spectral regions below  $1216(1+z) \text{ \AA}$  is suppressed due to the hydrogen absorption by intervening absorbing systems. This complicates the search for high-redshift objects. For redshifts above 7, only NIR observations are useful, because this affects only the bands bluer than the Lyman dropout. To distinguish between these effects it is important to have multi-band observations. Unfortunately, this is not always possible, and in some cases no optical/NIR emission from the afterglow is detected at all.

### (I) Extinction by dust

During the last years, two observational approaches were developed to test if the cause for the dark nature of a burst is additional dimming of the optical flux due to high redshift or dust extinction. Following Jakobsson et al. (2004), a GRB with a detected X-ray afterglow is considered as an optically dark burst if the optical-to-X-ray flux density ratio of its afterglow is smaller than expected for synchrotron spectrum. This definition relies on the standard framework of GRB afterglow theory (Sect. 2.2.3). According to the model, there are only two possibilities: either the optical and the X-ray band are in the same spectral branch, i.e., for the spectral slopes we have  $\beta_X = \beta_{\text{opt}}$ , or the cooling frequency  $\nu_c$  is in between the optical branch (spectral index  $(p-1)/2$ ) and the X-ray branch (spectral index  $p/2$ ). In the last case it is  $\beta_X = \beta_{\text{opt}} + 0.5$  (Sect. 2.2.3), a good observational demonstration of this effect is given by Zafar et al. (2011). Consequently, the spectral slope between the optical and the X-ray band,  $\beta_{\text{OX}}$ , cannot be smaller than  $(p-1)/2$ . Our recent work presented in Greiner et al. (2011) on early GROND observations of afterglows suggests that the order  $\nu_m < \nu_{\text{opt}} < \nu_c < \nu_X$  is a reasonable first guess also for optically dark events. Assuming  $p > 2$ , as favored by theory, any spectral slope  $\beta_{\text{OX}} < 0.5$  indicates additional dimming of the optical flux of the afterglow and defines a GRB as a dark burst.

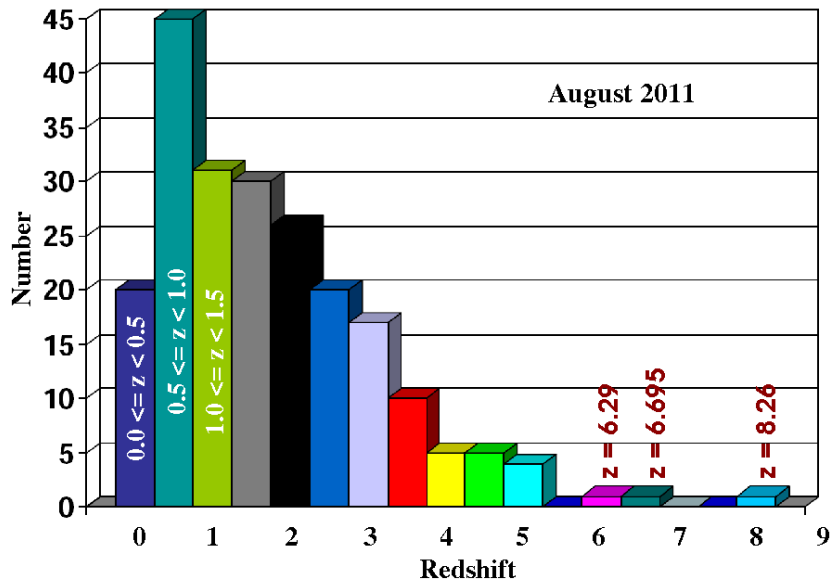
In an approach similar to Jakobsson et al. (2004), van der Horst et al. (2009) compared the observed  $\beta_{\text{OX}}$  with the spectral index of the X-ray afterglow. Within the context of synchrotron radiation, van der Horst et al. (2009) defined a burst as optically dark if  $\beta_{\text{OX}} < \beta_X - 0.5$  (see also Rol et al. 2005). This approach explicitly assumes that there is a spectral break between the optical and the X-ray regime. If, however, this break lies outside the optical/X-ray region, then the criterion for a dark burst according to van der Horst et al. (2009) would be  $\beta_{\text{OX}} < \beta_X$ . Observational evidence for this case might come from the observed value of  $\beta_X$  after correction for absorption by gas. Assuming that for the electron index  $2 < p < 3$  holds, any observed  $\beta_X < 1$  could indicate that the X-ray band is on the  $(p-1)/2$  spectral branch of the SED (i.e.,  $\nu_X < \nu_c$ ).

In Greiner et al. (2011) we also confirmed that the faintness of the optical afterglows is mainly

---

<sup>6</sup>Note that the definition of a dark burst does actually refer to the visibility of its optical afterglow only. It does not relate to the gamma-ray band. It does also no refer to the prompt emission phase, even though it is clear that here the same physical processes are at work: Lyman dropout and extinction by dust would affect the optical light of this phase in the same way as they affect the afterglow phase.

Figure 2.9: Histogram of the GRB redshift distribution based on 216 events up to August 2011. The three GRBs with the highest spectroscopic redshift are labeled: GRB 050904 ( $z = 6.29$ ), GRB 080913 ( $z = 6.695$ ) and GRB 090423 ( $z = 8.26$ ). Lyman dropout starts once  $1 + z > \lambda_{obs}/(1216 \text{ \AA})$ , where  $\lambda_{obs}$  stands for the wavelength of the filter band.



caused by dust extinction at moderate redshift (see also the ESO press release from 16 December 2010<sup>7</sup>). Moreover, we showed that the population of dust extinguished GRBs is between 25% and 40%. Moreover, our study was able for the first time to build SEDs with contemporary X-ray/optical/NIR data, without making any assumption on the light curves and the SEDs as in previous works (Cenko et al. 2009). These results were only possible thanks to the rapid optical/NIR multi-wavelength follow-up observations with the multi-channel imager GROND (see Sect. 1.4), supplemented by *Swift*/XRT spectra. This allowed to build multi-band light curves and broad-band SEDs and derive rest-frame extinctions.

## (II) High-redshift GRBs

When looking for very high-redshift galaxies ( $z \gtrsim 8$ ), only a handful of objects are found even with the Hubble Space Telescope (HST) (e.g. Bouwens et al. 2010, 2011), with the most distant object confirmed being at a spectroscopic  $z = 8.6$  Lehnert et al. (2010). However, these galaxies discovered using the best facilities might be just the tip of the iceberg.

GRBs have demonstrated to be a powerful alternative for identifying objects beyond a redshift 5 (Fig. 2.9). This is of primary interest because it allows us to study the nature of the first stars in the Universe. Moreover, since GRB progenitors are massive stars, and therefore have a lifetime in the order of million years only, they pick up the places of the most intense star formation. In other words, they are suspect to track the galaxy evolution (e.g., Bromm et al. 2009).

Thanks to my work with GROND on La Silla (Sect. 1.5) I had the opportunity to discover the optical/NIR afterglow of GRB 080913 ( $z = 6.695 \pm 0.025$ ; Rossi et al. 2008c; Greiner et al. 2009b), what at the time was the most distant GRB, and the second most distant object ever observed (Sect. 1.5). However, a few months later Tanvir et al. (2009), with the contribution of GROND data, reported a spectroscopic redshift of  $z = 8.26$  for GRB 090423. It was the second most distant object spectroscopically confirmed to date, after the galaxy studied by Lehnert et al. (2010) at  $z = 8.6$ . However, different from galaxies, SEDs of GRB afterglows are simple power laws, without emission lines. Therefore, the observation of the Lyman dropout is a very powerful tool to estimate the photometric redshift of

<sup>7</sup><http://www.eso.org/public/news/eso1049/>

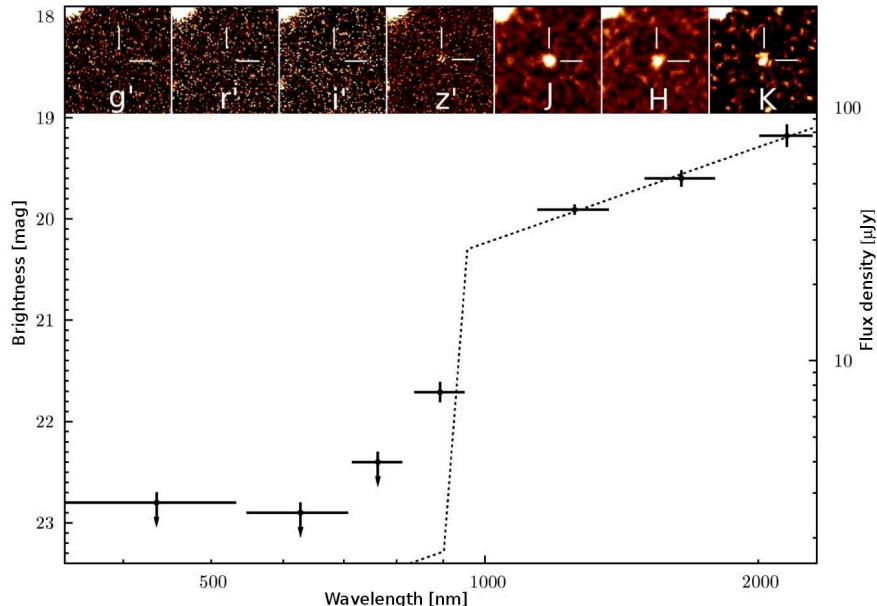


Figure 2.10: The SED of the afterglow of GRB 080913 observed by GROND (Rossi et al. 2008c). The zoom-in shows the position of the afterglow in the  $g'r'i'z'$  JHK bands. The SED is characterized by the lack of detection in  $g'r'i'$  and faintness in  $z'$ , while it is not affected by suppression in JHK. This can only be explained by intervening Lyman dropout, constraining the photometric redshift to  $z = 6.4 \pm 0.3$ . Adapted from Greiner et al. (2009b).

GRBs (Sect. 1.5). This technique led to estimate a photometric redshift of  $z \sim 9.4$  for GRB 090429B, again with fundamental contributions from GROND (Cucchiara et al. 2011). Figure 2.9 shows the redshift distribution of all GRBs with known redshift till August 2011.

### (III) Intrinsic low brightness

The Jakobsson et al. (2004) and van der Horst et al. (2009) criteria are a powerful tool to check if a burst was dark due to extinction in its host galaxy or due to cosmological Lyman drop out. If these criteria are fulfilled it is for sure that at least one of these two physical processes was at work. It means that there is no way to bring the observed optical flux into agreement with the observed X-ray flux, if this was synchrotron radiation (which might be considered as a secure assumption). Since in the case of a dark burst the afterglow was not detected in any optical/NIR band, a precise quantitative estimate of either  $A_V(host)$  or  $z$  cannot be given, however. This is contrary to the cases I will discuss in Chapter 3 and 4. Here multi-color data of an afterglow were available, i.e. the afterglow was detected, a broad-band SED could be constructed, and  $A_V(host)$  and/or  $z$  could be estimated. If, on the other hand, the Jakobsson et al. (2004) and van der Horst et al. (2009) are not fulfilled then this does not mean that extinction or Lyman drop out can be ruled out. Each of these two physical processes could still have been at work but the observations (upper limits) were simply not deep enough to claim this now with certainty.

There is still the possibility that an afterglow was not detected in any band even though its (non-detected) optical flux lies perfectly on the theoretical SED, i.e. none of the previous discussed two processes came into play at all. This can happen when the optical flux was simply too low for the observations performed. In other words, again, the observations were not deep enough. In fact, one can easily show that for positions of the cooling frequency  $\nu_c$  close to the soft X-ray band in



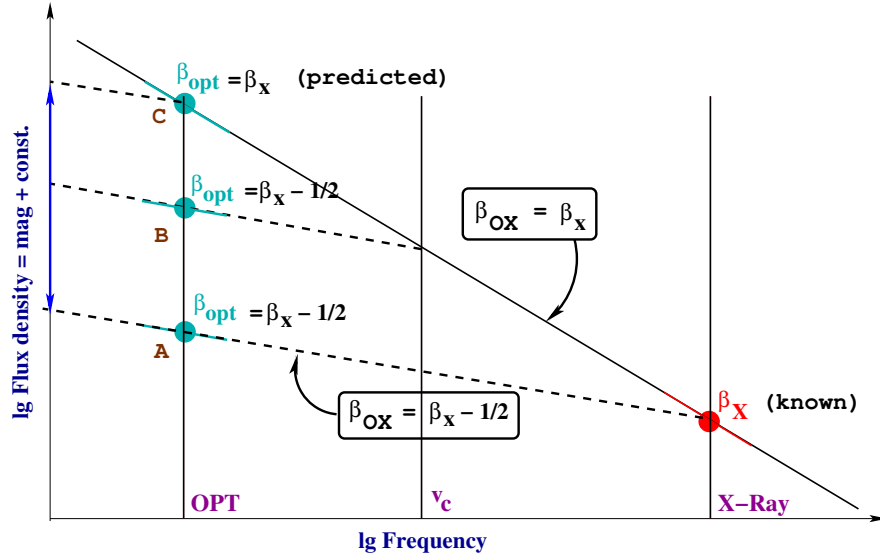


Figure 2.11: Sketch of the idea behind the Jakobsson et al. (2004) and van der Horst et al. (2009) criteria discussed in Sect. 2.3.4. In red is drawn the observed X-ray slope  $\beta_X$ . Depending on the position of the spectral break at the colling frequency  $\nu_c$ , the slope predicts the optical flux, since left to  $\nu_c$  the relation  $\beta = \beta_X - 0.5$  holds. There are two limiting cases: (A)  $\nu_c = \nu_X$  and (C)  $\nu_c = \nu_{\text{opt}}$ . The former predicts the lowest possible optical flux, the latter the highest. Finally (B) describes the most general case, namely  $\nu_{\text{opt}} < \nu_c < \nu_X$ . The van der Horst et al. (2009) criterion checks  $\beta_{\text{OX}}$ , the spectral slope between the optical and the X-ray band. Theoretically it can be at most as low as  $\beta_X - 0.5$ . If an observed upper limit provides a deduced  $\beta_{\text{OX}}$  lower than this value, then additional dimming of the afterglow must have come in to play.

combination with a spectral slope in the order of 1 between  $\nu_c$  and  $\nu_X$ , a detection of the afterglow with *Swift*/XRT can predict an optical flux too low for 2-m class optical telescopes, which are the biggest telescopes following up all observable afterglows. This is called intrinsic low brightness.

Phenomenologically all three processes, either operating alone or together, lead to the observational same result: they can make an afterglow undetectable even though reasonably deep and rapid follow-up observations were performed. The question then is, can one figure out in some way which of the three processes might in fact be dominating among the dark burst sample? Is it perhaps always extinction? Or always high redshift (Lyman drop out)? This will be studied in detail in Chapter 5, where I look deep into the arcsec-sized X-ray error circles of an ensemble of dark bursts. I will discuss that the nature of the galaxies seen (or not seen) in these small error circles is a reasonable tool to explore the nature of the dark bursts in a statistical sense.

## 2.4 GRB host galaxies

Before the first afterglow detection, GRBs were usually localized within huge error boxes of several degrees, what made the search of suitable candidates basically impossible. Finally, the detection of the first optical afterglows in the late 1990s (Sect. 1.1) changed this poor situation. GRB 970228, the first GRB with a detected optical afterglow, was also the first one where an extended source was found underlying the position of the afterglow. However, since at that time it was still not proven that GRBs were cosmological events, the association with this galaxy was still not sure. Fortunately few months later GRB 970508 was found to have a redshift of 0.835 (Metzger et al. 1997a,b), definitively confirming the extragalactic nature of GRBs, and therefore the extended source underlying GRB

970228 afterglow was definitively its host galaxy, later found to be at a redshift  $z = 0.695$  (Djorgovski et al. 1999). At this point it was also clear that GRBs allow us the detection of distant galaxies that are very difficult to detect with other methods (Natarajan et al. 1997).

### 2.4.1 The main GRB host galaxy population

*Swift's* ability to localize X-ray afterglows within 1-2 arcsec error circles substantially improved the possibility to find host galaxies, even without a sub-arcsecond optical localization of the corresponding afterglows. Optical follow-up observations, while important because of a better localization, are often limited by visibility constraints and the availability of telescope time. The new approach allowed to build complete samples of *Swift*/XRT-localized events and to search for their host galaxies within their corresponding small X-ray error circles.

Since long GRBs have proven to be related to the death of massive stars (Sect. 1.2), GRBs mark galaxies that have recently undergone episodes of intense star formation. This picture matches well with the sample of host galaxies of long GRBs observed up to a redshift of 5 (e.g., GRB 060510B; Chary et al. 2007), which are predominantly blue, star-forming galaxies with usually low and modest global extinction by dust (e.g., Christensen et al. 2004; Savaglio et al. 2009, but see Sect. 2.4.2). Moreover, since gamma-rays are not affected by obscuration by gas and dust along the line of sight, long GRBs are a powerful tool to highlight star-forming galaxies up to very high-redshifts (Sect. 2.3.4; Li 2008; Kistler et al. 2009). Therefore, GRB host galaxies might represent a subsample which is less biased against dusty and evolved galaxies, which are less bright in optical surveys. Indeed, we know already that some GRB hosts are extremely dust-obscured (Sect. 2.4.2). Moreover, we have recently shown that GRBs can also be hosted by massive and chemically evolved galaxies, like our neighbor M82 (e.g., Hunt et al. 2011; Krühler et al. 2011).

Long GRB host galaxies are very different in morphology, including spiral galaxies and more irregular galaxies (Fig. 2.12). In agreement with studies of the star formation rate, no early-type galaxy, or in general a galaxy with a passive stellar population, has ever been found to be associated with a long GRB. There is some indication that some host galaxies might be part of an interacting group of galaxies (e.g., Foley et al. 2006; Levan et al. 2006a), and the interaction may have triggered the star formation, including the progenitor of long GRBs, but the studies in this direction are not yet progressed enough.

Short GRBs pinpoint a different galaxy population, dominated by passive galaxies, like old spiral and elliptical galaxies (Berger et al. 2005; Berger 2009; Fong et al. 2010). This is in agreement with the suggested association of short GRBs with the merger of compact stellar objects (Sect. 1.2), because these stars might have a long lifetime before finally undergoing a merging episode (Belczynski et al. 2006). The search for the hosts of short GRBs is complicated by the fact that the progenitors may travel for several kpc away from their birthplaces, and therefore several arcseconds on the sky, making the association between them and their host galaxies difficult to prove in the absence of redshift measurements. In the following, and in particular in Chapter 5, I will concentrate only on long GRBs and their host galaxies.

### 2.4.2 Dark GRB host galaxies

In section 2.3.4 I have introduced the problem of dark GRBs. It is of fundamental importance to study the characteristics of their host galaxies if they can be identified on statistical arguments. Naively one can assume that they can be different compared to galaxies of not dark GRBs, e.g., with respect

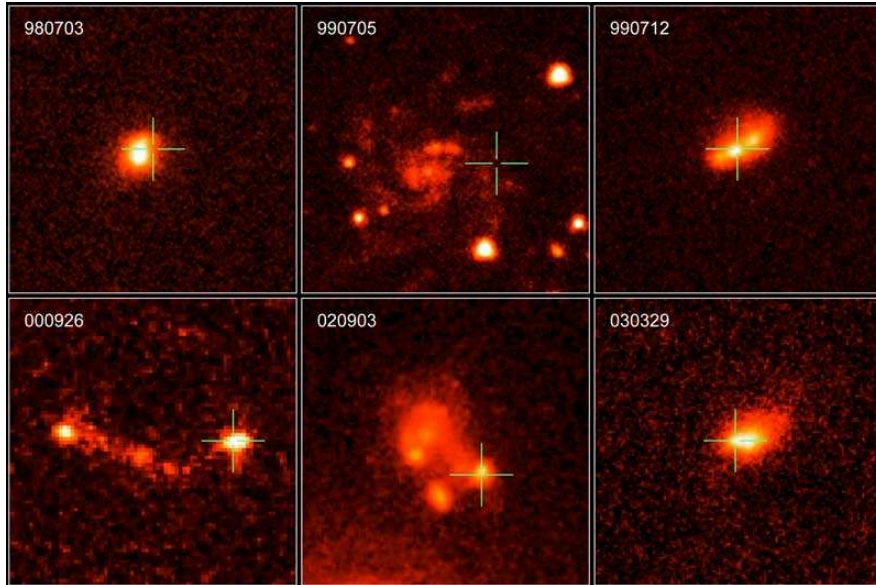


Figure 2.12: A mosaic of some GRB host galaxies imaged with HST in optical. Due to their redshift, the light we receive comes mainly from the blue and ultra-violet bright regions within the galaxies, produced by the massive stars in the hosts (adapted from Fruchter et al. 2006).

to their star formation rate, metallicity, dust content. Furthermore, in case of a high-redshift, these properties could be different compared with what is observed at lower redshifts.

While clear examples of high-redshift GRBs exist (Haislip et al. 2006; Kawai et al. 2006; Tagliaferri et al. 2005; Greiner et al. 2009b; Tanvir et al. 2009; Salvaterra et al. 2009; Pérez-Ramírez et al. 2010), these are rare events. Perley et al. (2009) found that a significant fraction of dark bursts occurred in highly obscured regions within their host galaxies. The galaxies themselves, however, have optical colors similar to blue, non-extinguished GRB hosts (e.g., Christensen et al. 2004), suggesting that in these cases the obscuring dust resides only in the local environment of the GRB progenitor and not farther out, like the case of GRB 000210 (Piro et al. 2002; Gorosabel et al. 2003). There exist, however, a handful of GRBs which reside in red and dusty galaxies (e.g., Levan et al. 2006a; Berger et al. 2007; Hashimoto et al. 2010; Chen et al. 2010, 2011). Recently in Greiner et al. (2011), using the multi-channel imager GROND, we showed that dust extinction in GRB host galaxies is the most likely reason for the optical dimness of these events.

Naturally, the absence of a precise localization of the optical/NIR counterpart of an X-ray afterglow makes the search for its host galaxy challenging, because many galaxies can lie inside an X-ray error circle even if it has a few arcsec radius only. Also, often GRB host galaxies are very faint, requiring a large amount of observing time with 8-m class optical telescopes to reach deep enough flux limits to identify them. In Chapter 5 I will show that it is possible to reduce the number of host galaxy candidates in arcsec-sized X-ray error circle by using special selection criteria.

The open questions are: i) Do the properties of the host galaxies of dust-extinguished GRBs differ from those of the main host galaxy population? ii) Does a study of the host galaxy properties confirm that extinction by dust, plus potentially a moderate redshift was the cause of the afterglow faintness? iii) Is high dust extinction a global property of these host galaxies or it is just restricted to the local environment of the GRB progenitor? I will touch these questions in Chapter 5.



## Chapter 3

# The prompt phase of GRB 080928 from optical to gamma-rays

In this chapter I study the prompt gamma-ray, X-ray and optical emission of GRB 080928. This burst was detected by *Swift*/BAT and *Fermi*/GBM but not seen by *Fermi*/LAT. The burst is of particular interest since both optical and X-ray emission was detected by *Swift*/UVOT and *Swift*/XRT, respectively, when the GRB was still radiating in the gamma-ray band. This makes it one of a rare number of cases (e.g., GRBs 041219A, 050820A, 051111, 061121; Shen & Zhang 2009; Götz et al. 2011), where a broad-band SED from about 1 eV to 150 keV can be constructed for the prompt emission phase.

In the following, I first present the observations obtained in gamma-rays, X-rays and optical, and afterwards I discuss the observations within the framework of the standard afterglow theory (Sect. 2.2). In particular, I show that the prompt radiation between 200 and 500 sec after the burst trigger has spectral properties in agreement with synchrotron emission. By combining optical to gamma-ray data, a sharp break is seen in the SED around 4 keV that moves to lower energies at late times. To the best of my knowledge, this is the first time that a sharp break is clearly visible in the optical to gamma-ray SED of the prompt emission phase of a GRB, and the first time that it is possible to confront such observations with the theory.

### 3.1 Data and analysis

#### 3.1.1 *Swift*/BAT and *Fermi*/GBM data

The long burst GRB 080928 triggered the Burst Alert Telescope of *Swift* at  $t_0 = 15:01:32.86$  UT (Sakamoto et al. 2008) on the 28th of September 2008. This was an image trigger lasting 112 seconds. The prompt emission detected in the BAT began with a faint precursor at  $t_0 - 90$  s, then weak emission starting at  $t_0 - 20$  s and lasting for 40 s, followed by a second, slightly brighter peak starting at 50 s and ending at 120 s after the trigger (Fig. 3.1). The main emission of the GRB started at  $t_0 + 170$  seconds, with two peaks at 204 and 215 seconds<sup>1</sup>. Another less significant peak is detected around 310 s before fading out to at least 400 seconds when *Swift* had to stop observing due to its entry into the South Atlantic Anomaly (SAA) and the noise level became too large for any late emission to be detected in the BAT (Cummings et al. 2008; Fenimore et al. 2008; Sakamoto et al. 2008).

---

<sup>1</sup>If not stated otherwise, for the rest of this chapter all times refer to the zero-point  $t_0$ .

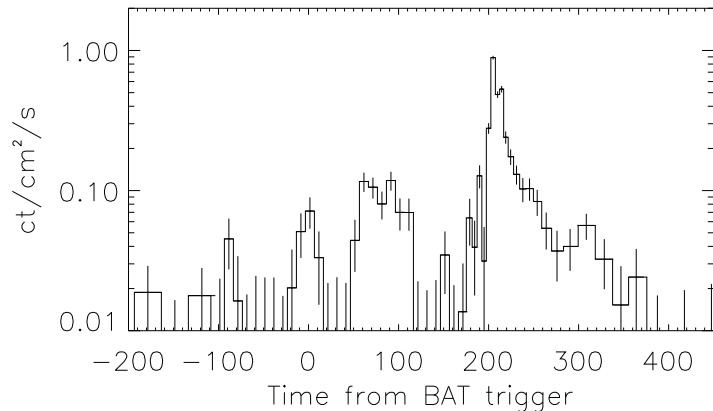


Figure 3.1: *The light curve of GRB 080928 as seen by Swift/BAT. Swift triggered at the gamma-ray peak at  $t_0 = 0$ , which was followed by at least two more peaks with the maximum flux at  $t_0 + 204$  s. There may be a faint precursor of the main burst at  $t_0 - 90$  s.*

The main burst emission also triggered the Gamma-Ray Burst Monitor onboard *Fermi* (Paciesas et al. 2008), while the INTEGRAL satellite was passing through the SAA during the time of GRB 080928 and thus could not observe the burst with the anti-coincidence shield of the spectrometer SPI (SPI-ACS, Rau et al. 2005). GBM has 2 sets of detectors which cover the energy band between 8 keV and 1 MeV, and between 150 keV and 40 MeV. Emission from the burst was predominately seen in the low energy detectors. The GBM light curve (Fig. 3.1) shows a single pulse corresponding to the emission maximum observed by *Swift* at

$$t_{0,\text{GBM}} = t_0 + 204 \text{ s}. \quad (3.1)$$

In Rossi et al. (2011b) we analyzed data collected by BAT between  $t_0 - 239$  s and  $t_0 + 494$  s in event mode with  $100 \mu\text{s}$  time resolution and about 6 keV energy resolution. The data were processed using standard BAT analysis tools. For spectral analysis, the data were binned so that the signal-to-noise ratio was at least 3.0. During the main peak, the bin edges were chosen to match the *Swift*/XRT spectral bins. The spectra were fit using Xspec v12.5.0.

The spectral analysis of the *Fermi* data is summarized in Rossi et al. (2011b). It is important to report that the GBM spectra was analyzed for two different time windows, one covering the broad emission maximum from  $t_{0,\text{GBM}} - 5.248$  s to  $t_{0,\text{GBM}} + 24.448$  s, while the second was constrained to  $\approx 4$  s around the light curve peak ( $t_{0,\text{GBM}} - 1.152$  s to  $t_{0,\text{GBM}} + 2.944$  s).

### 3.1.2 *Swift*/XRT data

*Swift*/XRT started to observe the BAT GRB error circle 170 seconds after the trigger and found an unknown X-ray source at coordinates R.A. (J2000)=  $6^{\text{h}}20^{\text{m}}16^{\text{s}}.87$ , Dec. =  $-55^{\circ}11'58''.5$ , with a final uncertainty of  $1''.4$  (Osborne et al. 2008; Sakamoto et al. 2008). Observations continued until 2.7 days after the GRB, when the source became too faint to be detected.

In Rossi et al. (2011b) we obtained the X-ray data from the *Swift* data archive and the light curve from the *Swift* light curve repository (Evans et al. 2007, 2009). To reduce the data, the software package HeaSoft 6.6.1 was used<sup>2</sup> with the calibration file version v011<sup>3</sup>. Data analysis was performed following the procedures described in Nousek et al. (2006). We found that the X-ray emission was only sufficiently bright to perform a spectral analysis in the first two observing blocks (000–001). However, the early windowed timing (wt) mode and photon counting (pc) mode data were highly

<sup>2</sup><http://heasarc.gsfc.nasa.gov/docs/software/lheasoft>

<sup>3</sup>[heasarc.gsfc.nasa.gov/docs/heasarc/caldb/swift](http://heasarc.gsfc.nasa.gov/docs/heasarc/caldb/swift)

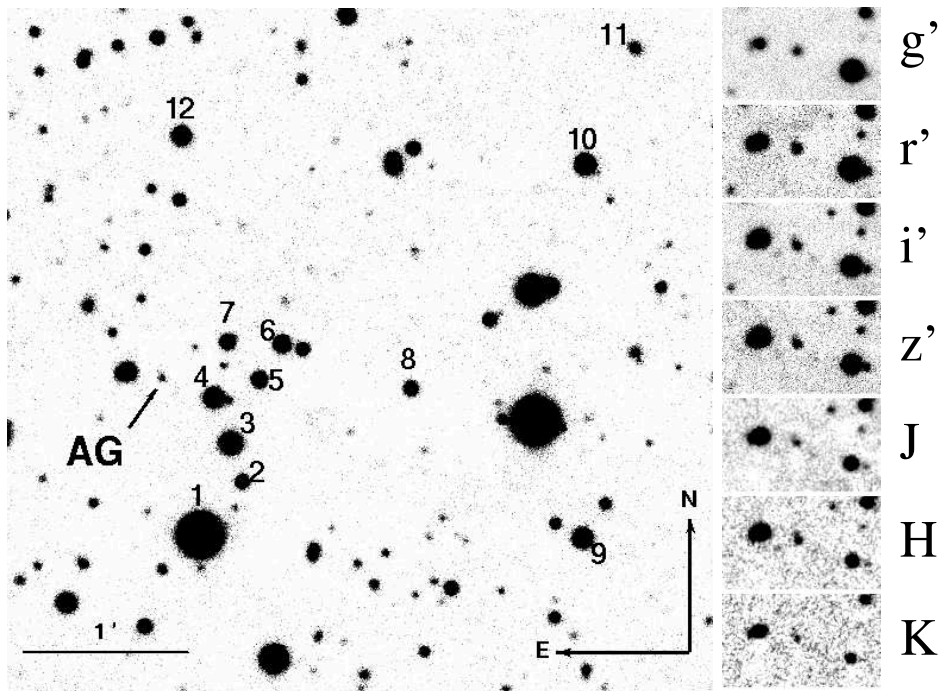


Figure 3.2: Finding chart of the afterglow of GRB 080928 (GROND  $i'$  band, at 0.603 days after the burst). The afterglow (AG) and the secondary photometric standards used (Table A.4) are indicated. On the right it is shown the afterglow as observed by GROND in all seven filters.

affected by pile-up. To account for this effect, the methods presented in Romano et al. (2006) and Vaughan et al. (2006) were applied. In total, from both observing blocks the SED was extracted for 27 epochs, covering 1.4 days.

Following Butler & Kocevski (2007), initially the pc-mode spectra were fitted with an absorbed power-law to obtain  $N_{\text{H}}^{\text{host}}$  using Xspec v12.5.0. This model consists of two absorption components, one in the host frame and another one in the Galaxy. For both absorbers the Tübingen abundance template by Wilms et al. (2000) was used, with the Galactic absorption fixed to  $N_{\text{H}}^{\text{Gal}} = 0.56 \times 10^{21} \text{ cm}^{-2}$  (Kalberla et al. 2005). The spectra were then fitted in two steps. First, all pc-mode spectra of the XRT observing block 000 were stacked using the FTOOL mathpha (Blackburn 1995)<sup>4</sup>. This spectrum contained about 1000 counts. The fitted absorbed power-law is characterized by a spectral slope of  $\beta_{\text{X}} = 1.09_{-0.10}^{+0.07}$  and an effective hydrogen column density of  $N_{\text{H}}^{\text{host}} = 3.6_{-2.2}^{+1.8} \times 10^{21} \text{ cm}^{-2}$ . The spectral slope agrees with the observed mean value of  $\beta_{\text{X}} \sim 1$  found by, e.g., Racusin et al. (2009) and Evans et al. (2009). Having derived  $N_{\text{H}}^{\text{host}}$  in this way, the early spectra (wt-data) were fitted with an absorbed power-law in which  $N_{\text{H}}^{\text{host}}$  was fixed to the previously derived value.

### 3.1.3 Optical/NIR data

Swift/UVOT started observing about 3 min after the trigger, still before the onset of the main emission of the GRB, and immediately found an optical afterglow candidate (Kuin et al. 2008; Sakamoto et al. 2008). The redshift reported by Vreeswijk et al. (2008) was later refined to  $z = 1.6919$  by Fynbo et al.

<sup>4</sup><http://heasarc.gsfc.nasa.gov/ftools/>

(2009).<sup>5</sup>

In Rossi et al. (2011b) *Swift*/UVOT data were analyzed using the standard analysis software distributed within FTOOLS, version 6.5.1. For all the detections, the source count rates were extracted within a 3'' aperture. An aperture correction was estimated from selected nearby point sources in each exposure and applied to obtain the standard UVOT photometry calibrated for a 5'' aperture.

Ground-based follow-up observations were performed using the ROTSE-IIIa 0.45m telescope in Australia (Rykoff et al. 2008) and the multichannel imager GROND on the 2.2m telescope on La Silla (Sect. 1.5). This data set (Tables A.1, A.2, A.3) was supplemented by data published from the VLT (Vreeswijk et al. 2008; Fynbo et al. 2009), and the 16'' Watcher telescope in South Africa (Ferrero et al. 2008).

ROTSE-IIIa data were analyzed with a PSF photometry package based on DAOPHOT following the procedure described in Quimby et al. (2006). GROND optical/NIR data were analyzed through standard PSF photometry using DAOPHOT tasks under IRAF (Tody 1993) similar to the procedure described in Krühler et al. (2008). Aperture photometry was applied when analyzing the field galaxies, using the DAOPHOT package (Warmels 1992). Afterglow coordinates were derived from the GROND 3rd epoch  $g'r'i'z'$ -band data. The stacked image has an astrometric precision of about 0.3 arcsec, corresponding to the RMS accuracy of the USNO-B1 catalogue (Monet et al. 2003). The coordinates of the optical afterglow (Fig. 3.2) are R.A. (J2000)= 06<sup>h</sup>20<sup>m</sup>16<sup>s</sup>.83, Dec. = -55°11'58".9 (Galactic coordinates  $l, b = 263^{\circ}.82, -26^{\circ}.31$ ). Magnitudes were corrected for Galactic extinction using the interstellar extinction curve derived by Cardelli et al. (1989) and by assuming  $E(B - V) = 0.07$  mag (Schlegel et al. 1998) and a ratio of total-to-selective extinction of  $R_V = 3.1$ .

During our first two epochs of GROND observations (Rossi et al. 2008a) the weather conditions were not good, with the seeing always higher than 2.5 arcsec and strong winds (> 10 m/s). Therefore, it was not possible to separate the afterglow from a nearby galaxy that first became separately visible on the third-epoch images (seeing 1.5 arcsec; see Sect. 4.2.4). To correct for the contribution of this galaxy, I performed image subtraction using the HOTPANTS package<sup>6</sup>. Image subtraction was applied on the first, second, and third epoch GROND images, using the fifth GROND epoch images as a template. This gave good results for all bands except  $g'$ , which is affected by a low-quality point spread function. Therefore, for this band I performed a simple subtraction of the flux of the galaxy component, with the flux derived from the fifth-epoch images. Calibration of the field in  $JHK_S$  was performed using 2MASS stars (Table A.4). The magnitudes of the selected stars were transformed into the GROND filter system and finally into AB magnitudes using  $J(AB) = J(Vega) + 0.91$ ,  $H(AB) = H(Vega) + 1.38$ ,  $K_s(AB) = K_s(Vega) + 1.79$  (Greiner et al. 2008).

Watcher data (Ferrero et al. 2008), VLT data (Vreeswijk et al. 2008; Fynbo et al. 2009), and ROTSE-IIIa data were calibrated using USNO-B1 field stars. In order to take these different calibrations into account, I compared the  $r'$ -band photometry of the GROND secondary standard stars with the corresponding  $R$ -band magnitudes from USNO-B1. In doing so, I obtained a correction of  $0.40 \pm 0.15$  mag for USNO-B1. After shifting these afterglow data to the GROND  $r'$  band, I finally subtracted the GROND fifth-epoch flux of the galaxy closest to the afterglow (see Sect. 4.2.4) from the Watcher and VLT observed magnitudes, which shifted the afterglow magnitude by +0.05 mag and +0.11 mag, respectively. The correction for the ROTSE-IIIa data was even smaller and, therefore, set to zero.

<sup>5</sup>For this redshift the distance modulus is  $m - M = 45.54$  mag, the luminosity distance  $3.95 \times 10^{28}$  cm, the look-back time 9.76 Gyr (3.91 Gyr after the Big Bang), and 1 arcsec on the sky corresponds to a projected distance of 8.56 kpc.

<sup>6</sup><http://www.astro.washington.edu/users/becker/hotpants.html>



Table 3.1: *Spectral fit results for Swift/BAT and Fermi/GBM.*

instrument	model	$\tilde{\beta}_1$	$E_1$	$\tilde{\beta}_2$	$E_2$	$\tilde{\beta}_3$	$\chi^2/\text{d.o.f.}$
<b>46.5 s &lt; <math>t_0</math> &lt; 121.0 s</b>							
BAT-GBM	db-pl	–	$12.37^{+1.52}_{-12.37}$	$1.92^{+0.13}_{-0.18}$	$143^{+37}_{-64}$	–	582 / 560
<b>202.848 s &lt; <math>t_0</math> &lt; 206.944 s = -1.152 s &lt; <math>t_{0,\text{GBM}}</math> &lt; 2.944 s</b>							
GBM	Band	–	–	$1.24 \pm 0.16$	$108 \pm 24$	$3.3 \pm 4.6$	411 / 436
XRT-BAT-GBM	db-pl	$0.62^{+0.10}_{-0.18}$	$3.94^{+0.56}_{-0.62}$	$1.74^{+0.05}_{-0.08}$	$131^{+6}_{-16}$	–	639 / 581
<b>198.752 s &lt; <math>t_0</math> &lt; 228.448 s = -5.248 s &lt; <math>t_{0,\text{GBM}}</math> &lt; 24.448 s</b>							
GBM	Band	–	–	$1.51 \pm 0.16$	$70 \pm 17$	$2.5 \pm 0.7$	564 / 436
XRT-BAT-GBM	db-pl	$1.14 \pm 0.03$	–	$1.81 \pm 0.05$	$132^{+49}_{-16}$	–	643 / 674

Notes: Spectral fit results for *Swift*/BAT and *Fermi*/GBM. BAT/GBM combines BAT and GBM data, XRT-BAT-GBM further uses the XRT data. In these cases the fit was performed using a double broken power-law (db-pl), with the corresponding break energies in units of keV. Note that in this notation  $\tilde{\beta}$  is the photon index and the observed photon flux is proportional to  $E^{-\tilde{\beta}}$  ( $\tilde{\beta} = \beta + 1$ ). Band stands for Band function (Sect. 2.1).

These data sets cover both prompt and afterglow phase. In the following, I will concentrate on early data obtained during prompt phase only (part of the UVOT and ROTSE data sets), while in Chapter 4 I will discuss the late-time observations.

## 3.2 The prompt phase

In this section I discuss first the high energy observations and I will interpret them in the context of the standard afterglow theory (Sect. 2.2). Afterwards, I will include optical observations and show that, during the prompt phase of GRB 080928, optical to gamma-ray emission had a common origin, namely synchrotron emission from an ensemble of hot electrons. GRB 080928 is also one of the few cases where the optical, X-ray and gamma-ray prompt emission is time-resolved in more than one epoch, and it is the first case that can be interpreted within the LAE model (Sect. 2.3.3). Moreover, I will show that gamma and optical data independently allow me to constrain the initial Lorentz factor of the relativistic outflow.

### 3.2.1 From gamma-rays to X-rays

The prompt gamma-ray emission is dominated by a strong peak starting at 170 s, which reached its maximum at 204 s and was detected by GBM and BAT and also seen by XRT. In addition, XRT also detected a second weaker peak at 357 s. The first peak was also detected by UVOT in the white band.

During the first peak of the prompt emission (in the interval  $t_0 - 23.5 \text{ s} < t < t_0 + 16.5 \text{ s}$ ) it is possible to fit only a simple power-law to the BAT data with a photon index  $1.67 \pm 0.34$ . It is also possible to fit the BAT-GBM data during the second peak ( $t_0 + 46.5 \text{ s} < t < t_0 + 121 \text{ s}$ ) and the XRT-BAT-GBM data during the main peak ( $t_0 + 198.75 \text{ s} < t < t_0 + 228.4 \text{ s}$ ). In (Rossi et al. 2011b), for both peaks we found a peak energy of  $\approx 130 \text{ keV}$ , though we could not constrain the index above the peak (Table 3.1). No spectral analysis was possible for the precursor.

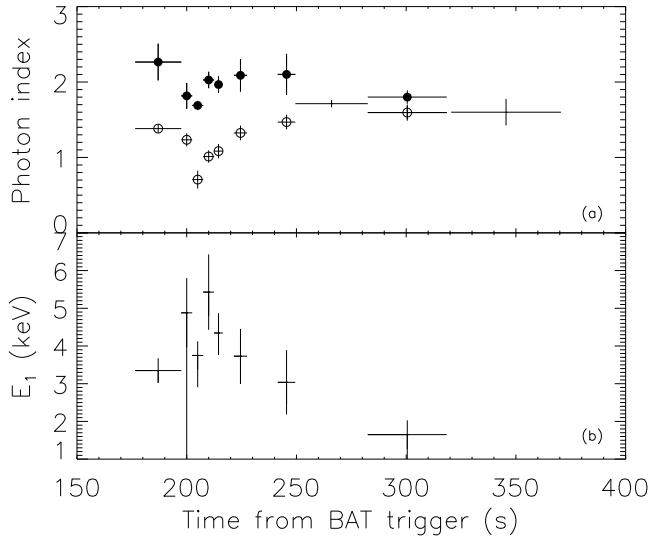


Figure 3.3: Spectral parameters of the prompt emission using the time-resolved XRT-BAT-GBM data. (a): The evolution of the photon index from fits to BAT-GBM and XRT data. Open circles show the low-energy index  $\beta_1$  below the break energy  $E_1$  of a single broken power-law and the filled circles represent the high-energy index  $\beta_2$  above  $E_1$ . Points with no plot symbols (error bars only) are the best-fit results using a simple power-law only. (b): The low-energy break energy,  $E_1$ , from fits to the BAT and XRT data. During the flare at 208 s spectral evolution is seen, similar to what was also detected in other afterglows (e.g., Falcone et al. 2007).

For the GBM-only data, two different empirical models were applied to fit the spectra: a simple power-law and a Band function (Band et al. 1993), which smoothly connects two power-laws. The burst was faint for GBM, especially at energies above 150 keV. Thus, the more complex model of a Band function could not be constrained sufficiently and the simple power-law is preferred for both time intervals.

Table 3.1 summarizes the fits of the SED for the XRT-BAT-GBM data for two time intervals around the main peak in the gamma-ray light curve. In particular, it was performed a spectral fit for the peak centered around 204 s. For joint fits with BAT and XRT, it was used an absorbed power-law with the Galactic and the GRB host column densities fixed to the values found in Sect. 3.1.2.

Figure 3.3 shows the time evolution of the SED in the BAT band and the joint BAT-XRT band during the first 400 s after the BAT trigger. For the three early peaks in the BAT light curve (Fig. 3.1) the error bars are too large to indicate any spectral evolution. During the main gamma-ray peak at 204 s, however, there is evidence for a spectral softening when the peak is developing and a spectral hardening after the peak. After the light curve peak, the situation is reversed. This behavior is similar to what has been found for GRB 060714 (Krimm et al. 2007). Also, the power-law indexes as well as the break energy are consistent with the corresponding values found in gamma-ray flares (Krimm et al. 2007).

In the cases where a broken power-law model is the best fit the break energy as well as the high-energy index and the low-energy index are well constrained. So, essentially BAT is fitting the high-energy index, XRT is fitting the low-energy index and the joint fit fits an average index, becoming dominated by the low-energy emission where the BAT statistics are poor. Remarkably, even though the break energy is always between 1 and 5 keV, i.e. well below the BAT and GBM window, the prompt emission flare is still very bright in BAT and GBM. Moreover, it is 10 times brighter than the peak on which BAT triggered.

### 3.2.2 From gamma-rays to optical bands

GRB 080928 is one of those exceptional cases where optical and X-ray data could be obtained while the source was still being detected in the gamma-ray band (Fig. 3.4). The analysis of the joint UVOT-XRT-BAT-GBM SED allowed me to follow the evolution of the prompt emission during all the main

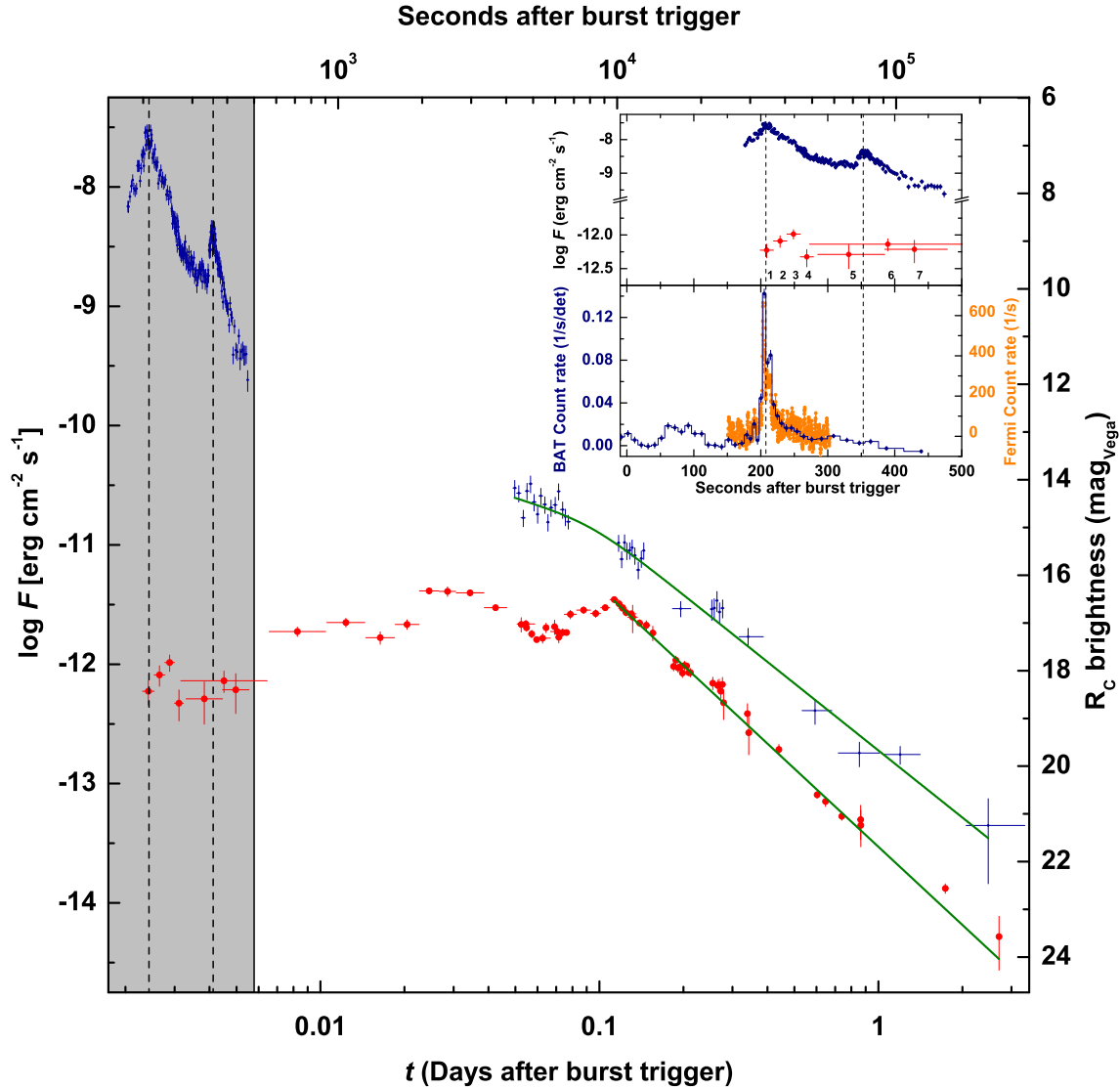


Figure 3.4: **Main figure:** Temporal evolution of the optical (composite light curve with all data shifted to the  $R_c$  band) and X-ray afterglow (0.3 to 10 keV) of GRB 080928 (optical: red circles, X-ray: blue error bars). The upper limits are not shown here to avoid confusion. In this Chapter I focus on the early phase (highlighted in gray) defined as the interval covering the gamma-ray observations. In the optical bands, this time-window is dominated by UVOT observations, with just a single data point (the 6th) from ROTSE-IIIa. In the main figure is also presented the late-time phase after 500 seconds (white background), when no gamma-ray emission was detected anymore. In Chapter 4, and in particular in Section 4.2, I will discuss this evolutionary phase. Between  $\sim 500$  and  $\sim 10^4$  seconds ( $\sim 0.006$ -0.15 days), the optical observations are covered by ROTSE and UVOT data. Unfortunately this interval is not entirely covered by Swift/XRT observations, because of observational constraints. This interval is peculiar for the bumpy optical light curve, which I will discuss in the next chapter. After  $\sim 10^4$  s ( $\sim 0.15$  days), the optical/NIR and X-ray afterglow show a constant fading, first covered by UVOT and ROTSE-IIIa, then by GROND. The data are complemented by VLT and Watcher optical observations. The green curves represent the best fit of the late-time data. **Zoom-in:** The zoom-in shows the early phase where optical/NIR and X-ray data are compared with the BAT-GBM prompt emission. In the upper panel, numbers from 1 to 7 label the optical observations during the early phase. The dashed vertical lines, both in the main figure and in the zoom-in, indicate the peak times of the two X-ray flares. **Note:** This figure appeared as a cover page of *Astron. & Astroph.*, 529, part II, where Rossi et al. (2011b) was published.

flaring activity observed between 199 and 557 seconds after the trigger from 1 eV to 150 keV.

The prompt gamma-ray emission detected by BAT and GBM is dominated by the strong peak at 204 s. Possibly physically related to that is a strong peak in the X-ray emission seen by XRT about 4 seconds later at 208 s, which was followed by a less intense X-ray peak at 357 s. The latter has no obvious counterpart in the gamma-ray emission. The optical light curve monitored by UVOT shows a first peak at  $(249 \pm 10)$  s, i.e. 45 seconds after the main peak of the prompt emission and 41 s after the main peak in the X-ray flux.

In order to gain deeper insight into the early emission properties and on their time evolution, I included the optical data and constructed the SED from the optical to the gamma-ray band for six time intervals defined by the first six optical detections by UVOT, starting at 199 s and finishing 479 s after the trigger (Table 3.2, Fig. 3.4). In doing so, I excluded the 6th optical measurement (ROTSE-IIIa) shown in Table 3.2 because it covers a rather big time interval.

During the first five time intervals BAT as well as GBM were still detecting gamma-ray emission (the main gamma-ray peak occurred when UVOT was already observing), while during the last two time intervals the fluence in the gamma-ray band was too low to constrain the spectral properties. Figure 3.5 shows the fit to the data from about 1 eV to up to 150 keV. In the following, I first focus on SED #1. Here, I fit the data with a broken power-law with the X-ray data corrected for Galactic and GRB host absorption (see Sect. 4.2.1) and the optical data corrected for the Galactic and GRB host extinction.

For the time interval #1 (Table 3.2) the first optical UVOT detection (Table A.2) has been combined with the XRT and the BAT-GBM detection from 202.8 s to 206.9 s. A sharp break is clearly visible at an energy around 5 keV (in case of SED #1 the soft X-ray data,  $E < 1$  keV, shows too much scatter and therefore could not be used for the analysis). Assuming that SED #1 represents the spectral energy distribution of synchrotron light of a single radiating component from about 1 eV to 150 keV (see also Shen & Zhang 2009), I fitted the data with a broken power-law while fixing the low-energy index to its theoretically expected value  $\beta = -1/3$  (i.e., rising with energy). The slope of the high-energy index is then found to be  $\beta = 0.72 \pm 0.06$  ( $\chi^2/\text{d.o.f.} = 66.8/75$ ) with a spectral break at an energy of  $4.30 \pm 0.45$  keV. The corresponding UVOT data point lies  $1\sigma$  below the best fit (Fig. 3.5).

If one identifies the break in the SED as the position of the minimum injection frequency  $\nu_m$  of an ensemble of relativistic electrons in the slow cooling regime ( $\nu_m < \nu_c$ , with  $\nu_c$  being the cooling frequency), then we expect a low-energy spectral index of  $-1/3$  and a high-energy spectral index of  $(p-1)/2$ , where  $p$  is the power-law index of the electron distribution function ( $N(\gamma)d\gamma \propto \gamma^{-p}d\gamma$ ). The measured low-energy spectral index ( $-0.39 \pm 0.06$ ) is basically in agreement with the theoretically expected value. The measured high-energy spectral index is  $0.72 \pm 0.06$ , leading to  $p = 2.44 \pm 0.12$ , which is a reasonable value for relativistic shocks, both theoretically (Achterberg et al. 2001; Kirk et al. 2000) as well as observationally (e.g., Kann et al. 2006; Starling et al. 2008; Curran et al. 2010).

On the other hand, if the break is the cooling frequency in the fast cooling regime ( $\nu_c < \nu_m$ ), then one expects a low-energy spectral index of  $-1/3$  and a high-energy spectral index of 0.5. Within errors the latter disagrees with the observations, the spectral slope is  $0.72 \pm 0.06$  and the discrepancy is  $3.7\sigma$ . However, it is quite possible that the snapshot of the high-energy part of the SED observed in the time window is the average of a rapidly evolving SED that accompanied the rapidly evolving light curve.

Making the step to the SEDs #2 to #4, one is faced with the problem that the break seen in SED #1 is not detectable anymore, most likely because the peak energy  $E_p$  has moved to lower energies. However, given that a large flare in the X-ray light curve is evident, part of the data allows

for investigating if the evolution of the SED is compatible with large-angle emission.

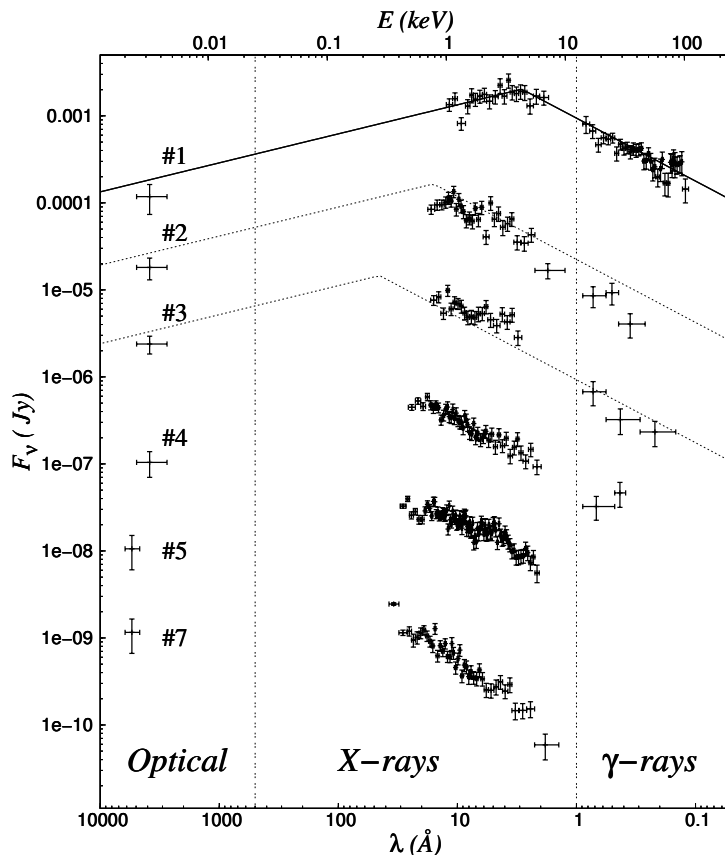


Figure 3.5: The spectral energy distribution of the optical to gamma-ray early emission, when the first three optical data points were obtained by Swift/UVOT white filters. The corresponding time intervals are listed in Table 3.2. The fluxes of the curves #2, 3, 4, 5, and 7 have been multiplied for clarity by  $10^{-1}$ ,  $10^{-2}$ ,  $10^{-3}$ ,  $10^{-4}$ , and  $10^{-5}$ , respectively. The fits for #2, 3 were obtained by fixing the high-energy slope to the corresponding slope obtained for SED #1, the low-energy slope to  $-1/3$ , and by matching the expected break energy following a non-standard LAE model (Sect. 3.2.3).

### 3.2.3 Evidence for large-angle emission from X-rays to the optical band

In Section 2.3.3 I have reviewed the large-angle emission model, which is used to interpret the flares observed in X-ray afterglow light curves. In particular, this model leads to the result that after the peak the flux should decrease as  $t^{-(2+\beta)}$ , where  $\beta$  is the spectral index.

Figure 3.4 shows that between epoch #3 and #4 the optical light curve is falling, while thereafter it remains constant (within errors). The figure also shows that after the 5th optical epoch the X-ray light curve has a 2nd flare. This makes it likely that the nature of the main emission component changed after the 3rd time interval. Having this in mind, I included only the first three data points in Table 3.2 in our analysis. In doing so, I fixed the value for the spectral slopes to the one for SED #1, i.e.,  $\beta = -1/3$  for the low-energy part as given by synchrotron theory and 0.72 for the high-energy part as it follows from the fit.

Within the LAE model, from assumption (1) that the electron population is the same at all angles  $\theta$  (Sect. 2.3.3), it follows that the peak energy should decrease as  $t^{-1}$ . In the  $\nu^{1/3}$  part of the spectrum, the optical LAE should then decay as  $t^{-5/3}$ . However, the data show that the optical flux is rising between epoch 1 and 3 (Fig. 3.4).

If the entire emission between the 1st and the 2nd X-ray flare is of LAE origin, then the fact that the optical flux increases at epochs 2 and 3 (instead of decreasing as  $t^{-5/3}$ ), while the X-ray flux decreases implies that the aforementioned assumption (1) of the LAE model is incorrect. In particular, it implies that  $E_p$  for the electrons at larger angles (corresponding to epoch 3) is lower than at smaller

Table 3.2: Results of the joint optical to gamma-ray spectral fit ( $\sim 1$  eV to  $\sim 150$  keV).

#	Optical		XRT-BAT-GBM		$E_{\text{break}}$ (keV)
	mean time	interval	mean time	interval	
1	208.7	199.0 - 219.0	204.8	202.8 - 206.9	4.30(45)
2	228.7	219.0 - 238.0	231.0	227.5 - 234.5	0.78(39)
3	248.7	239.0 - 258.0	245.5	241.5 - 249.5	0.28(18)
4	268.7	259.0 - 278.7	268.7	259.0 - 278.7	–
5	331.3	285.0 - 385.0	344.4	318.5 - 372.5	–
6	389.6	272.7 - 556.7	361.0	272.7 - 477.9	–
7	429.3	385.0 - 478.7	428.9	385.0 - 477.9	–

Notes: Here are shown seven time intervals (given in units of seconds) defined by the first seven optical data points (Fig. 3.4) during the early emission component of GRB 080928 (Fig. 3.5). The 6th optical measurement (ROTSE-IIIa) covers a rather big time interval, therefore it was not used for the study of the time evolution of the break energy. The 2nd and the 4th column give the logarithmic mean time. The last column gives the break energy including its error, computed inside the non-standard LAE model predictions, for epochs 1 to 3 assuming  $t_p = 185.9$  s. For further details see Sect. 3.2.2.

angles (corresponding to epoch 1), at the same lab-frame time. In other words, the rising optical flux is compatible with the LAE interpretation only if  $E_p$  decreases with observer time faster than  $t^{-1}$ .

Therefore, following a concept developed by A. Panaitescu (private communication), I applied a non-standard LAE model. Within this model, the local synchrotron peak flux  $F_p$  as well as the peak energy  $E_p$  depend on the viewing angle  $\theta$ . Furthermore, an observer located at an angle  $\theta$  relative to us would observe a peak flux and peak energy evolving as  $F_p(\theta) \propto \theta^{-2a}$  and  $E_p \propto \theta^{-2b}$ , respectively. The evolution of the measured peak flux and peak energy after relativistic boosting is then  $F_p \propto (t - t_p)^{-2-a}$  and  $E_p \propto (t - t_p)^{-1-b}$ , respectively, where  $t_p$  is the unknown zero-point. The resulting LAE X-ray light-curve above the peak energy  $E_p$  in the  $\nu^{-\beta}$  part of the SED is then

$$F_X \propto (t - t_p)^{-2-\beta-a-b\beta}, \quad (3.2)$$

while the LAE optical light-curve (below the peak energy, in the  $\nu^{1/3}$  part of the SED) is described by

$$F_{\text{opt}} \propto (t - t_p)^{-5/3-a+b/3}. \quad (3.3)$$

In order to check this model, the peak energy was fixed to  $E_p = 4.3$  keV at epoch 1 and the spectral slope was fixed to  $\beta = 0.72$  (Table 3.2). I fitted the X-ray and optical data between 205 and 250 s after the trigger, i.e., between epochs 1 and 3, when the optical light curve was rising (Fig. 3.6). This gives  $t_p = (185.9 \pm 7.5)$  s,  $a = -1.7 \pm 0.2$ , and  $b = 1.7 \pm 0.5$ , where the latter parameters follow via Eq. 3.3 from the derived decay slopes. Figure 3.5 shows how the fit is able to follow the SED during epochs #2 and #3. The fit puts the time zero-point at the beginning of the main emission of the proper GRB. This finding is qualitatively in line with other studies of other X-ray afterglows (e.g. Liang et al. 2006).

While the fit is satisfactory, one might wonder why at epoch 1 the low-energy part of the SED touches the optical data point only within  $1 \sigma$ . However, there is actually much more uncertainty in the extinction-corrected UVOT flux than it is simply given by the measurement error of 0.25 mag

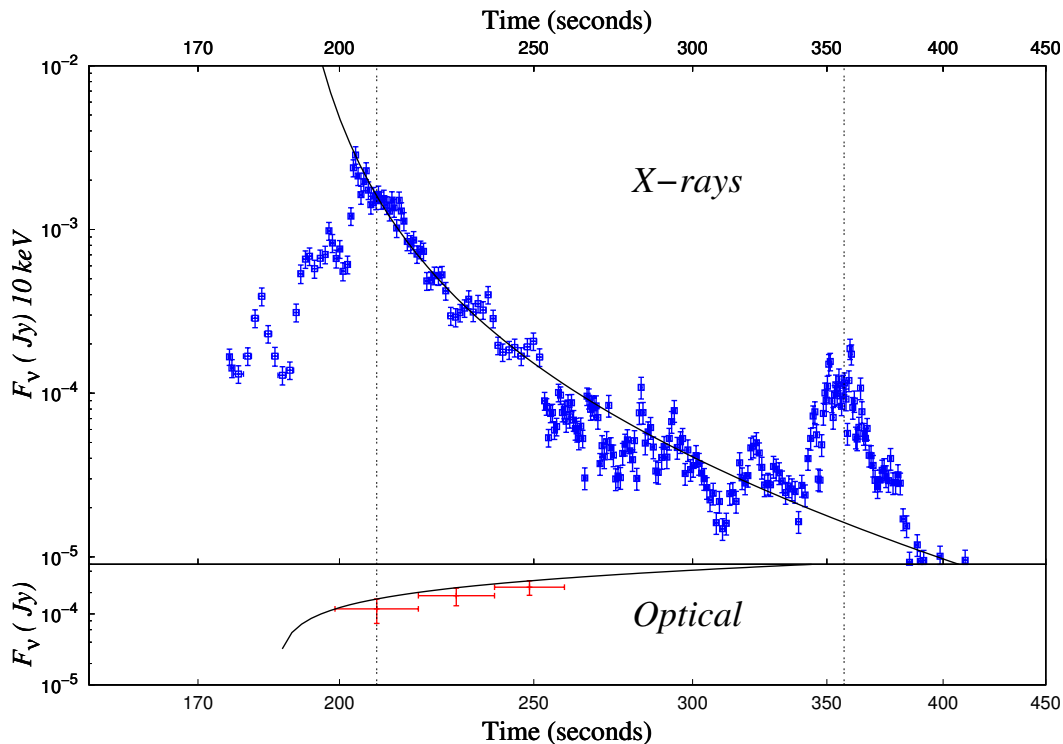


Figure 3.6: Fit of the X-ray and optical light curves in order to constrain the parameters  $a, b$  in the modified LAE model (Eqs. 3.2 and 3.3). Data after 250 seconds, i.e. epoch 3, are not considered here because the nature of the main emission component might have changed after the 3rd time interval (see text for details). Vertical lines highlight the position of both X-ray peaks. **Top:** 10 keV X-ray light curve between 170 and 500 s after the trigger, which includes the time interval between epochs 1 and 3, i.e. between 205 and 250 s after the trigger (source [www.swift.ac.uk/burst\\_analyser](http://www.swift.ac.uk/burst_analyser); Evans et al. 2010b). The data (blue crosses) are modeled according to the equation 3.2. **Bottom:** Fit of the optical data between epochs 1 and 3. The data (red crosses) are modeled following the equation 3.3. By fitting the optical data, I considered that in the first epoch the optical flux density as derived from the fit is slightly brighter than the observed flux density and, therefore, I applied the same shift to all epochs.

(white filter; Roming et al. 2009; see Table A.2). The biggest uncertainty<sup>7</sup> comes from the correction for extinction in the GRB host galaxy. Assuming a Milky Way extinction law, a ratio of total-to-selective extinction of  $R_V=3.08$  (i.e. the standard value), and  $A_V^{\text{host}} = 0.12$  mag (Table 4.4) gives a correction for host extinction in the UVOT white filter of 0.52 mag (including the cosmological  $k$ -correction and the correct CCD sensitivity characteristics in case of UVOT/white filter observations<sup>8</sup>). However,  $R_V$  in the star-forming region where the GRB went off is not exactly known. Its  $1\sigma$  error might well be in the order of 50%. Finally, the host extinction I have derived here (Table 4.4) is based on data taken 20 ks after the burst. It is an open question if the host extinction was the same amount already 200 s after the onset of the burst. In other words, the fact the UVOT white filter measurement does not exactly correspond to the low-energy SED extrapolated from the X-ray data should not be over interpreted. However, it naturally affects the test of the LAE model since it introduces additional uncertainties.

Liang et al. (2006) found that the time zero-points of the prompt emission tails and the tails of the

<sup>7</sup>A smaller uncertainty comes from the Galactic reddening derived from Schlegel et al. (1998), which percentage error can be large for low reddening values.

<sup>8</sup><http://heasarc.gsfc.nasa.gov/docs/heasarc/caldb/data/swift/uvota/>

flares are in agreement within the expectation of the internal shock models, indicating that each X-ray flare forms a distinct episode of the central engine activity. However, in their modeling of the light curves there is no dependence from the viewing angle  $\theta$ , i.e. the angle parameters  $a$  and  $b$  (Eqs. 3.2 and 3.3) are set to zero, as in the original LAE model. This is due to the fact that optical light curves are not included in the analysis, because often no optical data is available for the time when the X-ray flare is active. Therefore, it is always possible to find an agreement with the original LAE model, without requiring a dependence from the viewing angle  $\theta$ . In this respect, the modified LAE model as suggested by A. Panaitescu, and for the first time applied here, enables a better understanding of the evolution of X-ray flares.

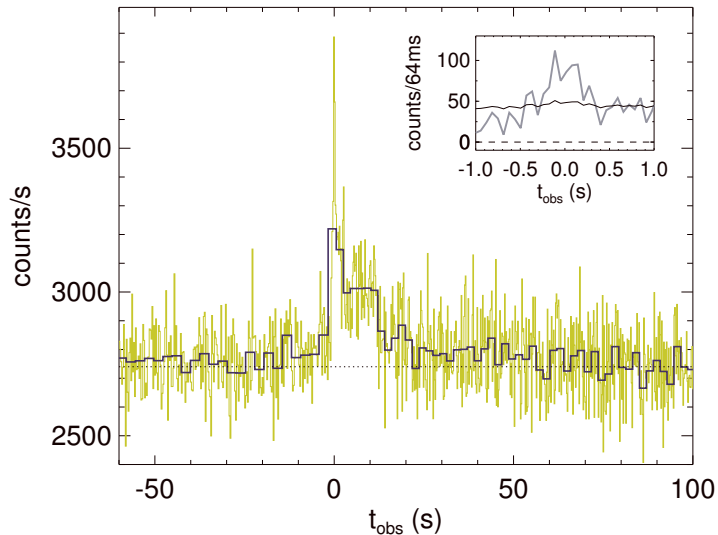


Figure 3.7: *Detailed Fermi/GBM light curve combined with 2 s resolution (black line) and 0.256 s resolution (yellow line). A zoom in the 64 ms binned, background subtracted light curve around the peak is shown in the inset. Variability on time scales of  $\sim 128$  ms is detected at  $3\sigma$  (solid grey line) above the background plus shot noise fluctuations. Note that in this figure the time zeropoint is the Fermi/GBM trigger time  $t_{0,\text{GBM}}$  (Eq. 3.1).*

### 3.2.4 The isotropic equivalent energy and gamma-ray peak luminosity

Given the results of the spectral fit in the high-energy domain one can estimate the isotropic-equivalent energy released during the prompt emission phase. Fitting the BAT and GBM data for the time of the gamma-ray precursor between 46.5 s and 121 s gives an isotropic equivalent energy of  $E_{\text{iso}}$  (1-10000 keV) =  $(0.40 \pm 0.03) \times 10^{52}$  erg, while a fit of the combined XRT-BAT-GBM data during the main peak emission between  $t_0 + 198.75$  s and  $t_0 + 228.4$  s leads to  $E_{\text{iso}} = (0.88 \pm 0.025) \times 10^{52}$  erg. Fixing the peak energy for the value found in the second interval ( $132_{-16}^{+49}$  keV; Table 3.1) one finds for the whole burst from  $t_0 - 23.5$  s to  $t_0 + 372.5$  s an isotropic energy of  $E_{\text{iso}} = (1.44 \pm 0.92) \times 10^{52}$  erg.

### 3.2.5 Constraints on the initial Lorentz factor of the outflow

As I have reviewed in Section 2.2.1, the observation of non-thermal gamma-rays in combination with the observed small variability timescale of the bursts implies that a GRB fireball is expanding relativistically towards the observer. While Section 2.2.1 only contained a qualitative estimate of the Lorentz factor obtained in this way, it can in fact be used to derive for individual bursts constraints on the initial Lorentz factor of the ejecta,  $\Gamma_0$ . This procedure can also be performed for GRB 080928, but the lack of a high-energy detection of the burst above 150 keV limits the accuracy of this approach.

Following Lithwick & Sari (2001), a lower limit on  $\Gamma_0$  due to Compton scattering of photons by pair-created electrons and positrons is given by

$$\Gamma_0 > \hat{\tau}^{1/(\beta+3)} (1+z)^{(\beta-1)/(\beta+3)}, \text{ with} \quad (3.4)$$



$$\hat{\tau} = \frac{\sigma d_L^2 (m_e c^2)^{1-\tilde{\beta}} f}{c^2 \delta t (\tilde{\beta} - 1)}. \quad (3.5)$$

Here,  $\sigma$  is the interaction cross section,  $d_L$  is the luminosity distance (see Sect. 3.1.1),  $\tilde{\beta}$  is the high-energy photon index,  $f$  is the normalization constant of the observed photon flux defined as  $N(E) = f E^{-\tilde{\beta}}$ , and  $\delta t$  is the smallest detectable variability time scale during the prompt emission. The parameters  $m_e$  and  $c$  are the electron mass and the velocity of light, respectively.

In the case of GRB 080928 neither GBM nor BAT detected photons of the burst at energies beyond 150 keV. Therefore, in order to apply the procedure of Lithwick & Sari (2001) one has to assume that the photon spectrum did extend up to energies  $\Gamma_0 m_e c^2$ . Thus, one has to extrapolate into the high-energy domain, assuming a power-law slope with the observed  $\tilde{\beta}$ . The GBM data from the time interval  $198.752 \text{ s} < t_0 < 228.448 \text{ s} = -5.248 \text{ s} < t_{0,\text{GBM}} < 24.448 \text{ s}$  can be fitted with a *Band* function with a break at  $70 \pm 17 \text{ keV}$ , a high energy index of  $2.5 \pm 0.7$  and photon flux in the 0.3 to 1 MeV band of  $0.023 \text{ ph/cm}^2/\text{s}$  (Table 3.1; see also Rossi et al. 2011b). So, I use here the GBM data for further analysis (Fig. 3.7).

The shortest time scale on which variability in the GBM data can be detected with high significance is  $\delta t = 128 \text{ ms}$  (see the inset of Fig. 3.1). Figure 3.8 shows the results obtained for the lower limit of the initial Lorentz factor of the outflow via Eqs. (1) and (2) based on Lithwick & Sari 2001 (their eqs. 4 and 8, and including a correction of  $(180/11)^{1/(6+2\tilde{\beta})}$  as explained by these authors). Basically, the uncertainty in  $\Gamma_0$  is dominated by the uncertainty of  $\tilde{\beta}$ . The potential parameter space found for  $\Gamma_0$  in this way (100...350) is in qualitative agreement with the corresponding values found for other bursts (Lithwick & Sari 2001; Molinari et al. 2007; Ferrero et al. 2009; Oates et al. 2009; Greiner et al. 2009a).

In principle, also the observed afterglow light curve (Fig. 3.4) can be used to set constraints on the initial Lorentz factor. Assuming that the peak time  $t_p$  of the optical light curve signals the start of the fireball deceleration phase,  $\Gamma_0$  can be deduced. Following Molinari et al. (2007) it is

$$\Gamma_0 = 2 \times \left( \frac{3 E_{\text{iso}} (1+z)^3}{32\pi n m_p c^5 \eta_\gamma t_p^3} \right)^{1/8}. \quad (3.6)$$

Using  $t_p = 1000 \text{ s}$  (Fig. 3.4), an isotropic equivalent energy of  $E_{\text{iso}} = 1.44 \pm 0.92 \times 10^{52} \text{ erg}$  (Sect. 3.2.4), a radiation efficiency  $\eta_\gamma$ , and a circumburst gas density  $n$  in units of  $\text{cm}^{-3}$ , it follows  $\Gamma_0 = 123_{-15}^{+7} (\eta_\gamma n)^{-1/8}$ , in qualitative agreement with the previous estimate based on the gamma-ray data. Note that this value scales  $\propto t_p^{-3/8}$ . A later peak time would thus imply a smaller  $\Gamma_0$  and vice versa. In principle, a comparison with the lower limit on  $\Gamma_0$  obtained via the constraint derived before based on the gamma-ray data should make it possible to constrain the product  $(\eta_\gamma n)^{-1/8}$ . However, given the larger error bars a reliable constraint on this product cannot be deduced.

### 3.3 Summary of the GRB 080928 prompt emission

GRB 080928 ( $z=1.692$ ) was a long burst that lasted for about 400 seconds. It was detected by *Swift*/BAT and *Fermi*/GBM and was followed up by *Swift*/XRT and *Swift*/UVOT. Ground-based follow-up observations were performed by the robotic ROTSE-IIIa telescope in Australia and the multi-channel imager GROND on La Silla. Its early X-ray light curve was dominated by two bright peaks that occurred within the first 400 seconds after the BAT trigger. The first peak was delayed by some seconds from the gamma-ray peak emission, while the second peak had no obvious counterpart

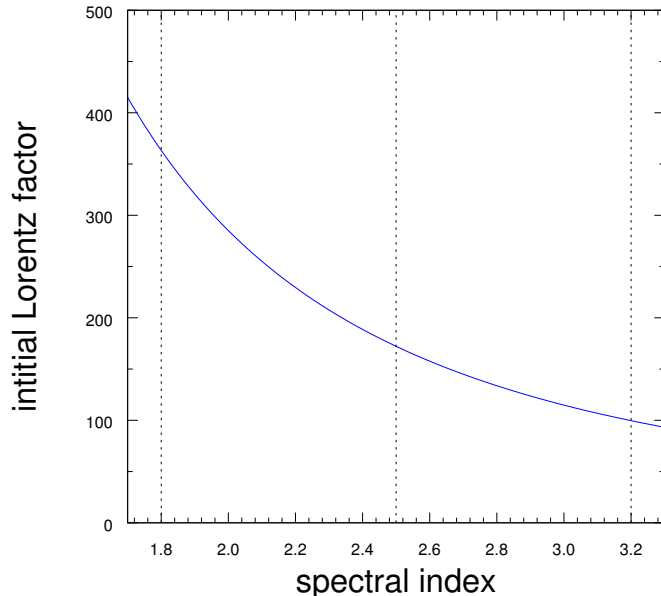


Figure 3.8: *The deduced value for the lower limit of the initial Lorentz factor  $\Gamma_0$  based on the Fermi/GBM data as a function of the photon index  $\tilde{\beta}$  according to Eq. (3.4) and using a photon flux of  $F_{ph}$  (0.3-1 MeV) = 0.023 ph/cm<sup>2</sup>/s in a 30 sec time interval around the GRB light curve peak. The vertical broken lines give the corresponding values and their  $1\sigma$  errors for the measured photon index of  $2.5 \pm 0.7$ .*

in the high-energy band. It occurred when the gamma-ray emission had already faded away. However, optical emission was detected while the burster was still active in the gamma-ray band. This allowed me in Rossi et al. (2011b) to obtain a detailed SED of the prompt phase from 1 eV to 150 keV, from optical to gamma-rays. The SED at early times clearly showed a well-sampled sharp break at 4 keV and the slopes of the SED on both sides of this peak strongly favored the conclusion that during the prompt phase the main emission mechanism was synchrotron radiation. To the best of my knowledge, this allowed us to characterize for the first time the continuum spectra of the prompt GRB emission in a frequency interval spanning from optical to gamma-rays through X-rays.

In addition, the optical and X-ray data confirmed that the radiation following the first strong peak seen in the X-ray light curve comes from large-angle emission. In particular, the observed rising optical emission contemporaneous to the decaying X-ray tail called for an alternative approach suggested by A. Panaitescu, where one of the assumptions made in the LAE model was relaxed, namely the assumption that the electron population is the same at all angles  $\theta$ . This implied the use of a generalized version of the LAE model, for which the flux and the energy of the peak are evolving as  $F_p \propto \theta^{-2-a}$  and  $E_p \propto \theta^{-1-b}$ , with  $a = -1.2 \pm 0.2$  and  $b = 1.1 \pm 0.5$ . It is important to note that the inclusion of optical data in the analysis provided a better understanding of the flare activity related to central engine, provided that it is possible to conclude that optical and X-ray data have a common origin. Indeed, only the inclusion of optical data revealed that the light curve parameters might depend from the viewing angle. Therefore, future studies of X-ray flares should include optical observations, when possible.

In conclusion, GRB 080928 has shown the fundamental importance of both timely response and a joint analysis of gamma-ray to optical data in order to shed more light on the details of the GRB physics. Indeed, in addition to the findings I have just summarized, the gamma-ray and optical observations allowed me to constrain independently the initial Lorentz factor  $\Gamma_0$  of the ejecta. In the next chapter I analyze the late time X-rays and optical/NIR light curve of GRB 080928 together with another burst (GRB 080514B), showing in both cases once more that the combination of gamma-ray, X-ray, and optical/NIR data is of fundamental importance for an understanding the GRB phenomenon.

## Chapter 4

# Afterglow studies from near-infrared to X-rays

In this chapter I will investigate the afterglows of GRB 080514B and GRB 080928, which have been published in Rossi et al. (2008b) and Rossi et al. (2011b) respectively. The first event was discovered by the AGILE satellite and, was at that time, was the first burst detected at energies above 30 MeV with a detected optical afterglow. This raised the question if the physical properties of its afterglow and host galaxy do stand out from the corresponding properties of the main GRB population which is not seen at such high energies. However, spectroscopic observations of the afterglow, and therefore measurements of the redshift, were unfortunately missing. In this work I estimate the photometric redshift of the afterglow, important for quantifying the energetics of the burst.

While GRB 080928 is also important for the simultaneous optical, X-rays and gamma-rays observations of the prompt emission, which I have discussed in the previous chapter, here I present its peculiar optical/NIR and X-rays light curve, characterized by several bumps in the optical. While this behavior was observed also for other bursts, still a clear and final interpretation is missing. In the following, I will also discuss the search for the host galaxy of GRB 080928 and the characterization of the field.

### 4.1 Follow-up observations of the AGILE high-energy burst GRB 080514B

The discovery of GRB 080514B by the Italian *AGILE* gamma-ray satellite (Tavani et al. 2008) on May 14, 2008 at 09:55:56 UT (Rapisarda et al. 2008) was of particular interest, because at that time no burst was detected at energies above 30 MeV has had an observed afterglow. *AGILE* carries three instruments covering the energy range from 20 keV to 50 GeV and detected GRB 080514B at energies well above 30 MeV (Giuliani et al. 2008a,b). GRB 080514B was a bright, multi-spiked event with a duration ( $T_{90}$ ) of 5.6 s, which implies that it is a long burst.

The burst was also observed by *Mars Odyssey*, operating as part of the Interplanetary Network (IPN; Hurley et al. 2006), making it possible to constrain the size of the error box to about 100 arcmin<sup>2</sup> (Rapisarda et al. 2008). This localization led to the discovery of its X-ray afterglow by the *Swift* satellite at coordinates R.A., Dec. (J2000) = 21<sup>h</sup>31<sup>m</sup>22<sup>s</sup>.62, +00°42′30″.3 with an uncertainty of 1′.6 (radius, 90% confidence) at 0.43 days after the trigger (Page et al. 2008). Before the announcement of the X-ray afterglow position, however, the optical afterglow had already been discovered by observing

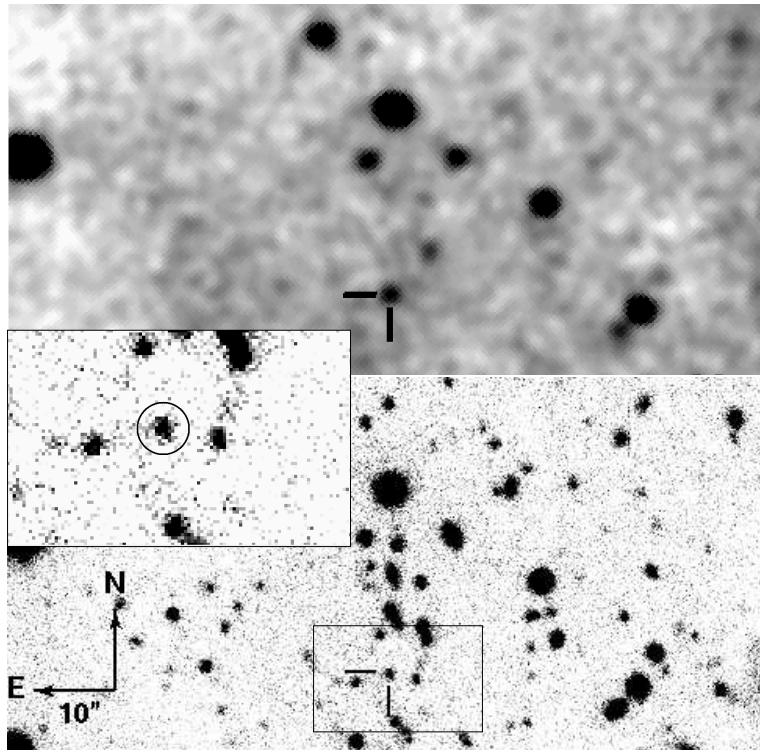


Figure 4.1: **Top:** IAC80 I-band discovery image of the optical afterglow of GRB 080514B. The afterglow is highlighted. **Bottom:** Keck R-band image obtained 24 days after the trigger. The underlying host galaxy is clearly detected. The zoom inset of the Keck image shows the host galaxy.

the complete IPN error box (Postigo et al. 2008a,b; Fig. 4.1). In the following, I present our ground-based follow-up observations of the afterglow of GRB 080514B, supplemented by *Swift*/UVOT and XRT data, starting 0.43 days after the trigger.

#### 4.1.1 Data gathering: optical/NIR and X-ray observations

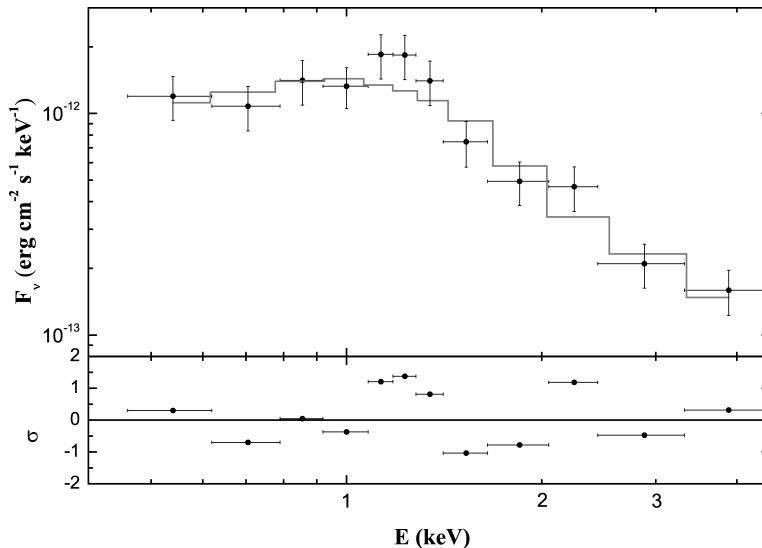
*Swift*XRT data were obtained from the *Swift* data archive and the light curve from the *Swift* light curve repository (Evans et al. 2007). To reduce the data, the software package HeaSoft 6.4 was used<sup>1</sup> with the calibration file version v011. Data analysis was performed following the procedures described in Nousek et al. (2006). Spectral analysis was completed with the software package Xspec v12, using the elemental abundance templates of the Galactic interstellar medium given by Wilms et al. (2000).

*Swift* UVOT observed the field in the broad-band  $v$ ,  $b$ ,  $u$ ,  $uvw1$ ,  $uvm2$ , and  $uvw2$  filters (Holland 2008; for the filter definitions, see Poole et al. 2008). A second set of observations were obtained in the *white* band about 2.5 days after the trigger.

Ground-based follow-up observations were performed using the 16'' Watcher telescope in South Africa, the IAC80 telescope at Observatorio del Teide, the MPG/ESO 2.2m telescope equipped with GROND (Sect. 1.5), the Nordic Optical Telescope, the Kitt Peak 4m telescope, the Gemini North 8m and the Keck 10m telescope. The data were analyzed using standard PSF photometry, while aperture photometry was applied only for the analysis of the host galaxy (Table B.1). No spectrum of the optical afterglow could be obtained.

<sup>1</sup><http://heasarc.gsfc.nasa.gov/docs/software/lheasoft>

Figure 4.2: The observed X-ray spectrum of the afterglow of GRB 080514B obtained in photon counting mode at 0.5 days (source [www.swift.ac.uk/xrt\\_spectra](http://www.swift.ac.uk/xrt_spectra); Evans et al. 2009). The spectrum was fitted with an absorbed power-law and a gas column density of  $1.4 \times 10^{21} \text{ cm}^{-2}$  (Sect. 3.1). The lower panel shows the residuals of the fit computed to be the difference between the observed data and the best-fit model, normalized to the error in the observed data.



#### 4.1.2 The Optical/NIR and X-ray afterglow: detection and light curve

Since GRB 080514B is the first burst having both detected high energy emission and a known afterglow, two points are of particular interest in two points: (a) Do the afterglow properties separate this burst from the long burst sample? (b) What is its redshift? While the former question is related to whether burst properties correlate with afterglow features, the latter is critical in quantifying the energetics of the burst.

**X-ray data** Because *Swift* did not begin observations until 0.43 days after the SuperAGILE/IPN detection, the quality of both the spectrum and the light curve of the X-ray afterglow suffer from a low count rate and data gaps due to *Swift*'s orbit. Fitting the afterglow X-ray spectrum of the first observing block (0.43–0.54 days; total exposure time 5916 s) with an absorbed power-law, results in a spectral slope of  $\beta_X = 1.01^{+0.28}_{-0.25}$  and an effective hydrogen column density of  $N_H = 1.4^{+0.9}_{-0.8} \times 10^{21} \text{ cm}^{-2}$  ( $\chi^2/\text{d.o.f.} = 7.97/9$ ;  $1\sigma$  uncertainties), in agreement with results reported by Page et al. (2008) (Fig. 4.2). No constraints on a possible spectral evolution could be set. The derived hydrogen column density is higher than the Galactic value of  $N_H = 0.38 \times 10^{21} \text{ cm}^{-2}$  based on radio observations (Kalberla et al. 2005). This implies that additional absorption by gas occurs inside the GRB host galaxy. It is important to note, however, that the error bars are large.

The canonical X-ray afterglow light curve (Sect. 2.3.1; Nousek et al. 2006) shows a transition from a plateau to a normal decay phase between about 0.1 and 1 days post-burst and a jet break thereafter. Unfortunately, for GRB 080514B at early times (0.43 to 0.54 days) the X-ray light curve exhibits substantial scatter, as has also been the case for other X-ray afterglows (cf. O'Brien et al. 2006). This, and the lack of data thereafter, makes it impossible to decide whether there was a plateau phase at early times (0.43 to 0.54 days), a flare, or a break in the decay between 0.54 and 2.5 days. Assuming a simple power-law decay, the light curve is well described by a temporal decay index of  $\alpha_X = 1.52 \pm 0.14$  ( $\chi^2/\text{d.o.f.} = 17.68/18$ ). A smoothly broken power-law is statistically unlikely (Fig. 4.3). The spectral fit was then used to derive an energy conversion factor of  $6.1 \times 10^{-11} \text{ erg cm}^{-2} \text{ counts}^{-1}$ .

Following Gehrels et al. (2008) and Schulze et al. (2011), the flux density  $F_{\nu,X}[\text{Jy}]$  at the fre-

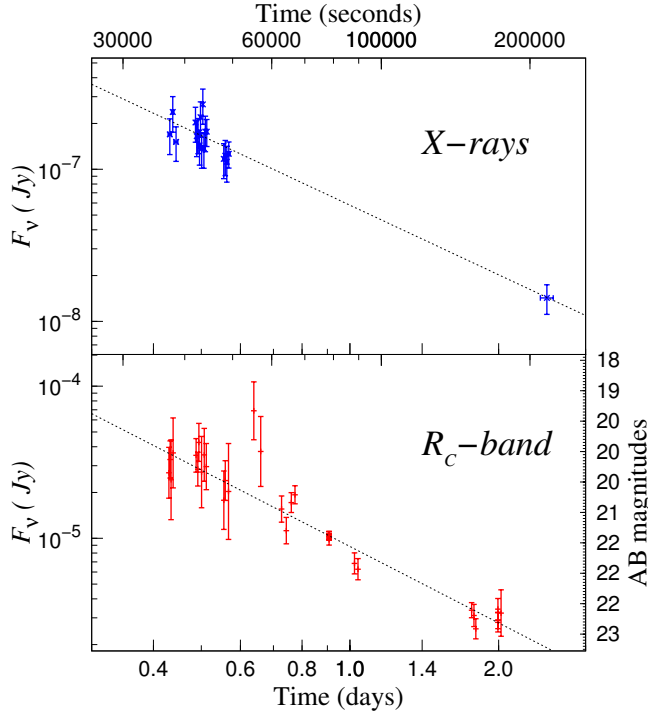


Figure 4.3: *Optical and X-ray light curves of the afterglow of GRB 080514B. Top:* X-ray light curve in the 0-3-10 keV band centered at 1.73 keV ( $\nu_X = 4.19 \times 10^{17}$  Hz). The thick line shows the best fit obtained with a power law with decay index  $\alpha_X = 1.52 \pm 0.14$ . **Bottom:** Optical light curve in the  $R_C$ -band, obtained from the data presented in Table B.1, The data are corrected for Galactic extinction, then shifted from the native filter wavelength to the  $R_C$ -band. In order to compare with the observed X-ray light curve, the host component, from the Keck observation at  $\sim 24$  days after the burst, has been subtracted. The thick line shows the best fit obtained with a power law with decay index  $\alpha_{\text{opt}} = 1.67 \pm 0.07$ .

quency  $\nu_X$  is given by

$$F_{\nu,X}[\text{Jy}] = 4.13 \times 10^5 \frac{(1 - \beta_X) F_X}{(10 \text{ keV})^{1-\beta_X} - (0.3 \text{ keV})^{1-\beta_X}} E_X^{-\beta_X}, \quad (4.1)$$

where  $\beta_X$  is the spectral slope in the X-ray band,  $F_X$  is the measured flux in the 0.3 – 10 keV range in units of  $\text{erg cm}^{-2} \text{s}^{-1}$  and the reference energy  $E_X$  is the logarithmic mean between 0.3 keV and 10 keV (1.73 keV,  $\nu_X = 4.19 \times 10^{17}$  Hz). The numerical constant converts the energy in units of keV to a frequency in units of Hz and the flux density from  $\text{erg cm}^{-2} \text{s}^{-1} \text{Hz}^{-1}$  to Jy. The obtained light curve is shown in Figure 4.3.

The observed time-dependent flux  $F_X(t_{\text{obs}})$  of the afterglow in the 0.3-10 keV window of *Swift*/XRT can be roughly described by the function

$$F_X(t_{\text{obs}})[\text{erg/cm}^2/\text{s}] = 4.5 \times 10^{-12} (t/t_1)^{-\alpha_X}, \quad (4.2)$$

where the time is measured in the observer frame,  $t_1 = 0.5$  days and  $\alpha_X = 1.52 \pm 0.14$  (Fig. 4.3). Following our paper on GRB 060605 (Ferrero et al. 2009), this can be translated into an X-ray luminosity (e.g., Nousek et al. 2006) of

$$L_X(t_{\text{host}}) = 4\pi d_L^2 (1+z)^{\beta_X-1} F_X(t_{\text{obs}}), \quad (4.3)$$

where  $d_L$  is the luminosity distance. Using  $z=1.8$  it is  $d_L = 4.26 \times 10^{28}$  cm, and assuming a spectral slope of  $\beta_X = 1.0$  (see above), the time evolution of the X-ray luminosity of the afterglow in the 0.3-10 keV energy window is given by

$$L_X(t)[\text{erg/s}] = 1.0 \times 10^{47} (t/t_1)^{-\alpha_X}, \quad (4.4)$$

where now  $t$  is measured in the GRB host frame. Based on these numbers the isotropic energy release of the afterglow in the X-ray band was about  $4.7 \times 10^{51}$  erg between 0.5 and 2.5 days, which corresponds to 2% of its isotropic energy release of  $2.6 \times 10^{53}$  erg in the gamma-ray band (Rossi et al. 2008b).

**Optical data** Afterglow coordinates were derived from the GROND first epoch stacked  $r'$ -band image, which has an astrometric precision of about  $0''.2$ , corresponding to the RMS accuracy of the USNO-B1 catalogue (Monet et al. 2003). The coordinates of the optical afterglow are R.A., Dec. (J2000) =  $21^{\text{h}}31^{\text{m}}22^{\text{s}}.69$ ,  $+00^{\circ}42'28''.6$  (Galactic coordinates  $l, b = 54^{\circ}.57, -34^{\circ}.49$ ). Magnitudes were corrected for extinction according to the interstellar extinction curve provided by Cardelli et al. (1989) and by assuming both a colour excess  $E(B - V) = 0.06$  mag (Schlegel et al. 1998) and  $R_V = 3.1$ .

While the optical afterglow is detected in a broad range of filters, from the *Swift* UVOT  $uvw2$  band to the  $H$  band (160–1700 nm), the data set is sparse with some scatter (Table B.1). To determine the slope of the light-curve decay as well as the spectral energy distribution (SED) of the afterglow, in Rossi et al. (2008b) we performed a simultaneous fit for all 14 photometric bands exhibiting detections with a single power-law (excluding the UVOT *white* filter measurement) and an added host component for those bands in which the late flattening indicates that the afterglow has become fainter than the host. From this fit ( $\chi^2_{red}/\text{d.o.f.} = 1.51/25$ ), it is derived a decay slope  $\alpha_{opt} = 1.67 \pm 0.07$ . Unfortunately, this value alone is insufficient to decide whether this is a pre-break or a post-break decay. Light curves with such a (steep) pre-jet break decay slope or with such a (flat) post-jet break decay slope have both been observed (for compilations of optical afterglow data see, e.g. Zeh et al. 2006; Kann et al. 2008). Therefore, there is no clear evidence for a jet break.

### 4.1.3 The SED and the photometric redshift

The simultaneous fitting procedure described in Sect. 4.1.2 yields magnitudes normalized to one day after the GRB for each band, which define the SED of the afterglow. In doing so, no evidence for chromatic evolution is found but one should caution that the data are sparse and is often of low signal-to-noise ratio. The SED is described well by a simple power-law with spectral slope  $\beta_{opt} = 0.64 \pm 0.03$  ( $\chi^2/\text{d.o.f.} = 8.58/10$ ) from the  $H$  band to the  $U$  band (Table 4.1 and Fig. 4.4). There is no evidence for dust in the host galaxy, which would create spectral curvature. On the other hand, the three UVOT UV filters show a much steeper slope, which can be attributed to Lyman dropout.

Using *HyperZ* (Bolzonella et al. 2000), the best fit solution provides a photometric redshift of  $z = 1.8^{+0.4}_{-0.3}$  ( $1\sigma$  uncertainties, see Avni 1976), and without any sign for a dust extinction component, and therefore resulting in  $A_V^{\text{host}} = 0$ . The redshift estimate is in agreement with the constraint of  $z < 2.3$  based on Gemini-North observations (Perley et al. 2008a) and the pseudo-redshift of  $z = 1.76 \pm 0.30$  based on the burst spectrum (Pelangeon & Atteia 2008). On the other hand, it is intermediate between the two redshift estimations presented by Gendre et al. (2008). Exclusion of the  $uvw2$  filter from the fit did not alter the obtained photometric redshift. The doubling of the assumed Galactic reddening to  $E(B - V) = 0.12$  also did not change the deduced photometric redshift significantly.

Using the derived redshift  $z = 1.8$  and the prompt emission properties as measured by *Konus-Wind* (Golenetskii et al. 2008), the bolometric isotropic energy release is  $E_{iso} = (2.63^{+0.22}_{-0.23}) \times 10^{53}$  erg and the peak luminosity  $L_{iso} = (4.73 \pm 0.99) \times 10^{53}$  erg  $s^{-1}$ , which are high but not exceptional values. The host-frame peak energy of  $E_{peak} = 627^{+64}_{-62}$  keV is unremarkable. Therefore, it is possible that the *AGILE* detection at high energies is of such high significance because of the high luminosity of this event.

Fixing  $z = 1.8$ , in Rossi et al. (2008b) we refit the SED (now excluding the UVOT UV filters) with dust models for the Milky Way, Large and Small Magellanic Clouds (for the procedure, see Kann et al. 2006). In all cases, adding  $A_V$  as an additional parameter did not improve the fits significantly, and the derived extinction is also zero within errors in all three cases (at  $3\sigma$  confidence,  $A_V \leq 0.06$

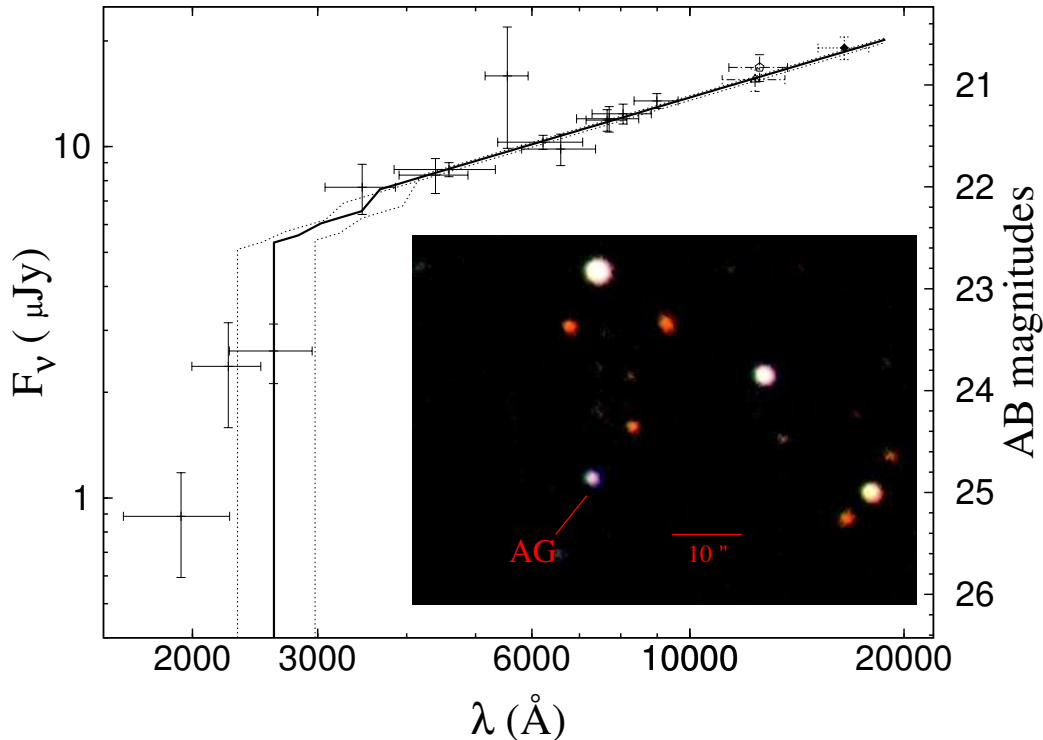


Figure 4.4: The SED of the afterglow at 1 day after the burst fitted using the HyperZ tool (solid line; the dotted lines show the  $1\sigma$  uncertainties). From left to right are shown the data presented in Table 4.3. The UVOT  $v$  band is affected by a short exposure time, the low sensitivity of the detector at longer wavelengths and high background. The steep decline blueward  $3000 \text{ \AA}$  is interpreted as intergalactic Lyman dropout and therefore it constrains the redshift of the afterglow. The blue color of the afterglow is clearly seen in the inset, which is a color composite of GROND  $g'$ ,  $r'$  and  $i'$ -band images.

for MW,  $\leq 0.17$  for LMC, and  $\leq 0.14$  for SMC dust). No evidence for a  $2175 \text{ \AA}$  feature (which would lie close to the  $R_C$  and  $r'$  bands) is apparent, and no discrimination is possible between dust models. The assumption of zero extinction is consistent with several studies (Starling et al. 2007; Schady et al. 2007, 2010) on the dust-to-gas ratios in GRB host galaxies.

#### 4.1.4 Optical/NIR to X-ray SED from GROND and *Swift*

By fixing the Galactic hydrogen column density to the value given by Kalberla et al. (2005), and setting  $z=1.8$ , one finds  $N_{\text{H}}^{\text{host}} = 8.7^{+9.0}_{-7.3} \times 10^{21} \text{ cm}^{-2}$  and  $\beta_{\text{X}} = 0.94^{+0.24}_{-0.21}$  ( $\chi^2/\text{d.o.f.} = 8.12/9$ ). While the deduced  $N_{\text{H}}^{\text{host}}$  allows potentially for a substantial host extinction when using the Galactic gas-to-dust ratio, within the large  $1\sigma$  errors this result is not in conflict with the non-detection of host extinction in the optical bands. The measured spectral slope is consistent with the mean value found for *Swift* X-ray afterglows (O'Brien et al. 2006). Using the derived spectral slope and redshift, the absolute magnitude of the afterglow is  $M_B = -22.17 \pm 0.2$  and  $M_B = -20.17 \pm 0.5$ , at one and four days after the GRB, respectively (for the method see Kann et al. 2006, 2008; no extinction is assumed). These are typical values for a GRB afterglow, i.e. GRB 080514B is neither exceptionally bright or faint.

As mentioned in Sect. 4.1.2, based on the light curve alone one cannot decide whether the data belong to the pre-jet break phase or to the post-jet break phase. Using the  $\alpha - \beta$  closure relations (Zhang & Mészáros 2004), the optical/NIR data at 1 day are consistent with a wind medium with



Table 4.1: *The values plotted in Fig. 4.4.*

Filter	$\lambda$ (nm)	$\lambda/(1+z)$ (nm)	AB mag	$F_\nu$ ( $\mu\text{Jy}$ )
UVOT <i>uvw2</i>	203.0	72.50	$24.03 \pm 0.36$	$0.887 \pm 0.294$
UVOT <i>uvm2</i>	223.1	79.68	$22.96 \pm 0.36$	$2.369 \pm 0.786$
UVOT <i>uvw1</i>	263.4	94.07	$22.86 \pm 0.21$	$2.615 \pm 0.505$
UVOT <i>u</i>	365.2	130.43	$21.69 \pm 0.18$	$7.663 \pm 1.259$
UVOT <i>b</i>	444.8	158.86	$21.60 \pm 0.12$	$8.3 \pm 0.951$
GROND <i>g'</i>	455.2	162.57	$21.56 \pm 0.04$	$8.616 \pm 0.356$
UVOT <i>v</i>	550.5	196.61	$20.90 \pm 0.41$	$15.894 \pm 6.014$
GROND <i>r'</i>	627.0	223.93	$21.37 \pm 0.03$	$10.269 \pm 0.284$
<i>Rc</i>	658.8	235.29	$21.42 \pm 0.11$	$9.841 \pm 1.016$
GROND <i>i'</i>	762.6	272.36	$21.21 \pm 0.07$	$11.923 \pm 0.833$
Gemini <i>i'</i>	770.6	275.21	$21.20 \pm 0.09$	$12.003 \pm 0.995$
<i>Ic</i>	806.0	287.86	$21.17 \pm 0.07$	$12.371 \pm 0.805$
GROND <i>z'</i>	893.0	318.93	$21.07 \pm 0.05$	$13.509 \pm 0.659$
NEWFIRM <i>J</i>	1235.1	441.11	$20.93 \pm 0.08$	$16.797 \pm 1.47$
GROND <i>J</i>	1256.1	448.61	$20.84 \pm 0.09$	$15.463 \pm 1.139$
GROND <i>H</i>	1646.7	588.11	$20.70 \pm 0.08$	$19.111 \pm 1.408$

Notes: The data refer to  $t = 1$  day. Data are corrected for Galactic extinction and are given in AB magnitudes and flux density. The third column shows the observed central wavelengths in the host frame at  $z = 1.8$ .

the cooling frequency bluewards of the optical/NIR bands and a light curve in the pre-break regime (Table 4.2 and Fig. 4.5; see also Sect. 2.2.3). The much larger error bars in the X-ray data are less of a constraint here.

In particular, the X-ray data seem to favor an ISM medium, with the cooling frequency above the X-ray band (0.3-10 keV). However, the difference in the observed spectral slopes of the SED between optical and X-rays disfavors this idea since it requires a break of the SED between the two bands. It is important to note that, while the optical light curve is constrained and well sampled until 2 days after the burst, the X-ray light curve has a big gap after 0.6 days ( $\sim 50000$  s; Fig. 4.3). Therefore, the obtained  $\alpha_X = 1.52 \pm 0.14$  is probably more indicative of a fading than of a real evolution, as discussed in Section 4.1.2. However, within  $1\sigma$  the closure relations are in agreement with a wind medium, for  $\nu_c > \nu_X$ . This matches with the analysis of the optical SED. The finding of a wind medium would be indicative of a massive star progenitor, probably a Wolf-Rayet star (Sect. 1.2 and 2.2.3). Indeed, in Schulze et al. (2011) we have analyzed several optical and X-ray light curves to derive the density profile in the proximity of GRB progenitors, and the analysis showed that the afterglow of GRB 080514B is one of the few ones, with a wind profile.

Within the considerations above, it is possible to fit the optical and X-rays data together, after shifting both dataset to the same time after the burst (Fig. 4.5). In doing so, since the X-ray light curve behavior was less constrained than the optical, I shifted the optical/NIR SED at 1 day to 0.5 days, i.e. the mid-time of the X-ray spectrum, taking in account that the optical afterglow was decaying with  $\alpha_{\text{opt}} = 1.67$  (Sect. 4.1.2). For fitting the complete data-set no additional contribution from the ISM in the GRB host galaxy was considered, as resulted from the optical/NIR analysis. In agreement with

Table 4.2: Predicted temporal slopes  $\alpha$  for various afterglow scenarios.

afterglow model	Optical		X-ray	
	$\alpha_{\text{opt}}$	$\sigma$ -level	$\alpha_X$	$\sigma$ -level
iso				
ISM, wind, $\nu_c < \nu$	$0.46 \pm 0.05$	-14.54	$1.02^{+0.42}_{-0.38}$	-1.14
ISM, $\nu < \nu_c$	$0.96 \pm 0.05$	-8.53	$1.52^{+0.42}_{-0.38}$	-0.01
<b>wind</b> , $\nu < \nu_c$	$1.46 \pm 0.05$	-2.52	$2.02^{+0.42}_{-0.38}$	1.24
jet				
ISM, wind, $\nu_c < \nu$	$1.28 \pm 0.06$	-4.23	$2.02^{+0.56}_{-0.50}$	0.96
ISM, wind, $\nu < \nu_c$	$2.28 \pm 0.06$	6.62	$3.02^{+0.56}_{-0.50}$	2.89

Notes: The results are based on the measured spectral slopes  $\beta_{\text{opt}} = 0.64 \pm 0.03$  (Sect. 4.1.3) and  $\beta_X = 1.01^{+0.28}_{-0.25}$  (Sect. 4.1.2). These values have to be compared with the measured  $\alpha_{\text{opt}} = 1.67 \pm 0.07$  and  $\alpha_X = 1.52 \pm 0.14$ . Assuming a jet, for  $t < t_{\text{break}}$  the isotropic model holds, whereas for  $t > t_{\text{break}}$  the jet model applies (Sect. 2.2.3). The  $\sigma$ -level represents the difference between the predicted and the observed temporal slope, normalized to the square root of the sum of their quadratic errors. The favoured model is highlighted.

the findings from the closure relations, the X-ray data were fitted considering a Galactic gas column density of  $N_{\text{H}}^{\text{Gal}} = 3.8 \times 10^{20} \text{ cm}^{-2}$ . The optical/NIR and X-ray data were well fitted by a single broken power law with the condition  $\beta_X = \beta_{\text{opt}} + 0.5$ , i.e. with a cooling frequency between the optical and the X-ray frequencies ( $\chi^2/\text{d.o.f.} = 10.5/14$ ). The fit confirmed the optical spectral slope of  $0.64 \pm 0.01$  and, in addition, found  $\beta_X = 1.14 \pm 0.01$ , in agreement with Sect. 4.1.3. Hence, the spectral slope did not evolve between 0.5 days and 1 day after the burst. The fit finds for the cooling frequency a value of  $\nu_c = 0.26 \pm 0.12 \text{ keV}$  and a host gas column density of  $N_{\text{H}}^{\text{host}} = 1.27^{+0.49}_{-0.42} \times 10^{22} \text{ cm}^{-2}$ , in agreement with the result from the X-ray spectral analysis alone, but much well constrained.

Such a high value for the gas column density it is not unusual and in fact much higher values have been found, basically always indicating that the dust-to-gas ratio is substantially reduced along GRB sight lines (e.g., Galama & Wijers 2001; Kann et al. 2006; Mao 2010). Several explanations for this phenomenon have been put forward by e.g. Schady et al. (2010, 2011)). In Krühler et al. (2011) we argue that dust destruction by the intense fireball light, as it is discussed by e.g. Fruchter et al. (2001), remains the most favorable model to explain these observations.

#### 4.1.5 The host galaxy of GRB 080514B

A galaxy underlying the position of the optical transient is detected in all GROND optical bands at 8.9 days as well as in the deep Keck  $g$  and  $R$ -band images obtained 24.13 days post-burst. Using the stacked GROND  $g'r'i'z'$  images, its coordinates are R.A., Dec. (J2000) =  $21^{\text{h}}31^{\text{m}}22^{\text{s}}.68$ ,  $+00^{\circ}42'28''.8$ , which is offset by  $0'.3 \pm 0'.2$  from the position of the optical afterglow. Assuming a cosmological model with  $H_0 = 71 \text{ km s}^{-1} \text{ Mpc}^{-1}$ ,  $\Omega_{\text{M}} = 0.27$ ,  $\Omega_{\Lambda} = 0.73$  (Spergel et al. Spergel et al. (2003)), for  $z = 1.8$  the offset of the optical transient from the centre of this galaxy is  $2.6 \pm 1.7 \text{ kpc}$ .

By assuming a power-law spectrum for the putative host galaxy of the form  $F_{\nu} \propto \nu^{-\beta_{\text{gal}}}$ , its absolute  $R$ -band magnitude is  $M_R = 24.73 - \mu - k$ , where  $\mu = 45.70 \text{ mag}$  is the distance modulus and  $k$  is the cosmological  $k$ -correction,  $k = -2.5(1 - \beta_{\text{gal}}) \log(1 + z)$ . For  $\beta_{\text{gal}} = 0.45$ , as it follows from

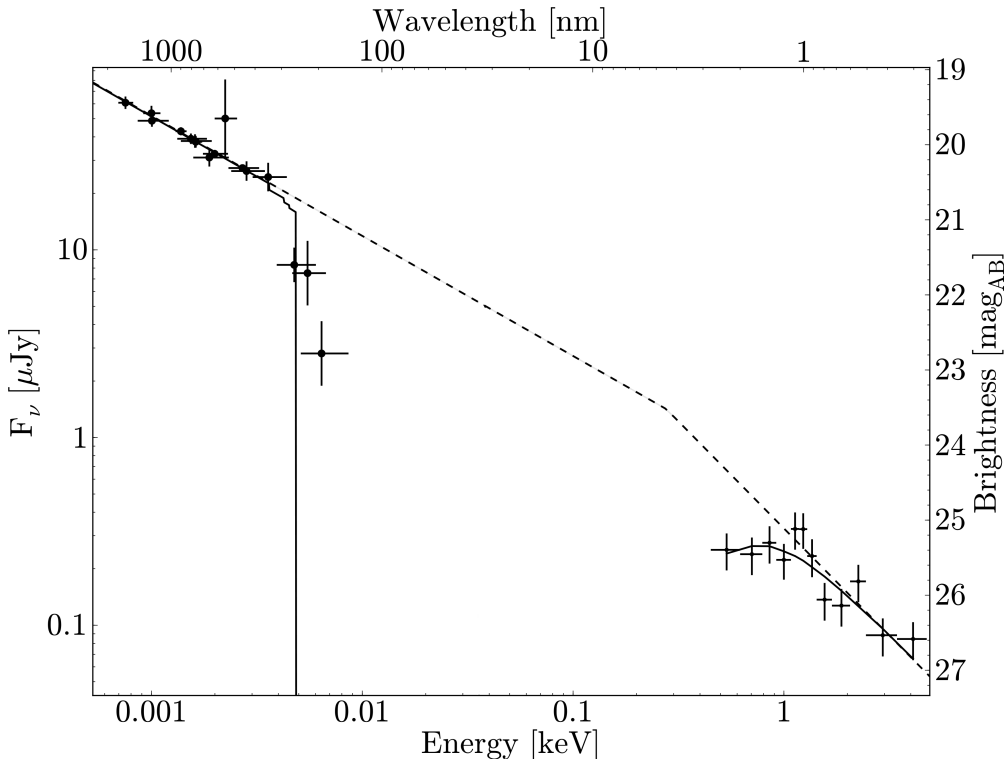


Figure 4.5: *Optical/NIR to X-ray SED of the afterglow of GRB 080514B in the observer frame. The broad band SED at 1 day after (Table. 4.3, Fig. 4.4) the burst was shifted to 0.5 days in order to be fitted together with the X-ray data (see text in Sect. 4.1.4 for details). The SED is well fitted by a broken power law with  $\beta_{\text{opt}} = 0.64 \pm 0.01$  and  $\beta_{\text{X}} = \beta_{\text{opt}} + 0.5$  and the fit finds for the cooling frequency a value of  $h\nu_c = 0.26 \pm 0.12$  keV ( $\nu_c = 6.3 \pm 2.9$  Hz). The thick line shows the SED continuum, affected by Lyman dropout in the optical and gas absorption in the X-ray band, while the dashed line shows the SED not affected by intervening absorption.*

the third epoch GROND  $g'r'i'z'$  data, this galaxy has  $M_R = -20.9$ , which is about 0.5 mag more luminous than the characteristic magnitude of the Schechter  $r$ -band luminosity function of galaxies in the Las Campanas redshift survey (Lin et al. 1996). Its  $R$ -band magnitude agrees well with the distribution of long-burst host magnitudes for this redshift (Guziy et al. 2005a; Savaglio et al. 2009).

## 4.2 The afterglow of the long GRB 080928

In Section 3 I have discussed in detail that GRB 080928 is one of the few events where a broad-band SED from optical to gamma-rays can be constructed for the prompt emission phase. The afterglow of this event was rapidly found, and Vreeswijk et al. (2008) measured a redshift of  $z = 1.692$ . Here, I describe the analysis of the optical and X-ray afterglow of GRB 080928, as well as the search for its host galaxy. Data gathering and analysis is already discussed in Sections 3.1.2 and 3.1.3.

### 4.2.1 The X-ray and optical/NIR light curve

At early times, up to 470 s after the trigger, the X-ray light curve is dominated by two strong peaks (Fig. 3.4). The first peak is 4 seconds after the peak seen by BAT and GBM. The optical light curve is similarly complex, showing bumps up to about 10 ks after the trigger. Unfortunately, the gap in the X-ray data does not allow for a comparison between the two bands during this timespan.

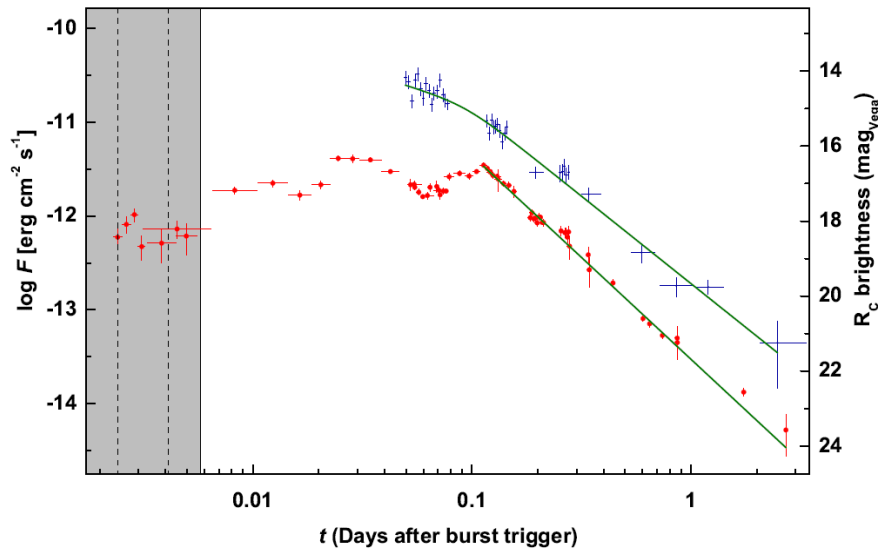


Figure 4.6: *The optical and X-ray light curve of GRB 080928 (see Figure 3.4).*

Despite the rich variability in the early afterglow, the late time evolution is consistent with a power-law decay. After 4.2 ks the X-ray light curve can be described by a broken power-law, in the form introduced by Beuermann et al. (1999):

$$F_{\nu}(t) = \text{const.} \cdot \left[ \left( \frac{t}{t_b} \right)^{-\alpha_1 n} + \left( \frac{t}{t_b} \right)^{-\alpha_2 n} \right]^{-\frac{1}{n}} \quad (4.5)$$

where the decay indexes are  $\alpha_1^X = 0.72 \pm 0.35$  and  $\alpha_2^X = 1.87 \pm 0.07$ , and the break is at  $t_b = (8100 \pm 1600)\text{s}$  (observer frame). The smoothness of the break is fixed  $n = 5$ . The broken power-law results in a good fit solution with  $\chi^2/\text{d.o.f.} = 55.4/33 = 1.68$  (Fig. 3.4).

The optical data do not allow for a fit with a broken power-law due to the multiple bumps in the light curve. For  $t_{\text{obs}} > 10$  ks the fit with a single power-law gives  $\alpha_{\text{opt}} = 2.17 \pm 0.02$  ( $\chi^2/\text{d.o.f.} = 56.8/34 = 1.67$ ). The optical/NIR and X-ray data suggest similar small variability after 20 ks, which however it is not possible to study further due to the sparsity of the data. The break in the X-ray light curve could be a jet break, but as I will argue later, the detailed modeling of the afterglow does not support this conclusion (Sect. 4.2.3).

In Fig. 4.7 the X-ray afterglow of GRB 080928 is compared with all X-ray afterglows found up to April 2010 in a redshift interval of  $\Delta z = 0.1$  around the redshift of GRB 080928 (1.6919), namely GRB 050802 ( $z = 1.7102$ ; Fynbo et al. 2009), 071003 ( $z = 1.60435$ ; Perley et al. 2008c), 080603A ( $z = 1.6880$ ; Perley et al. 2008b), 080605 ( $z = 1.6403$ ; Fynbo et al. 2009), 090418 ( $z = 1.608$ ; Chornock et al. 2009), 091020 ( $z = 1.71$ ; Xu et al. 2009), and 100425A ( $z = 1.755$ ; Goldoni et al. 2010). In comparison to these, the early X-ray emission of GRB 080928 is about 1.6 dex more luminous, probably due to its physical connection to the prompt emission. Even compared to the entire ensemble of 190 X-ray light curves, it is more luminous than the average. However, after the light curve break at 8.1 ks (observer frame; 3 ks host frame) the afterglow rapidly becomes sub-luminous with respect to the ensemble. Interestingly, except for GRB 080603A and 100425A, the other afterglows have a similar break time and post-break decay slope.

In the optical bands the afterglow tends to vary between two extremes. The afterglow was corrected for the extinction derived below (Sect. 4.2.2) and shifted it to  $z = 1$  following Kann et al. (2006). Compared to the ensemble of optical afterglows with reasonable data (Kann et al. 2010), at early times it is comparatively faint, nearly eight magnitudes fainter than the brightest events

Figure 4.7: The X-ray luminosity of 190 Swift GRBs and their afterglows in the range of 0.3 to 10 keV between Jan 26, 2005, and Apr 25, 2010. GRB 080928 is shown in black. For comparison all six GRBs within a redshift interval of 0.1 around the redshift of GRB 080928 are highlighted in dark gray. The luminosity of the afterglow of GRB 080928 was basically in the mean of the X-ray luminosities which have so far been observed. For the theoretical procedure see Section 4.1.2 (Eq. 4.3).

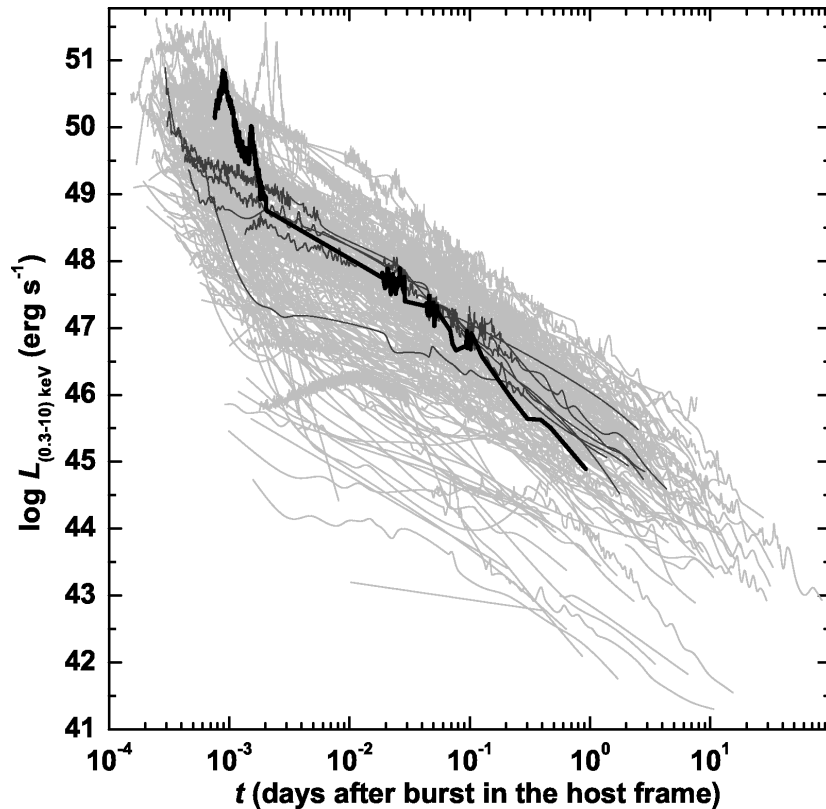
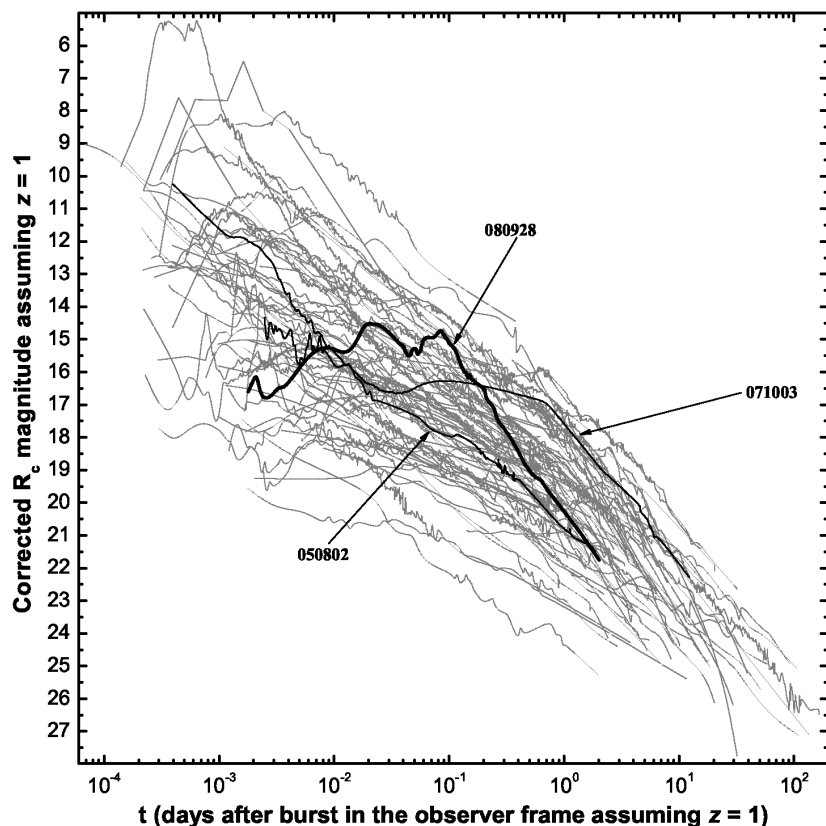


Figure 4.8: The optical afterglow of GRB 080928 (thick line) compared with the sample of extinction-corrected afterglows shifted to  $z = 1$  from Kann et al. (2010). For comparison, the GRBs within a redshift interval of 0.1 around the redshift of GRB 080928 for which there are optical data are highlighted and labeled. All magnitudes are Vega magnitudes.



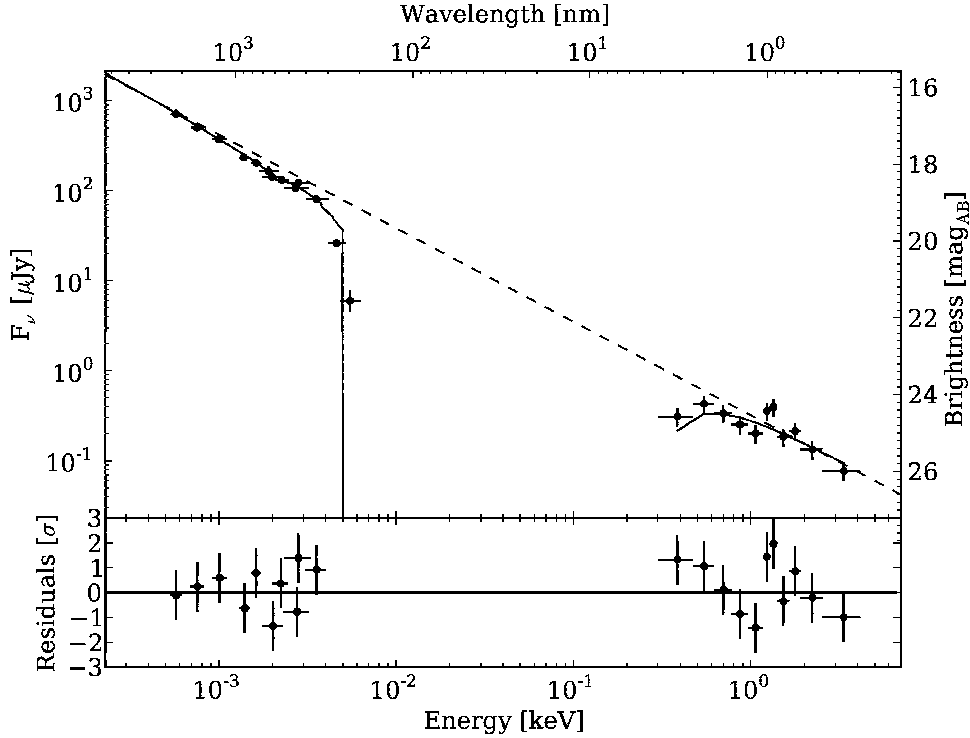


Figure 4.9: *The observed SED of the X-ray/optical/NIR afterglow of GRB 080928 at  $t=20$  ks, after correction for Galactic extinction by dust and Galactic absorption by gas. The joint X-ray/optical SED is almost a pure power-law (dashed line) affected by only a small amount of host extinction by dust (Table 4.4) and  $3.5 \times 10^{21} \text{ cm}^{-2}$  of host absorption by the gas. The UV bands are affected by Lyman dropout. Residuals refer to the plot with  $\beta_{\text{OX}} = 1.02$  (broken line).*

(Fig. 4.8). Its multiple re-brightenings, which are a notable signature of this afterglow, then bring the late-time light curve close to the mean magnitude of the distribution at one day after the GRB (at  $z = 1$ ). In between, at about 0.1 days (at  $z=1$ ), they make the afterglow about 2 mags brighter than the average, shifting it into the group of the 10 top brightest optical afterglows at that time.

#### 4.2.2 GROND and *Swift* optical/NIR to X-ray SED

In order to fit the unabsorbed SED from the optical to the X-ray band I selected the X-ray data from 12.4 ks to 25 ks (mean photon arrival time 20 ks). Since no evidence for color variations was found in the optical data, I then shifted the optical light curve to this time (Table 4.3; corrected for a Galactic extinction of  $E(B - V) = 0.07$  mag). In addition to the GROND and UVOT data I used the VLT detection corrected to the  $R_C$  band (Sect. 3.1.3). In doing the fit, the redshift was fixed to 1.692, the host galaxy hydrogen column density to  $N_{\text{H}} = 3.5 \times 10^{21} \text{ cm}^{-2}$  and the Galactic hydrogen column density to  $N_{\text{H}} = 0.56 \times 10^{21} \text{ cm}^{-2}$  (Sect. 3.1.2). The resulting SED is shown in Fig. 4.9 (left) and Table 4.4. There is no spectral break between the X-ray band and the optical. Between 4 ks until the end of the X-ray observations at around 120 ks (1.4 days) no evidence for spectral evolution was found.

In Rossi et al. (2008b), we find that SMC and LMC dust provided an acceptable fit, although MW dust improved the fit (Table 4.4). The 2175Å feature is less strong than in the case of GRB 070802 (Krühler et al. 2008; Elíasdóttir et al. 2009), however. The derived host extinction is clearly

Table 4.3: *The values plotted in Fig. 4.9.*

Filter	$\lambda$ (nm)	$E$ (eV)	AB mag	$F_\nu$ ( $\mu$ Jy)
<i>uvw2</i>	203.0	6.12	> 19.33	< 11.4
<i>uvm2</i>	223.1	5.57	$20.18 \pm 0.31$	$5.40 \pm 1.51$
<i>uvw1</i>	263.4	4.71	$18.87 \pm 0.11$	$23.8 \pm 2.38$
<i>u</i>	365.2	3.40	$18.26 \pm 0.04$	$73.7 \pm 2.81$
<i>b</i>	444.8	2.79	$18.87 \pm 0.08$	$111.7 \pm 8.64$
<i>g'</i>	455.2	2.73	$18.99 \pm 0.10$	$97.8 \pm 9.07$
<i>v</i>	550.5	2.26	$18.68 \pm 0.10$	$119.4 \pm 11.0$
<i>r'</i>	627.0	1.98	$18.44 \pm 0.05$	$129.6 \pm 6.05$
<i>R<sub>C</sub></i>	658.8	1.88	$18.53 \pm 0.15$	$140.0 \pm 19.4$
<i>i'</i>	762.6	1.63	$17.82 \pm 0.05$	$186.2 \pm 9.29$
<i>z'</i>	893.0	1.39	$17.53 \pm 0.06$	$213.4 \pm 11.4$
<i>J</i>	1256.1	0.99	$16.64 \pm 0.09$	$340.0 \pm 26.6$
<i>H</i>	1646.7	0.75	$15.85 \pm 0.12$	$460.7 \pm 52.7$
<i>K<sub>s</sub></i>	2151.2	0.58	$15.00 \pm 0.17$	$653.8 \pm 102.4$

Notes: The values plotted in Fig. 4.9. The data refer to  $t = 20$  ks. Data are corrected for Galactic extinction and are given in AB magnitudes. The  $R_C$ -band value is based on Vreeswijk et al. (2008); the other data refer to the GROND and the UVOT filter bands.

Table 4.4: *Results of the joint optical to X-ray spectral fit. The first column gives the dust model, the following columns the deduced host extinction, the spectral slope from the optical to the X-ray band and the  $\chi^2$  with the corresponding degrees of freedom.*

Dust model	$A_V^{\text{host}}$	$\beta_{\text{OX}}$	$\chi^2/\text{d.o.f}$
MW	$0.12 \pm 0.03$	$1.03 \pm 0.01$	20.2/18
LMC	$0.07 \pm 0.02$	$1.02 \pm 0.01$	24.5/18
SMC	$0.04 \pm 0.01$	$1.01 \pm 0.01$	26.6/18

unremarkable within the sample of Kann et al. (2010).

In a way similar as for GRB 080514B (Sect. 4.1.4), for a Milky Way interstellar medium the deduced high  $N_{\text{H}}$  would imply a host extinction of  $A_V^{\text{host}} = 2_{-1.2}^{+1.0}$  mag. This value, like in the case of GRB 080514B (Sect. 4.1.4), is in contrast to the small value found here. However, several GRB afterglows studies have found that, despite a very large scatter in the  $N_{\text{H}}/A_V$  ratio, the  $N_{\text{H}}$  is always significantly larger than that observed in the local Universe (e.g., Galama & Wijers 2001; Stratta et al. 2004; Kann et al. 2006; Starling et al. 2007; Schady et al. 2007, 2010), a phenomenon that potentially could be explained by dust destruction by the intense fireball light (Fruchter et al. 2001; Watson et al. 2007).

### 4.2.3 Theoretical interpretation of the light curve

Using the forward shock afterglow model (e.g., Panaitescu & Kumar 2000; Zhang & Mészáros 2004; Piran 2005), it is difficult to explain the different slopes of the optical and X-ray light curves given that they are on the same power-law segment of the spectrum. Assuming the cooling frequency,  $\nu_c$ , is

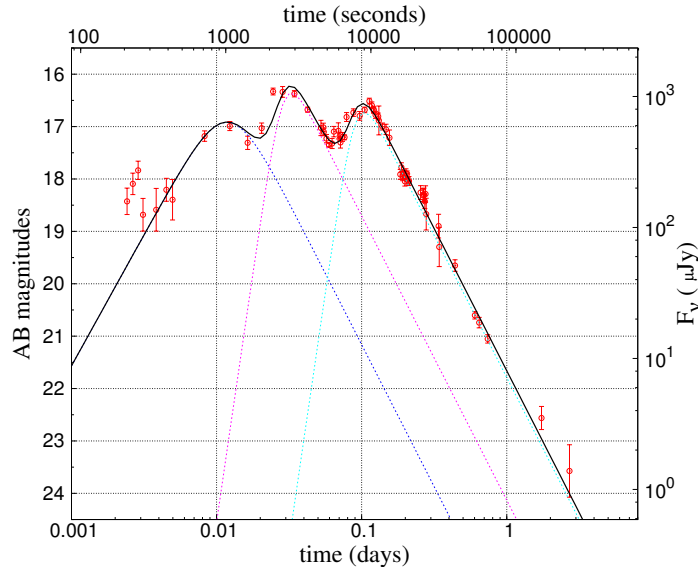


Figure 4.10: *The best fit light curves of the optical afterglow of GRB 080928. In agreement with the energy injection model, to explain the presence of three bumps, three broken power laws are needed. Therefore, the optical data were fitted such that the decay indexes after the peaks are the same for the three broken power laws and fixed to the value obtained after 10 ks.*

above the X-ray band, the spectral slope gives an electron energy index of  $p = 2\beta + 1 \approx 3$ . The light curve slope of  $\alpha \approx 2$  then indicates a pre-break evolution in a stellar wind. This would be problematic for the early-time evolution, as it is difficult to get a rising afterglow with a stellar wind external medium. The second possibility is that  $\nu_c$  is below the optical band, resulting in  $p = 2\beta \approx 2$ . The light curve slope then indicates a post-break evolution. Having  $\nu_c$  below the optical band is, however, difficult to achieve as it is shown below.

The early optical light curve is rich in variability. Unfortunately, there are no XRT measurements during the optical fluctuations to verify the correlation between X-ray and optical light curves, but there are a couple of other cases where high-energy flares are seen in the optical too, e.g., GRB 041219A (Vestrand et al. 2005; Blake et al. 2005), GRB 050820A (Vestrand et al. 2006), GRB 060526 (Thöne et al. 2010), GRB 061121 (Page et al. 2007) and XRF 071031 (Krühler et al. 2009). In particular, the general behaviour of the afterglow recalls the cases of GRB 060904B (Klotz et al. 2008; Kann et al. 2010) and GRB 060906 (Cenko et al. 2009). The optical fluctuations have a long timescale which is more consistent with energy injection into the forward shock than with central engine activity.

In Rossi et al. (2011b), one of the co-authors (Jóhannesson, G.) used the numerical model introduced in Jóhannesson et al. (2006) and Jóhannesson (2006) to fit the afterglow data. The data taken in the first 500 s after the trigger were excluded, as they are most likely explained by internal shocks. The data are still kept in the fit as upper limits: not accounted if the model is below, but added to the  $\chi^2$  value like normal points if the model is above. Two different times were explored as the initial time for the calculation: the trigger time  $t_0$  and the start of the main prompt emission at  $t_0 + 170$  s. Since a wind-like medium will over-predict the early data, this analysis was limited to a constant-density medium. The assumption was that the first peak in the optical light curve at  $\sim 1000$  s is the onset of the afterglow and the following two bumps at  $\sim 2$  ks and  $\sim 10$  ks are caused by energy injections (Fig. 4.10). Host extinction was assumed to be Milky-Way like as found from the spectral analysis but the host extinction  $A_V^{\text{host}}$  was allowed to vary during the fit. The Ly  $\alpha$  absorption was accounted following the method of Madau (1995).

The numerical model prefers the start time of  $t_0 + 170$  s where most of the constraints come from the optical data contemporaneous with the high-energy prompt emission. The model over-predicts



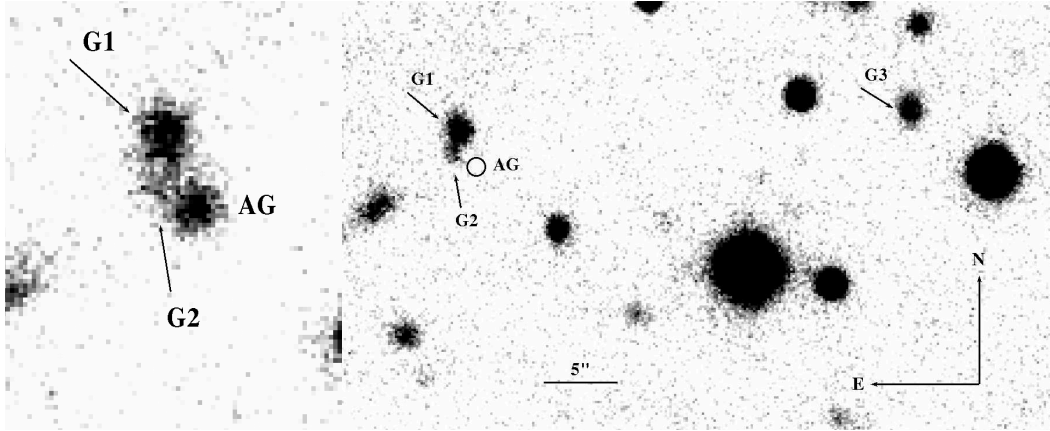


Figure 4.11: A view of the region around GRB 080928. **Left:** Zoom-in of the GROND combined  $g'r'i'z'$ -band image obtained 1.74 days after the burst at a seeing of  $1''.5$ . It shows the afterglow (AG) and the brightest galaxies close to it. **Right:** Zoom-in of the stacked GROND optical  $g'r'i'z'$ -band images obtained on May 15, 2009, 6.5 months after the burst (5th epoch) when the afterglow had faded away. It also shows the galaxy (G3) that was coincidentally covered by the slit of the spectrograph when the redshift of the afterglow was measured with the ESO/VLT (Vreeswijk et al. 2008; Fynbo et al. 2009). Data for G1 to G3 are summarized in Table 4.5.

Table 4.5: Coordinates and AB magnitudes of objects G1, G2 and G3 close in projection to the afterglow of GRB 080928. Magnitudes are not corrected for Galactic extinction.

Object, R.A., Dec. (J2000)	$g'$	$r'$	$i'$	$z'$	$J$	$H$	$K_s$
G1, 06:20:16.96, -55:11:56.6	24.22(15)	23.41(05)	22.43(08)	22.03(08)	20.89(09)	20.55(30)	20.00(50)
G2, 06:20:16.99, -55:11:58.0	25.20(50)	24.50(06)	23.26(09)	22.70(05)	21.50(20)	21.20(30)	> 20.7
G3, 06:20:13.35, -55:11:54.9	23.13(12)	23.12(05)	22.63(07)	22.20(05)	> 22.0	> 21.6	> 20.9

the data in this epoch when the start time is  $t_0$ . The best fit results in  $\chi^2/\text{d.o.f.} = 307/187 = 1.64$ , which is comparable to the power-law fits shown earlier despite fitting more data. It is important to note that the value found for the initial Lorentz factor of the outflow ( $\Gamma_0 = 77^{+120}_{-28}$ ) is in agreement with the results found in Section 3.2.5. However, the fit does not do a good job with the X-ray light curve, because it is slightly under-predicting the X-ray emission before the second injection and it is over-predicting it afterwards. This seems to indicate that there is some other mechanism at work than energy injections, but the lack of simultaneous X-ray observations during the optical rise makes it difficult to interpret what is going on.

#### 4.2.4 The search for the host galaxy of GRB 080928

The deep 5th epoch GROND images taken 6.5 months after the trigger of GRB 080928 at a seeing of  $\sim 1''$  do not show any galaxy underlying the position of the optical transient down to the following  $3\sigma$  upper limits (AB magnitudes):  $g' = 25.4, r' = 25.6, i' = 24.6, z' = 24.3, J = 22.0, H = 21.6, K_s = 20.9$ . Assuming for simplicity a power-law spectrum for this galaxy as described in 4.1.5, for the  $r'$ -band, distance modulus  $\mu = 45.54$  and a representative value of  $\beta_{\text{gal}}=1$ , one can obtain a lower limit of  $M_{r'} > -19.94$ , which is in agreement with the luminosities found so far for the GRB host galaxy population. In fact, much less luminous hosts are known (see Savaglio et al. 2009). However,

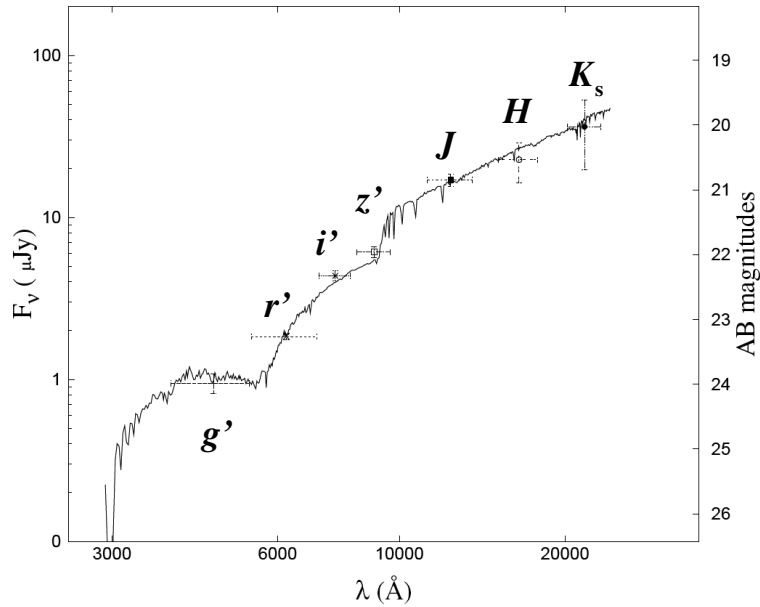


Figure 4.12: The broad-band SED of galaxy G1 close to the afterglow of GRB 080928 (see Fig. 4.11), obtained from images taken with GROND 6.5 months after the burst ( $g'r'i'z'$  JHK<sub>s</sub> filters). Shown is the best HyperZ fit that is based on the template of a dusty starburst galaxy at a redshift of  $z=1.46$ .

Table 4.6: Results obtained modeling the SED of galaxies in the field of GRB 080928 (Fig. 4.11).

Object	$\chi^2_{0.7359}$	Dust	$A_V^{\text{host}}$	$\chi^2_{1.6919}$	Dust	$A_V^{\text{host}}$
G1 starburst	3.98	LMC	1.0	3.47	SMC	0.8
G2 irregular	1.07	LMC	0.7	3.49	MW	0.8
G3 irregular	1.01	–	0.0	3.76	–	0.0

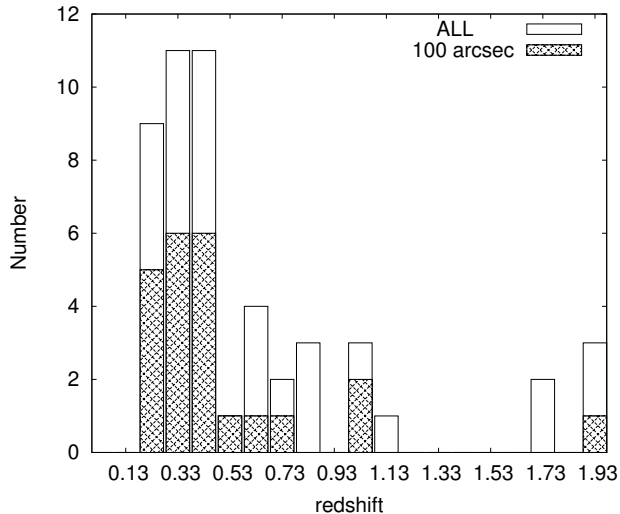
Notes: *HyperZ* results for the fit of the SED of G1, G2, and G3 based on GROND data obtained 6.5 months after the burst. The redshift was fixed the first time to the value of the absorber foreground the afterglow ( $z =$ ), and the second time to the afterglow redshift (see text). Also given are the corresponding values for the deduced host extinction  $A_V^{\text{host}}$  and the preferred host extinction law (SMC, LMC, or Milky Way).

could one of the galaxies seen in projection close to the afterglow be the host?

Close to the position of the afterglow there is a relatively bright galaxy (labeled G1 in Fig. 4.11) with  $r' = 23.41 \pm 0.05$ . Using the stacked GROND  $g'r'i'z'$ -band images from the 5th epoch, its central coordinates (Table 4.5) are offset by  $2''.6 \pm 0''.3$  from the position of the optical afterglow. If this galaxy is at the redshift of the burst, then the projected offset of the optical transient from its centre is  $(22.2 \pm 2.6)$  kpc. This is almost 20 times larger than the median projected angular offset of 1.31 kpc found by Bloom et al. (2002) for a sample of 20 host galaxies of long bursts, making it unlikely that this is the host galaxy of GRB 080928.

Some arcseconds south of G1 lies a diffuse object which could either be physically associated to G1 or represent another foreground/background galaxy. This object (G2 in Fig. 4.11) is  $1''.5 \pm 0''.3$  away from the afterglow position. If it is at the redshift of the burst, its projected distance from the afterglow is  $(13 \pm 2.6)$  kpc, again hardly in agreement with the observed GRB offset distribution. However, both objects/galaxies are potentially close enough in projection to imprint a signal on the GRB afterglow spectrum. Indeed, Fynbo et al. (2009) report a foreground absorption line system exhibiting several strong Fe, Mg and Ca lines at a redshift of  $z = 0.7359$ . In the  $1''$  slit passing over the afterglow, Fynbo et al. (2009) identify a galaxy  $30''$  away from the afterglow at a redshift

Figure 4.13: *The redshift distribution for all galaxies in the 5x5 arcmin GROND field of view of GRB 080928 and for all galaxies within 100 arcsec around the position of the afterglow based on HyperZ and the 5th epoch GROND images. A galaxy entered the resulting statistics only when its derived redshift estimate had a probability value of greater than 90%, which is not the case for the galaxies detected near the afterglow position (Table 4.6). The typical  $1\sigma$  error in the photometric redshift is 0.1.*



of  $z = 0.736$ . This redshift is identical to the value found for the absorbing system (Vreeswijk et al. 2008). We labelled this galaxy as G3.

Using *HyperZ* (Bolzonella et al. 2000), I used the multi-color presented here photometry to obtain the photometric redshift of the galaxies in the field to identify the objects correlated to the absorbing system and the afterglow. The aperture photometry (see Tab. 4.5) was performed on the GROND seven band images, after correcting for the different PSFs used through PSF-matching techniques using IRAF tasks (see Alcock et al. 1999).

In Table 4.6, I provide the best fit in terms of  $\chi^2/\text{d.o.f.}$  of the observed broad-band SEDs of G1 to G3 if one fixes the redshift of these objects at  $z = 0.736$  (the redshift of the intervening system seen by Fynbo et al. 2009) and at  $z = 1.6919$  (the redshift of the afterglow). The results indicate that with high probability no one of the galaxies is the host galaxy and that G1 is not the foreground absorber seen in the afterglow spectrum.

For object G3, I find a *HyperZ* solution in very good agreement with the value of  $z = 0.736$  reported by Vreeswijk et al. (2008) ( $\chi^2/\text{d.o.f.} = 1.01$ ). However, the detection in only the four optical bands does not allow me to constrain the dust extinction in this galaxy. Unfortunately, in the case of G2 a *HyperZ* fit with the redshift as a free parameter leads to no conclusive results, the resulting error bars are very large and the photometry can be affected by the nearby galaxy G1. On the other hand, a *HyperZ* fit with the redshift fixed at  $z = 0.736$  gives a reasonable photometric solution ( $\chi^2/\text{d.o.f.} = 1.07$ ; Table 4.6). This makes it possible that G2 is responsible for the absorption line system seen in the afterglow spectrum, given the proximity of G2 to the spectral slit passing over G3 and the afterglow.

When one treats the redshift as a free parameter, not fixing it to the value of the afterglow or the absorbing system, he finds that the best *HyperZ* solution for G1 is  $z = 1.46^{+0.15}_{-0.10}$  (Fig. 4.12), in both cases (whether G2 is considered to be a separate galaxy or not), confirming that G1 is not related to any other object.

Finally, I analyzed if the finding of Vreeswijk et al. (2008), that two galaxies close to the afterglow have a redshift around 0.736, points to a potential overdensity of galaxies in the field at this redshift. Therefore, I have used deep GROND 5th epoch images to perform a  $g'r'i'z'JHK_s$  photometry of all objects in the field that appear to be non-stellar in order to estimate their redshift. Then, I created two samples, one sample including all galaxies in the field, the other sample including only galaxies within

100 arcsec around the afterglow position. I then used *HyperZ* to derive the photometric redshifts. Using a bin width of  $dz=0.1$ , a binning of the results was performed in such a way that a redshift of 0.74 lies in the middle of a bin. The results are shown in Fig. 4.13. No overdensity of galaxies is seen around the redshift of interest (note that Table 4.6 did not enter Fig. 4.13 since for no galaxy in this table *HyperZ* found a solution for the redshift that has a probability of better than 90%).

### 4.3 Summary of the afterglow and host observations

The richness in the phenomenology of GRB afterglows becomes apparent when high- and low-energy data are combined. GRB 080514B was outstanding because of its high-energy emission above 30 MeV. Unfortunately, no spectroscopic redshift could be measured for its afterglow. However, thanks to the database collected here, I was able to determine its photometric redshift ( $z = 1.8^{+0.4}_{-0.3}$ ) and, based on this result, to determine its energetics. In particular, in Rossi et al. (2008b) I paid attention to the question whether the properties of the X-ray and optical afterglow as well as of the host of this burst were different from the corresponding properties of the main GRB population that is not seen at such high gamma-ray energies at all. Interestingly, no evidence for anything special was found, supporting the picture that the gamma-ray emission during the prompt phase on the one hand and the afterglow properties on the other hand are not physically related to each other. It indicates that both processes are decoupled to a high degree as it is suggested by/inherent to the standard GRB model.

Very different to GRB 080514B ( $z = 1.8^{+0.4}_{-0.3}$ ) was GRB 080928 ( $z=1.692$ ). It had no high energy emission, was not even seen above 150 keV. Its afterglow light curve, however, was very bumpy, probably due to long-lasting engine activity. Thanks to GROND and *Swift*/XRT data it was possible to analyze the optical/NIR to X-rays SED of the late afterglow after the last peak at  $\sim 10$  ks, and I could show that both emissions have a common origin. The SED follows a simple power-law, i.e. the cooling frequency lies outside the NIR-Xray frequency interval. Finally, the search for the host was not conclusive, and therefore no visible host galaxy can be associated with GRB 080928.

GRB 080514B as well as GRB 080928 occurred at approximately the same redshift, the absolute magnitudes of their hosts differed by about 1 mag in *R* at least, since there is only an upper limit for 080928 host. The offset of GRB 080514B from its host galaxy was  $2.6 \pm 1.7$  kpc, therefore it was quite small, in agreement with other studies (e.g., Kann et al. 2011). However, in case of GRB 080928, the closest visible galaxy would be at a projected distance of  $22.6 \pm 2.6$  kpc, a difference by nearly a factor of 10. This argument, together with analysis of the SED of the objects closest to the afterglow which lead to redshift solutions not in agreement with the afterglow one, showed that no visible galaxy can be associated with GRB 080928. The following Chapter 5 deals with bursts where no optical afterglow was detected at all and hence only arcsec-sized X-ray error circles are known. Contrary to the main GRB population with detected optical afterglows in such cases only host galaxy candidates can be identified.

## Chapter 5

# Host galaxies of dark GRBs

The previous two chapters were devoted to GRBs that developed well-observed optical/NIR afterglows. In other words, they could be localized to the sub-arcsec scale. Here, I now report on the results of a search for the potential GRB host galaxies (in the following GRBHs) of a sample of 18 bursts with no detected optical/NIR afterglow, i.e., dark GRBs (see also Sects. 2.3.4 and 2.4.2). The absence of optical detection implies that it was not possible to determine the redshift of these 18 GRBs. All bursts in the sample have a detected X-ray afterglow with an error circle between  $1''$  and  $6''$  in radius and all have an observed duration in the *Swift*/BAT energy window of  $T_{90} > 2$  seconds (i.e., long GRBs; Kouveliotou et al. 1993). In nine of these 18 cases *Swift*/UVOT started observing the field within some dozen seconds or a few minutes after the corresponding GRB trigger, but no afterglow could be found. All events were followed-up with ground-based optical/NIR telescopes, sometimes with response times as short as only minutes after the corresponding burst and no afterglow was detected. If there were optical afterglows, then they must have been very faint with respect of the average brightness of the well-observed long GRB afterglows known so far (Kann et al. 2010).

Most observations reported here were performed with the VLT 8.2-m telescopes. In addition, I re-analyzed several rapid response observations of some of these events performed with the multi-channel imager GROND mounted at the 2.2-m telescope on La Silla. By looking deep into the X-ray error circles, the main questions are: (i) which are the likely host galaxy candidates, what are their coordinates and angular sizes, their  $R$ ,  $K$ -band magnitudes and colors, what are their morphological shapes and is there potential evidence for galaxy-galaxy interactions? (ii) What is the main reason for the optical dimness of the corresponding afterglows? Could it have been high redshift or is it extinction by dust in the GRB host galaxy, which is generally thought to be more likely?

Given that long bursts are related to the death of very massive stars, of particular interest are very dusty galaxies. Spiral galaxies have a maximum  $(R - K)_{AB}$  color of about 3.5 mag ( $\sim 5.2$  mag in the Vega system) before the Lyman dropout at high  $z$  comes into play. Galaxies with a larger  $(R - K)_{AB}$  color are therefore of special interest. These galaxies are usually called extremely red objects (EROs) and they were first addressed in the context of deep NIR surveys (Elston et al. 1988). Recent work show that the host galaxies of most dust-extinguished dark GRBs, can be very red or they have highly obscured regions where the GRB progenitor resides (e.g., Perley et al. 2009; Krühler et al. 2011). To date, a handful of GRB hosts are known to be EROs, and in all cases they are the hosts of dark GRBs: 020127 (Berger et al. 2007), 030115 (Levan et al. 2006a), 080325 (Hashimoto et al. 2010), 080607 (Chen et al. 2010, 2011). With this thesis, and in Rossi et al. (2011a), I increase the known number of EROs hosting GRBs. In Hunt et al. (2011) we have recently shown that one of the EROs discussed in this Chapter is indeed not only an extremely red object, but also a very massive dust-obscured galaxy.

Table 5.1: *Characterization of the GRB fields studied in Chapter 5.*

#	GRB	$T_{90}$ seconds	R.A., Dec. (J2000) XRT	error arcsec	Galactic coordinates ( $l, b$ ) degrees	$E(B - V)$ mag
1	050717	85	14:17:24.44, -50:32:00.5	1.5	316.61, 10.04	0.238
2	050922B	150.9	00:23:13.39, -05:36:18.0	1.7	104.35, -67.45	0.037
3	060211A	126.3	03:53:32.59, +21:29:19.1	1.5	169.74, -24.40	0.192
4	060805A	5.3	14:43:43.45, +12:35:11.6	1.6	9.53, 59.97	0.024
5	060919	9.1	18:27:41.74, -51:00:52.5	1.7	343.87, -17.50	0.071
6	060923B	8.6	15:52:46.68, -30:54:13.7	1.8	342.74, 17.61	0.148
7	061102	45.6	09:53:37.84, -17:01:26.0	2.9	253.43, 28.29	0.042
8	070429A	163.3	19:50:48.93, -32:24:17.6	2.1	8.06, -25.90	0.170
9	070517A	7.6	18:30:28.93, -62:17:51.7	2.1	332.76, -21.47	0.152
10	080123	115	22:35:46.17, -64:54:02.7	1.7	323.07, -46.57	0.025
11	080207	340	13:50:02.99, +07:30:07.8	1.4	340.92, 65.95	0.023
12	080218B	6.2	11:51:49.75, -53:05:49.2	1.6	293.94, 8.73	0.174
13	080602	74	01:16:42.18, -09:13:55.7	1.7	142.56, -71.13	0.028
14	080727A	4.9	13:53:33.76, -18:32:40.9	1.6	322.88, 41.91	0.073
15	080915A	14	01:11:47.63, -76:01:13.1	3.7	301.30, -41.04	0.049
16	081012	29	02:00:48.21, -17:38:18.1	1.8	185.87, -71.40	0.023
17	081105	~ 10	00:15:48.50, +03:28:15.5	4.8	105.87, -58.22	0.029
18	081204	~ 20	23:19:09.13, -60:13:31.7	5.3	321.96, -53.36	0.028

Notes: (1) The *Swift*/XRT positions for GRB 061102 and GRB 070517A are from N. Butler's webpage ([http://astro.berkeley.edu/~nat/swift/xrt\\_pos.html](http://astro.berkeley.edu/~nat/swift/xrt_pos.html)) (Butler 2007). The XRT position for GRB 080915A, GRB 081105, and GRB 081204 are from Oates et al. (2008b), Beardmore & Cummings (2008), and Mangano et al. (2008a), respectively. All other XRT data are from [http://www.swift.ac.uk/xrt\\_positions/index.php](http://www.swift.ac.uk/xrt_positions/index.php). (2) The burst duration,  $T_{90}$ , was mostly taken from <http://heasarc.gsfc.nasa.gov/docs/swift/archive/grbtable/>. For GRB 081105 the reference is Cummings et al. (2008), for GRB 080727A it is McLean et al. (2008), and for GRB 081204 it is Götz et al. (2008). (3)  $E(B - V)$  was obtained from the NASA Extragalactic Database Coordinate Transformation and Extinction calculator at <http://nedwww.ipac.caltech.edu/forms/calculator.html>.

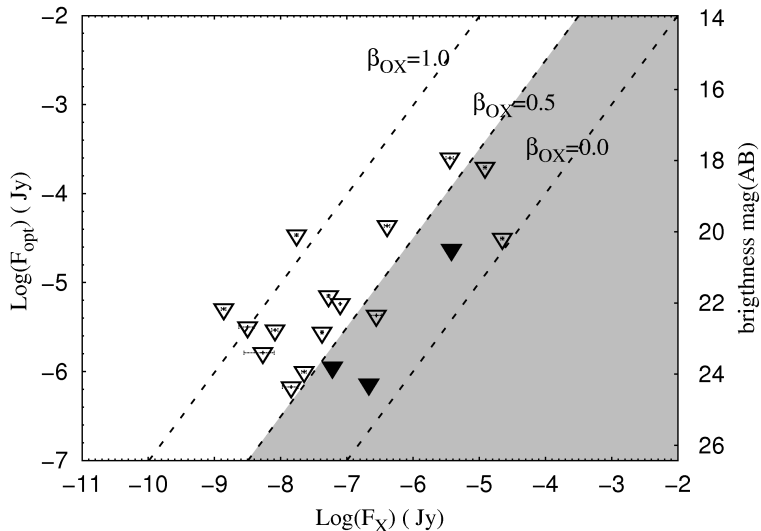
## 5.1 The GRB sample

The input sample consists of bursts detected by *Swift*/BAT (Barthelmy et al. 2005a) in the years 2005 (when *Swift*/XRT started flight-localizing GRBs) to 2008. These events are selected from a sample of bursts which share the following properties: (1) a detected X-ray afterglow by *Swift*/XRT with an error circle of less than 6 arcsec radius;<sup>1</sup> (2) a non-detected optical/NIR afterglow and optical upper limits at the faint end of the known brightness distribution of GRB afterglow light curves (see below); (3) a Galactic visual extinction  $A_V$  of less than 1 mag along the line of sight in order to avoid large Galactic extinction uncertainties and to avoid crowded stellar fields; (4) visibility from ESO La Silla and Paranal.

Altogether 45 events fulfill these criteria. This sample size is big, however, and had to be reduced

<sup>1</sup>The input here is based on the official XRT enhanced positions at [http://www.swift.ac.uk/xrt\\_positions/index.php](http://www.swift.ac.uk/xrt_positions/index.php). If an XRT position was not available there, I used the positions published on N. Butler's web-page [www page http://astro.berkeley.edu/~nat/swift/xrt\\_pos.html](http://astro.berkeley.edu/~nat/swift/xrt_pos.html), or I made use of other references.

Figure 5.1: **Jakobsson plot:** Observed upper limits in the  $R_C$  band compared to the measured flux density at 1.73 keV (the logarithmic mean of the Swift/XRT window, 0.3–10 keV) for the 18 bursts in this sample. The bursts falling in the gray area fulfill the JO4 criterion (Sect. 2.3.4). Unfortunately, some of them cannot be surely classified due to complications in the analysis (see Sect. 5.1.2). The bursts entering the golden dark burst subsample are marked with a filled black triangle.



to 18 due to constraints given by the available telescope time on the ESO/VLT. All these 18 bursts have reported upper limits on their optical afterglow magnitudes that lie at least 1.5 mag below the mean value of the afterglow brightness distribution in the sample of Kann et al. (2010). All upper limits are such that they characterize these afterglows as being fainter in  $R$  than about 80% of all afterglows with known redshift for the given observing time after the corresponding burst. The observed GRB fields are summarized in Table 5.1, further details are given in Appendix C.1.

Deep follow-up observations of 16 of these 18 XRT error circles were performed with VLT/FORS1, FORS2, VIMOS, ISAAC, and HAWK-I in the years 2008 to 2010, months to years after the corresponding burst (Table C.2). Limiting AB magnitudes were typically  $R_C=26.5$  and  $K_s=23.5$ . In the case of GRB 050717 and GRB 060211A multi-band imaging was performed using GROND on La Silla and the near-infrared imager NEWFIRM mounted on the 4-m Mayall telescope at Kitt Peak National Observatory. In the case of GRB 081204, a late  $J$ -band observation was obtained using NTT/SOFI on La Silla.

### 5.1.1 Optical/NIR data analysis of ESO/VLT and GROND observations

VLT, GROND, and NEWFIRM data were reduced using IRAF tasks<sup>2</sup> and analyzed through point-spread function (PSF) and aperture photometry using DAOPHOT and APPHOT (Tody 1993). The procedure is mainly based on the pipeline written to reduce GROND data (e.g., Krühler et al. 2008). Aperture photometry, if not otherwise specified, was performed by using an aperture diameter of twice the Full Width Half Maximum (FWHM) of the stellar PSF. ISAAC, HAWK-I and GROND NIR fields were calibrated using 2MASS field stars. VLT optical data were calibrated on standard star fields for the Vega photometric system, while the calibration performed for the optical  $g'r'i'z'$  images of GROND used SDSS stars (Table C.2).

### 5.1.2 Optical and X-ray data to define a golden dark burst subsample

Following the discussion in Section 2.3.4, if a burst is dark and fulfills both the criteria of Jakobsson et al. (2004) and van der Horst et al. (2009) (in the following J04 and V09, respectively), then the

<sup>2</sup><http://iraf.noao.edu>

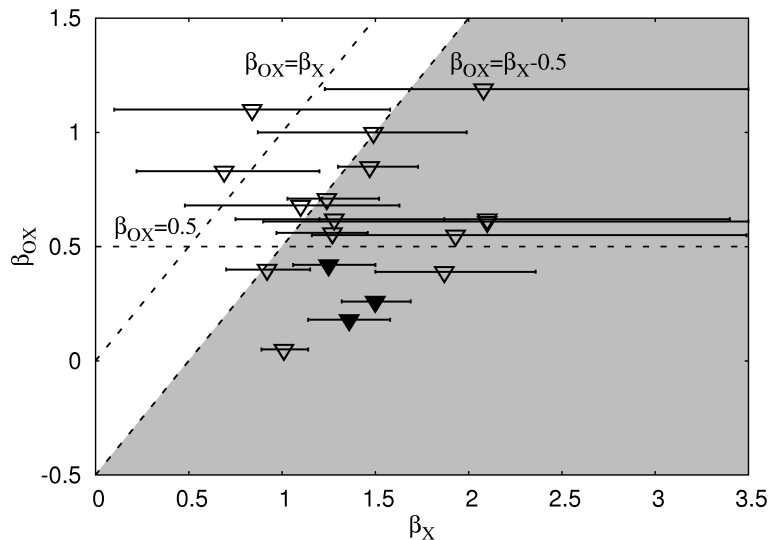


Figure 5.2: **Van der Horst plot:** Deduced upper limits for the spectral slope  $\beta_{\text{OX}}$  compared to the measured spectral slope of the afterglow in the X-ray band. The bursts falling in the gray area fulfill the V09 criterion (Sect. 2.3.4). Here  $\beta_{\text{OX}} = 0.5$  is highlighted in order to compare with the J04 criterion (Fig. 5.1). The bursts entering the golden dark burst subsample are marked with a filled black triangle.

dimness of the optical flux must be caused either by dust extinction or by high redshift, or a mixture of both. If the JO4 and V09 criteria are not fulfilled, then the optical upper limits are not deep enough to test if dust extinction or high redshift was the reason for the dimness of the optical flux, and low brightness (see Sect. 2.3.4) could also be the reason for the dark nature of the corresponding burst.

When estimating the minimum optical flux based on the observed X-ray flux, i.e. assuming the case  $\nu_c = \nu_X$ , here and in the following I set  $\nu_X = 1.73$  keV, which is the logarithmic mean of the *Swift*/XRT window (0.3 – 10 keV). Even though the X-ray window of *Swift* starts at 0.3 keV, here the flux is strongly affected by gas absorption, which produces a relatively large uncertainty. Therefore, I preferred a more conservative approach and set  $\nu_X = 1.73$  keV, having in mind that for  $\nu_X = 0.3$  keV even more bursts of my sample could fulfill JO4 and V09 criteria.

X-ray light curve data were taken from the *Swift*/XRT GRB light curve repository and spectroscopic data from the *Swift*/XRT GRB spectrum repository (Evans et al. 2007, 2009) and corrected for Galactic absorption. For the computation of  $\beta_{\text{OX}}$  I used the upper limits in the  $R_C$  band. When no  $R_C$ -band upper limits were available, I used the deepest upper limit obtained in the filter with the longer wavelength. Having the flux density  $F_{\nu, X} [\text{Jy}]$  at the frequency  $\nu_X$ , and the flux density  $F_{\nu, \text{opt}} [\text{Jy}]$  corresponding to the optical  $R_C$ -band upper limit, I used these values to obtain  $\beta_{\text{OX}}$ :

$$\beta_{\text{OX}} = \log \left( \frac{F_{\nu, X}}{F_{\nu, \text{opt}}} \right) / \log \left( \frac{\nu_{\text{opt}}}{\nu_X} \right). \quad (5.1)$$

The two flux densities must to be obtained at the same time, therefore the X-ray value is derived after fitting the X-ray light curve. In doing so, I focused on those time intervals where the X-ray light curves were smoothly decaying, which is different from burst to burst. Table 5.2 summarizes the properties of the 18 bursts considered here, where I defined the parameter

$$\Delta = \beta_X - \beta_{\text{OX}} - 0.5. \quad (5.2)$$

In particular, I used the minimum value  $\Delta_{\text{min}}$  based on the 90% confidence error of  $\beta_X$ . If  $\Delta_{\text{min}} > 0$  then a burst fulfills the V09 criterion (Table 5.2).

Then the value  $\Delta$  equals the amount of spectral slope that is missing in order to join the X-ray with the optical observations, assuming a break at  $\nu_c = \nu_X$ . It can be translated into a missing flux density in the optical bands (see also Rol et al. 2005 who extensively applied this approach). In



Table 5.2: Summary of the darkness properties of the sample of 18 bursts considered here.

#	GRB	Time (s)	UL	Filter	UL <sub>R</sub>	Ref.	$\beta_{\text{OX}}$	$\beta_{\text{X}}$	$\Delta_{\text{min}}$	Comments
(1)	(2)	(3)	(4)	(5)	(6)	(7)	(8)	(9)	(10)	(11)
1	050717	420	19.0	$\nu$	18.2	GCN 3638	< 0.40	$0.92^{+0.23}_{-0.22}$	-0.20	a; b
2	050922B	49000	22.5	$r'$	22.3	GCN 4025	< 0.39	$1.87^{+0.49}_{-0.37}$	0.61	c
3	060211A	19980	22.0	$R_C$	21.8	GCN 4927	< 0.71	$1.24^{+0.28}_{-0.21}$	-0.18	-
4	060805A	63000	22.9	$r'$	22.7	GCN 5406	< 1.00	$1.49^{+0.50}_{-0.62}$	-0.63	-
5	060919	918	20.2	$\nu$	19.8	GCN 5580	< 0.68	$1.10^{+0.53}_{-0.62}$	-0.70	a
6	060923B	295	18.5	$\nu$	17.9	GCN 5603	< 0.62	$1.28^{+0.59}_{-0.53}$	-0.37	b
7	061102	1480	20.5	$\nu$	20.1	GCN 5784	< 1.10	$0.84^{+0.74}_{-0.74}$	-1.50	d
8	070429A	44064	24.0	$R_C$	23.8	GCN 6371	< 0.42	$1.25^{+0.25}_{-0.19}$	0.14	•; g
9	070517A	57600	24.5	$i'$	24.3	GCN 6420	< 0.56	$1.27^{+0.19}_{-0.30}$	-0.09	f
10	080123	58732	22.6	$\nu$	22.2	UVOT	< 1.19	$2.08^{+1.42}_{-0.85}$	-0.46	b; d; h; i
11	080207	5364	20.3	$R_C$	20.5	GCN 7333	< 0.26	$1.50^{+0.19}_{-0.18}$	0.56	•
12	080218B	11520	24.7	$r'$	24.3	Table C.3	< 0.18	$1.36^{+0.22}_{-0.22}$	0.46	•
13	080602	504	20.3	$\nu$	20.2	GCN Rep. 145.1	< 0.05	$1.01^{+0.13}_{-0.12}$	0.34	e
14	080727A	2268	19.8	$K$	22.8	GCN 8048	< 0.85	$1.47^{+0.26}_{-0.17}$	-0.05	-
15	080915A	6840	22.1	$I_C$	22.1	GCN 8248	< 0.62	$2.10^{+1.30}_{-0.90}$	0.08	d
16	081012	69660	23.5	$r'$	23.4	Table C.3	< 0.83	$0.69^{+0.51}_{-0.47}$	-1.11	-
17	081105	46224	23.0	$r'$	22.8	Table C.3	< 0.61	$2.10^{+1.70}_{-1.20}$	-0.21	d
18	081204	34560	24.1	$r'$	23.9	Table C.3	< 0.55	$1.93^{+1.56}_{-0.77}$	0.11	d

Notes: *Columns:* (3 to 5) Time after the burst and reported upper limits (UL) of the afterglow (observed magnitudes);  $r'$ -band magnitudes are given in the AB system, all others in the Vega/UVOT system. (6) Deduced UL in the  $R_C$  band (AB system) after correcting for Galactic extinction and shifting from the native filter wavelength (column 5) to the  $R_C$  band using the upper limit on  $\beta_{\text{OX}}$ . (8) If  $\beta_{\text{OX}} < 0.5$  then a burst fulfills the J04 criterion. (10) The minimum value (based on the 90% confidence error of  $\beta_{\text{X}}$ ) of the quantity  $\Delta = \beta_{\text{X}} - \beta_{\text{OX}} - 0.5$ . If  $\Delta_{\text{min}} > 0$  then a burst fulfills the V09 criterion. (11) (a) During the time of the observed UL the SED in the X-ray band is not constant. (b) The observed UL lies close to the end of the prompt GRB phase. (c) No X-ray data exist at the time when the UL was obtained. (d) Very faint X-ray flux; no well-defined X-ray light curve. (e) Flat X-ray light curve during the time when the UL was obtained. (f) The optical afterglow was detected; see Sect. 5.2.1. (g) No UL is reported in the corresponding GCN (Price 2007). We used  $R_C = 24.0$  based on the original data which are available in the Gemini archive. (h) This burst is a possible short GRB (see Sec. C.1). (i) Reference for 080123 upper limit comes from the automated UVOT messages webpage at [http://heasarc.gsfc.nasa.gov/docs/swift/uvot\\_tdrss/301578](http://heasarc.gsfc.nasa.gov/docs/swift/uvot_tdrss/301578). A bullet (•) indicates that the burst entered our golden dark burst sample (Sect. 5.1.2). *Column 7, References:* (1.) Blustin et al. 2005; (2.) Guziy et al. 2005; (3.) Sharapov et al. 2006; (4.) Rol & Page 2006; (5.) Breeveld & Guidorzi 2006; (6.) Holland & Cucchiara 2006; (7.) Holland 2006; (8.) Price 2007; (9.) Fox et al. 2007; (10.) Cucchiara & Ukwatta 2008; (11.) Andreev et al. 2008; (13.) Beardmore et al. 2008e; (14.) Levan & Wiersema 2008; (15.) Rossi et al. 2008b

Table 5.3 I summarize the results obtained using this method, where the flux densities in the optical are transformed into AB magnitudes. Altogether 8 of the 18 bursts considered here meet either the J04 or the V09 criterion. Among them, 5 events, namely GRB 050922B, GRB 070429A, GRB 080207, GRB 080602, and GRB 080218B, fulfill both criteria, while GRB 050717 fulfills only the J04 criterion and GRB 080915A as well as GRB 081204 fulfill only the V09 criterion (Figures 5.1 and 5.2).

However, some caution is required. At the time when the optical upper limits were obtained some shortcomings can limit the validity of this approach: (1) an X-ray light curve that is rather flat than decaying might point to an additional X-ray component and hence call the aforementioned theoretical relations for a single radiation component into question (GRB 080602); (2) a gap in the X-ray data base (GRB 050922B); (3) an evolving X-ray spectral slope (GRB 050717); (4) or a large measurement error ( $> 1$ ) of the X-ray spectral slope (GRB 080915A, GRB 081105, GRB 081204). Only three events in the sample of 18 bursts can be considered as securely fulfilling the J04 and V09

Table 5.3: Summary of the optical flux extrapolated from X-ray observations.

#	GRB	Time (s)	R-band UL	X-ray $F_{\nu_X}$ [Jy]	$\beta_X$	$R_C$ ( $\nu_c = \nu_X$ )	$R_C$ ( $\nu_c = \nu_{\text{opt}}$ )
(1)	(2)	(3)	(4)	(5)	(6)	(7)	(8)
1	050717	420	>18.2	$1.22 \pm 0.06 \times 10^{-5}$	$0.92^{+0.23}_{-0.22}$	$18.2^{+1.6}_{-1.7}$	$14.5^{+1.6}_{-1.7}$
2	050922B	49000	>22.3	$2.78 \pm 0.54 \times 10^{-7}$	$1.87^{+0.49}_{-0.37}$	$14.8^{+2.7}_{-3.7}$	$11.1^{+2.7}_{-3.7}$
3	060211A	19980	>21.8	$5.28 \pm 0.24 \times 10^{-8}$	$1.24^{+0.28}_{-0.21}$	$21.9^{+1.5}_{-2.2}$	$18.1^{+1.5}_{-2.2}$
4	060805A	63000	>22.7	$3.16 \pm 0.83 \times 10^{-9}$	$1.49^{+0.50}_{-0.62}$	$22.8^{+3.5}_{-4.5}$	$19.1^{+3.5}_{-4.5}$
5	060919	918	>19.8	$4.06 \pm 0.37 \times 10^{-7}$	$1.10^{+0.53}_{-0.62}$	$20.4^{+3.7}_{-4.5}$	$16.7^{+3.7}_{-4.5}$
6	060923B	295	>17.9	$3.60 \pm 0.46 \times 10^{-6}$	$1.28^{+0.59}_{-0.53}$	$16.5^{+3.7}_{-4.4}$	$12.8^{+3.7}_{-4.4}$
7	061102	1480	>20.1	$1.74 \pm 0.10 \times 10^{-8}$	$0.84^{+0.75}_{-0.71}$	$26.1^{+5.2}_{-5.6}$	$22.3^{+5.2}_{-5.6}$
8	070429A	44064	>23.8	$6.05 \pm 0.48 \times 10^{-8}$	$1.25^{+0.25}_{-0.19}$	$21.0^{+1.4}_{-1.9}$	$17.3^{+1.4}_{-1.9}$
9	070517A	57600	>24.3	$1.44 \pm 0.38 \times 10^{-8}$	$1.27^{+0.19}_{-0.30}$	$22.5^{+2.2}_{-1.5}$	$18.8^{+2.2}_{-1.5}$
10	080123	58732	>22.2	$1.38 \pm 0.11 \times 10^{-9}$	$2.08^{+1.42}_{-0.85}$	$19.1^{+5.9}_{-10.4}$	$15.4^{+5.9}_{-10.4}$
11	080207	5364	>20.5	$3.80 \pm 0.08 \times 10^{-6}$	$1.50^{+0.19}_{-0.18}$	$15.0^{+1.3}_{-1.4}$	$11.3^{+1.3}_{-1.4}$
12	080218B	11520	>24.3	$2.15 \pm 0.32 \times 10^{-7}$	$1.36^{+0.22}_{-0.21}$	$18.9^{+1.6}_{-1.6}$	$15.1^{+1.6}_{-1.6}$
13	080602	504	>20.2	$2.23 \pm 0.12 \times 10^{-5}$	$1.01^{+0.13}_{-0.12}$	$16.7^{+0.9}_{-1.0}$	$13.0^{+0.9}_{-1.0}$
14	080727A	2268	>22.8	$8.20 \pm 0.86 \times 10^{-9}$	$1.47^{+0.26}_{-0.17}$	$21.7^{+1.3}_{-1.9}$	$17.9^{+1.3}_{-1.9}$
15	080915A	6840	>22.1	$7.93 \pm 0.09 \times 10^{-8}$	$2.10^{+1.30}_{-0.90}$	$14.7^{+6.7}_{-9.7}$	$11.0^{+6.7}_{-9.7}$
16	081012	69660	>23.4	$5.38 \pm 2.59 \times 10^{-9}$	$0.69^{+0.51}_{-0.47}$	$28.1^{+3.5}_{-3.8}$	$24.4^{+3.5}_{-3.8}$
17	081105	46224	>22.8	$4.22 \pm 0.16 \times 10^{-8}$	$2.10^{+1.70}_{-1.20}$	$15.4^{+8.1}_{-12.6}$	$11.7^{+8.1}_{-12.6}$
18	081204	34560	>23.9	$2.26 \pm 0.18 \times 10^{-8}$	$1.93^{+1.56}_{-0.77}$	$17.3^{+5.7}_{-11.2}$	$13.8^{+5.7}_{-11.2}$

Notes: Columns (3) and (4) Time after the burst and reported upper limits (UL). They are the same as columns (3) and (6) in Table 5.2. (5) X-ray Flux density at 1.73 keV in units of *Jansky*. (6)  $\beta_X$  reported from Table 5.2. (7)  $R_C$ -band (AB magnitudes) extrapolated from the X-ray flux assuming a break at  $\nu_c = \nu_X$ . (8)  $R_C$ -band (AB magnitudes) extrapolated from the X-ray flux assuming a break at  $\nu_c = \nu_{\text{opt}}$ . The *V09 criteria* is fulfilled if the upper limit (4) is higher within the errors than the predicted magnitude in the case of  $\nu_c = \nu_X$  (column 7).

criteria (GRB 070429A, GRB 080207A, GRB 080218B). I consider them as the *golden dark burst subsample* (Figs. 5.1, 5.2).

As explained above, among the 8 events which fulfill the J04 and V09 criteria, for 5 bursts the JO4 and V09 criteria might not be applicable, while for the remaining 10 events the optical follow-up observations were not deep enough to decide if, according to synchrotron theory, the optical flux was too small compared to the observed X-ray flux. Therefore, it is not possible to conclude with certainty which was the reason for the dimness of the optical flux. Nevertheless, the precise X-ray localization of their afterglows on the one hand, but the non-detection of their corresponding optical counterparts on the other hand, puts all of them into the same phenomenological class: these are dark GRBs. The task then is to figure out for each case what might have been the potential GRBH then. Is there at least one galaxy detectable within such a small X-ray error circle? And if there is more than one galaxy in such an error circle, is one of them special in some sense? The basic idea is: even if the JO4 and the V09 criteria could not be applied for these remaining 10 events, do perhaps the observed properties of their suspected GRBHs point to the possibility that either high redshift (Lyman dropout) or high extinction might have affected the corresponding optical afterglow?

## 5.2 Detailed overview of the ESO/VLT and GROND observations

In the following I report the result of our observations for each GRB field. The results are summarized in Tables 5.4, 5.5 and 5.6. Finding charts are provided in Figs. C.2, C.3, and C.4.

If not stated otherwise, in the following  $R_C$ ,  $K$  magnitudes and colors are given in the AB magnitude system, in order to allow for a direct comparison with data of confirmed GRB host galaxies, i.e. those identified via the subarcsecond accurate optical afterglow detections) compiled by Savaglio et al. (2009, in the following SBG09). All  $(R_C - K)$  colors are corrected for Galactic extinction, estimated using the extinction maps published by Schlegel et al. (1998). Thereby, the following transformations were used: (1) FORS1:  $R_{AB} = R_{Vega} + 0.23$  mag (Klose et al. 2004), and I assumed that this holds also for FORS2 and VIMOS; (2) ISAAC:  $K_{AB} = K_{s,Vega} + 1.86$  mag (Klose et al. 2004), and I used this transformation also for HAWK-I and NEWFIRM. I further assumed that all  $R$ -band filters correspond to the  $R_C$  band. For GROND the Vega to AB conversion is  $K_{AB} = K_{s,Vega} + 1.80$  mag, except for observations after an intervention on the instrument on March 2008, for which  $K_{AB} = K_{s,Vega} + 1.86$  mag. Extinction corrections for the GROND filters are:  $A(g') = 1.253 A_V$ ,  $A(r') = 0.799 A_V$ ,  $A(i') = 0.615 A_V$ ,  $A(z') = 0.454 A_V$ ,  $A(J) = 0.292 A_V$ ,  $A(H) = 0.184 A_V$ ,  $A(K) = 0.136 A_V$ , while for all other instruments it was assumed the standard values  $A(R_C) = 0.748 A_V$ ,  $A(K) = 0.112 A_V$  (Rieke & Lebofsky 1985). It was always set  $A_V = 3.1 E(B - V)$ .

Following Bloom et al. (2002) and Perley et al. (2009), for every object it was calculated the probability  $p$  of finding a galaxy of any type of the given (extinction-corrected)  $R_C$ -band magnitude  $m$  in a region of radius  $r$ , where  $r$  is the radius of the associated error circle. It is

$$p(m) = 1 - \exp(-\pi r^2 \sigma(\leq m)), \quad (5.3)$$

where  $\sigma(\leq m)$  is the surface density of galaxies with magnitudes  $\leq m$ . If the object I have found is located within the 90% XRT error circle of radius  $r_0$ , then I set  $r = r_0$ , if it is placed within  $[r_0, n r_0]$ , then I set  $r = n r_0$ . The input for  $\sigma(\leq m)$  is the relation derived by Hogg et al. (1997), which is based on galaxy counts down to about  $R_{Vega} = 26.5$ . In addition, in the case of EROs, number counts of these galaxies are available now too (Gonzalez-Perez et al. 2009; Hempel et al. 2011; Kim et al. 2011), and will be used in equation 5.3 to calculate the probability  $p$  of finding a ERO of the given magnitude, in the same way explained above.

### 5.2.1 Notes for individual targets

**GRB 050717** The burst occurred at relatively low Galactic latitude ( $b = 10^\circ$ ), and the field is relatively crowded with stars. The foreground Galactic reddening is moderate,  $E(B - V) = 0.24$  mag, the highest in the sample. The 90% XRT error circle radius is very small ( $r_0 = 1''.5$ ; Fig. C.2).

The field was observed with GROND two years after the burst. Within the 90% XRT error circle two extended objects (A and B) are visible in the  $r'i'z'$ -band images (Fig. 5.3). Object A ( $R_{AB} = 23.6$ ) has a size of about  $2''.1 \times 3''.9$ . Based on its visual appearance this might be a faint galaxy. It extends into the 90% XRT error circle. The fainter object B ( $R_{AB} = 24.5$ ) lies at the southern boundary of the error circle. Neither object is detected in  $g'$  and also not seen in the NIR bands (Table 5.5). Given the non-detection in the NIR ( $K_{AB} > 22.1$ ), for both objects only an upper limit for  $(R - K)_{AB}$  can be given ( $< 2.6$  mag and  $< 3.4$  mag, respectively).

Assuming that A and B are galaxies, the probability  $p$  of finding a galaxy of the given  $R_C$ -band magnitude in the 90% XRT error circle is about 0.08 and 0.16, respectively. I consider both objects as potential GRB host galaxy candidates.

Table 5.4: Summary of the photometry of all objects found in the XRT error circles based on the VLT observations.

# GRB	Object	R.A., Dec. (J2000)	$R_{AB}$	$K_{AB}$	UL <sub>R</sub> UL <sub>K</sub>	$R_{AB} - K_{AB}$	Pos
2 050922B	A	00:23:13.36, -05:36:18.3	~26.5	>22.8	26.5 22.8	<3.7	1
5 060919	A	18:27:41.78, -51:00:51.0	26.14(24)	>23.4	26.5 23.4	<2.7	1
6 060923B	A <sup>a</sup>	15:52:46.49, -30:54:12.3	23.10(11)	21.76(09)	26.6 24.3	1.34(14)	2
	B <sup>a</sup>	15:52:46.61, -30:54:10.3	21.67(02)	18.95(03)	26.6 24.3	2.72(03)	2
	C <sup>a</sup>	15:52:46.56, -30:54:14.6	24.49(04)	22.87(15)	26.6 24.3	1.62(16)	1
	D <sup>a</sup>	15:52:46.63, -30:54:16.4	25.74(12)	21.63(06)	26.6 24.3	4.11(13)	2
	E <sup>a</sup>	15:52:46.66, -30:54:12.9	blended with A	blended with A	26.6 24.3	-	1
7 061102	A	09:53:37.93, -17:01:22.7	24.10(06)	>22.8	26.9 22.8	<1.3	2
	B	09:53:37.89, -17:01:30.8	23.96(06)	>22.8	26.9 22.8	<1.2	2
8 070429A	A	19:50:48.78, -32:24:13.6	25.01(20)	22.57(25)	26.5 23.8	2.44(32)	2
	B <sup>a</sup>	19:50:48.78, -32:24:18.1	24.14(09)	22.39(21)	26.5 23.8	1.75(23)	1
	C <sup>a</sup>	19:50:48.90, -32:24:17.4	24.32(08)	21.89(14)	26.5 23.8	2.43(16)	1
9 070517A	A	18:30:29.08, -62:17:53.0	25.39(21)	>23.4	26.6 23.4	<2.0	1
10 080123	A	22:35:46.18, -64:54:04.1	25.52(17)	>23.3	27.0 23.3	<2.2	1
	B	22:35:45.73, -64:54:03.8	25.73(20)	>23.3	27.0 23.3	<2.4	2
	C	22:35:46.92, -64:53:55.1	21.01(01)	19.60(01)	27.1 23.6	1.41(01)	5
	D	22:35:45.48, -64:53:56.4	23.49(09)	>23.3	27.1 23.6	<-0.1	5
11 080207	A	13:50:03.03, +07:30:09.3	25.15(17)	23.02(39)	26.9 23.6	2.13(42)	2
	B	13:50:02.97, +07:30:07.2	26.49(37)	21.77(14)	26.9 23.6	4.72(40)	1
12 080218B	A	11:51:49.69, -53:05:49.1	26.23(13)	21.74(10)	27.3 24.0	4.49(16)	1
	B	11:51:50.00, -53:05:47.4	24.62(04)	22.74(24)	27.3 24.0	1.88(24)	2
13 080602	A	01:16:42.15, -09:13:55.0	22.95(02)	22.55(05)	26.9 23.5	0.40(05)	1
	B	01:16:42.12, -09:13:57.5	24.00(06)	>23.5	26.9 23.5	<0.5	2
	C	01:16:42.14, -09:13:53.4	>26.9	22.49(14)	26.9 23.5	>4.4	2
14 080727A	-	no candidates	>26.3	>23.0	26.3 23.0	-	
15 080915A	A	01:11:47.80, -76:01:13.9	21.63(01)	20.42(02)	26.3 23.4	1.21(02)	1
	B	01:11:45.27, -76:01:10.4	21.28(01)	19.19(01)	26.3 23.4	2.09(01)	3
	C <sup>a</sup>	01:11:47.47, -76:01:10.0	24.71(07)	>23.4	26.3 23.4	<1.3	1
	D <sup>a</sup>	01:11:46.98, -76:01:09.5	24.57(08)	>23.4	26.3 23.4	<1.2	2
	E <sup>a</sup>	01:11:47.16, -76:01:15.1	25.44(15)	>23.4	26.3 23.4	<2.0	1
16 081012	A	02:00:48.18, -17:38:15.2	25.16(17)	>23.9	26.7 23.9	<1.3	2
17 081105	A	00:15:48.46, +03:28:10.7	23.73(08)	22.78(18)	26.1 24.5	0.95(15)	1
	B	00:15:48.30, +03:28:13.8	24.34(13)	22.13(14)	26.1 24.5	2.21(19)	1
	C	00:15:48.42, +03:28:11.6	>25.3	21.74(13)	26.1 24.5	>3.56	1
18 081204	A <sup>b</sup>	23:19:09.39, -60:13:31.5	23.21(04)	22.37(16)	26.4 24.3	0.84(17)	1
	B <sup>a</sup>	23:19:09.13, -60:13:30.2	23.46(04)	21.59(08)	26.4 24.3	1.87(09)	1
	C	23:19:08.99, -60:13:23.4	23.16(07)	22.06(11)	26.4 24.3	1.10(13)	2
	D	23:19:08.89, -60:13:37.6	24.19(10)	22.16(15)	26.4 24.3	2.03(18)	2
	E	23:19:09.10, -60:13:39.4	24.32(12)	>24.3	26.4 24.3	<0.0	2
	F <sup>a</sup>	23:19:09.24, -60:13:29.4	24.65(50)	21.53(07)	26.4 24.3	3.12(50)	1
	G	23:19:08.30, -60:13:39.0	blended with a star	21.57(15)	26.4 24.3	-	2

Notes: GRB 050717, GRB 060211A, and GRB 060805A are the only bursts in our sample for which we do not have VLT data (see Table 5.5). Magnitudes and colors are not corrected for Galactic extinction. UL stands for upper limit. Magnitude errors are given in units of 10 mmag. The last column defines the distance of the object from the center of the 90% XRT error circle of radius  $r_0$ . A value  $n$  means that the source lies within  $r \leq nr_0$ . *Special notes about the photometry:* All magnitudes are based on (2× FWHM) aperture photometry, except for those cases where the object was affected by near-by objects. Then we used either (a) PSF photometry or (b) 1× FWHM aperture photometry. In particular, we gave preference to the latter in the case of elongated objects.

Table 5.5: Summary of the photometry of all objects found in the XRT error circles based on observations with GROND.

#	GRB	Obj.	R.A., Dec. (J2000)	$g'_{AB}$	$r'_{AB}$	$i'_{AB}$	$z'_{AB}$	$J_{AB}$	$H_{AB}$	$K_{AB}$	$r'_{AB} - K_{AB}$	Pos
1	050717	A	14:17:24.56, -50:31:58.7	> 25.4	23.65(10)	23.01(11)	23.40(30)	>22.6	>21.9	>21.1	<2.6	2
		B <sup>b</sup>	14:17:24.58, -50:32:01.6	> 25.4	24.50(40)	23.50(40)	22.80(30)	>22.6	>21.9	>21.1	<3.4	2
3	060211A	A	03:53:32.66, +21:29:19.8	> 25.2	24.51(20)	> 24.8	> 24.4	>22.8	>21.6	>21.6	<2.9	1
		B	03:53:32.43, +21:29:16.3	23.60(08)	23.09(06)	22.76(09)	23.31(10)	>22.8	>21.6	21.50(20)	1.59(21)	2
4	060805A	A	14:43:43.49, +12:35:12.5	>25.5	25.4(40)	> 24.6	> 24.2	>22.9	>21.8	>21.1	<4.3	1
		B	14:43:43.39, +12:35:10.1	23.42(16)	23.68(12)	> 24.6	> 24.2	>22.9	>21.8	>21.1	<2.6	2
11	080207	–	no candidates	>25.4	>24.9	>23.9	>23.8	>22.0	>20.8	>20.1	–	–
12	080218B	A	see Table 5.4	>25.5	>24.9	>24.2	>24.1	>22.8	>21.4	>21.2	–	1
		B	11:51:50.00, -53:05:47.4	25.10(30)	24.30(30)	–	23.27(10)	>22.8	>21.4	>21.2	<3.0	2
13	080602	A	01:16:42.15, -09:13:55.0	22.96(10)	22.93(08)	22.86(13)	22.60(14)	>21.4	>21.0	>20.6	<2.3	1
		B	01:16:42.12, -09:13:57.5	>25.3	23.73(12)	23.90(29)	22.97(17)	>21.4	>21.0	>20.6	<3.1	2
		C	see Table 5.4	>25.3	>25.5	>24.9	>24.6	>21.4	>21.0	>20.6	–	2
15	080915A	A	01:11:47.80, -76:01:13.9	22.05(10)	21.27(10)	21.21(10)	20.80(10)	20.53(02)	20.37(03)	20.39(15)	0.88(15)	1
		B	01:11:45.27, -76:01:10.4	23.30(30)	21.14(05)	20.88(06)	20.28(12)	19.74(06)	19.33(06)	19.00(08)	2.14(09)	3
		≥ C	see Table 5.4	>24.0	>24.3	>24.1	>23.9	>22.1	>21.3	>21.3	–	1
16	081012	–	no candidates	>23.8	>23.8	>23.4	>23.2	>21.8	>21.3	>21.0	–	–
17	081105	–	no candidates	>24.0	>23.9	>23.3	>22.9	>21.4	>20.7	>20.3	–	–
18	081204	A <sup>b</sup>	23:19:09.39, -60:13:31.5	23.69(10)	23.74(08)	23.25(11)	23.09(15)	>22.0	>21.6	>20.9	<2.8	1
		B <sup>b</sup>	23:19:09.13, -60:13:30.2	24.18(30)	23.74(08)	23.53(14)	23.29(17)	>22.0	21.67(26)	>20.9	<2.8	1
		C	23:19:08.99, -60:13:23.4	>25.0	23.96(17)	23.62(28)	>24.0	21.39(19)	>21.6	>20.9	<3.1	2
		≥ D	see Table 5.4	>25.0	>25.0	>24.7	>24.0	>22.0	>21.6	>20.9	<3.1	2

Notes: Magnitudes are not corrected for Galactic extinction. In case of GRB 060211A we report the NEWFIRM  $K_s$ -band results, while for GRB 080218B the  $i'$ -band data are affected by a ghost image from a bright star. *Special notes about the photometry:* (b) see Table 5.4.

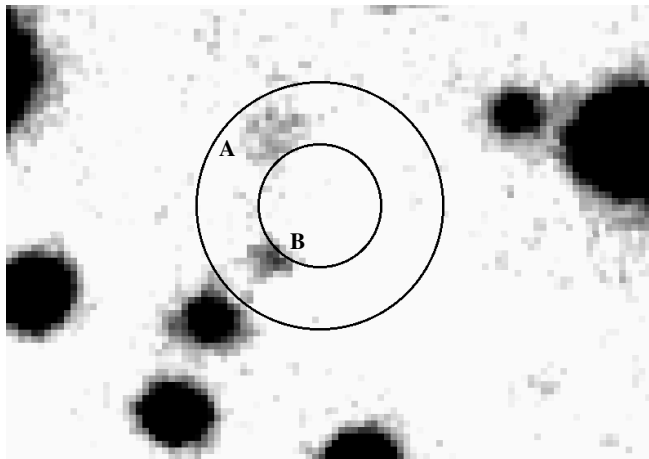


Figure 5.3: Combined GROND  $r'i'z'$ -band image of the field of GRB 050717, including the 90% XRT error circle ( $r_0 = 1''.5$ ) as well as an error circle of radius  $2r_0$ . The combined image shows the faint, extended object A. Here and in all finding charts shown in the following, North is up and East is left.

**GRB 050922B** The burst occurred at high Galactic latitude ( $b = -67^\circ$ ); the field is not crowded by stars. The foreground Galactic reddening is very small,  $E(B - V) = 0.04$  mag. The 90% XRT error circle is small,  $r_0 = 1''.7$  (Fig. C.2).

The field of GRB 050922B was observed with NEWFIRM in the  $K_s$ -band about 3 years after the burst. Additional data were obtained with FORS2 and ISAAC under good seeing conditions (a stellar FWHM of  $0''.7$ ) one year later.

Within the 90% XRT error circle a faint object (A;  $R_{AB} \sim 26.5$ ) emerges in the FORS2/ $R$ -band image, but it is close the detection limit. It is not visible in the NEWFIRM and the ISAAC NIR  $K_s$ -band images. No other object is detected within the  $2r_0$  XRT error circle down to  $3\sigma$  upper limits of  $R_{AB} > 26.5$  and  $K_{AB} > 22.8$ .

A galaxy (object G;  $R_{AB} \sim 24$ ;  $2''.5 \times 3''.0$ ) is located about  $5''.0$  southwest from the center of the XRT error circle at R.A., Dec. (J2000) = 00:23:13.56,  $-05:36:22.6$ , well outside the  $2r_0$  XRT error circle. The minimum distance between the center of this galaxy and the outer boundary of the 90% XRT error circle is  $3''.5$ , making it unlikely to be the GRB host galaxy.

Object A is very faint and, therefore, it is difficult to discern its morphology. If it is a galaxy, it is among the optically faintest GRB host galaxies known to date. The probability  $p$  of finding a galaxy of this  $R_C$ -band magnitude in the 90% XRT error circle is about 0.3. I consider this object as the GRB host galaxy candidate.

**GRB 060211A** The field of GRB 060211A lies at relatively low Galactic latitude ( $b = -24^\circ$ ) but it is not crowded with stars. The foreground Galactic reddening is moderate,  $E(B - V) = 0.19$  mag. The 90% XRT error circle is very small ( $r_0 = 1''.5$ ; Fig. C.2).

The field was observed 1.5 and 3 years after the burst with GROND and NEWFIRM ( $J$  and  $K$ ), respectively. In the 90% XRT error circle I find one object (A) in the GROND  $r'$  band, which looks slightly extended in N-S direction ( $1''.1 \times 1''.2$ ). The object is not visible in the other GROND bands. Complementary NEWFIRM observations did not detect any object down to  $J_{AB} = 23.6$  and  $K_{AB} = 21.6$  either. Therefore, only an upper limit on the  $(R - K)_{AB}$  color of object A can be given ( $< 2.5$  mag).

In addition to A, an extended fuzzy object (B) is located S-E of the doubled ( $r = 2r_0$ ) XRT error circle, about  $4''.0$  away from the center of the error circle (see Fig. C.2). This object is also seen in the NEWFIRM  $J$ -band image, where it appears resolved into two or three sources (Fig. 5.4). It is also

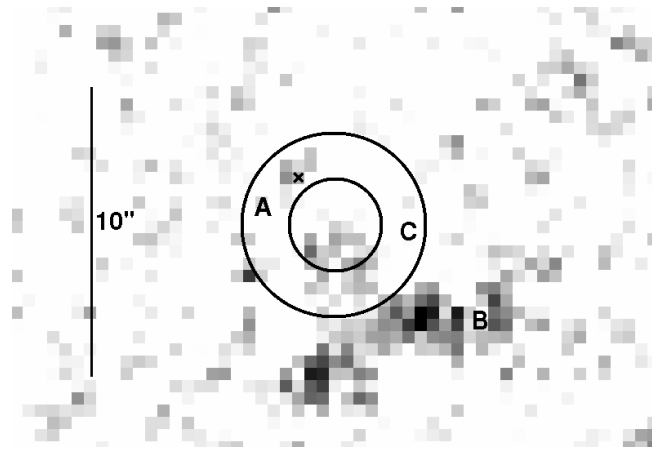


Figure 5.4: *NEWFIRM J-band* image of the field of GRB 060211A. It shows the 90% XRT error circle ( $r_0 = 1''.5$ ) as well as a circle of radius  $2r_0$ .

detected with GROND in  $g'r'i'z'$ . In the  $r'$  band its size is about  $3''.8 \times 2''.2$ . The *NEWFIRM J-band* image reveals another very faint, possibly extended object within the 90% XRT error circle (C) that could be related to object A (Fig. 5.4). It is not seen in any other band.

Assuming that A is a single galaxy, the probability  $p$  of finding a galaxy of the measured  $R_C$ -band magnitude within the 90% XRT error circle is about 0.05, I consider A and C as GRB host galaxy candidates.

**GRB 060805A** The field lies at relatively high Galactic latitude ( $b = 60^\circ$ ). It is not crowded by stars but it is located close to a bright star ( $R_C = 13.5$ ) at RA, Dec. (J2000) = 14:43:42.098, +12:35:20.63 (USNO-B1 catalog), which may affect the background estimation. The foreground Galactic reddening is small,  $E(B - V) = 0.02$  mag, among the smallest in the sample. The corresponding 90% XRT error circle is very small ( $r_0 = 1''.6$ ; Fig. C.2).

The field was observed with GROND two years after the burst. In the  $r'$ -band image two sources are detected (A, B; Fig. C.2) at the S-E boundary of the 90% XRT error circle with magnitudes  $R_{AB} = 25.0$  and 23.6, respectively. Both objects appear extended. Object B, with a size of  $2''.7 \times 1''.3$ , lies about  $2''.0$  away from the center of the XRT error circle; its outer regions extend into the 90% XRT error circle. Contrary to object A, object B is also detected in the  $g'$ -band ( $\sim 23.6$ ) with a  $(g' - r')_{AB}$  color consistent with a flat SED in this wavelength region. It could imply that this galaxy is dominated by a young stellar population. Object A is not detected in the GROND  $i'z'$  and both are not detected in *JHK* bands, where only deep upper limits could be derived (Table 5.5). The  $(R - K)_{AB}$  colors of A and B are  $< 4.3$  mag and  $< 2.6$  mag, respectively. Note that the photometry of both objects is slightly affected by the bright nearby star.

Assuming that A and B are galaxies, the probability  $p$  of finding a galaxy of the measured  $R_C$ -band magnitude in the XRT error circle is about 0.11 for object A within  $r_0$  and 0.14 for object B within  $2r_0$ . I consider both, A and B, as GRB host galaxy candidates. The same conclusion was drawn by Perley et al. (2009), who observed this field in  $g'$  and  $R_C$  using the Keck telescopes.

**GRB 060919** The field of this burst lies at low Galactic latitude ( $b = -17^\circ$ ) but is not crowded with stars. The foreground Galactic reddening is small,  $E(B - V) = 0.07$  mag, and the 90% XRT error circle is again among the smallest in my sample ( $r_0 = 1''.7$ ; Fig. C.2).

The field was observed with FORS1 and ISAAC (stellar FWHM of  $0''.8$  and  $0''.6$ , respectively) about 2 years after the burst in  $R_C$  and  $K_s$ , respectively. I find only a single  $R_C$ -band source within the

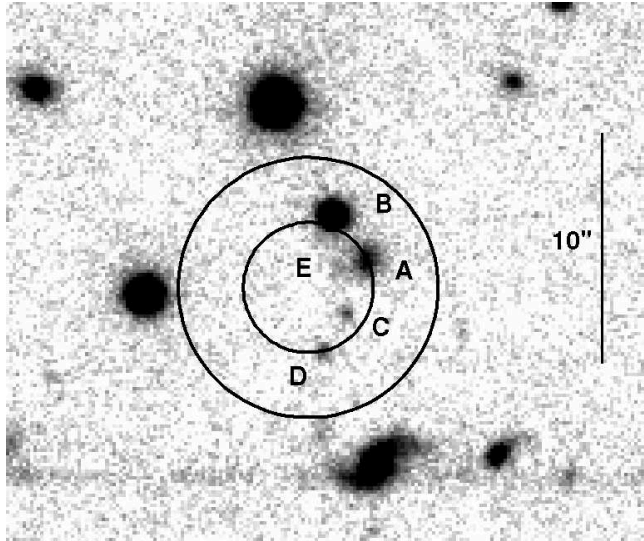


Figure 5.5: ISAAC  $K_s$ -band image of the field of GRB 060923B. Also shown is the 90% XRT error circle ( $r_0 = 2''.8$ ) as well as a circle of radius  $2r_0$ . The image reveals that object A is a galaxy.

90% XRT error circle (A), no other objects are visible even within  $2r_0$ . In the  $R_C$ -band image object A seems to be extended along the E-W direction ( $1''.5 \times 1''.4$ ;  $R_{AB} = 26.1$ ). It is not detected in the ISAAC image down to deep flux limits ( $K_{AB} > 23.4$ ). Its  $(R - K)_{AB}$  color is thus  $< 2.6$  mag, well within the range of the colors of the known GRB host galaxy population (SBG09). If this object is not the host, then one can provide the following upper limits for the GRB host galaxy:  $R_{AB} > 26.5$  and  $K_{AB} > 23.4$ .

The probability of finding a galaxy of the measured  $R_C$ -band magnitude in a region of radius  $r_0$  is 0.25. This is a high probability, but given that object A is the only object detected within the  $2r_0$  XRT error circle, I suggest that it is the potential GRB host galaxy. It is one of the faintest host galaxy candidates in the sample.

**GRB 060923B** The field is at relatively low Galactic latitude ( $b = 18^\circ$ ) and it is relatively crowded with bright stars. The foreground Galactic reddening is moderate,  $E(B - V) = 0.15$  mag. The corresponding 90% XRT error circle is of moderate size ( $r_0 = 2''.8$ ; Fig. C.2).

The field was observed with FORS1 and ISAAC about 1.5 years after the burst (stellar FWHM of  $0''.8$  and  $0''.5$ , respectively). FORS1  $R_C$ -band as well as ISAAC  $K_s$ -band observations show two objects (C,E, Fig. C.2) inside the 90% XRT error circle, while objects A, B, D lie within the  $2r_0$  error circle.

Object C ( $R_{AB} \sim 24.5$ ), has a point-like PSF but it is probably too faint for detecting the faintest region of a galaxy with comparable brightness. Therefore I am not sure about its nature. Objects A ( $R_{AB} = 23.1$ ) and E are very close to each other, making it difficult to get a reliable  $R$ -band photometry, especially for object E. Object B, slightly outside  $1r_0$  ( $R_{AB} = 21.7$ ) has a PSF that is point-like. On the deep  $K_s$ -band image object A shows an extended morphology ( $2.2'' \times 2.1''$ ; Fig. 5.5). Therefore, I identify it as a galaxy. The probability  $p$  of finding a galaxy like A of the measured  $R$ -band magnitude inside a region of radius  $2r_0$  is 0.10. Object D ( $R_{AB} = 25.7$ ) has a very red  $(R - K)_{AB}$  color ( $\sim 3.8$  mag) and appears elongated in optical and NIR images, while A and C have a modest color of 1.1 mag and 1.3 mag, respectively.

Objects E and C are the only ones within  $r_0$ , but it is difficult to conclude anything about their nature. If E is a galaxy it would be attractive because of its position close to the galaxy A, suggesting a possible interaction. I also note that object D has a very red color. Given that I am sure about the



galactic nature of objects A and D only, and D is a rare red object, I consider D as the best host galaxy candidate (see Sect. 5.3.10).

**GRB 061102** The field is at moderate Galactic latitude ( $b = 28^\circ$ ). The foreground Galactic reddening is small,  $E(B - V) = 0.04$  mag. The corresponding 90% XRT error circle is of moderate size ( $r_0 = 2''.9$ ; Fig. C.3).

The field was observed with FORS1 and ISAAC in  $R_C$  and  $K_s$ , respectively, about 1.5 years after the burst under very good seeing conditions (PSF FWHM of  $0''.7$ ). The VLT images show no object within the 90% XRT error circle down to  $R_{AB} = 26.9$  and  $K_{AB} = 22.8$ . Two objects (A, B) are found within the doubled XRT error circle ( $r = 2r_0$ ; Fig. C.3). They are only detected in  $R_C$  but not in  $K$ . Both objects are clearly extended ( $2''.5 \times 1''.5$  and  $1''.8 \times 1''.9$ , respectively). Their  $(R - K)_{AB}$  color ( $\lesssim 1.2$  mag and  $\lesssim 1.1$  mag, respectively) match with the corresponding color of the GRB host galaxy population at a redshift around  $z = 1$  (SBG09). In both cases, the probability of finding a galaxy of the given  $R_C$ -band magnitude inside a region of  $2r_0$  is 0.5.

Objects A and B could be members of a loose group of galaxies (which also includes the galaxy about  $10''.0$  south-east of B, see Fig. C.3). I also note that the field lies close to an anonymous (foreground?) group or even cluster of galaxies that is apparent in FORS1  $R_C$ -band image, which could have its center about  $1''.5$  north of the XRT error circle. The brightest members of this group or cluster have USNO A2-magnitudes of  $R \sim 18$ .

I consider galaxies A and B as equally likely hosts, even though object A touches the inner part of the 90% XRT error circle with its outer region, while galaxy B probably does not. If none of these sources is the host galaxy, then the measured deep  $R_C$  and  $K_s$ -band upper limits would make the host galaxy of GRB 061102 one of the faintest in the sample.

**GRB 070429A** The field lies at moderate Galactic latitude ( $b = -26^\circ$ ). It is not crowded with stars. The foreground Galactic reddening is modest,  $E(B - V) = 0.17$  mag. The corresponding 90% XRT error circle is of moderate size ( $r_0 = 2''.1$ ; Fig. C.3). This burst enters the golden dark burst subsample (see Sec. 5.1.2 and C.1).

The field was observed with FORS1 and ISAAC about 1 year after the burst (stars FWHM  $1''.0$  in  $R_C$  and  $0''.6$  in  $K_s$ ). In the FORS1  $R_C$ -band image (Fig. C.3) I find one object (A) at the border of the  $2r_0$  XRT error circle and two other sources inside the 90% XRT error circle (B,C). All three objects are extended (between  $1''.7$  and  $3''.8$  in their major axis), i.e., they are galaxies. Objects B and C could be an interacting pair since they show a fuzzy structure. Their individual  $R_C$ ,  $K_s$  magnitudes (Table 5.4) and  $(R - K)_{AB}$  colors (Table 5.6) are compatible with the GRB host population at a redshift  $z < 2$  (SBG09).

The observed color of objects A, B, and C does not characterize any of them as very red. In other words, if one of them is the GRB host, then the afterglow was not optically dim because of high-redshift or global host galaxy extinction. The probability-magnitude criterion gives the following numbers for the three galaxies (A-C): 0.45, 0.07 and 0.08, respectively. Given that B and C are well placed inside the 90% XRT error circle, I consider both as equally likely host galaxy candidates.

**GRB 070517A** This burst is unique in the sample, because I could identify its afterglow by comparing late-time observations with the follow-up observations reported by Fox et al. (2007).

The field was observed with FORS1 and ISAAC about 1 year after the burst in very good seeing conditions (FWHM of  $0''.5$  and  $0''.6$ , respectively). The field is at relatively low Galactic latitude ( $b =$

$-21^\circ$ ) but not very crowded with stars. The foreground Galactic reddening is modest,  $E(B-V) = 0.15$  mag. The corresponding 90% XRT error circle is of moderate size ( $r_0 = 2''.1$ ; Fig. C.3).

In the  $R_C$ -band image only one object is detected (A, Fig. C.3) inside the 90% XRT error circle. No further objects are apparent within the doubled XRT error circle ( $r = 2r_0$ ). In particular, I do not detect the  $r' = 22.1$  afterglow candidate at RA, Dec. (J2000) = 18:30:29.12,  $-62:17:50.7$  (uncertainty of  $< 0''.75$  in each coordinate), which was reported by Fox et al. (2007) based on Gemini-South observations about 16 hr after the burst (indicated by a cross in Fig. C.3). I conclude that in fact this was the GRB afterglow, and therefore this burst cannot be considered as dark anymore, and it will be removed from the sample in the following discussion.

The second object observed by Fox et al. (2007) lies within the 90% XRT error circle at RA, Dec. (J2000) = 18:30:29.08,  $-62:17:53.0$  (object A in the finding chart). I measure  $R_{AB} = 25.39 \pm 0.21$  and  $K_{AB} > 23.4$  and these authors found  $i' = 24.5$ . This object lies  $1''.6 \pm 0''.3$  south of the optical transient. Based on the images, I cannot decide if A is a galaxy or a star. If it is the GRB host galaxy, then its  $(R-K)_{AB}$  color of  $< 1.7$  mag is compatible with the GRB host galaxy population for a redshift around  $z = 1$  (SBG09). No underlying galaxy is found at the position of the suspected optical afterglow down to  $R_{AB} = 26.6$  and  $K_{AB} = 23.4$ .

The angular distance between the afterglow and object A is  $1''.6 \pm 0''.3$ . The probability  $p$  to find a galaxy of the given  $R_C$ -band magnitude in a circle with this radius is 0.11, classifying object A in this way as a reasonable GRB host galaxy candidate. However, if A was the host galaxy of GRB 070517A, then its angular distance translates to a projected distance of  $12.8 \pm 2.4$  kpc, assuming a redshift of  $z = 1$ . This is 10 times larger than the median projected angular offset of 1.3 kpc found by Bloom et al. (2002) for a sample of 20 host galaxies of long bursts, making object A not the favourite host. On the other hand, if I require a projected angular distance of less than 10 kpc, then the upper limit on the redshift of this galaxy is  $z = 0.4$ . In this case A would be a very faint galaxy when compared to the sample of SBG09. Alternatively, of course, the true host galaxy could underlie the optical position and lie beneath the detection limits.

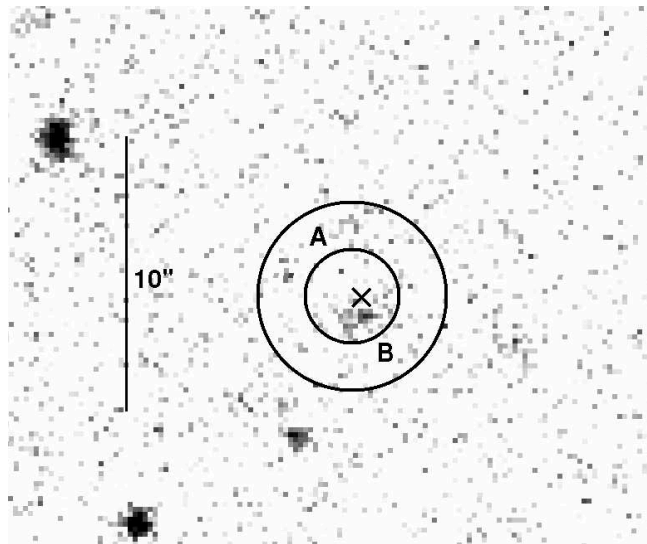
**GRB 080123** Uehara et al. (2008) characterize this event as a short burst due to its short duration in the *Suzaku*/WAM energy band, while the duration measured by *Swift*/BAT is larger than 100 seconds (Ukwatta et al. 2008c). In the Appendix (C.1) I show that an analysis of the gamma-ray light curve and its spectral properties classifies this event as a short burst. However, given that the bursts included in my sample are long according to their  $T_{90}$  measured by *Swift*/BAT, this GRB has been kept on the list.

The GRB field is at moderate Galactic latitude ( $b = -47^\circ$ ), not very crowded with stars. The Galactic reddening is very small,  $E(B-V) = 0.02$  mag. The 90% XRT error circle is among the smallest in the sample ( $r_0 = 1''.7$ ; Fig. C.3).

The field was observed with FORS2 and ISAAC about 1.5 years after the burst. The most obvious feature of the field is the presence of a bright ( $R_{AB} = 21.01$ ,  $K_{AB} = 19.6$ ; using a  $3 \times$  FWHM aperture) and relatively large ( $7''.3 \times 3''.1$ ) anonymous galaxy (object C, Fig. C.3) with its center about  $9''.0$  N-W of the center of the XRT error circle at RA, Dec. (J2000) = 22:35:46.92,  $-64:53:55.1$ . A less bright and less extended (about 1/3 of C) galaxy (D) lies about  $10''.0$  east of C and about  $8''.0$  N-E of the center of the XRT error circle at R.A., Dec. (J2000) = 22:35:45.48,  $-64:53:56.4$  with  $R_{AB} = 23.49$ ,  $K_{AB} > 23.3$ . Given that GRB 080123 might be classified as a short burst, Leibler & Berger (2010) considered C as the most likely GRB host galaxy candidate<sup>3</sup> and report a redshift of  $z = 0.495$ .

<sup>3</sup>Their reported coordinates refer to the X-ray error box known at that time, the position of which is slightly different to

Figure 5.6: ISAAC  $K_s$ -band image of the field of GRB 080207, including the 90% XRT error circle ( $r_0 = 1''.4$ ) as well as a circle of radius  $2r_0$ . Object A is well visible in the VLT/VIMOS  $R_C$ -band image only. (see Fig. C.3). Also shown by a cross is the position of the Chandra X-ray source (see text).



The deep FORS2 image shows only one source (A) within the 90% XRT error circle. According to its morphological appearance it could be a galaxy. An additional object (B) is seen inside  $2r_0$ . Neither A nor B is detected in ISAAC  $K_s$ -band image down to  $K_{AB} = 23.3$ . Probably, B is a galaxy too. With  $(R - K)_{AB} < 2.2$  mag and  $< 2.4$  mag, respectively, both objects match into the sample of GRBHs for redshifts around  $z = 1$  (SBG09).

In agreement with Uehara et al. (2008) also the analysis of the GRB properties based on the Amati relation supports the conclusion that GRB 080123 was a short burst (see Sect. C.1). Based on its short burst classification, Leibler & Berger (2010) had already considered galaxy C as the best host galaxy candidate. Indeed, the probability  $p$  of finding such a bright galaxy in a circular area of radius  $8''.0$  is just 0.13. Also, its redshift is typical of the short burst population (e.g., Kann et al. 2011). The projected angular offset of the burst from the center of this galaxy in units of light radii would then be remarkable, however. On the other hand, the probability of finding a galaxy with the  $R$ -band magnitude of object A within the 90% XRT error circle is similarly small ( $p=0.17$ ). Therefore, object C is also a host galaxy candidate, even though its faintness might imply a redshift beyond 1. In this context I note that GRB 060121 was also found to be related to a quite faint host and its photometric redshift has been determined to be above 4 de Ugarte Postigo et al. (2006); Levan et al. (2006b).

**GRB 080207** The burst occurred at high Galactic latitude ( $b = 66^\circ$ ), the field is not crowded by stars. The Galactic reddening is very small,  $E(B - V) = 0.02$  mag. The 90% XRT error circle is the smallest in the sample ( $r_0 = 1''.4$ ; Fig. C.3). This burst enters the golden dark burst subsample (see Sec. 5.1.2 and C.1).

The field was observed 2 years after the burst with VLT/VIMOS in  $R_C$  and ISAAC in  $K_s$  under good seeing conditions (FWHM of  $0''.8$  and  $0''.6$ , respectively). In addition, deep GROND imaging was performed at a mean time of 10 hours after the burst, but no afterglow was detected (Table C.3). Deep VIMOS  $R_C$ -band image shows one fuzzy object ( $2''.4 \times 1''.3$ ) at the northern boundary of the 90% XRT error circle (A, Fig. C.3). This object is very faint in  $K_s$ -band ISAAC images, but I obtained a weak detection ( $2.5\sigma$ ) coincident with the  $R_C$ -band position. In addition, the ISAAC image shows another, elongated source (B;  $1''.6 \times 0''.9$ ) within the XRT error circle that has a very faint  $R_C$ -band

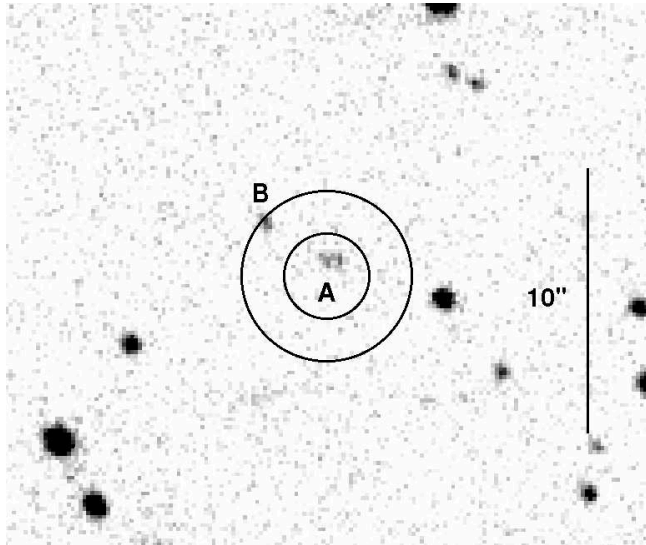


Figure 5.7: ISAAC  $K_s$ -band image of the field of GRB 080218B, including the 90% XRT error circle ( $r_0 = 1''.6$ ) as well as a circle of radius  $2r_0$ .

counterpart with  $R_{AB} = 26.49$  (Fig. 5.6). GROND did not detect these sources in any band, only upper limits can be provided (Table 5.5).

The magnitudes of A as well as its  $(R - K)_{AB}$  color (2.1 mag) match into the properties of the known GRB galaxy population for a redshift around 1 (SBG09). In contrast to this, object B is very red,  $(R - K)_{AB} = 4.7$  mag. Given its very red color and its position within the 90% XRT error circle, I consider B as the most likely GRB host candidate (see Sect. 5.3.10).

When this work was in its finalization, the *Chandra* source catalogue (Evans et al. 2010a) became public. Inspection of the catalogue shows that a X-ray observation of the field was performed 8 days after the burst and a point source was detected (CXO J135002.9+073007) at coordinates RA, Dec. (J2000) = 13:50:02.97, 07:30:07.8 ( $\pm 0''.6$ ). The position of this source is within  $1\sigma$  consistent with the position of object B. Therefore, I conclude that this is the host galaxy of GRB 080207. Moreover Hunt et al. (2011) have recently obtained a photometric redshift of about 2.2 for this galaxy, therefore I can exclude that its red color is due to Lyman dropout.

Assuming for simplicity a power law spectrum for this galaxy of the form  $F_\nu \propto \nu^{-\beta_{\text{gal}}}$ , then for a representative value of  $\beta_{\text{gal}}=1$  and a redshift of  $z=2.2$ , this gives  $M_K = -24.4$ , which is at the bright end of the luminosities found so far for the GRB host galaxy population (SBG09, their figure 7).<sup>4</sup>

**GRB 080218B** The field is at relatively low Galactic latitude ( $b = 9^\circ$ ), the lowest in the sample. However, it is only moderately crowded with stars. The Galactic reddening along the line of sight is modest,  $E(B - V) = 0.17$  mag. The 90% XRT error circle is small ( $r_0 = 1''.6$ ; Fig. C.3). This burst enters the golden dark burst subsample (see Sec. 5.1.2 and C.1).

The field was observed with FORS2 and ISAAC about 1 year after the burst under very good seeing conditions (FWHM =  $0''.5$ ). In addition, deep GROND imaging was performed at a mean time of about 0.75 hr after the burst, but no afterglow was detected (Table C.3). Deep FORS2  $R_C$ -band image reveals one faint ( $R_{AB} = 26.2$ ), extended object (A) within the 90% XRT error circle and another object (B;  $R_{AB} = 24.6$ ) inside  $2r_0$ . Both objects are also detected with ISAAC at magnitudes  $K_{AB} = 21.7$  and 22.7, respectively (Fig. 5.7). Object A is too faint to be detected by GROND, while B is detected in  $g'r'z'$  (Table 5.5; it is not seen in  $i'$  due to ghost images in the field).

<sup>4</sup>The absolute  $K_s$ -band magnitude is given by  $M_K = m_K - \mu - k$ , where  $\mu$  is the distance modulus and  $k$  is the cosmological  $k$ -correction,  $k = -2.5(1 - \beta_{\text{gal}})\log(1 + z)$ .

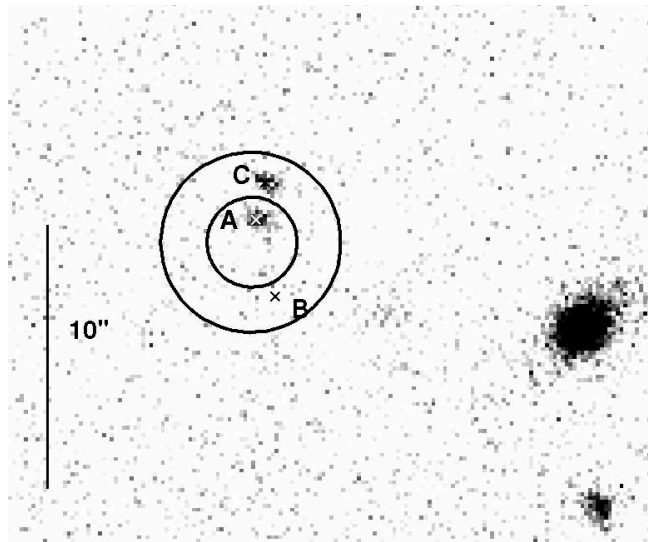


Figure 5.8: ISAAC  $K_s$ -band image of the field of GRB 080602, including the 90% XRT error circle ( $r_0 = 1''.7$ ) as well as a circle of radius  $2r_0$ .

Object A is elongated in SE-NW direction ( $2''.5 \times 1''.1$ ). It could be a spiral galaxy seen nearly edge-on or a tight group of galaxies. If it is a single galaxy, then its large  $(R - K)_{AB}$  color (4.2 mag) suggests a high global extinction, which could explain the dimness of the optical afterglow. The probability of finding a galaxy of this  $R_C$ -band magnitude within an area of radius  $r = r_0$  on the sky is about 0.2. Given its red color and its position inside the 90% XRT error circle, I consider A as the most likely GRB host galaxy (see Sect. 5.3.10).

**GRB 080602** The field is at high Galactic latitude ( $b = -71^\circ$ ), among the highest in the sample. The Galactic reddening is very small,  $E(B - V) = 0.03$  mag. The 90% XRT error circle is small, too ( $r_0 = 1''.7$ ; Fig. C.4).

I retrieved VLT/FORS2 and ISAAC data obtained about 1 year after the burst from the ESO archive (program ID 081.A-0856; PI: P. Vreeswijk). These observations were performed under good seeing conditions (stellar FWHM  $0''.8$  and  $0''.7$ , respectively). In addition, deep GROND multi-color imaging was performed 1.5 years after the burst.

In the FORS2  $R_C$ -band image I find one object (A;  $R_{AB} = 22.9$ ) inside the 90% XRT error circle. It is also detected in all GROND optical bands and also seen in the ISAAC  $K_s$ -band image ( $K_{AB} = 22.5$ ), where it splits into two separate (interacting?) objects, with the second one (C)  $1''.3$  north of A (Fig. 5.8). At the southern boundary of the 90% XRT error circle lies another object (B; size  $2''.0 \times 1''.8$ ), possibly another galaxy. Object A looks fuzzy and extended ( $2''.6 \times 2''.0$ ), while the nature of C is less obvious. Assuming that A (merged with C in all bands except the ISAAC  $K_s$ -band image) is a single galaxy, a fit of its SED with *Hyperz* (Bolzonella et al. 2000) gives good solutions for a spiral galaxy with no intrinsic extinction at a redshift of  $z = 1.40_{-0.15}^{+0.30}$  ( $\chi^2/\text{d.o.f} = 0.074$ ) as well as for a starburst galaxy at a redshift of  $z = 2.10_{-0.35}^{+0.20}$  and a moderate MW extinction of  $A_V = 0.4$  mag ( $\chi^2/\text{d.o.f} = 0.050$ ; Fig. 5.9). This double solution is due to the fact that the  $z'$ -band magnitude can well fit both the  $4000\text{\AA}$  Balmer jump as well as a moderate  $2175\text{\AA}$  feature from a MW (or LMC) extinction law. I caution however that while the first solution implies a absolute magnitude  $M_B \sim -23.0$ , in case of the  $z \sim 2.1$  solution I obtain  $M_B \sim -24.0$ , which is very unlikely when compared with the luminosity function presented in the Las Campanas redshift survey (Lin et al. 1996)). Therefore, I consider  $z = 1.4_{-0.15}^{+0.30}$  as the most likely redshift estimation.

Object A as well as B have colors  $(R - K)_{AB} = 0.3$  mag and  $< 0.4$  mag, respectively, which is

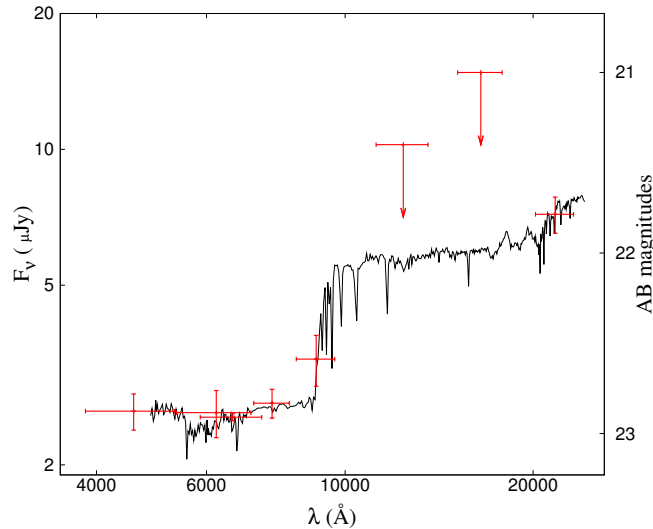


Figure 5.9: Hyperz best-fit solution of the broad-band SED of object A in the XRT error circle of GRB 080602, in case of a spiral galaxy at a redshift of  $z = 1.40^{+0.30}_{-0.15}$  with no intrinsic extinction ( $\chi^2/d.o.f = 0.074$ ).

well within the range of the observed colors for GRB host galaxies (SBG09). In the case of object A, the probability of finding a galaxy of the given  $R_C$ -band magnitude inside a circular area of radius  $r_0$  is 0.03, while for B the corresponding value is 0.21 (within  $2r_0$ ). However, the probability to find a galaxy with the red color of object C within the same area is also small (see Sect. 5.3.10). Therefore, I consider object A and C as equally likely GRB host galaxy.

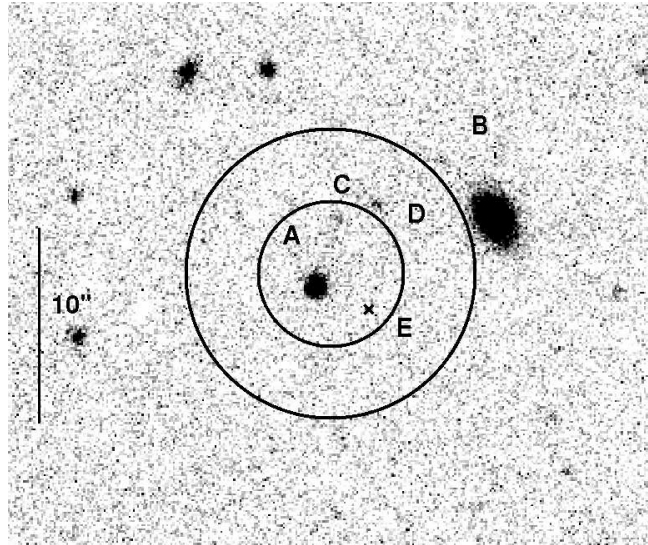
**GRB 080727A** The field lies at moderate Galactic latitude ( $b = 42^\circ$ ) and is not crowded by stars. The Galactic reddening is very small,  $E(B - V) = 0.07$  mag. The 90% XRT error circle is small, too ( $r_0 = 1''.6$ ; Fig. C.4).

The field was observed with ISAAC about 1.5 years after the burst under very good seeing conditions (stellar FWHM of  $0''.6$ ). The deep FORS1  $R_C$ -band image was taken from the ESO archive (program ID 081.A-0856; PI P. Vreeswijk; FWHM of  $0''.8$ ). No GRB host galaxy candidate is detected, neither inside the 90% XRT error circle down to  $R_{AB} = 26.3$  and  $K_{AB} = 23.0$ , nor inside the doubled ( $r = 2r_0$ ) XRT error circle. This is the second case next to GRB 050922B in the sample where only deep upper limits on any host galaxy can be provided. A moderately bright, anonymous, and nearly edge-on galaxy ( $R_{AB} = 23.4$ ; size  $4''.5 \times 2''.0$ ) lies  $10''.0$  (5 projected light radii) east of the center of the XRT error circle. However, I consider this object as too far away from the XRT error circle in order to be physically related to the GRB. I conclude that the host galaxy of this burst belongs to the faintest GRBHs known so far. It is also possible that the afterglow was not seen in the optical bands due to Lyman dropout, i.e., high-redshift.

**GRB 080915A** The field does not lie at low Galactic latitude ( $b = -41^\circ$ ), but it is relatively crowded with stars. The Galactic reddening is very small,  $E(B - V) = 0.05$  mag. The 90% XRT error circle is large ( $r_0 = 3''.7$ ; Fig. C.4).

The field was observed with HAWK-I in Target of Opportunity mode starting 28 hours after the burst, the observation lasted for 14 minutes. Observations were performed under very good seeing conditions (FWHM of  $0''.6$ ). No candidate NIR afterglow was found inside the doubled XRT error circle down to  $K_{AB} = 23.4$ . Additional  $R_C$ -band data were obtained with FORS1 12 days after the burst (FWHM of  $1''.4$ ). The FORS1 image reveals three sources (A, C, E) in the 90% XRT error circle. Another object (D) lies at the border of the 90% error circle. Object A has a PSF that is compatible

Figure 5.10: Deep VLT/HAWKI  $K_s$ -band image of the XRT error circle of GRB 080915A taken 28 hr after the burst. Also shown is the 90% XRT error circle ( $r_0 = 3''.7$ ) as well as a circle of radius  $2r_0$ . Here E is not visible and therefore it is indicated by a cross. All objects are detected in the deep VLT/FORS1 image taken 11 days later.



with a point source, while C and D appear fuzzy and could be galaxies. Object E is very faint, close to the detection limit. It is difficult to decipher if it is a galaxy or not.

Outside the  $2 \times 90\%$  XRT error circle there is a bright object (B), which is a galaxy ( $5''.6 \times 4''.5$  in the FORS1 image). It stands out because of its relatively large  $(g' - r')_{AB}$  color (2.0 mag). Also, several other galaxies in the GROND field of view have this color.

For objects C and D the probability of finding a galaxy with the corresponding  $R_C$ -band magnitude inside a circle of radius  $r_0$  and  $2r_0$  on the sky is  $p = 0.13$  and  $0.52$ , respectively. Besides object B, objects C and D are also detected as very faint sources in the HAWK-I  $K_s$ -band image (Fig. 5.10).

Given their position inside and, respectively, very close to the 90% XRT error circle, I consider C and D as GRB host galaxy candidates. Objects C and D could be a pair of interacting galaxies.

**GRB 081012** The field is at high Galactic latitude ( $b = -71^\circ$ ), it is not crowded with stars. The Galactic reddening is very small,  $E(B - V) = 0.02$  mag, among the lowest in the sample. The 90% XRT error circle is relatively small ( $r_0 = 1''.8$ ; Fig. C.4).

The field was observed with VIMOS and ISAAC nearly exactly 1 year after the burst under good seeing (FWHM of  $0''.8$  and  $0''.4$ , respectively). Deep VIMOS  $R_C$ -band image shows no source within the 90% XRT error circle down to  $R_{AB} = 26.7$ . One object (A, Fig. C.4) is detected within the annulus between  $r_0$  and  $2r_0$ . It has a cometary shape ( $1''.8 \times 1''.5$ ) and a magnitude of  $R_{AB} = 25.16 \pm 0.17$ . It is possible that this is an irregular galaxy or a galaxy with a Galactic foreground star superposed its southern part. The object is not visible in the ISAAC image down to  $K_{AB} = 23.9$ . An upper limit of  $(R - K)_{AB} < 1.2$  mag can be set, but given the potential foreground star, this color should be considered with caution. The field was also observed by GROND while searching for the afterglow at a mean time of 19.3 hr after the burst. Neither object A nor any transient source were detected in any band (Filgas et al. 2008; Tables 5.5, C.3).

Given the absence of any other source within the 90% XRT error circle, I consider object A as the likely GRB host galaxy. This does not exclude the possibility that the host is indeed fainter than the detection limits ( $R_{AB} > 26.7$ ,  $K_{AB} > 23.9$ ).

**GRB 081105** The field is at moderately high Galactic latitude ( $b = -58^\circ$ ), not very crowded by stars. The Galactic reddening is very small,  $E(B - V) = 0.03$  mag. The 90% XRT error circle is

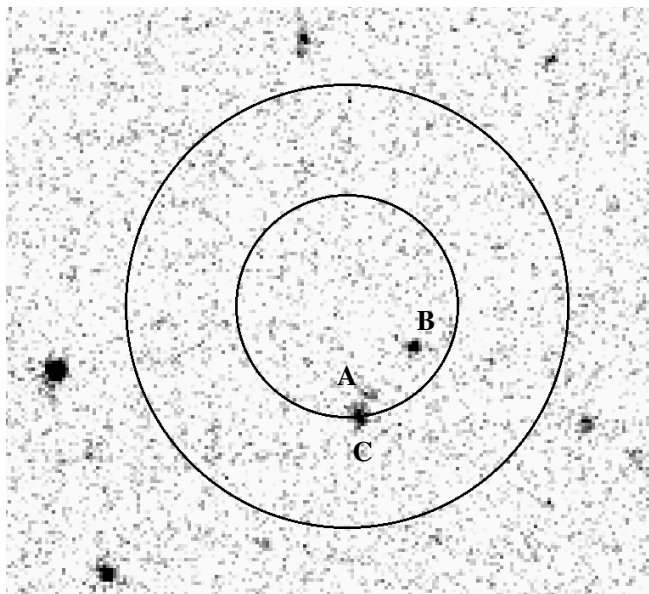


Figure 5.11: ISAAC  $K_s$ -band image of the field of GRB 081105. Also shown is the 90% XRT error circle ( $r_0 = 4''.8$ ) as well as a circle of radius  $2r_0$ .

relatively large ( $r_0 = 4''.8$ ; Fig. C.4).

The field was observed with VIMOS and ISAAC about 1 year after the burst. In spite of the relatively large size of the XRT error circle, in the deep VIMOS  $R_C$ -band image only two objects is detected (A, B, Fig. C.4). A third one (C) is seen in the deep ISAAC  $K_s$ -band image about  $1''.0$  south of A, but only a local upper limit of 25.5 can be obtain in the  $R_C$ -band. (Fig. 5.11). In the  $K_s$ -band image, which was taken during a very good average seeing (FWHM of  $0''.4$  compared to  $1''.0$  in the  $R_C$ -band image), objects A and C appear slightly extended, i.e., these might be (interacting) galaxies. In case of B one cannot determine if it is a star or a galaxy. The field was also observed by GROND while searching for the afterglow, starting about 13 hr after the burst. No transient source was detected in any band, only deep upper limits could be obtained (Clemens et al. 2008; Table C.3). None of the three objects (A,B,C) was detected either (Table 5.5).

The  $(R - K)_{AB}$  colors of objects A and B (about 0.9 mag and 2.1 mag, respectively) match those of the sample of GRBHs at a redshift around  $z = 1$  (SBG09). But object C has a very red color ( $(R - K)_{AB} > 3.5$ ), making it an interesting very red object, among the reddest in the sample. The probability of finding a galaxy with the  $R_C$ -band magnitudes of objects A and B inside a field of radius  $r = r_0$  is  $p = 0.31$  and  $0.45$ , respectively. Given the red color of galaxy C, I consider this as the most likely host galaxy candidate (see Sect. 5.3.10).

**GRB 081204** The field is at moderate Galactic latitude ( $b = -53^\circ$ ) and not very crowded with stars. The Galactic reddening is very small,  $E(B - V) = 0.03$  mag. The 90% XRT error circle is the largest in the sample ( $r_0 = 5''.3$ ; Fig. C.4).

The field was observed with VIMOS and ISAAC about 1 year after the burst under good seeing (FWHM of  $1''.0$  and  $0''.5$ , respectively). Further  $J$ -band imaging was performed with SOFI at the NTT nearly 2 years after the event. Two galaxies (A, B in Fig. C.4) are visible in deep VIMOS  $R_C$  and ISAAC  $K_s$ -band images within the 90% XRT error circle, while a similarly bright galaxy with similar  $R-K$  colors lies in the region between 1 and  $2r_0$ . Object A is elongated in E-W direction ( $2''.1 \times 1''.4$ ), while B shows a clear bulge-halo structure and is of similar size ( $2''.7 \times 1''.4$ ). Most interesting, N-W from object B lies a faint, elongated object (F), which clearly stands out as a relatively bright point-like source in the ISAAC image (Fig. 5.13). In addition, in the VIMOS image north from F



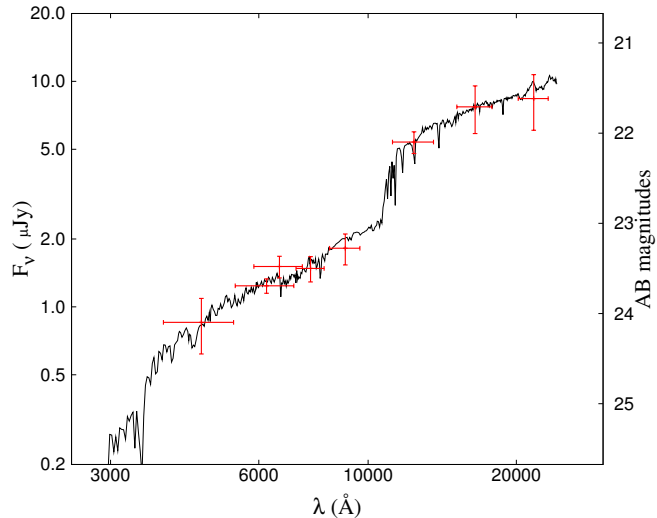


Figure 5.12: Hyperz best-fit solution of the broad-band SED of object B in the XRT error circle of GRB 081204, in case of a spiral galaxy at a redshift of  $z = 1.7 \pm 0.3$  with moderate intrinsic SMC extinction of  $A_V = 0.3$  ( $\chi^2/d.o.f = 0.3$ ).

lies another object, but it is too faint for further analysis. It seems reasonable to assume that all these objects, which stand together within  $5''.0$ , represent an interacting group of galaxies.

Deep follow-up observations of the field were also performed with GROND while (unsuccessfully) searching for the afterglow about 10 hr after the burst (Table C.3; Updike et al. 2008). Objects A and B are detected in  $g'r'i'z'$  (A also in  $H$ ), while C was only seen in  $r'i'J$ . Unfortunately, photometric redshift estimates are not very accurate for these galaxies. In case of B the  $4000\text{\AA}$  Balmer break is possibly placed between the  $z'$  and the  $J$  band, indicating a redshift of  $1.7 \pm 0.3$  (Fig. 5.12). No such feature is seen for galaxy C and *Hyperz* finds solutions within the redshift interval  $1 < z < 2$  with different sets of extinction laws, galaxy templates and host extinction.

Galaxy A is blue, its SED is essentially flat between  $R_C$  and  $K_s$  ( $(R-K)_{AB} = 0.8 \pm 0.2$  mag), while B is redder ( $(R-K)_{AB} = 1.8 \pm 0.1$  mag). The  $R_C$ -band magnitude measurement of F is complicated by the closer galaxy B but it is possible to give a reasonable estimate of  $R_{AB} = 24.65$ . The magnitude-probability criterion gives  $p(A) = 0.26$  and  $p(B) = 0.31$ , which does not prefer one galaxy over the other. In the  $K_s$ -band image object F appears as a fuzzy source with a bright core ( $K_{AB} = 21.5$ ), as bright as B. Probably this is the central bulge of this galaxy. The  $(R-K)_{AB} = 3.1$  makes galaxy F an interesting very red object, among the reddest in the sample. The probability to find a galaxy with the red color of F within an area of radius  $r = r_0$  is 0.09.

In the deep VIMOS image, inside the XRT error annulus between  $r_0$  and  $2r_0$ , three further objects are visible (C, D, E). Object C ( $R_{AB} \sim 23.2$ ) is elongated and angular in size ( $2''.2 \times 1''.7$ ) as well as shape, similar to galaxies A and B. Objects D and E are fainter ( $R_{AB} = 24.2$  and  $24.3$ , respectively) and have a rather blue color of  $(R-K)_{AB} < 2.0$  mag and  $< 0.0$  mag, respectively.

To summarize, objects A, B, and F are extended objects. All lie inside the 90% XRT error circle. Given the connection of long GRBs with young stellar populations, it is appealing to have an interacting pair (or even quadruplet) of galaxies inside the error circle. It is also very unlikely to find a red galaxy like F within the small area of the XRT error circle. Therefore, I consider F as likely GRB host galaxy candidate, followed by object B and A.

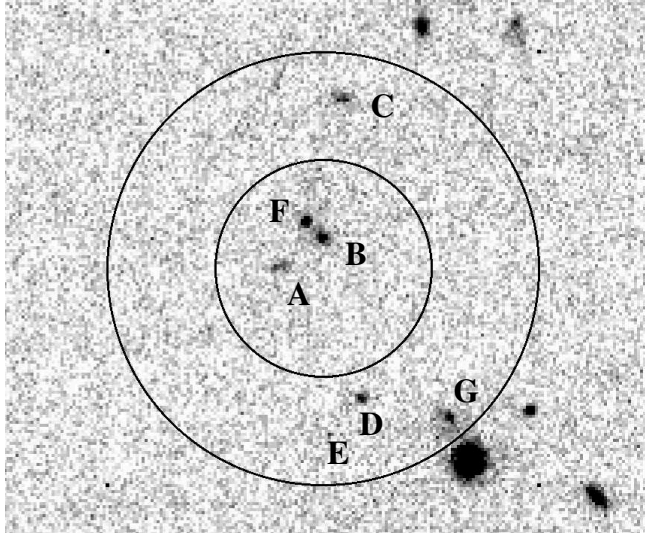


Figure 5.13: *ISAAC K<sub>s</sub>*-band image of the field of GRB 081204. Also shown is the 90% XRT error circle ( $r_0 = 5''.3$ ) as well as a circle of radius  $2r_0$ .

### 5.3 The properties of the host galaxy population

Even in the case of arcsec-sized error boxes it is usually difficult or even impossible to reveal the best GRB host galaxy candidate. The approach I used here to identify a putative host is identical to the approach adopted 15 years ago, when no afterglows were known at all and at best only arcmin-sized error boxes obtained via satellite triangulation were available (e.g., Klose et al. 1996; Vrba et al. 1999). The main observational difference is the size of the XRT error circles provided by *Swift*/XRT that can go down to 1-2 arcsec, allowing meaningful searches for host galaxies (see also Perley et al. 2009; Laskar et al. 2011). The question is: Is there anything special in the field? To answer this question, several criteria were used.

#### 5.3.1 The magnitude-probability criterion

I consider galaxies (i.e., extended objects) of all types as very likely GRB host galaxy candidates if the chance probability  $p$  to find such an object of the given  $R_C$ -band magnitude in the corresponding error circle is less than 10% (see Eq. 5.3). Altogether seven bursts fulfill this criteria (Table 5.6): GRB 050717, object A; GRB 060211A, object A; GRB 060805A, object A; GRB 060923B, object A; GRB 070429A, objects B and C; GRB 070517A, object A; and GRB 080602, object A. Note that in the case of GRB 070429A two galaxies fulfill this criterion, and the VLT data reveal that they might constitute an interacting system. Note also that in case of GRB 070517A the optical afterglow has been identified in the present work (Sect. 5.2.1) and  $p$  gives the corresponding probability to find the galaxy labeled A (Fig. C.3) at the given angular distance from the afterglow position.

In most cases the magnitude-probability criterion based on all types of galaxies provides however chance probability values  $p > 0.1$ . This is because either the detected galaxies are too faint, the XRT error circles are too big (even though some arcsec only), or a mixture of both. Also, if more than one galaxy is found inside an XRT error circle, this criterion often does not help to prefer one candidate over the other since the differences in the corresponding  $p$ -values are not sufficiently big (e.g., GRB 050717 and GRB 061102; Table 5.6). This situation changes, however, if one considers number counts of extremely red objects only (see Sect. 5.3.10).

Table 5.6: Summary of the morphological properties of the objects found in the XRT error circles.

#	GRB	Object	R-band size	$K_s$ -band size	Note	$(R - K)_{AB}$	$(R - K)_{Vega}$	Pos	$p$	$P_{ERO}$
1	050717	•A	$2.1 \times 3.9$	not visible	G	< 1.98	< 3.61	2	$0.08 \pm 0.01$	
		•B	$1.2 \times 1.3$	not visible		< 2.83	< 4.46	2	$0.16 \pm 0.04$	
2	050922B	•A	$0.7 \times 0.9$	not visible		< 3.7	< 5.3	1	$0.32 \pm 0.04$	
		•A	$1.1 \times 1.2$	not visible	G	< 2.53	< 4.16	1	$0.05 \pm 0.01$	
3	060211A	B	$3.8 \times 2.2$	3 sources	G	< 1.21	$2.84 \pm 0.21$	3	$0.14 \pm 0.01$	
		•C	only in $J$	–	G	–	–	1	–	
		•A	$1.5 \times 1.1$	not visible	G	< 4.3	< 5.9	1	$0.11 \pm 0.01$	
4	060805A	•B	$2.7 \times 1.3$	not visible	G	< 2.5	< 4.1	2	$0.14 \pm 0.01$	
		•A	$1.5 \times 1.4$	not visible		< 2.60	< 4.23	1	$0.24 \pm 0.04$	
6	060923B	A	$2.1 \times 2.2$	$2.2 \times 1.8$	G	1.05	$2.68 \pm 0.14$	2	$0.10 \pm 0.01$	
		B	$2.0 \times 2.0$	$1.9 \times 1.9$	S	2.43	$4.06 \pm 0.04$	2	–	
		C	$1.1 \times 1.0$	$0.8 \times 0.8$		1.33	$2.96 \pm 0.16$	1	$0.07 \pm 0.01$	
		•D	$1.3 \times 1.3$	$0.8 \times 0.8$	G	3.82	$5.45 \pm 0.13$	2	$0.55 \pm 0.03$	$0.04 \pm 0.01$
		E	blended with A					1	–	
7	061102	•A	$2.5 \times 1.5$	not visible	G	< 1.22	< 2.85	2	$0.51 \pm 0.02$	
		•B	$1.8 \times 1.9$	not visible	G	< 1.08	< 2.71	2	$0.47 \pm 0.02$	
8	<b>070429A</b>	A	$3.8 \times 1.4$	$1.9 \times 1.1$	G	2.10	$3.73 \pm 0.32$	2	$0.45 \pm 0.05$	
		•B	$2.8 \times 1.4$	blended with C	G	1.41	$3.04 \pm 0.23$	1	$0.07 \pm 0.01$	
		•C	$1.7 \times 1.5$	$1.5 \times 1.0$	G	2.09	$3.72 \pm 0.16$	1	$0.08 \pm 0.01$	
9	070517A	A	$1.6 \times 1.3$	not visible	G	< 1.69	< 3.32	1	$0.11 \pm 0.02$	
10	080123	•A	$1.4 \times 1.1$	not visible	G	< 2.17	< 3.80	1	$0.17 \pm 0.02$	
		B	$1.2 \times 0.7$	not visible	G	< 2.38	< 4.01	2	$0.58 \pm 0.06$	
		•C	$7.3 \times 3.1$	$1.9 \times 1.1$	G	1.36	$2.99 \pm 0.01$	5	$0.13 \pm 0.01$	
		D	$1.9 \times 1.4$	not visible	G	< -0.16	< 1.47	5	$0.62 \pm 0.03$	
11	<b>080207</b>	A	$2.4 \times 1.3$	not visible	G	2.08	$3.71 \pm 0.43$	2	$0.32 \pm 0.03$	
		•B	$2.1 \times 1.1$	$1.6 \times 0.9$	G	4.66	$6.29 \pm 0.40$	1	$0.23 \pm 0.06$	$0.01 \pm 0.01$
12	<b>080218B</b>	•A	$2.5 \times 1.1$	$1.4 \times 0.7$	G	4.15	$5.78 \pm 0.16$	1	$0.20 \pm 0.02$	0.01
		B	$1.6 \times 1.5$	$0.8 \times 0.8$		1.54	$3.17 \pm 0.24$	2	$0.22 \pm 0.01$	
13	080602	•A	$2.6 \times 2.0$	$1.2 \times 0.8$	G	0.34	$1.97 \pm 0.05$	1	$0.03 \pm 0.01$	
		B	$2.0 \times 1.8$	not visible	G	< 0.44	< 2.07	2	$0.21 \pm 0.01$	
		•C	not visible	$1.2 \times 0.8$	G	> 4.35	> 5.98	2	–	$0.04 \pm 0.01$
14	080727A	no candidates					1	–		
15	080915A	A	$3.5 \times 3.5$	$1.2 \times 1.2$	S	1.11	$2.74 \pm 0.02$	1	–	
		B	$5.6 \times 4.5$	$3.4 \times 1.8$	G	1.99	$3.62 \pm 0.01$	3	$0.25 \pm 0.01$	
		•C	$1.2 \times 1.2$	not visible	G	< -0.29	< 1.34	1	$0.13 \pm 0.01$	
		•D	$1.2 \times 1.2$	not visible	G	< 0.03	< 1.66	2	$0.52 \pm 0.02$	
		E	$1.5 \times 1.5$	not visible		< 1.94	< 3.57	1	$0.21 \pm 0.01$	
16	081012	•A	$1.8 \times 1.5$	not visible	G	< 1.21	< 2.84	2	$0.47 \pm 0.04$	
17	081105	A	$1.2 \times 1.2$	$1.0 \times 1.0$	G	0.89	$3.56 \pm 0.15$	1	$0.31 \pm 0.02$	
		B	$1.1 \times 1.1$	$0.8 \times 0.8$		2.15	$3.78 \pm 0.19$	1	$0.45 \pm 0.03$	
		•C	not visible	$0.8 \times 0.5$	G	> 3.50	> 5.13	1	–	$0.08 \pm 0.01$
18	081204	A	$2.1 \times 1.4$	$0.9 \times 0.5$	G	0.79	$1.61 \pm 0.16$	1	$0.26 \pm 0.01$	
		B	$2.7 \times 1.4$	$1.1 \times 0.8$	G	1.82	$2.74 \pm 0.09$	1	$0.31 \pm 0.01$	
		C	$2.2 \times 1.7$	$0.9 \times 0.6$	G	1.05	$2.58 \pm 0.13$	2	$0.69 \pm 0.02$	
		D	$1.2 \times 1.2$	$0.5 \times 0.5$		1.98	< 1.46	2	$0.92 \pm 0.01$	
		E	$1.2 \times 1.2$	not visible		< -0.04	< 1.59	2	$0.94 \pm 0.02$	
		•F	~ 1	$0.6 \times 0.6$	G	3.1	$4.7 \pm 0.50$	1	$0.84 \pm 0.09$	$0.09 \pm 0.01$
		G	blended with a star	$1.5 \times 1.5$		–	–	2	–	

Notes: (1) A bullet • in column 2 indicates the most likely GRB host candidate. If more than one candidate is marked then we cannot decide which is the best. For details about the selection, see Sect. 5.2.1. GRBs that enter the *golden dark burst subsample* are highlighted in boldface. (2) Sizes are given in units of arcsec. (3) Magnitude errors in  $(R - K)_{AB}$  are identical to the corresponding errors for  $(R - K)_{Vega}$ . Colors are corrected for Galactic extinction. (4) The last two columns gives the chance probability  $p$  of finding a galaxy of the corresponding extinction-corrected (Vega)  $R$ -band magnitude on the sky in a region with the size of the corresponding X-ray error circle with a radius  $r = \text{Pos} \times r_0$  (Eq. 5.3). Thereby the first column refers to number counts of galaxies of all kinds. If the object is for sure a star, then no value is given. The second column refers to number counts of EROs only (see Sect. 5.3.10). (5) Comment “G” stands for galaxy, “S” for star; if no letter is given then we could not decide if this is a star or a galaxy. (6) In case of GRB 070517A the probability  $p$  is based on the distance between the afterglow and galaxy A,  $1''6$  (Sect. 5.2.1).

Table 5.7:  $R, K$ -band magnitudes of host galaxies of dark bursts and bursts with detected highly reddened optical afterglows.

GRB	Comment	Redshift	$R_{AB}$	$K_{AB}$	$(R - K)_{AB}$	Ref.
970828	no afterglow	0.957	$24.6 \pm 0.2$	$22.6 \pm 0.2$	$2.0 \pm 0.3$	[1]
990506	radio afterglow	1.310	$25.7 \pm 0.2$	$23.4 \pm 0.2$	$2.3 \pm 0.2$	[2]
020127	no afterglow	$1.9^{+0.2}_{-0.4}$	$24.96 \pm 0.15$	$20.40 \pm 0.05$	$4.56 \pm 0.16$	[3]
030115	$(R - K)_{AB}^{OT} = 4.1$ mag	$2.5 \pm 0.2$	$25.3 \pm 0.3$	$22.21 \pm 0.15$	$3.1 \pm 0.3$	[4]
050223	no afterglow	0.584	$21.78 \pm 0.05$	$20.71 \pm 0.02$	$1.07 \pm 0.06$	[5]
051022	no afterglow	0.809	$21.7 \pm 0.1$	$20.01 \pm 0.23$	$1.7 \pm 0.25$	[6]
060923A	$A_V^{host} = 2...5$ mag	1.8...2.8	$25.88 \pm 0.12$	$23.6 \pm 0.4$	$2.28 \pm 0.42$	[7]
070306	$A_V^{host} = 5.4 \pm 0.6$ mag	1.496	$22.98 \pm 0.23$	$21.47 \pm 0.20$	$1.51 \pm 0.30$	[8]
080325	$A_V^{host} = 0.8$ mag	1.9	$25.5 \pm 0.16$	$21.7 \pm 0.06$	$3.8 \pm 0.16$	[9]
080607	$A_V^{host} = 1...2$ mag	3.036	$>27.0$	$24.8 \pm 0.7$	$>2.2$	[10]

[1] Djorgovski et al. (2001); [2] Le Floch et al. (2003); Bloom et al. (2003); [3] Berger et al. (2007), the redshift is photometric; [4] Levan et al. (2006a); Dullighan et al. (2004), the redshift is photometric; here we used the  $R$ -band reported by Dullighan et al. (2004), which was obtained later than the value reported by Levan et al. (2006a), from which we used the NICMOS  $K$ -band value; [5] Pellizza et al. (2006); [6] Castro-Tirado et al. (2007); Rol et al. (2007); [7] Tanvir et al. (2008); [8] Jaunsen et al. (2008); [9] Hashimoto et al. (2010), the redshift is photometric; [10] Chen et al. (2010, 2011); Perley et al. (2011). OT stands for optical transient. Note that this list is not meant to be complete.

### 5.3.2 Dust extinction and edge-on galaxies

A high inclination angle of a spiral host galaxy might result in a notable host extinction of the optical afterglow because the line of sight is crossing the galaxy's dusty disk. Unfortunately, the host galaxy candidates in the sample are usually so faint that one cannot determine what their inclination angle is. Nevertheless, two cases stand out. These are the very elongated host galaxy candidate A in the field of GRB 080207 as well as object A in the field of GRB 080218B. However, for the latter it is not possible to rule out that what is seen here is the unresolved superposition of two or more fainter sources, while the host of 080207 is probably the starburst galaxy B (see below). Therefore, I conclude that there is no strong observational evidence that any afterglow in the sample considered above remained optically undetected because its host is an edge-on but otherwise normal spiral galaxy.

### 5.3.3 Extremely red objects (EROs)

Long bursts trace the birth places of the most massive stars (e.g., Fruchter et al. 2006), which leads to the expectation that a certain percentage of all hosts of long bursts could be dust-enshrouded starburst galaxies, appearing as red objects. Indeed, several such cases are reported in the literature (Table 5.7). A representative example is the host galaxy of the highly extinguished afterglow of GRB 080607 (Perley et al. 2011;  $A_V^{host} > 1$  mag), which is a massive galaxy with moderate star formation (Chen et al. 2010, 2011).

Red objects, if they are galaxies, can point either to a high global extinction inside an actively star-forming irregular galaxy (e.g., Chen et al. 2010), a galaxy dominated by an old population of stars, or to cosmological Lyman dropout. In my sample six objects found in the XRT error circles fall (within their  $1\sigma$  magnitude error) into this category (Table 5.6). These are: GRB 060923B, object D with  $(R - K)_{AB} = 3.82 \pm 0.13$  mag; GRB 080207, object B with  $4.66 \pm 0.40$  mag; GRB 080218B, object A with  $4.15 \pm 0.16$  mag; GRB 080602, object C with  $> 4.3$  mag; GRB 081105, object C with

$> 3.5$  mag; GRB 081204, object F with  $3.1 \pm 0.5$  mag. Considering only the most secure GRB-host associations in the sample (GRB 080218B and GRB 080207), the observations almost double the number of known very red GRBHs with  $(R - K)_{AB} > 3.5$ .

Compared to the general GRB host galaxy population (e.g., SBG09; their figure 2), the EROs are very bright in  $K$  and, therefore, possibly massive galaxies, especially the host of GRB 080207. Using complementary *Spitzer* satellite long-wavelength data, in Hunt et al. (2011) we have recently obtained a photometric redshift of about 2.2 for this galaxy. Unfortunately, in the case of GRB 080218B/object A no photometric redshift is known. In the case of GRB 080602 and GRB 081204, the ERO lies close to a galaxy with a photometric redshift  $\lesssim 2$  (see Sect. 5.2.1).

In a recent work on host galaxies of 14 dark bursts, mainly based on optical observations, Perley et al. (2009) unveiled one ERO associated to a GRB in their sample (GRB 070521). This raises the question why I find two EROs among three dark bursts, while these authors find only one ERO in their sample of 14 dark bursts. The main reason might be that their search for host galaxies concentrated on optical observations. Also, they used slightly different criteria to define their sample compared to what it is used here. For example, if I had used the J04 criterion only, the dark burst golden subsample would increase to 6 events (Table 5.2). Independent of this, both surveys demonstrate that optically dark bursts are tracers of very red galaxies.

Finally I note that in the case of GRB 080602 object A has low probability of  $p = 0.03$  of being located within the XRT error circle. In the same field object C (within the  $2r_0$  error circle) has a very red color of  $(R - K)_{AB} > 4.3$  mag, i.e. is an ERO. Therefore, there are two candidates based on two different selection criteria. This demonstrates once more how difficult it is to identify GRBHs in arcsec-sized XRT error circles when no optical afterglow was detected, i.e. when the error circle is larger than, say, 1 arcsec.

### 5.3.4 Lyman-dropout candidates

In one case of the input sample no objects are found down to deep VLT flux limits in  $R$  and  $K_s$  within the associated 90% XRT error circles (Table 5.6; GRB 080727A). In two other cases a candidate host galaxy is detected only in the deep  $K_s$ -band image (GRB 080602/object C, GRB 081105/object C). All three objects are candidates for a Lyman dropouts in the  $R_C$  band, i.e., for a redshift  $z \gtrsim 4.5$ . So, if my interpretation is correct, at most about 20% of all optically dim burst investigated here could lie at such redshifts. This is in qualitative agreement with Perley et al. (2009), who found that in their sample of optically non-detected afterglows at most 14% are at a redshift  $z > 5$ .

Can the GRBs mentioned above be defined as dark bursts? All three bursts fail to enter the golden dark GRB sample due to the large uncertainties in their optical-to-X-rays spectral index. In particular, in case of GRB 050922B there is a gap in the X-ray data at the time when the upper limit was obtained (at 49 ks). Therefore, I did not consider it as a well-defined dark burst. If, however, one extrapolates backwards in time based on the X-ray light curve after 100 ks, then the burst is dark according to J04 as well as V09. GRB 080727A, on the other hand, would become a dark burst according to the criterion proposed by V09, if one uses the  $1 \sigma$  error bar of  $\beta_X$  and not the more restrictive 90% confidence level. Finally, GRB 080602 did not enter the golden sample because the flat X-ray light curve might point to an additional X-ray component with potentially no corresponding optical counterpart (and no further X-ray data were obtained after about 2 ks; Evans et al. 2007, 2009).

### 5.3.5 Interacting pairs of galaxies as host galaxy candidates

Since long bursts are related to star formation, their host galaxies could be interacting, morphologically disturbed galaxies, where a star burst was triggered by galaxy-galaxy-interaction (e.g., Fruchter et al. 1999). In the present work, I do indeed find five potential cases of interacting pairs inside the XRT error circles. These are GRB 070429A, objects B and C ( $R_C$  band; Fig. C.3); GRB 080602, objects A and C ( $K_s$  band; Fig. 5.8); GRB 080915A, objects C and D ( $R_C$  and  $K_s$  band; Figs. C.4, 5.10); GRB 081105, objects A and C ( $K_s$  band; Fig. 5.11) as well as GRB 081204, objects B and F ( $R_C$  and  $K_s$  band; Figs. C.4, 5.13). Among these the most obvious cases for an interacting pair or group of galaxies are represented by GRB 070429A and GRB 081204.

Even though there are no statistics at hand that could provide chance probability values for finding an interacting pair of galaxies in a randomly chosen small area on the sky, it is worth to study if this is a good selection criterion for host galaxy identifications in *Swift*/XRT error circles of dark bursts (see also Wainwright et al. 2007).

### 5.3.6 Redshift estimates

No precise redshifts are known for the galaxies I have found in the XRT error circles. In the case of GRB 080602 and GRB 081204 the redshift is surely below 3.5 due to the detection of the object in the GROND  $g'$ -band but no further constraints can be set. Therefore, I tried the following to obtain redshift estimates.

Table C.1 provides estimated redshifts by assuming for all galaxies absolute magnitudes of  $M_R = -22, -20,$  and  $-18,$  respectively. The first value is about 1 mag below the most luminous galaxies found in the Las Campanas redshift survey ( $M_R = -23$ ; Lin et al. 1996), the middle value is approximately the characteristic  $M^*$  of the corresponding Schechter  $r$ -band luminosity function, while the third value roughly corresponds to the absolute magnitude of the Large Magellanic Cloud. By adopting a power-law spectrum for the SED of the form  $F_\nu \propto \nu^{-\beta}$ , the corresponding redshift was then calculated for two different spectral slopes ( $\beta = 0.0$  and  $1.0$ ).<sup>5</sup> If the deduced redshift was larger than 5, Lyman dropout in the  $R$ -band could have affected the apparent magnitudes and no values for  $z$  are given. I find that most galaxies, if not more luminous than the Milky Way, probably lie at redshifts smaller than  $z = 2$ .

### 5.3.7 Burst locations close to very bright galaxies and groups or clusters of galaxies

In four cases the XRT error boxes are situated relatively close to very bright galaxies or to a potential anonymous group or cluster of galaxies. Any physical relation with the corresponding GRB is difficult to establish, though. I note however that only 15 years ago any such relation might have been considered more seriously (e.g., Hurley et al. 1997; Gorosabel & Castro-Tirado 1997). My sub-sample of such associations includes GRB 061102, where a group of galaxies (possibly a cluster) is centered about 1.5 north of the XRT error circle, and GRB 081105, which has an XRT error circle that lies about 30 arcsec south of a bright, morphologically disturbed spiral that itself might belong to a relatively nearby, anonymous group or cluster of galaxies. I also note that galaxy B in the field of GRB 080915A has colors and a morphology similar to a galaxy about 30 arcsec north of the XRT error circle and similar to several other galaxies in the field.

---

<sup>5</sup>for the equation see Sect. 5.2.1

Finally, GRB 080123 also belongs to this subsample, where the XRT error circle is located 9'0 North-East of a bright spiral. Since this burst is classified as short (Ukwatta et al. 2008b,c; see also Sect. 5.2.1), this could be the host galaxy of this burst (Leibler & Berger 2010). However, the fact that deep VLT/FORS images reveal at least one galaxy in the 90% XRT error circle leaves open alternative candidates.

### 5.3.8 Host galaxy candidates of the golden dark burst sample

The golden dark burst subsample includes GRB 070429A, GRB 080207, and GRB 080218B (see Sect. 5.1.2). Interestingly, GRB 080207 and GRB 080218B also belong to the small subsample of bursts with extremely red host galaxy candidates (see Sect. 5.3.3). This supports the idea that global dust extinction was responsible for dimming the afterglow of these events in the optical bands. This holds especially for GRB 080207, for which one can be sure the host galaxy is without any doubt object B, thanks to the precise localization of its X-ray afterglow by *Chandra*.

In the case of GRB 080218B, a host galaxy candidate is visible in the  $R_C$ -band, constraining its redshift to  $\lesssim 4.5$ . For this event, Greiner et al. (2011) find that different pairs of  $(z, A_V)$  solutions can explain the non-detection of the optical/NIR afterglow by GROND. For example, for a redshift of 3.5 a host extinction of  $A_V^{\text{host}} = 1.5$  mag is required. A lower redshift would increase the deduced amount of host extinction. This supports the finding presented here that dust extinction in GRBHs plays an important role for the explanation of the dimness of optically dark bursts (see also Cenko et al. 2009; Perley et al. 2009). On the other hand, the host galaxy candidates in the case of GRB 070429A show a  $(R - K)$  color which is not particularly red. This points out that, if one of these galaxies is the host, *global* extinction by dust was not the reason for the dimness of this burst. However, the dust distribution could be patchy or the burst simply embedded within a dusty star-forming region in its host galaxy.

Could the other four bursts with very red host galaxy candidates (GRB 060923B, GRB 080602, GRB 081105 and GRB 081204) also enter the golden dark burst subsample? Unfortunately, the data quality is not good enough to tell. GRB 081204 did not enter it because of the large error of the X-ray spectral slope. The case of GRB 080602 was already discussed in Sect. 5.3.4 and in the case of GRB 060923B and GRB 081105 the reported upper limit in the optical bands (see Table 5.2) are not deep enough to provide a clue on the reason for the optical dimness of these events.

### 5.3.9 What makes dark bursts: it is not high redshift

For 17 of the 18 bursts investigated here it is possible to find galaxies inside the corresponding 90% XRT error circles (radius  $r_0$ ). This high detection rate is in agreement with the study of Perley et al. (2009). The only exception in my study is GRB 080727A, where no object is seen down to deep flux limits even inside a circle with radius  $2r_0$ . In six cases only one galaxy is visible in the corresponding 90% XRT error circle, making it the only detected host galaxy candidate (GRB 050922B, GRB 060805A, GRB 060919, GRB 080207, GRB 080218B and GRB 080602), while in six other cases more than one galaxy is detected inside  $r_0$  (GRB 060211A, GRB 060923B, GRB 070429A, GRB 080915A, GRB 081105 and GRB 081204). Finally, for two bursts, no galaxy is seen within  $r_0$  at all but at least one galaxy is detected within  $2r_0$  (GRB 061102 and GRB 081012). For GRB 050717 galaxy A extends into  $r_0$  but probably has its luminosity center outside the 90% error circle.

The fields of GRB 061102, GRB 080123, and GRB 081012 stand out in some way. In these cases galaxies are seen in the corresponding XRT error circle, at least within  $2r_0$ , but there is neither an

ERO found among them, nor evidence for an interacting pair of galaxies, nor does the magnitude- $p$  relation select a certain galaxy (all have  $p > 0.1$ ). As discussed in Sects. 5.2.1 and C.1, GRB 080123 is classified as a short burst according to its high-energy data and a bright galaxy 9'0 N-E of it is a good host galaxy candidate ( $p = 0.13 \pm 0.01$ ). For the other two bursts one must conclude however that, if one of these is the host, then it is a rather normal galaxy, i.e., typical for host galaxies of unextinguished GRBs.

Fynbo et al. (2009) shows that at least 39% of optically dim GRB afterglows are dark according to J04. If my sample of 16 true long bursts with no detected optical afterglow is representative for the entire ensemble of long dark bursts<sup>6</sup>, I conclude that cosmological Lyman dropout, i.e., high-redshift, is not required to explain the optical dimness of these events in most cases, because for most events (~90%) there is no lack of optically detected galaxies in *Swift*/XRT error circles. Most of them are faint, between  $R = 23$  and 26, a substantial fraction (about 1/3) might belong to an interacting pair of galaxies, a sign for triggered star formation. A fraction of at most 10% with redshifts  $z > 5$  brings the sample in agreement with what is known about the redshift distribution of long bursts with detected optical afterglows. In other words, the population of the dark bursts most likely does not represent a hidden long tail of missed high- $z$  events in the GRB redshift distribution. This finding is in agreement with Perley et al. (2009) and confirms the picture suggested in earlier studies (e.g., Klose et al. 2003; Tanvir et al. 2008; Fynbo et al. 2009; Cenko et al. 2009). In particular, these conclusions are in agreement with the results obtained by Greiner et al. (2011) that are based on rapid follow-up observations of GRB afterglows with the multi-channel imager GROND: it is extinction by dust and not a high redshift that dominates the dark burst population.

### 5.3.10 EROs as an important subpopulation of GRB host galaxies of dark GRBs

The six EROs I have found have a magnitude between  $K_{AB} = 21.6$  and 22.5, i.e.  $K_{Vega} = 19.8$  to 20.7 (Table 5.4). For these  $K$ -band magnitudes the number density of EROs on the sky is about 1 per 1000 arcsec<sup>2</sup> (Gonzalez-Perez et al. 2009; Hempel et al. 2011; Kim et al. 2011). These findings then point to an overdensity of EROs in the XRT error circles I have studied here and makes all of them to primary host galaxy candidates (Table 5.6). The physical association of long GRBs with the formation and death of the most massive stars naturally points to these galaxies, too. Four of the six EROs found in this work lie inside their corresponding 90% XRT error circle. In the remaining 2 cases (GRB 060923B and GRB 080602) the ERO lies just close the border of the 90% error circle and it is still among the best candidate when compared to the other galaxies (see Sect. 5.2.1).

The immediate conclusion one can draw from this study is that bursts with optically non-detected afterglows (but rapid and deep follow-up observations) trace a subpopulation of galaxies undergoing violent star formation. In particular: two of the three bursts that belong to the golden dark burst sample have an ERO within their XRT error circle (GRB 080207 and GRB 080218B). If one considers as dark all GRBs that follow the J04 or V09 criterion (but keeping in mind that this includes now events where the X-ray data are not so easily interpreted; Sect. 5.1.2), then 8 GRBs enter in this sample (Table 5.2) and 4 of them have an ERO in their XRT error circle (in addition these are GRB 080602 and GRB 081204). It should be stressed: in principle all GRBs studied here except GRB 070517A (for which I identified the afterglow; Sect. 5.2.1) could fulfill the criterion from J04 and V09, i.e. they were dark because of either dust extinction or high redshift. However, there are not deep enough

---

<sup>6</sup>excluding GRB 070517, where the optical afterglow was finally identified (Sect. 5.2.1) and excluding GRB 080123, which might have been a short burst but with  $T_{90} > 2$  s in the *Swift*/BAT energy window (Sect. 5.2.1 and C.1)



optical limits to arrive at this conclusion.

Several previous studies have already targeted GRBHs (e.g., Le Floc'h et al. 2003; Christensen et al. 2004; Fruchter et al. 2006; Ovaldsen et al. 2007; Svensson et al. 2010 and SBG09). They concentrated on the low-redshift regime (up to  $z \sim 1.5$ ) and showed that most hosts are subluminal ( $L < L^*$ ), blue, of low metallicity and with a moderate star formation rate ( $\sim 1 - 10 M_{\odot} \text{yr}^{-1}$ ). However, my results indicate that an infrared-bright subpopulation of very dusty GRB host galaxies exists, which stands out from the main GRB host galaxy population.

Redshift measurements for the EROs I have found here are missing in most cases so far. However, for the ERO related to GRB 080207 a photometric redshift could be deduced recently (Hunt et al. 2011). Its observed broad-band SED implies a very luminous ( $M_K \sim 24.4$ ), infrared-bright galaxy, very different from the sample of GRBHs compiled by SBG09. This galaxy is in color, luminosity, and redshift similar to the host of the dark bursts GRB 080325 (Hashimoto et al. 2010) and GRB 080607 (Chen et al. 2010, 2011). These findings suggest a possible bias in the GRB host samples studied so far, which are dominated by host galaxies of optically detected afterglows. This conclusion is in agreement with a recent work on dark bursts observed with GROND (Krühler et al. 2011), where it is shown that highly extinguished afterglows trace a subpopulation of more luminous, massive, metal-rich, and chemically evolved GRB host galaxies that was missed in previous surveys.

One might wonder if EROs could, on average, have a higher metallicity than the bluer and globally not dust-enshrouded main population of GRB host galaxies. Since the single-star scenario for long burst progenitors favours low metallicities theoretically (e.g., Hirschi et al. 2005; Langer & Norman 2006) as well as observationally (e.g., Gorosabel et al. 2005; Han et al. 2010; Rau et al. 2010), the occurrence of EROs as GRB host galaxies could point to a second evolutionary channel that can produce GRB progenitors. In fact, it has been suggested that the long-burst population splits into single star progenitors and those belonging to a merging binary system, with the latter not being strongly dependent on metallicity issues (e.g., Fryer et al. 2007; Georgy et al. 2009). A statistical study of the circumburst environments into which the afterglows develop also suggests the existence of two populations of GRB progenitors (Schulze et al. 2011).

## 5.4 Summary of the host galaxies of dark GRBs

Motivated by the non-detection of the optical afterglows of a substantial fraction of *Swift* bursts with well-observed X-ray afterglows, I have selected 18 such events with small *Swift*/XRT error circles and searched for the potential host galaxies of these bursts using deep multi-colour imaging. The primary telescope of this study was the VLT equipped with FORS1, FORS2, & VIMOS for  $R_C$ -band imaging and ISAAC & HAWK-I for  $K_s$ -band imaging. This was supplemented by observations with the 7-channel imager GROND mounted at the 2.2-m MPG/ESO telescope on La Silla and by the infrared imager NEWFIRM mounted at the 4-m Mayall telescope on Kitt Peak. The limiting magnitudes achieved were deep, usually  $R_{AB} = 26.5$  and  $K_{AB} = 23.5$  as well as  $g'r'i'z'JHK = 25.5, 25, 24.5, 24, 22.5, 21.5, 21$  for GROND. The latter data included late-time imaging as well as data gained in Rapid Response Mode, where I did not find evidence for a fading afterglow.

In the sample I have studied, I found only three cases where the corresponding GRB host galaxy could have a Lyman dropout in the  $R_C$  band (GRB 080602, GRB 080727A, GRB 081105). This included one case where no object was seen at all within the corresponding XRT error circle down to deep magnitudes ( $R_{AB} > 26$ ,  $K_{AB} > 23$ ; GRB 080727A) and two bursts where a galaxy was detected only in the  $K_s$ -band (GRB 080602/object C, GRB 081105/object C) and lied very close to an optically

brighter galaxy. The latter two belong to a subsample of six events for which I found extremely red objects (EROs;  $(R - K)_{AB} > 3.5$  mag) inside the corresponding XRT error circle (the other four EROs are detected also in the  $R$ -band). Given that EROs represent a unique galaxy population with respect to their global physical parameters, a physical relation of them to the corresponding GRBs seems appealing. This implies that extinction by host galaxy dust (either local or global) is the most natural explanation for the optical dimness of these events. Lyman dropout in the optical bands due to high-redshift is usually not required. This conclusion is not contradicted by the fact that the latter four events do not fulfill the J04 as well as the V09 criterion, which then still leaves open the possibility that these afterglows have only been intrinsically faint. In fact, for all six events the probability of finding an ERO within the corresponding XRT error circle turned out to be less than 10%. This is a strong statistical argument in favor of the idea that extinction by dust in their host galaxies was the main reason for the optical non-detection of these afterglows and not just their intrinsic faintness.

While the  $(R - K)$  color of galaxies turned out to be a powerful criterion to find host galaxy candidates, I also considered chance-probability constraints based on published number counts of galaxies on the sky. In seven cases the chance probability  $p$  to find a galaxy of the detected  $R_C$ -band magnitude in the corresponding 90% XRT error circle was  $\lesssim 10\%$ , that makes them good host galaxy candidates. In the remaining cases, host galaxy candidates were found but they are not special in some way, neither with respect to their  $(R - K)$  colors, nor their magnitudes, nor their  $p$ -values. However, in five events studied here, I found pairs of probably interacting galaxies in the XRT error circles, potentially a sign of triggered star-formation.

The connection between star-forming activity and dark bursts is even more intriguing for the six EROs found in this sample. This is the most outstanding discovery of this investigation. It points to the existence of a subpopulation of GRB host galaxies that is characterized by violent star formation that is missed by host galaxy surveys of bursts with well-observed optical afterglows. The putative host of GRB 080207 is the most remarkable example ( $(R - K)_{AB} = 4.66 \pm 0.40$  mag; see also Hunt et al. 2011). The possibility that a non-negligible fraction of dark bursts traces highly dust-enshrouded and possibly submm-bright galaxies makes these bursts an interesting tool to obtain deeper insight into the optically hidden star formation history of the Universe.

# Chapter 6

## Summary

Gamma-ray bursts are outstanding phenomena for what concerns the physical origin, the released energy, the cosmological distance and for highlighting galaxies with peculiar properties. Today a big effort is devoted to the discovery, the localization and the follow-up of GRBs and their afterglows in gamma-rays, X-rays and the optical/NIR bands with instruments on board the *Swift* satellite and dedicated ground-based facilities like the seven-channel imager GROND. While the gamma-ray light curves show much variability, optical/NIR and X-ray light curves of afterglows can be characterized by few several power-law segments. The diversity is however high and complicated by several possible concurring events like jet breaks, flares and more exotic possibilities like energy injections.

The spectral energy distribution, both during the prompt and the subsequent afterglow phase, shows a power-law or a broken power-law structure. The standard fireball model succeeded in describing the power-law shape of the light curves and the SEDs of the prompt and of the afterglow phase as synchrotron radiation released due to relativistic shocks. However, for the prompt emission phase still it was missing a complete optical to gamma-rays SED, well-sampled in frequency domain and in time. This holds in particular during the bright flares often observed during a GRB, which origin and physics still have to be understood.

In Chapter 3 I first reported on the gamma-ray, X-ray and optical observations of the prompt phase of GRB 080928. GRB 080928 was a long burst, lasting for about 400 seconds, detected by *Swift*/BAT and *Fermi*/GBM and its prompt emission was followed up by XRT and UVOT on board the *Swift* satellite. These observations were complemented by ground-based data obtained with the ROTSE-IIIa optical telescope. The prompt emission of this burst was dominated by a bright peak, which was observed in gamma-rays and X-rays. A second flare was visible in X-rays only. For this phase, I was able to build and follow the optical to gamma-ray SED for a total of seven epochs, the first three during the first bright flare. I could show that the SED during the first epoch shows a clear break around 4 keV, and the slopes of the low and high energy branch are in good agreement with the expectation from synchrotron theory, implying that the radiation comes from the same ensemble of hot electrons. To the best of my knowledge, it was for the first time that this could be shown. Furthermore, thanks to the good sampling of the SED during the main flare, a generalized large-angle emission model suggested by A. Panaitescu (private communication) was applied. Within this model the observed parameters, the peak flux and the peak energy, depend from the viewing angle. The model gave a good prediction of the optical, X-ray and gamma-ray SEDs in the following two epochs. Unfortunately, it was not possible to apply the model to the following epochs, because of a possible contamination of the observed flux from the second X-ray flare.

In Chapter 4 I studied the afterglows of GRB 080514B and GRB 080928. The former was a

high-energy, long GRB detected by *AGILE* with photons emitted above 30 MeV and it was the first high-energy event that could be followed up by *Swift* and ground-based observatories like GROND. The light curve showed a single power-law decay and the SED showed a break between the X-rays and the optical/NIR bands, in full accordance with synchrotron emission. The combined analysis of the light curve and the SED, favors a wind profile of the GRB environment, implying a massive star to be the progenitor of this long GRB. The main result on the study of GRB 080514B was the estimation of its photometric redshift,  $z = 1.8_{-0.3}^{+0.4}$ , an important result due to the lack of spectroscopic measurements. This finding allowed me to determine the energy budget of the burst. Thanks to this analysis, I could show that while GRB 080514B was outstanding for its high-energy photons released, it was followed by an X-ray and an optical/NIR afterglow without peculiar properties. This fact implies that high-energy emission in the gamma-ray band does not correlate with the occurrence of special features in the corresponding afterglow light. The detected underlying GRB host galaxy showed no outstanding properties, too.

Very different to GRB 080514B was GRB 080928 ( $z = 1.692$ ). While they were at a similar redshift, GRB 080928 had no high energy emission, it was not seen above 150 keV. The afterglow light curve was also different, i.e., not a simple power-law, but it showed a peculiar behavior with several re-brightenings, which could be explained as energy injections. After this phase, the optical and X-ray afterglow light curve both evolved with a power-law decay. The observed spectral slope of the SED followed the expectations from the theoretical closure relations. No host galaxy was found and no other galaxy (or groups) lied at the same redshift of the burst. Assuming a typical host galaxy template, I obtained a lower limit for its absolute magnitude of  $M_r > -19.94$ , which is in agreement with the luminosities found so far for the GRB host galaxy population. In fact, much less luminous hosts are known.

Chapter 5 was finally dedicated to the problem of GRBs with detected X-ray but no detected optical/NIR afterglow, the so-called dark GRBs. The possible causes are: an afterglow with low brightness, a dropout due to very high-redshift when Lyman absorption moves into the optical bands, or extinction by dust in the interstellar medium of the corresponding GRB host galaxy. Here, I studied a sample of 18 dark bursts with arcsec-sized X-ray error circle and searched for their host galaxies. This sample was mainly build up from several approved observing proposals for the ESO/VLT 8.2m telescopes. The sample of dark GRBs had to be reduced to 16 after the discovery of the afterglow of a GRB 070517 and a detailed analysis about the long duration nature of GRB 080123. The analysis of the deep imaging data within the arcsec-size XRT error circle of the remaining 16 dark GRBs, led to the discovery of 6 extremely red objects (EROs) as the host galaxies of the corresponding dark bursts. These galaxies might be reddened by their extreme dust content. This implies that dark bursts might trace a subpopulation of extremely red, globally dust-enshrouded galaxies, markedly different from the main body of the GRB host galaxy population, which are blue, sub-luminous, compact galaxies. This subpopulation might be missed by host galaxy surveys of bursts with well-observed optical afterglows. Statistical arguments led to the conclusion that all 6 extremely red objects are physically related to the corresponding GRB. In other words, most likely these are the corresponding GRB host galaxies. This implies that for at least 6 of the 16 events investigated here, extinction by cosmic dust in their host galaxies was the reason for the optical dimness of these bursts. The non-detection of any optically visible galaxy in 3 of the 16 X-ray error circles down to very deep flux limits indicates that for this small fraction of dark GRBs a high redshift could have been the reason for the optical dimness of the corresponding bursts. Finally, it is noteworthy that 5 of the 16 dark GRBs have pairs of galaxies (potentially interacting) in their arcsec-sized X-ray error circles. This implies, in agreement

with the general picture of the nature of the long burst population, that actively star-forming galaxies represent an important subpopulation of the host galaxies of long bursts.

In this thesis I have used a combination of optical/NIR data to study GRBs, their afterglows, and their host galaxies. This approach turned out to be very successful for unveiling the physical processes behind these events. Future studies still have to clarify a lot of open questions like the physical interpretation very complicate prompt and afterglow light curve, like in the case of GRB 080928 afterglow, or the importance or EROs among the GRB host galaxy population.

## Bibliography

- Achterberg, A., Gallant, Y. A., Kirk, J. G., & Guthmann, A. W. 2001, *Mon. Not. R. Astron. Soc.*, 328, 393
- Akerlof, C. W., Kehoe, R. L., McKay, T. A., et al. 2003, *Publ. Astron. Soc. Pacific*, 115, 132
- Alcock, C., Allsman, R. A., Alves, D., et al. 1999, *Astroph. J.*, 521, 602
- Amati, L. 2006, *Mon. Not. R. Astron. Soc.*, 372, 233
- Amati, L., Frontera, F., & Guidorzi, C. 2009, *Astron. & Astroph.*, 508, 173
- Amati, L., Frontera, F., Tavani, M., et al. 2002, *Astron. & Astroph.*, 390, 81
- Antonelli, L. A., D'Avanzo, P., Perna, R., et al. 2009, *Astron. & Astroph.*, 507, L45
- Atwood, W. B., Abdo, A. A., Ackermann, M., et al. 2009, *Astroph. J.*, 697, 1071
- Avni, Y. 1976, *Astroph. J.*, 210, 642
- Band, D., Matteson, J., Ford, L., et al. 1993, *Astroph. J.*, 413, 281
- Barthelmy, S. D., Barbier, L. M., Cummings, J. R., et al. 2005a, *Space Sci. Rev.*, 120, 143
- Barthelmy, S. D., Chincarini, G., Burrows, D. N., et al. 2005b, *Nature*, 438, 994
- Beardmore, A. P., Burrows, D. N., & Cummings, J. R. 2008, *GCN Circ.*, 8522
- Belczynski, K., Perna, R., Bulik, T., et al. 2006, *Astroph. J.*, 648, 1110
- Berger, E. 2009, *Astroph. J.*, 690, 231
- Berger, E., Fox, D. B., Kulkarni, S. R., Frail, D. A., & Djorgovski, S. G. 2007, *Astroph. J.*, 660, 504
- Berger, E., Price, P. A., Cenko, S. B., et al. 2005, *Nature*, 438, 988
- Beuermann, K., Hessman, F. V., Reinsch, K., et al. 1999, *Astron. & Astroph.*, 352, L26
- Blackburn, J. K. 1995, in *Astronomical Society of the Pacific Conference Series*, Vol. 77, *Astronomical Data Analysis Software and Systems IV*, ed. R. A. Shaw, H. E. Payne, & J. J. E. Hayes, 367
- Blake, C. H., Bloom, J. S., Starr, D. L., et al. 2005, *Nature*, 435, 181
- Blandford, R. D. & Znajek, R. L. 1977, *Mon. Not. R. Astron. Soc.*, 179, 433
- Bloom, J. S., Berger, E., Kulkarni, S. R., Djorgovski, S. G., & Frail, D. A. 2003, *Astron. J.*, 125, 999
- Bloom, J. S., Frail, D. A., & Sari, R. 2001, *Astron. J.*, 121, 2879
- Bloom, J. S., Kulkarni, S. R., & Djorgovski, S. G. 2002, *Astron. J.*, 123, 1111
- Bloom, J. S., Starr, D. L., Blake, C. H., Skrutskie, M. F., & Falco, E. E. 2006, in *Astronomical Society of the Pacific Conference Series*, Vol. 351, *Astronomical Data Analysis Software and Systems XV*, ed. C. Gabriel, C. Arviset, D. Ponz, & S. Enrique, 751
- Boella, G., Butler, R. C., Perola, G. C., et al. 1997a, *Astron. & Astroph. Suppl.*, 122, 299
- Boella, G., Chiappetti, L., Conti, G., et al. 1997b, *Astron. & Astroph. Suppl.*, 122, 327
- Bolzonella, M., Miralles, J.-M., & Pelló, R. 2000, *Astron. & Astroph.*, 363, 476
- Bouwens, R. J., Illingworth, G. D., Labbe, I., et al. 2011, *Nature*, 469, 504
- Bouwens, R. J., Illingworth, G. D., Oesch, P. A., et al. 2010, *Astroph. J.*, 709, L133
- Bromm, V., Yoshida, N., Hernquist, L., & McKee, C. F. 2009, *Nature*, 459, 49
- Burrows, D. N., Hill, J. E., Nousek, J. A., et al. 2005a, *Space Sci. Rev.*, 120, 165
- Burrows, D. N., Romano, P., Falcone, A., et al. 2005b, *Science*, 309, 1833
- Butler, N. R. 2007, *Astron. J.*, 133, 1027
- Butler, N. R. & Kocevski, D. 2007, *Astroph. J.*, 663, 407
- Cardelli, J. A., Clayton, G. C., & Mathis, J. S. 1989, *Astroph. J.*, 345, 245
- Castro-Tirado, A. J., Bremer, M., McBreen, S., et al. 2007, *A&A*, 475, 101
- Castro-Tirado, A. J., Soldán, J., Bernas, M., et al. 1999, *Astron. & Astroph. Suppl.*, 138, 583
- Cenko, S. B., Fox, D. B., Moon, D.-S., et al. 2006, *Publ. Astron. Soc. Pacific*, 118, 1396
- Cenko, S. B., Kelemen, J., Harrison, F. A., et al. 2009, *Astroph. J.*, 693, 1484
- Chary, R., Berger, E., & Cowie, L. 2007, *Astroph. J.*, 671, 272
- Chen, H., Perley, D. A., Wilson, C. D., et al. 2010, *Astroph. J.*, 723, L218
- Chen, H., Perley, D. A., Wilson, C. D., et al. 2011, *Astroph. J.*, 727, L53

- Chevalier, R. A. & Li, Z.-Y. 2000, *Astroph. J.*, 536, 195
- Chincarini, G., Mao, J., Margutti, R., et al. 2010, *Mon. Not. R. Astron. Soc.*, 406, 2113
- Chincarini, G., Moretti, A., Romano, P., et al. 2007, *Astroph. J.*, 671, 1903
- Chornock, R., Berger, E., Levesque, E. M., et al. 2010, *Astroph. J.*, submitted (arXiv:1004.2262)
- Chornock, R., Cenko, S. B., Griffith, C. V., et al. 2009, *GCN Circ.*, 9151
- Christensen, L., Hjorth, J., & Gorosabel, J. 2004, *Astron. & Astroph.*, 425, 913
- Clemens, C., Rossi, A., Greiner, J., & McBreen, S. 2008, *GCN Circ.*, 8257, 1
- Costa, E., Feroci, M., Piro, L., et al. 1997a, *IAU Circ.*, 6576
- Costa, E., Frontera, F., Heise, J., et al. 1997b, *Nature*, 387, 783
- Cucchiara, A., Levan, A. J., Fox, D. B., et al. 2011, *Astroph. J.*, 736, 7
- Cucchiara, A. & Ukwatta, T. N. 2008, *GCN Circ.*, 7207
- Cummings, J., Barthelmy, S. D., Baumgartner, W., et al. 2008, *GCN Circ.*, 8294
- Curran, P. A., Evans, P. A., de Pasquale, M., Page, M. J., & van der Horst, A. J. 2010, *Astroph. J.*, 716, L135
- de Pasquale, M., Evans, P., Oates, S., et al. 2009, *Mon. Not. R. Astron. Soc.*, 392, 153
- De Pasquale, M., Schady, P., Kuin, N. P. M., et al. 2010, *Astroph. J.*, 709, L146
- de Ugarte Postigo, A., Castro-Tirado, A. J., Guziy, S., et al. 2006, *Astroph. J.*, 648, L83
- de Ugarte Postigo, A., Thöne, C. C., Goldoni, P., Fynbo, J. P. U., & the X-shooter GRB collaboration. 2011, *Astronomische Nachrichten*, 332, 297
- Djorgovski, S. G., Frail, D. A., Kulkarni, S. R., et al. 2001, *ApJ*, 562, 654
- Djorgovski, S. G., Kulkarni, S. R., Bloom, J. S., & Frail, D. A. 1999, *GCN Circ.*, 289
- Donaghy, T. Q., Lamb, D. Q., Sakamoto, T., et al. 2006, *Astroph. J.*, submitted (astro-ph/0605570)
- Dullighan, A., Ricker, G., Butler, N., & Vanderspek, R. 2004, in *American Institute of Physics Conference Series*, Vol. 727, *Gamma-Ray Bursts: 30 Years of Discovery*, ed. E. Fenimore & M. Galassi, 467–470
- Elíasdóttir, Á., Fynbo, J. P. U., Hjorth, J., et al. 2009, *Astroph. J.*, 697, 1725
- Elston, R., Rieke, G. H., & Rieke, M. J. 1988, *Astroph. J.*, 331, L77
- Evans, I. N., Primini, F. A., Glotfelty, K. J., et al. 2010a, *Astroph. J. Suppl.*, 189, 37
- Evans, P. A., Beardmore, A. P., Page, K. L., et al. 2009, *Mon. Not. R. Astron. Soc.*, 397, 1177
- Evans, P. A., Beardmore, A. P., Page, K. L., et al. 2007, *Astron. & Astroph.*, 469, 379
- Evans, P. A., Willingale, R., Osborne, J. P., et al. 2010b, *Astron. & Astroph.*, 519, A102
- Falcone, A. D., Morris, D., Racusin, J., et al. 2007, *Astroph. J.*, 671, 1921
- Fenimore, E., Barthelmy, S. D., Baumgartner, W., et al. 2008, *GCN Circ.*, 8297
- Fenimore, E. & Sumner, M. 1997, in *All-Sky X-ray Observations in the Next Decade*, ed. M. Matsuoka & N. Kawai, 167
- Ferrero, A., French, J., & Melady, G. 2008, *GCN Circ.*, 8303
- Ferrero, P., Kloke, S., Kann, D. A., et al. 2009, *Astron. & Astroph.*, 497, 729
- Filgas, R., Kruehler, T., Greiner, J., et al. 2008, *GCN Circ.*, 8373
- Fishman, G. J., Meegan, C. A., Parnell, T. A., et al. 1985, in *International Cosmic Ray Conference*, Vol. 3, *International Cosmic Ray Conference*, ed. F. C. Jones, 343–346
- Fishman, G. J., Meegan, C. A., Wilson, R. B., et al. 1994, *Astroph. J. Suppl.*, 92, 229
- Foley, S., Watson, D., Gorosabel, J., et al. 2006, *Astron. & Astroph.*, 447, 891
- Fong, W., Berger, E., & Fox, D. B. 2010, *Astroph. J.*, 708, 9
- Fox, D. B., Price, P. A., & Berger, E. 2007, *GCN Circ.*, 6420
- Frail, D. A., Kulkarni, S. R., Nicastro, L., Feroci, M., & Taylor, G. B. 1997, *Nature*, 389, 261
- Frail, D. A., Kulkarni, S. R., Sari, R., et al. 2001, *Astroph. J.*, 562, L55
- Frontera, F., Costa, E., dal Fiume, D., et al. 1997, *Astron. & Astroph. Suppl.*, 122, 357
- Fruchter, A., Krolik, J. H., & Rhoads, J. E. 2001, *Astroph. J.*, 563, 597
- Fruchter, A. S., Levan, A. J., Strolger, L., et al. 2006, *Nature*, 441, 463
- Fruchter, A. S., Thorsett, S. E., Metzger, M. R., et al. 1999, *Astroph. J.*, 519, L13

- Fryer, C. L., Mazzali, P. A., Prochaska, J., et al. 2007, *Publ. Astron. Soc. Pacific*, 119, 1211
- Fynbo, J. P. U., Jakobsson, P., Prochaska, J. X., et al. 2009, *Astroph. J. Suppl.*, 185, 526
- Fynbo, J. U., Jensen, B. L., Gorosabel, J., et al. 2001, *A&A*, 369, 373
- Galama, T. J., Vreeswijk, P. M., van Paradijs, J., et al. 1998, *Nature*, 395, 670
- Galama, T. J. & Wijers, R. A. M. J. 2001, *Astroph. J.*, 549, L209
- Gehrels, N., Barthelmy, S. D., Burrows, D. N., et al. 2008, *Astroph. J.*, 689, 1161
- Gehrels, N., Chincarini, G., Giommi, P., et al. 2004, *Astroph. J.*, 611, 1005
- Gehrels, N., Ramirez-Ruiz, E., & Fox, D. B. 2009, *Annu. Rev. Astro. Astroph.*, 47, 567
- Gehrels, N., Sarazin, C. L., O'Brien, P. T., et al. 2005, *Nature*, 437, 851
- Gendre, B., Galli, A., & Bor, M. 2008, *GCN Circ.*, 7730, 1
- Georgy, C., Meynet, G., Walder, R., Folini, D., & Maeder, A. 2009, *Astron. & Astroph.*, 502, 611
- Giuliani, A., Fornari, F., Mereghetti, S., et al. 2008a, *GCN Circ.*, 7716, 1
- Giuliani, A., Mereghetti, S., Fornari, F., et al. 2008b, *Astron. & Astroph.*, 491, L25
- G.J. Fishman. 1999, *Astron. Astrophys. Suppl. Ser.*, 138, 395
- Goldoni, P., Flores, H., Malesani, D., et al. 2010, *GCN Circ.*, 10684
- Golenetskii, S., Aptekar, R., Mazets, E., et al. 2008, *GCN Circ.*, 7751, 1
- Gonzalez-Perez, V., Baugh, C. M., Lacey, C. G., & Almeida, C. 2009, *Mon. Not. R. Astron. Soc.*, 398, 497
- Goodman, J. 1997, *New Astronomy*, 2, 449
- Gorosabel, J. & Castro-Tirado, A. J. 1997, *Astroph. J.*, 483, L83
- Gorosabel, J., Christensen, L., Hjorth, J., et al. 2003, *Astron. & Astroph.*, 400, 127
- Gorosabel, J., Pérez-Ramírez, D., Sollerman, J., et al. 2005, *Astron. & Astroph.*, 444, 711
- Götz, D., Covino, S., Hascoët, R., et al. 2011, *Mon. Not. R. Astron. Soc.*, 413, 2173
- Granot, J. & Ramirez-Ruiz, E. 2010, *ArXiv e-prints: astro-ph: 1012.5101*
- Greiner, J., Bornemann, W., Clemens, C., et al. 2008a, *Publ. Astron. Soc. Pacific*, 120, 405
- Greiner, J., Bornemann, W., Clemens, C., et al. 2007, *The Messenger*, 130, 12
- Greiner, J., Clemens, C., Krühler, T., et al. 2009a, *Astron. & Astroph.*, 498, 89
- Greiner, J., Kruehler, T., & Rossi, A. 2008b, *GCN Circ.*, 8223
- Greiner, J., Krühler, T., Fynbo, J. P. U., et al. 2009b, *Astroph. J.*, 693, 1610
- Greiner, J., Krühler, T., Klose, S., et al. 2011, *Astron. & Astroph.*, 526, A30
- Greiner, J., Peimbert, M., Estaban, C., et al. 2003, *GCN Circ.*, 2020, 1
- Groot, P. J., Galama, T. J., van Paradijs, J., et al. 1998, *ApJ*, 493, L27
- Guziy, S., Gorosabel, J., Castro-Tirado, A. J., et al. 2005a, *Astron. & Astroph.*, 441, 975
- Guziy, S., Jelinek, M., Gorosabel, J., et al. 2005b, *GCN Circ.*, 4025
- Haislip, J. B., Nysewander, M. C., Reichart, D. E., et al. 2006, *Nature*, 440, 181
- Han, X. H., Hammer, F., Liang, Y. C., et al. 2010, *Astron. & Astroph.*, 514, A24
- Hashimoto, T., Ohta, K., Aoki, K., et al. 2010, *Astroph. J.*, 719, 378
- Hempel, A., Cristóbal-Hornillos, D., Prieto, M., et al. 2011, *ArXiv e-prints: astro-ph: 1102.3302*
- Hirschi, R., Meynet, G., & Maeder, A. 2005, *Astron. & Astroph.*, 443, 581
- Hjorth, J., Sollerman, J., Møller, P., et al. 2003, *Nature*, 423, 847
- Hogg, D. W., Pahre, M. A., McCarthy, J. K., et al. 1997, *Mon. Not. R. Astron. Soc.*, 288, 404
- Holland, S. T. 2008, *GCN Circ.*, 7759, 1
- Horváth, I. 1998, *Astroph. J.*, 508, 757
- Horváth, I., Balázs, L. G., Bagoly, Z., Ryde, F., & Mészáros, A. 2006, *Astron. & Astroph.*, 447, 23
- Hunt, L., Palazzi, E., Rossi, A., et al. 2011, *Astroph. J.*, 736, L36
- Hurkett, C., Page, K., Burrows, D., et al. 2005, *GRB Coordinates Network*, 3636, 1
- Hurley, K., Hartmann, D., Kouveliotou, C., et al. 1997, *Astroph. J.*, 479, L113
- Hurley, K., Mitrofanov, I., Kozyrev, A., et al. 2006, *Astroph. J. Suppl.*, 164, 124
- Iwamoto, K., Mazzali, P. A., Nomoto, K., et al. 1998, *Nature*, 395, 672



- Jager, R., Mels, W. A., Brinkman, A. C., et al. 1997, *Astron. & Astroph. Suppl.*, 125, 557
- Jakobsson, P., Hjorth, J., Fynbo, J. P. U., et al. 2004, *ApJ*, 617, L21
- Jaunsen, A. O., Rol, E., Watson, D. J., et al. 2008, *Astroph. J.*, 681, 453
- Jóhannesson, G. 2006, PhD thesis, University of Iceland
- Jóhannesson, G., Björnsson, G., & Gudmundsson, E. H. 2006, *Astroph. J.*, 647, 1238
- Kalberla, P. M. W., Burton, W. B., Hartmann, D., et al. 2005, *Astron. & Astroph.*, 440, 775
- Kann, D. A., Klose, S., & Zeh, A. 2006, *Astroph. J.*, 641, 993
- Kann, D. A., Klose, S., Zhang, B., et al. 2011, *Astroph. J.*, 734, 96
- Kann, D. A., Klose, S., Zhang, B., et al. 2010, *Astroph. J.*, 720, 1513
- Kann, D. A., Klose, S., Zhang, B., et al. 2008, *Astroph. J.*, submitted, arXiv:0804.1959
- Kawai, N., Kosugi, G., Aoki, K., et al. 2006, *Nature*, 440, 184
- Kennea, J. A., Burrows, D. N., Hurkett, C., Page, K., & Gehrels, N. 2005, *GRB Coordinates Network*, 3634
- Kim, J.-W., Edge, A. C., Wake, D. A., & Stott, J. P. 2011, *Mon. Not. R. Astron. Soc.*, 410, 241
- Kirk, J. G., Guthmann, A. W., Gallant, Y. A., & Achterberg, A. 2000, *Astroph. J.*, 542, 235
- Kistler, M. D., Yüksel, H., Beacom, J. F., Hopkins, A. M., & Wyithe, J. S. B. 2009, *Astroph. J.*, 705, L104
- Klebesadel, R. W., Strong, I. B., & Olson, R. A. 1973, *Astroph. J.*, 182, L85
- Klose, S., Eisloffel, J., & Richter, S. 1996, *Astroph. J.*, 470, L93
- Klose, S., Greiner, J., Rau, A., et al. 2004, *Astron. J.*, 128, 1942
- Klose, S., Henden, A. A., Greiner, J., et al. 2003, *ApJ*, 592, 1025
- Klotz, A., Gendre, B., Stratta, G., et al. 2008, *Astron. & Astroph.*, 483, 847
- Kouveliotou, C., Meegan, C. A., Fishman, G. J., et al. 1993, *Astroph. J.*, 413, L101
- Krimm, H. A., Granot, J., Marshall, F. E., et al. 2007, *Astroph. J.*, 665, 554
- Krimm, H. A., Hurkett, C., Pal'shin, V., et al. 2006, *ApJ*, 648, 1117
- Krühler, T., Greiner, J., McBreen, S., et al. 2009, *Astroph. J.*, 697, 758
- Krühler, T., Greiner, J., Schady, P., et al. 2011, *ArXiv e-prints*
- Krühler, T., Küpcü Yoldaş, A., Greiner, J., et al. 2008, *Astroph. J.*, 685, 376
- Kuin, N. P. M., Sakamoto, T., & Holland, S. 2008, *GCN Circ.*, 8298
- Kumar, P. & Panaitescu, A. 2000, *Astroph. J.*, 541, L51
- Langer, N. & Norman, C. A. 2006, *Astroph. J.*, 638, L63
- Laskar, T., Berger, E., & Chary, R.-R. 2011, *Astroph. J.*, submitted (arXiv:1102.1019)
- Lazzati, D., Covino, S., & Ghisellini, G. 2002, *Mon. Not. R. Astron. Soc.*, 330, 583
- Le Floch, E., Duc, P., Mirabel, I. F., et al. 2003, *Astron. & Astroph.*, 400, 499
- Lee, H. K., Wijers, R. A. M. J., & Brown, G. E. 2000, *Physics Reports*, 325, 83
- Lee, W. H. & Ramirez-Ruiz, E. 2007, *New Journal of Physics*, 9, 17
- Lehnert, M. D., Nesvadba, N. P. H., Cuby, J.-G., et al. 2010, *Nature*, 467, 940
- Leibler, C. N. & Berger, E. 2010, *Astroph. J.*, 725, 1202
- Levan, A., Fruchter, A., Rhoads, J., et al. 2006a, *Astroph. J.*, 647, 471
- Levan, A. J., Tanvir, N. R., Fruchter, A. S., et al. 2006b, *Astroph. J.*, 648, L9
- Li, L. 2008, *Mon. Not. R. Astron. Soc.*, 388, 1487
- Liang, E.-W., Racusin, J. L., Zhang, B., Zhang, B.-B., & Burrows, D. N. 2008, *Astroph. J.*, 675, 528
- Liang, E. W., Zhang, B., O'Brien, P. T., et al. 2006, *Astroph. J.*, 646, 351
- Liang, E.-W., Zhang, B.-B., & Zhang, B. 2007, *Astroph. J.*, 670, 565
- Lin, H., Kirshner, R. P., Sheckman, S. A., et al. 1996, *Astroph. J.*, 464, 60
- Lithwick, Y. & Sari, R. 2001, *Astroph. J.*, 555, 540
- Longair, M. S. 1994, *High energy astrophysics. Volume 2. Stars, the Galaxy and the interstellar medium.*
- Madau, P. 1995, *Astroph. J.*, 441, 18
- Malesani, D., Quirion, P., Fynbo, J. P. U., & Jakobsson, P. 2008, *GRB Coordinates Network*, 7783, 1
- Manzo, G., Giarrusso, S., Santangelo, A., et al. 1997, *Astron. & Astroph. Suppl.*, 122, 341

- Mao, J. 2010, *Astroph. J.*, 717, 140
- Mazets, E. P., Golenetskii, S. V., Ilyinskii, V. N., et al. 1981, *Astroph. & Space Sc.*, 80, 119
- McBreen, S., Krühler, T., Rau, A., et al. 2010, *Astron. & Astroph.*, in press, arXiv:1003.3885
- McLean, K., Barthelmy, S. D., Baumgartner, W., et al. 2008, *GCN Circ.*, 8029
- Meegan, C., Lichti, G., Bhat, P. N., et al. 2009, *Astroph. J.*, 702, 791
- Metzger, M. R., Cohen, J. L., Chaffee, F. H., & Blandford, R. D. 1997a, *IAU Circ.*, 6676, 3
- Metzger, M. R., Djorgovski, S. G., Kulkarni, S. R., et al. 1997b, *Nature*, 387, 878
- Molinari, E., Vergani, S. D., Malesani, D., et al. 2007, *Astron. & Astroph.*, 469, L13
- Monet, D. G., Levine, S. E., Canzian, B., et al. 2003, *Astron. J.*, 125, 984
- Mukherjee, S., Feigelson, E. D., Jogesh Babu, G., et al. 1998, *Astroph. J.*, 508, 314
- Myers, J., D. 2009, Swift GRB Table and Lookup, [http://heasarc.gsfc.nasa.gov/docs/swift/archive/grb\\_table/](http://heasarc.gsfc.nasa.gov/docs/swift/archive/grb_table/)
- Nakar, E. 2007, *Physics Reports*, 442, 166
- Nardini, M., Greiner, J., Krühler, T., et al. 2011, *Astron. & Astroph.*, 531, A39
- Natarajan, P., Bloom, J. S., Sigurdsson, S., et al. 1997, *New Astronomy*, 2, 471
- Nicuesa Guelbenzu, A., Klose, S., Rossi, A., et al. 2011, *Astron. & Astroph.*, 531, L6
- Nousek, J. A., Kouveliotou, C., Grupe, D., et al. 2006, *Astroph. J.*, 642, 389
- Oates, S. R., Page, M. J., Schady, P., et al. 2009, *Mon. Not. R. Astron. Soc.*, 395, 490
- O'Brien, P. T., Willingale, R., Osborne, J., et al. 2006, *Astroph. J.*, 647, 1213
- Olivares E., F., Greiner, J., Krühler, T., et al. 2011, in prep.
- Osborne, J. P., Beardmore, A. P., Evans, P. A., & Goad, M. R. 2008, *GCN Circ.*, 8295
- Ovaldsen, J.-E., Jaunsen, A. O., Fynbo, J. P. U., et al. 2007, *Astroph. J.*, 662, 294
- Paciesas, B., Briggs, M., & Preece, R. 2008, *GCN Circ.*, 8316
- Page, K. L., Beardmore, A. P., Mereghetti, S., Feroci, M., & Tavani, M. 2008, *GCN Circ.*, 7723, 1
- Page, K. L., Willingale, R., Osborne, J. P., et al. 2007, *Astroph. J.*, 663, 1125
- Panaiteacu, A. 2007, *Mon. Not. R. Astron. Soc.*, 380, 374
- Panaiteacu, A. & Kumar, P. 2000, *Astroph. J.*, 543, 66
- Parmar, A. N., Martin, D. D. E., Bavdaz, M., et al. 1997, *Astron. & Astroph. Suppl.*, 122, 309
- Pelangeon, A. & Atteia, J. 2008, *GCN Circ.*, 7760, 1
- Pellizza, L. J., Duc, P.-A., Le Floch, E., et al. 2006, *Astron. & Astroph.*, 459, L5
- Pérez-Ramírez, D., de Ugarte Postigo, A., Gorosabel, J., et al. 2010, *Astron. & Astroph.*, 510, 105
- Perley, D. A., Bloom, J. S., Chen, H., et al. 2008a, *GCN Circ.*, 7874, 1
- Perley, D. A., Bloom, J. S., & Prochaska, J. X. 2008b, *GCN Circ.*, 7791
- Perley, D. A., Cenko, S. B., Bloom, J. S., et al. 2009, *Astron. J.*, 138, 1690
- Perley, D. A., Li, W., Chornock, R., et al. 2008c, *Astroph. J.*, 688, 470
- Perley, D. A., Morgan, A. N., Updike, A., et al. 2011, *Astron. J.*, 141, 36
- Pian, E., Mazzali, P. A., Masetti, N., et al. 2006, *Nature*, 442, 1011
- Piran, T. 1997, in *Unsolved Problems in Astrophysics*, ed. J. Bahcall & J. Ostriker (Princeton University Press), 343–377
- Piran, T. 2005, *Reviews of Modern Physics*, 76, 1143
- Piro, L., Frail, D. A., Gorosabel, J., et al. 2002, *Astroph. J.*, 577, 680
- Poole, T. S., Breeveld, A. A., Page, M. J., et al. 2008, *Mon. Not. R. Astron. Soc.*, 383, 627
- Postigo, A. d. U., Castro-Tirado, A., Gorosabel, J., et al. 2008a, *GCN Circ.*, 7719
- Postigo, A. d. U., Castro-Tirado, A., Gorosabel, J., et al. 2008b, *GCN Circ.*, 7720
- Quimby, R. M., Rykoff, E. S., Yost, S. A., et al. 2006, *Astroph. J.*, 640, 402
- Racusin, J. L., Karpov, S. V., Sokolowski, M., et al. 2008, *Nature*, 455, 183
- Racusin, J. L., Liang, E. W., Burrows, D. N., et al. 2009, *Astroph. J.*, 698, 43
- Rapisarda, M., Costa, E., Monte, E. D., et al. 2008, *GCN Circ.*, 7715, 1
- Rau, A., Kienlin, A. V., Hurley, K., & Lichti, G. G. 2005, *Astron. & Astroph.*, 438, 1175

- Rau, A., Savaglio, S., Krühler, T., et al. 2010, *Astroph. J.*, 720, 862
- Rees, M. J. & Mészáros, P. 1992, *Mon. Not. R. Astron. Soc.*, 258, 41P
- Rhoads, J. E. 1999, *Astroph. J.*, 525, 737
- Ricker, G. R. 2003, *IAU Circ.*, 8101
- Rieke, G. H. & Lebofsky, M. J. 1985, *Astroph. J.*, 288, 618
- Rol, E., van der Horst, A., Wiersema, K., et al. 2007, *Astroph. J.*, 669, 1098
- Rol, E., Wijers, R. A. M. J., Kouveliotou, C., Kaper, L., & Kaneko, Y. 2005, *ApJ*, 624, 868
- Romano, P., Campana, S., Chincarini, G., et al. 2006, *Astron. & Astroph.*, 456, 917
- Roming, P. W. A., Kennedy, T. E., Mason, K. O., et al. 2005, *Space Sci. Rev.*, 120, 95
- Roming, P. W. A., Koch, T. S., Oates, S. R., et al. 2009, *Astroph. J.*, 690, 163
- Rossi, A., Clemens, C., Greiner, J., et al. 2008a, *GCN Circ.*, 8296
- Rossi, A., de Ugarte Postigo, A., Ferrero, P., et al. 2008b, *Astron. & Astroph.*, 491, L29
- Rossi, A., Greiner, J., Kruehler, T., et al. 2008c, *GCN Circ.*, 8218, 1
- Rossi, A., Klose, S., Ferrero, P., Greiner, J., & et al. 2011a, *Astron. & Astroph.*, submitted
- Rossi, A., Schulze, S., Klose, S., et al. 2011b, *Astron. & Astroph.*, 529, A142
- Ruffert, M. & Janka, H.-T. 2001, *Astron. & Astroph.*, 380, 544
- Ruffert, M. & Janka, H.-T. 2010, *Astron. & Astroph.*, 514, A66
- Rybicki, G. B. & Lightman, A. P. 1979, *Radiative processes in astrophysics*
- Rykoff, E. S., Yuan, F., & McKay, T. A. 2008, *GCN Circ.*, 8293
- Sakamoto, T., Barthelmy, S. D., Evans, P. A., et al. 2008, *GCN Circ.*, 8292
- Salvaterra, R., Della Valle, M., Campana, S., et al. 2009, *Nature*, 461, 1258
- Sari, R., Piran, T., & Halpern, J. P. 1999, *Astroph. J.*, 519, L17
- Sari, R., Piran, T., & Narayan, R. 1998, *Astroph. J.*, 497, L17
- Savaglio, S., Glazebrook, K., & Le Borgne, D. 2009, *Astroph. J.*, 691, 182
- Schady, P., Mason, K. O., Page, M. J., et al. 2007, *Mon. Not. R. Astron. Soc.*, 377, 273
- Schady, P., Page, M. J., Oates, S. R., et al. 2010, *Mon. Not. R. Astron. Soc.*, 401, 2773
- Schady, P., Savaglio, S., Krühler, T., Greiner, J., & Rau, A. 2011, *Astron. & Astroph.*, 525, A113
- Schaefer, B. E. 2007, *Astroph. J.*, 660, 16
- Schlegel, D. J., Finkbeiner, D. P., & Davis, M. 1998, *Astroph. J.*, 500, 525
- Schulze, S., Klose, S., Björnsson, G., et al. 2011, *Astron. & Astroph.*, 526, A23
- Shen, R. & Zhang, B. 2009, *Mon. Not. R. Astron. Soc.*, 398, 1936
- Spergel, D. N., Verde, L., Peiris, H. V., et al. 2003, *Astroph. J. Suppl*, 148, 175
- Stanek, K. Z., Matheson, T., Garnavich, P. M., et al. 2003, *Astroph. J.*, 591, L17
- Starling, R. L. C., van der Horst, A. J., Rol, E., et al. 2008, *Astroph. J.*, 672, 433
- Starling, R. L. C., Wijers, R. A. M. J., Wiersema, K., et al. 2007, *Astroph. J.*, 661, 787
- Stratta, G., Fiore, F., Antonelli, L. A., Piro, L., & De Pasquale, M. 2004, *Astroph. J.*, 608, 846
- Svensson, K. M., Levan, A. J., Tanvir, N. R., Fruchter, A. S., & Strolger, L. 2010, *Mon. Not. R. Astron. Soc.*, 405, 57
- Tagliaferri, G., Antonelli, L. A., Chincarini, G., et al. 2005, *Astron. & Astroph.*, 443, L1
- Tanvir, N. R., Fox, D. B., Levan, A. J., et al. 2009, *Nature*, 461, 1254
- Tanvir, N. R., Levan, A. J., Rol, E., et al. 2008, *Mon. Not. R. Astron. Soc.*, 388, 1743
- Tavani, M., Barbiellini, G., Argan, A., et al. 2009, *Astron. & Astroph.*, 502, 995
- Tavani, M., Barbiellini, G., Argan, A., et al. 2008, *Nuclear Instruments and Methods in Physics Research A*, 588, 52
- Thöne, C. C., Kann, D. A., Jóhannesson, G., et al. 2010, *Astron. & Astroph.*, 523, A70
- Tody, D. 1993, in *Astronomical Society of the Pacific Conference Series*, Vol. 52, *Astronomical Data Analysis Software and Systems II*, ed. R. J. Hanisch, R. J. V. Brissenden, & J. Barnes, 173
- Tueller, J., Barthelmy, S. D., Cummings, J., et al. 2008, *GCN Circ.*, 7205

- Uehara, T., Ohno, M., Takahashi, T., et al. 2008, GCN Circ., 7223
- Ukwatta, T. N., Baumgartner, W. H., Chester, M. M., et al. 2008a, GCN Circ., 7203
- Ukwatta, T. N., Tueller, J., Mangano, V., et al. 2008b, GCN Report, 111
- Updike, A., Clemens, C., & Greiner, J. 2008, GCN Circ., 8627
- van der Horst, A. J., Kouveliotou, C., Gehrels, N., et al. 2009, *Astroph. J.*, 699, 1087
- van Paradijs, J., Groot, P. J., Galama, T., et al. 1997, *Nature*, 386, 686
- Vanderspek, R., Villaseñor, J., Doty, J., et al. 1999, *Astron. & Astroph. Suppl.*, 138, 565
- Vaughan, S., Goad, M. R., Beardmore, A. P., et al. 2006, *Astroph. J.*, 638, 920
- Veres, P., Bagoly, Z., Horváth, I., et al. 2010, in *American Institute of Physics Conference Series*, Vol. 1279, American Institute of Physics Conference Series, ed. N. Kawai & S. Nagasaki, 457–459
- Vestrand, W. T., Wozniak, P. R., Wren, J. A., et al. 2005, *Nature*, 435, 178
- Vestrand, W. T., Wren, J. A., Wozniak, P. R., et al. 2006, *Nature*, 442, 172
- Vianello, G., Götz, D., & Mereghetti, S. 2009, *Astron. & Astroph.*, 495, 1005
- Vrba, F. J., Luginbuhl, C. B., Jennings, M. C., & Hartmann, D. H. 1999, *Astroph. J.*, 511, 298
- Vreeswijk, P., Malesani, D., Fynbo, J., et al. 2008, GCN Circ., 8301
- Wainwright, C., Berger, E., & Penprase, B. E. 2007, *Astroph. J.*, 657, 367
- Warmels, R. H. 1992, in *Astronomical Society of the Pacific Conference Series*, Vol. 25, *Astronomical Data Analysis Software and Systems I*, ed. D. M. Worrall, C. Biemesderfer, & J. Barnes, 115
- Watson, D., Hjorth, J., Fynbo, J. P. U., et al. 2007, *Astroph. J.*, 660, L101
- Waxman, E., Kulkarni, S. R., & Frail, D. A. 1998, *Astroph. J.*, 497, 288
- Wilms, J., Allen, A., & McCray, R. 2000, *Astroph. J.*, 542, 914
- Woosley, S. E. 1993, *Astroph. J.*, 405, 273
- Woosley, S. E. & Bloom, J. S. 2006, *Annu. Rev. Astro. Astroph.*, 44, 507
- Xu, D., Fynbo, J. P. U., Tanvir, N. R., et al. 2009, GCN Circ., 10053
- Zafar, T., Watson, D., Fynbo, J. P. U., et al. 2011, ArXiv e-prints: astro-ph: 1102.1469
- Zeh, A., Kann, D. A., Klose, S., & Hartmann, D. H. 2005, *Nuovo Cimento C Geophysics Space Physics C*, 28, 617
- Zeh, A., Klose, S., & Kann, D. A. 2006, *Astroph. J.*, 637, 889
- Zerbi, R. M., Chincarini, G., Ghisellini, G., et al. 2001, *Astronomische Nachrichten*, 322, 275
- Zhang, B. 2007, *Chin. J. Astron. Astroph.*, 7, 1
- Zhang, B., Fan, Y. Z., Dyks, J., et al. 2006, *Astroph. J.*, 642, 354
- Zhang, B. & Mészáros, P. 2004, *International Journal of Modern Physics A*, 19, 2385
- Zhang, B., Zhang, B.-B., Virgili, F. J., et al. 2009, *Astroph. J.*, 703, 1696

# Appendix A

## The optical/NIR data set of GRB 080928 and its afterglow

Table A.1: Log of the ROTSE-IIIa telescope observations of GRB 080928 (see Sect. 4.2.1).

Time (days)	Time (s)	$T_{start}$ (s)	$T_{stop}$ (s)	CR Magnitude
0.002160	186.7	132.0	263.9	> 18.5
0.004509	389.6	272.8	556.3	$18.38 \pm 0.22$
0.008266	714.2	565.6	901.8	$17.35 \pm 0.10$
0.012341	1066.3	911.2	1247.7	$17.16 \pm 0.09$
0.016375	1414.8	1256.7	1592.9	$17.48 \pm 0.13$
0.020442	1766.2	1602.1	1947.2	$17.20 \pm 0.10$
0.024512	2117.8	1956.1	2293.0	$16.50 \pm 0.06$
0.028530	2465.0	2302.2	2639.3	$16.51 \pm 0.10$
0.034383	2970.7	2648.7	3331.8	$16.54 \pm 0.06$
0.042429	3665.9	3340.8	4022.6	$16.85 \pm 0.05$
0.054459	4705.3	4373.1	5062.8	$17.18 \pm 0.08$
0.062571	5406.2	5071.8	5762.6	$17.49 \pm 0.10$
0.070628	6102.2	5771.4	6452.0	$17.35 \pm 0.08$
0.078676	6797.6	6461.6	7151.1	$16.99 \pm 0.09$
0.087760	7582.5	7160.1	8029.8	$16.90 \pm 0.07$
0.096907	8372.8	8038.5	8720.9	$16.96 \pm 0.08$
0.104911	9064.3	8729.8	9411.6	$16.85 \pm 0.05$
0.112957	9759.5	9420.7	10110.5	$16.68 \pm 0.06$
0.121012	10455.4	10119.7	10802.3	$16.86 \pm 0.05$
0.130107	11241.2	10811.6	11687.9	$16.97 \pm 0.06$
0.139266	12032.6	11696.8	12378.0	$17.17 \pm 0.07$
0.147299	12726.6	12386.8	13075.8	$17.22 \pm 0.10$
0.155384	13425.2	13084.4	13774.8	$17.38 \pm 0.15$

Notes: magnitudes are Vega magnitudes (unfiltered  $R$ -equivalent data, see Quimby et al. 2006), not corrected for Galactic extinction (Sect. 3.1.3). Midtimes have been derived logarithmically.

Table A.2: Log of the Swift/UVOT observations of GRB 080928 (see Sect. 4.2.1).

Time (days)	Time (s)	$T_{start}$ (s)	$T_{stop}$ (s)	Magnitude	Filter
0.001909	164.9	160.4	169.7	> 17.1	<i>v</i>
0.002184	188.7	179.0	199.0	> 19.7	<i>white</i>
0.002416	208.7	199.0	219.0	19.03 ± 0.25	<i>white</i>
0.002648	228.7	219.0	239.0	18.70 ± 0.21	<i>white</i>
0.002879	248.8	239.0	259.0	18.44 ± 0.17	<i>white</i>
0.003110	268.7	259.0	278.7	19.29 ± 0.31	<i>white</i>
0.003834	331.2	285.0	385.0	19.15 ± 0.41	<i>v</i>
0.004969	429.3	385.0	478.7	18.96 ± 0.39	<i>v</i>
0.050063	4325.4	4226.7	4426.5	> 19.1	<i>uvm2</i>
0.052440	4530.8	4432.0	4631.8	18.02 ± 0.15	<i>uvw1</i>
0.054817	4736.2	4637.3	4837.1	17.54 ± 0.07	<i>u</i>
0.057191	4941.3	4842.5	5042.2	18.05 ± 0.08	<i>b</i>
0.059573	5147.1	5048.2	5247.9	17.96 ± 0.04	<i>white</i>
0.061956	5353.0	5254.0	5453.8	> 19.3	<i>uvw2</i>
0.064332	5558.3	5459.3	5659.1	17.66 ± 0.10	<i>v</i>
0.066706	5763.4	5664.3	5864.1	> 19.0	<i>uvm2</i>
0.069081	5968.6	5869.6	6069.3	18.07 ± 0.15	<i>uvw1</i>
0.071451	6173.4	6074.3	6274.1	17.74 ± 0.11	<i>u</i>
0.073834	6379.2	6280.1	6479.9	18.02 ± 0.08	<i>b</i>
0.076205	6584.1	6485.0	6684.7	17.81 ± 0.05	<i>white</i>
0.078267	6762.3	6690.7	6834.6	> 18.8	<i>uvw2</i>
0.117545	10155.9	10007.1	10306.9	17.16 ± 0.07	<i>v</i>
0.121060	10459.6	10310.8	10610.6	17.24 ± 0.06	<i>v</i>
0.124573	10763.1	10614.3	10914.0	17.34 ± 0.07	<i>v</i>
0.131495	11361.1	10920.2	11819.9	19.66 ± 0.28	<i>uvm2</i>
0.141377	12214.9	11826.8	12615.8	18.28 ± 0.10	<i>uvw1</i>
0.184457	15937.1	15787.9	16087.7	18.35 ± 0.09	<i>u</i>
0.187971	16240.7	16091.5	16391.3	18.21 ± 0.09	<i>u</i>
0.191485	16544.3	16395.1	16694.9	18.38 ± 0.09	<i>u</i>
0.195021	16849.8	16700.6	17000.3	18.74 ± 0.08	<i>b</i>
0.198535	17153.4	17004.2	17304.0	18.87 ± 0.09	<i>b</i>
0.202048	17456.9	17307.7	17607.5	18.71 ± 0.09	<i>b</i>
0.205580	17762.1	17612.9	17912.6	18.51 ± 0.06	<i>white</i>
0.209096	18065.9	17916.6	18216.4	18.64 ± 0.06	<i>white</i>
0.211904	18308.5	18220.2	18397.2	18.65 ± 0.09	<i>white</i>
0.254794	22014.2	21568.9	22468.7	19.25 ± 0.13	<i>uvw1</i>
0.261860	22624.7	22475.3	22775.1	18.45 ± 0.10	<i>u</i>
0.265374	22928.4	22779.0	23078.7	18.75 ± 0.12	<i>u</i>
0.268888	23231.9	23082.5	23382.3	18.74 ± 0.13	<i>u</i>
0.272424	23537.4	23388.0	23687.8	19.25 ± 0.14	<i>b</i>
0.275939	23841.1	23691.7	23991.5	19.11 ± 0.16	<i>b</i>
0.278780	24086.6	23995.4	24178.3	19.49 ± 0.30	<i>b</i>
0.321708	27795.5	27349.3	28249.1	> 20.2	<i>uvm2</i>
0.332203	28702.3	28256.0	29155.7	19.71 ± 0.18	<i>uvw1</i>
0.339259	29312.0	29162.5	29462.3	19.34 ± 0.23	<i>u</i>
0.342773	29615.6	29466.1	29765.8	19.73 ± 0.37	<i>u</i>
0.345653	29864.5	29770.2	29959.0	> 18.9	<i>u</i>
0.385349	33294.2	33157.3	33431.6	> 19.6	<i>uvw2</i>
0.841783	72730.0	46011.4	114964.1	> 21.9	<i>uvw2</i>
0.853404	73734.1	46917.8	115877.5	21.14 ± 0.31	<i>v</i>
0.903886	78095.7	52273.5	116673.6	> 21.5	<i>uvm2</i>
0.954216	82444.2	56280.7	120770.5	> 21.8	<i>uvw1</i>
1.005800	86901.3	62061.1	121684.1	21.31 ± 0.22	<i>u</i>
1.095660	94665.0	73622.3	121722.0	> 21.3	<i>b</i>
0.864812	74719.8	74534.4	74905.6	21.85 ± 0.36	<i>white</i>
0.864400	74684.2	74534.4	74834.2	21.73 ± 0.34	<i>white</i>
1.811460	156510.0	121764.2	201170.5	> 20.5	<i>v</i>
2.194020	189563.0	178401.4	201423.3	> 21.1	<i>u</i>
2.196340	189764.0	178556.9	201674.8	> 21.4	<i>b</i>
2.199990	190079.0	178715.3	202165.7	> 21.3	<i>uvw1</i>
3.177100	274501.0	260418.7	289345.7	> 21.9	<i>u</i>

Notes: magnitudes are Vega magnitudes, not corrected for Galactic extinction (Sect. 3.1.3). Midtimes have been derived logarithmically.

Table A.3: Log of the GROND multi-color observations of GRB 080928 (see Sect. 4.2.1).

Time (days)	Filter	Exposure (s)	Brightness (mag <sub>AB</sub> )
0.6031	$g'r'iz'$	12 × 370	21.40 ± 0.15 / 21.03 ± 0.07 / 20.54 ± 0.07 / 20.43 ± 0.08
0.6031	$JHK_s$	240 × 10	19.83 ± 0.10 / 19.49 ± 0.15 / 19.11 ± 0.15
0.7398	$g'r'iz'$	12 × 370	21.93 ± 0.16 / 21.48 ± 0.08 / 21.13 ± 0.10 / 20.78 ± 0.10
0.7398	$JHK_s$	360 × 10	20.40 ± 0.16 / 20.01 ± 0.22 / 19.60 ± 0.30
1.7370	$g'r'iz'$	12 × 370	23.35 ± 0.25 / 22.99 ± 0.10 / 22.56 ± 0.16 / 22.53 ± 0.16
1.7370	$JHK_s$	360 × 10	> 21.8 / > 20.9 / > 20.4
2.708	$g'r'iz'$	4 × 370	> 24.3 / 23.41 ± 0.40 / 23.35 ± 0.73 / > 23.2
2.708	$JHK_s$	120 × 10	> 21.2 / > 20.4 / > 19.8
201	$g'r'iz'$	12 × 370	> 25.4 / > 25.6 / > 24.6 / > 24.3
201	$JHK_s$	360 × 10	> 22.0 / > 21.6 / > 20.9

Notes: The first column provides the midtime in days after the onset of the burst. The last (5th) epoch data were used to characterize the field galaxy population and to set constraints on the magnitudes of a galaxy close to the optical/NIR afterglow. Magnitudes are given in the AB photometric system, not corrected for Galactic extinction (Sect. 3.1.3). Midtimes have been derived logarithmically.

Table A.4: Secondary standard stars within 4 arcmin of the afterglow position (Fig. 3.2).

#	R.A., Dec. (J2000)	$g'$	$r'$	$i'$	$z'$	$J$	$H$	$K_s$
1	06:20:15.23 –55:12:45.4	14.426(01)	13.727(01)	13.269(01)	13.102(01)	12.753(01)	12.613(02)	12.880(02)
2	06:20:13.45 –55:12:32.5	19.427(05)	18.987(05)	18.593(05)	18.478(08)	18.267(05)	18.219(10)	18.435(23)
3	06:20:13.87 –55:12:17.1	17.291(01)	16.982(01)	16.709(01)	16.668(02)	16.568(03)	16.673(03)	16.780(07)
4	06:20:14.65 –55:12:01.1	17.513(02)	17.366(02)	17.103(02)	17.072(03)	16.988(03)	17.100(03)	17.208(10)
5	06:20:12.70 –55:11:55.1	20.734(14)	19.460(08)	18.017(03)	17.450(04)	16.886(03)	16.778(04)	16.853(07)
6	06:20:12.21 –55:11:45.9	18.307(02)	18.061(03)	17.734(03)	17.643(04)	17.508(04)	17.509(05)	17.711(23)
7	06:20:14.51 –55:11:45.1	19.989(08)	18.962(05)	18.204(04)	17.946(05)	17.561(03)	17.341(05)	17.378(11)
8	06:20:06.18 –55:12:02.1	20.499(05)	19.456(03)	18.453(03)	18.077(02)	17.598(06)	17.353(08)	17.556(05)
9	06:19:58.96 –55:12:57.4	17.430(03)	17.413(02)	17.206(02)	17.185(01)	17.123(04)	17.312(07)	17.553(07)
10	06:19:58.75 –55:10:40.3	19.275(03)	18.121(02)	17.026(02)	16.613(01)	16.110(05)	16.022(05)	16.143(02)
11	06:19:56.64 –55:09:57.4	20.949(14)	20.212(14)	19.672(13)	19.389(14)	18.794(08)	18.609(12)	18.403(13)
12	06:20:16.00 –55:10:28.9	18.087(03)	17.755(02)	17.442(03)	17.370(01)	17.168(05)	17.218(06)	17.313(04)

Notes: Calibration of the field in  $JHK_s$  was performed using 2MASS stars. The magnitudes of the selected 2MASS stars were then transformed into the GROND filter system and finally into AB magnitudes using  $J(AB) = J(Vega) + 0.91$ ,  $H(AB) = H(Vega) + 1.38$ ,  $K_s(AB) = K_s(Vega) + 1.79$  (Greiner et al. 2008). Numbers in parentheses give the photometric  $1\sigma$  statistical uncertainty of the secondary standards in units of milli-mag.





## Appendix B

# The optical/NIR data set of the afterglow of GRB 080514B

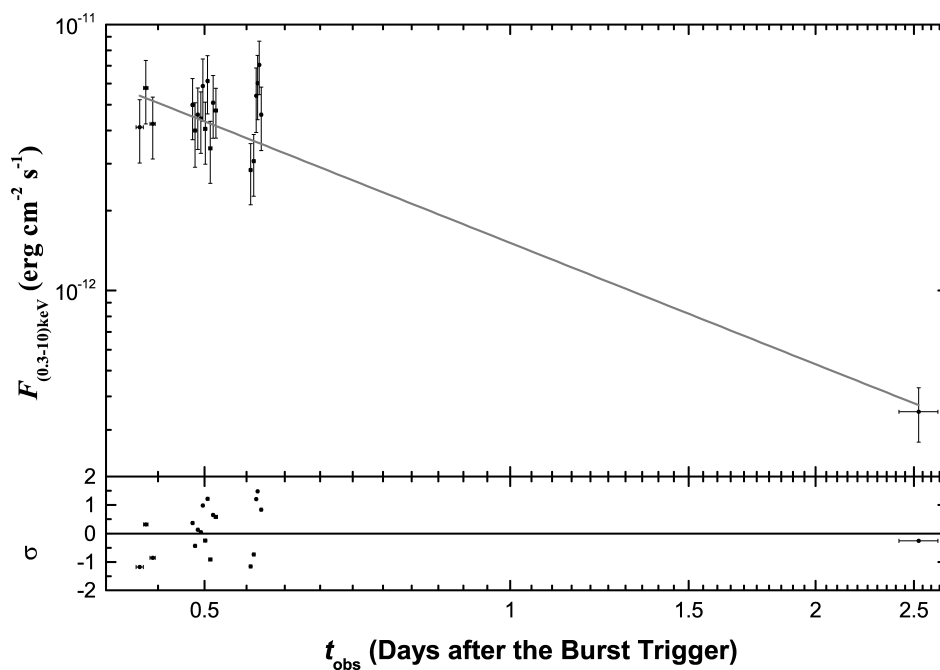


Figure B.1: The X-ray light curve of the afterglow of GRB 080514B observed by Swift/XRT.

Table B.1: Log of optical/NIR observations of the GRB 080514B afterglow (see Sect. 4.1).

Time (days)	Filter	Instr./Telesc.	Exposure (s)	Magnitudes
0.430	<i>uvw1</i>	UVOT	284	20.45 ± 0.40
0.432	<i>u</i>	UVOT	142	19.75 ± 0.30
0.434	<i>b</i>	UVOT	142	21.00 ± 0.63
0.438	<i>uvw2</i>	UVOT	568	21.47 ± 0.56
0.443	<i>v</i>	UVOT	142	>20.9
0.446	<i>uvm2</i>	UVOT	413	>22.0
0.488	<i>uvw1</i>	UVOT	419	20.17 ± 0.27
0.492	<i>u</i>	UVOT	209	19.91 ± 0.27
0.494	<i>b</i>	UVOT	209	20.40 ± 0.31
0.501	<i>uvw2</i>	UVOT	838	21.78 ± 0.57
0.507	<i>v</i>	UVOT	209	19.74 ± 0.42
0.512	<i>uvm2</i>	UVOT	616	20.63 ± 0.37
0.555	<i>uvw1</i>	UVOT	415	20.88 ± 0.46
0.559	<i>u</i>	UVOT	207	20.09 ± 0.32
0.561	<i>b</i>	UVOT	207	21.62 ± 0.91
0.567	<i>uvw2</i>	UVOT	791	22.09 ± 0.76
0.640	<i>R<sub>C</sub></i>	Watcher	120x14	19.23 ± 0.47
0.660	<i>R<sub>C</sub></i>	Watcher	120x15	19.89 ± 0.56
0.727	<i>I<sub>C</sub></i>	IAC 80	3x300	20.26 ± 0.21
0.743	<i>I<sub>C</sub></i>	IAC 80	3x300	20.59 ± 0.20
0.761	<i>I<sub>C</sub></i>	IAC 80	3x300	20.16 ± 0.16
0.774	<i>I<sub>C</sub></i>	IAC 80	3x300	20.03 ± 0.14
0.907	<i>g'</i>	GROND/2.2m	3x1501	21.53 ± 0.04
0.907	<i>r'</i>	GROND/2.2m	3x1501	21.16 ± 0.03
0.907	<i>i'</i>	GROND/2.2m	3x1501	20.77 ± 0.08
0.907	<i>z'</i>	GROND/2.2m	3x1501	20.43 ± 0.05
0.907	<i>J</i>	GROND/2.2m	3x1200	19.82 ± 0.03
0.907	<i>H</i>	GROND/2.2m	3x1200	19.10 ± 0.04
0.907	<i>K</i>	GROND/2.2m	2x1200	>17.5
1.021	<i>J</i>	NEWFIRM/KPNO	23x30x2	19.84 ± 0.14
1.038	<i>J</i>	NEWFIRM/KPNO	15x30x2	20.06 ± 0.07
1.763	<i>R<sub>C</sub></i>	NOT	1x300	22.31 ± 0.08
1.782	<i>B</i>	NOT	1x300	23.03 ± 0.13
1.798	<i>I<sub>C</sub></i>	NOT	1x300	22.00 ± 0.10
1.899	<i>i'</i>	GMOS/Gemini	1x200	21.83 ± 0.06
1.993	<i>g'</i>	GROND/2.2m	1x1501	22.74 ± 0.08
1.993	<i>r'</i>	GROND/2.2m	1x1501	22.38 ± 0.10
1.993	<i>i'</i>	GROND/2.2m	1x1501	21.78 ± 0.13
1.993	<i>z'</i>	GROND/2.2m	1x1501	>21.6
1.993	<i>J</i>	GROND/2.2m	1x1200	>20.3
1.993	<i>H</i>	GROND/2.2m	1x1200	>19.1
1.993	<i>K</i>	GROND/2.2m	1x1200	>17.7
2.023	<i>J</i>	NEWFIRM/KPNO	15x30x2	20.95 ± 0.30
2.039	<i>H</i>	NEWFIRM/KPNO	15x15x4	>20.3
2.536	<i>white</i>	UVOT	5361	22.19 ± 0.17
8.965	<i>g'</i>	GROND/2.2m	4x1501	24.05 ± 0.17
8.965	<i>r'</i>	GROND/2.2m	4x1501	24.40 ± 0.25
8.965	<i>i'</i>	GROND/2.2m	4x1501	23.35 ± 0.26
8.965	<i>z'</i>	GROND/2.2m	4x1501	23.28 ± 0.24
8.965	<i>J</i>	GROND/2.2m	4x1200	>21.9
8.965	<i>H</i>	GROND/2.2m	4x1200	>20.5
8.965	<i>K</i>	GROND/2.2m	3x1200	>18.4
24.13	<i>R<sub>C</sub></i>	Keck	960	24.17 ± 0.33
24.13	<i>g'</i>	Keck	1080	24.73 ± 0.34

Notes: The first column provides the mid-time in days after the GRB. Vega magnitudes are not corrected for Galactic extinction. The upper limits are  $3\sigma$  above the background. The data given in the table supersede the corresponding magnitudes reported in de Ugarte Postigo et al. (2008a,b), Rossi et al. (2008a,b), Urdike et al. (2008a,b), Malesani et al. (2008), and Perley et al. (2008).

# Appendix C

## Notes, tables and figures on the host galaxy search

### C.1 Additional notes on individual targets for the host galaxy search: observations by Swift and other facilities

#### GRB 050717

GRB 050717 triggered *Swift*/BAT at 10:30:52 UT (Hurkett et al. 2005b). It was a long burst with a duration of  $T_{90}(15 - 350 \text{ keV}) = (86 \pm 2) \text{ s}$  (Cummings et al. 2005a) which was also detected by *Konus-Wind* (Golenetskii et al. 2005). *Swift*/XRT began observing 79 s after the trigger and found a bright, fading X-ray source, while simultaneous *Swift*/UVOT observations started 78 s after the trigger and resulted only in upper limits (Hurkett et al. 2005b; Blustin et al. 2005). Unfortunately, XRT was unable to automatically centroid on the burst, leading to a delay of 2.5 hr in the determination of the X-ray position (error circle radius  $6''0$ ; Kennea et al. 2005; see also Hurkett et al. 2005a). The burst is discussed by Krimm et al. (2006b) in detail, it was very luminous and has one of the highest-ever measured peak energies, with a probable redshift  $z > 2.7$ . Deep ground-based *K*-band follow-up observations were performed with the du Pont 100-inch telescope at Las Campanas Observatory with a first run starting 37.7 hr after the burst. No fading NIR source was detected (Berger & Lopez-Morales 2005; Berger et al. 2005). Optical observations with the Tenagra 0.35-m telescope at Perth, Australia, did not find a new source down to the limit of the DSS2 red survey (Luckas et al. 2005). Also, PROMPT-5 at Cerro Tololo Inter-American Observatory in Chile automatically observed the field starting 13 hr after the burst. No fading source was found down to  $R_C = 21.7$  and  $I_C = 21.5$  (MacLeod et al. 2005).

UVOT obtained an upper limit of  $\nu > 19.0$  for any afterglow at 420 s (mid-time) after the onset of the burst (Blustin et al. 2005), corresponding to  $\nu > 18.3$  after correction for Galactic extinction. Using the observed constraint on the spectral slope  $\beta_{\text{OX}} < 0.40$  at the time of the UVOT observations, this corresponds to an upper limit of  $R_{\text{AB}} > 18.2$ . In the same way, following Rol et al. (2005), at the time of the optical observation the observed (mean) X-ray flux together with the observed (mean) spectral slope  $\beta_X$  predicts a non-extinguished  $R_{\text{AB}}$ -band magnitude between  $14.5^{+1.6}_{-1.7}$  and  $18.2^{+1.6}_{-1.7}$ , where the brighter magnitude corresponds to  $\nu_c = \nu_{\text{opt}}$  and the fainter magnitude to  $\nu_c = \nu_X$  ( $\nu_c$  is the cooling frequency; Sect. 2.3.1). The burst fulfills the J04 criterion but it does not fulfill the V09 criterion (Table 5.2 and Sect. 5.1.2). GRB 050717 did not enter the golden dark burst sample.

#### GRB 050922B

*Swift*/BAT detected the burst at 15:02:00 UT. It was an image trigger lasting for 168 seconds (Norris et al. 2005). Cummings et al. (2005b) give  $T_{90}(15 - 150 \text{ keV}) = (250 \pm 20) \text{ s}$ . Because of the image trigger history, Norris et al. (2005) speculated that it could be a high-redshift event similar to GRB 050904. *Swift*/XRT started observing 342 s after the trigger, UVOT one second later (Norris et al. 2005). A decaying X-ray afterglow was detected (Godet et al. 2005) but no optical counterpart (Pasquale et al. 2005). Several ground-based small telescopes responded to the trigger but found no afterglow candidate either: ROTSE IIIa (upper limit  $CR = 17.3$  at 3 min; Schaefer et al. 2005), the 14-inch Automated Response Telescope at the University of Osaka, Japan

(upper limit  $CR = 15.1$  at 3 min; Torii 2005), the 0.4-m telescope of Ussuriysk Astrophysical Observatory, Russia (upper limit  $CR = 16.0$  at 15 min; Kornienko et al. 2005), and the 30-cm telescope at University of Miyazaki, Japan (upper limit  $CR = 16.1$  at 21 min; Sonoda et al. 2005).

The INT 2.5-m telescope at Observatorio del Roque de los Muchachos on La Palma obtained an upper limit on the afterglow of  $r' > 22.5$  at 49 ks (mid-time) after the onset of the burst (Guziy et al. 2005), corresponding to  $r' > 22.4$  after correction for Galactic extinction. There are no X-ray data for the time between about  $t = 10$  ks and 100 ks after the burst, but there are for observations from  $t \sim 100$  ks to about 1 Ms. The latter data can be used to extrapolate to the X-ray flux at  $t = 49$  ks. The spectral slope is then  $\beta_{\text{OX}} < 0.39$ , corresponding to an upper limit of about  $R_{\text{AB}} > 22.3$ . Similarly, the observed X-ray flux together with the observed spectral slope  $\beta_{\text{X}}$  at  $t = 49$  ks predicts a non-extinguished  $R_{\text{AB}}$ -band magnitude between  $11.1^{+2.7}_{-3.7}$  and  $14.8^{+2.7}_{-3.7}$ . Using  $\beta_{\text{OX}}$  and  $\beta_{\text{X}}$ , the burst fulfills the criterion of J04 as well as V09 (Table 5.2). However, due to the large gap in the X-ray data base, GRB 050922B did not enter the golden dark burst sample.

### GRB 060211A

*Swift*/BAT triggered on GRB 060211A at 09:39:11 UT (Hurkett et al. 2006). It was a long burst with a duration of  $T_{90}$  (15–350 keV) =  $126 \pm 5$  s (Sato et al. 2006a; Krimm et al. 2006a). The spacecraft slewed promptly to the BAT position and *Swift*/XRT found a bright, fading X-ray source, while *Swift*/UVOT started observing 183 seconds after the trigger but did not detect any afterglow candidate (Hurkett et al. 2006). ROTSE IIIa, located at Siding Spring Observatory, Australia, and the Moscow Union 'Optic' MASTER robotic system responded to GRB 060211 immediately. ROTSE's automated response took the first image 147 s after the burst, under twilight conditions, while MASTER started 202 s after the GRB trigger. Only upper limits could be reported (Rujopakarn et al. 2006; Lipunov et al. 2006; see also Urata et al. 2006). Also the 2-m Faulkes Telescope North robotically followed-up GRB 060211 starting 5.4 min after the trigger. No fading optical counterpart down to  $R \approx 18.5$  was found (Gomboc et al. 2006). Deep upper limits were also reported by Norris et al. (2006),  $J > 19.1$  at 17 hr after the burst, and Sharapov et al. (2006),  $R > 22$  at 5.5 hr after the burst.

The 1.5-m telescope of Maidanak Astronomical Observatory obtained for the afterglow an upper limit of  $R = 22.0$  at  $\sim 20$  ks (mid-time) after the onset of the burst (Sharapov et al. 2006), corresponding to  $R = 21.6$  after correction for Galactic extinction. This corresponds to an upper limit of  $R_{\text{AB}} > 21.8$ . Among all available upper limits for this burst this observation provides the tightest constraints on the spectral properties of the afterglow from the optical to the X-ray band. According to these data, though, GRB 060211A does not fulfill the JO4 as well as the V09 criterion (Table 5.2).

### GRB 060805A

The burst triggered *Swift*/BAT on May 8, 2006 at 04:47:49 UT (Ziaeeepour et al. 2006). It had a duration of  $T_{90}(15 - 350 \text{ keV}) = 5.4 \pm 0.5$  s (Barbier et al. 2006a). *Swift*/XRT began taking data 93 seconds after the BAT trigger. Ground analysis revealed a faint, uncatalogued X-ray source. *Swift*/UVOT started observing 97 seconds after the trigger but no afterglow candidate was detected in any band (Ziaeeepour et al. 2006; Pandey et al. 2006). Further ground-based observations could only provide upper limits. The robotic 0.76-m Katzman Automatic Imaging Telescope (KAIT) at Lick Observatory started observing the field 119 s after the BAT trigger but no afterglow was found ( $V > 16.8$ ,  $I > 16.7$ ; Li 2006). The automated Palomar 60-inch telescope responded to GRB 060805A and started observing 3 min after the burst trigger. No source down to  $R > 19$  was found in the XRT error circle (Cenko 2006). Additional upper limits were obtained by the 1.3-m Skinakas Observatory (University of Crete, Heraklion, Greece):  $R > 21.5$  at 14 hr after the burst (Muehleger et al. 2006) and by the 2-m Liverpool Telescope on La Palma:  $r' > 22.9$  and  $i' > 22.6$  at 0.725 and 0.748 days, respectively, after the burst (Rol & Page 2006).

The 2-m Liverpool Telescope observations correspond to  $r' > 22.7$ , after correction for Galactic extinction. Using  $\beta_{\text{OX}} < 1.00$ , this corresponds to an upper limit of  $R_{\text{AB}} > 22.7$ . Among all available upper limits for this burst this observation provides the tightest constraint on  $\beta_{\text{OX}}$  and  $\beta_{\text{X}}$  (Table 5.2). However, GRB 060805A does not fulfill the JO4 as well as the V09 criterion (Table 5.2).

### GRB 060919

GRB 060919 triggered *Swift*/BAT at 07:48:38 UT (Guidorzi et al. 2006a). It was a long burst with a duration of  $T_{90} = (15 - 350 \text{ keV}) = 9.1 \pm 0.2$  s (Sato et al. 2006b). *Swift*/XRT began taking data 87 seconds after the

BAT trigger. Ground analysis revealed a faint X-ray source with an revised error circle of  $r = 4'1$  (Guidorzi et al. 2006a,b). *Swift*/UVOT started observing the field 73 seconds after the burst but did not detect an optical counterpart in any band down to deep flux limits (Breeveld & Guidorzi 2006). The robotic TAROT telescope on La Silla started observing 28 s after the trigger. No optical transient was found down to  $R > 15.4$  in the first 60 seconds of observations. An upper limit of  $R > 15.8$  could be set for any transient up to 382 s after the trigger (Klotz et al. 2006). The Faulkes Telescope South started observing about 2.8 hours after the event. No optical transient was detected down to a limiting magnitude of  $R > 19.5$  (Melandri et al. 2006).

The UVOT upper limit at 918 s corresponds to  $\nu > 20.0$ , after correction for Galactic extinction. Using  $\beta_{\text{OX}} < 0.68$ , this corresponds to an upper limit of  $R_{\text{AB}} > 19.8$ . Similar to the previous two bursts, this observation provides the tightest constraints on the spectral properties of the afterglow. Based on these data, GRB 060919 does not fulfill the JO4 as well as the V09 criterion (Table 5.2).

### GRB 060923B

*Swift*/BAT triggered on GRB 060923B at 11:38:06 UT (Stamatikos et al. 2006). It was a single-peaked burst with a duration of  $T_{90}(15 - 350 \text{ keV}) = 8.8 \pm 0.1 \text{ s}$  (Barbier et al. 2006b). *Swift*/XRT began observing the field 114 seconds after the BAT trigger and found an uncatalogued X-ray source with a positional accuracy of  $2'8$ . *Swift*/UVOT started observing 122 seconds after the burst with the *white* filter but could not detect an afterglow candidate (Stamatikos et al. 2006; Holland & Cucchiara 2006). No further ground-based follow-up observations were reported in the literature.

UVOT obtained an afterglow upper limit of  $\nu > 18.1$  at 295 s (mid-time) after the burst (Holland & Cucchiara 2006), corresponding to  $\nu > 18.0$  after correction for Galactic extinction. Using  $\beta_{\text{OX}} < 0.62$ , this corresponds to an upper limit of  $R_{\text{AB}} > 17.9$ . Among all available upper limits for this burst this observation provides the tightest constraint on  $\beta_{\text{OX}}$  and  $\beta_{\text{X}}$  (Table 5.2). However, GRB 060923B does not fulfill the JO4 as well as the V09 criterion (Table 5.2).

### GRB 061102

GRB 061102 triggered *Swift*/BAT at 01:00:31 UT (Holland et al. 2006). It was a long burst with a duration of  $T_{90}(15 - 350 \text{ keV}) = 17.6 \pm 1 \text{ s}$  (Tueller et al. 2006). *Swift*/XRT began observing the field 100 seconds after the BAT trigger and found an uncatalogued, fading X-ray source (Holland et al. 2006; Starling et al. 2006). *Swift*/UVOT started observing 110 seconds after the trigger with the *white* filter but no afterglow candidate was seen down to a  $3\sigma$  upper limit of *white*  $< 18.5$  (Holland et al. 2006). Continued observations provided only upper limits in all UVOT bands (Holland 2006). No further ground-based follow-up observations of this event are reported in the literature.

UVOT obtained an even deeper upper limit of  $\nu > 20.5$  at 1480 s (mid-time) after the onset of the burst (Holland 2006), corresponding to  $\nu > 20.4$  after correction for Galactic extinction. Using the observed  $\beta_{\text{OX}} < 1.10$ , this corresponds to an upper limit of  $R_{\text{AB}} > 20.1$ . Among all available upper limits this observation provides the tightest constraints on the afterglow SED. However, GRB 061102 does not fulfill the JO4 as well as the V09 criterion (Table 5.2).

### GRB 070429A

The burst 070429A triggered *Swift*/BAT at 01:35:10 UT (Barthelmy et al. 2007). It was a long burst with  $T_{90}(15 - 350 \text{ keV}) = 163 \pm 5 \text{ s}$  (Cannizzo et al. 2007). *Swift*/XRT started observing 153 s after the trigger and found a fading, uncatalogued X-ray source, while *Swift*/UVOT started observing 211 seconds after the trigger but did not detect an optical counterpart in any band (Schady & Cannizzo 2007). ROTSE-IIIc, located at Mt. Gamsberg, Namibia, started observing 97 s after the burst. No afterglow candidate was found down to  $CR > 17.3$  (unfiltered images) for images taken within 3 min after the trigger and down to  $CR > 18.0$  within 8 min (Rykoff et al. 2007). Additional data were obtained with the 0.6-m BOOTES-IR/T60 robotic telescope (Castro-Tirado et al. 2006), starting 3.25 hr after the burst but no afterglow was found (de Ugarte Postigo et al. 2007). Deep *K*-band observations with the 4.2-m William Herschel Telescope on La Palma beginning 4.1 hr after the burst detected a faint source in the XRT error circle, but no fading behavior was found (de Ugarte Postigo et al. 2007).

The Gemini North telescope mounted with the GMOS camera observed the field in  $i'$  and  $z'$  44 ks (mid-time) after the burst. No afterglow candidate was found (Price 2007). Unfortunately, no magnitude limits were

reported. Therefore, I used a conservative upper limit of  $R > 24.0$  based on the original Gemini data available in the Gemini archive<sup>1</sup>. This corresponds to an upper limit of  $R_{AB} > 23.8$ . Together with the measured X-ray flux at the same time this leads to  $\beta_{OX} < 0.42$  and  $\beta_X - \beta_{OX} - 0.5 > 0.14$ . These values fulfill the JO4 as well as the V09 criterion. The observed X-ray flux predicts a non-extinguished  $R_{AB}$ -band magnitude between  $17.3^{+1.4}_{-1.9}$  and  $21.0^{+1.4}_{-1.9}$ . Since the *Swift*/XRT light curve shows a constant decay with a constant spectral slope during the time when the optical upper limit was obtained, I included GRB 070429A in the golden dark burst sample.

### GRB 070517A

The burst triggered *Swift*/BAT at 11:20:58 UT (Vergani et al. 2007a).  $T_{90}$  was  $9 \pm 1$  s (Vergani et al. 2007b). *Swift*/XRT clearly detected an afterglow and could even see evidence for a break in the X-ray light curve. *Swift*/UVOT could not observe, however, due to a 4 mag bright star in the field of view. Ground-based optical follow-up was only reported by Gilmore (2007) (UL = DSS2 Infrared at 2.7 hr after the burst) and Fox et al. (2007) using Gemini-South about 16 hr after the burst. The latter authors suggested two afterglow candidates in the XRT error circle but no further observations of these sources were reported in the literature. Therefore, I used their faintest detection ( $i' > 24.5$ ) as an upper limit at 57600 s. Using the corresponding  $\beta_{OX} < 0.56$ , this translates to an upper limit of  $R_{AB} > 24.3$ , thus GRB 070517A does not fulfill the JO4 and the V09 criteria (Table 5.2). However, in late-time follow-up observations with VLT/FORS1 the brighter object reported by Fox et al. (2007) ( $r' = 22.1$ ) is not visible anymore. Thus, I conclude that this was the optical afterglow of GRB 070517A.

### GRB 080123

GRB 080123 triggered *Swift*/BAT at  $T_0=04:21:57$  UT (Ukwatta et al. 2008b).  $T_{90}$  was  $115 \pm 30$  s (Tueller et al. 2008; Ukwatta et al. 2008c; Myers 2009). The *Swift*/BAT light curve was dominated by a double-peaked structure with a duration of about 0.5 s with two well-separated peaks at  $T_0 + 0.3$  s and  $T_0 + 0.6$  s (Ukwatta et al. 2008b,c). *Suzaku*/WAM observations in the 50 keV to 5 MeV window classified GRB 080123 as a short burst due to the observed  $T_{90}$  of 0.40 s Uehara et al. (2008). The potential short-burst nature of this event is supported by the analysis performed by one of mine collaborators (L. Amati) of its peak energy spectrum compared to its isotropic equivalent energy ( $E_p$  vs.  $E_{iso}$ ; Amati 2006; Fig. C.1), assuming a redshift of  $z = 0.495$  (Leibler & Berger 2010). While due the low photon statistics it is only possible to derive limits on  $E_p$ , the analysis shows that the short spike is inconsistent with the  $E_p - E_{iso}$  relation for long bursts, while the long soft tail is consistent, in a similar way to what was seen in case of GRB 050724 (Barthelmy et al. 2005) and other short GRBs. In the present work I included the burst because of its  $T_{90} > 2$  s in the BAT instrumental window.

*Swift*/XRT detected the burst during the first 10 ks of the light curve, which begins with a steep decay and becomes flatter at later times. *Swift*/UVOT started following up GRB 080123 111 seconds after the BAT trigger. An upper limit of  $white > 20.5$  at 170 s after the trigger was reported (Ukwatta et al. 2008c), a time when the prompt emission was still visible in the XRT. No further optical/NIR observations are reported in the literature. However, a  $v$ -band upper limit of 22.6 at 58732 s is found in the automated UVOT messages webpage at [http://heasarc.gsfc.nasa.gov/docs/swift/uvot\\_jdrss/301578](http://heasarc.gsfc.nasa.gov/docs/swift/uvot_jdrss/301578). This upper limit does not constrain the afterglow SED enough to fulfill the JO4 as well as the V09 criterion (Table 5.2).

### GRB 080207

GRB 080207 triggered *Swift*/BAT at 21:30:21 UT (Racusin et al. 2008), and had a duration of  $T_{90} = 340 \pm 20$  s (Stamatikos et al. 2008). XRT started observing the field 124 seconds after the BAT trigger and detected a bright source in WT mode. After  $\sim 5000$  s it continued observing in PC mode, showing a light curve with a constant decay index. UVOT did not find the afterglow in early observations after 140 s in a  $white$  finding chart and in later deeper observations ( $> 1.5$  hours, Cucchiara & Racusin 2008). Several limiting magnitudes based on ground-based observations have been reported:  $R > 14.3$  at 1607 s (0.45 hours) and  $R > 19.0$  at 5049 s (1.45 hours) (TAROT at the Calern observatory, Klotz et al. 2008);  $J > 16.7$ ,  $H > 15.9$ ,  $K > 13.9$  at 7.8 hr, 7.7 hr and 10.1 hr after the trigger respectively (60-cm REM telescope on La Silla, D'Avanzo et al. 2008);  $R > 21.8$  at 0.759 hr (RTT150 on 1.5-m telescope at the TUBITAK National Observatory, Khamitov et al. 2008);  $R > 20.8$  at 13.7 hrs (Super-LOTIS telescope on Kitt Peak observatory, Updike et al. 2008); GMOS

<sup>1</sup><http://cadwww.dao.nrc.ca/gsa/>

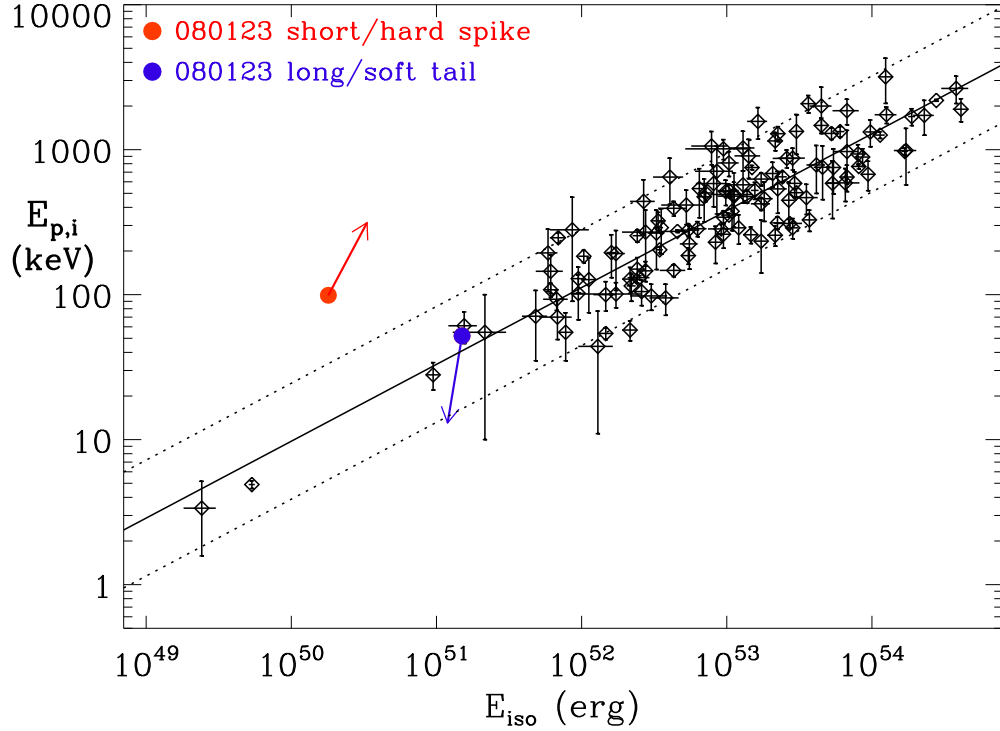


Figure C.1: Location of GRB 080123 in the  $E_p - E_{\text{iso}}$  plane (the red and blue arrows correspond to the initial short pulse and the long soft tail, respectively). In addition, long GRBs (diamonds) with known redshift and available estimates of  $E_p$  are shown (Amati 2006). The limits to  $E_p$  for GRB 080123 have been estimated based on the Swift/BAT and Suzaku/WAM spectral analysis (see text). The continuous line is the power-law best fit of the  $E_p - E_{\text{iso}}$  correlation and the dashed lines delimit the  $2\sigma$  confidence region.

camera on the Gemini South telescope, did not detect the afterglow down to  $g'r'iz' = 24.1, 24.5, 24.2, 25.0$  at 9.8 hr (Cucchiara & Fox 2008);  $R > 23.5$  at 9.75 hr (MOSCA mounted at NOT on La Palma; Marin et al. 2008);  $J > 23.5, H > 22.8, K > 21.5$  (VLT/SINFONI, Fugazza et al. 2008);  $R > 20.3$  at 1.49 hr and  $R > 21.0$  at 4.94 hr (Zeiss-600 at Mt. Terskol observatory, Andreev et al. 2008). Also, GROND did not detect the afterglow in any band down to deep flux limits (Table C.3).

The Zeiss-600 telescope upper limit at 1.69 hr corresponds to an upper limit of  $R_{\text{AB}} > 20.5$ . The observed X-ray flux predicts a non-extinguished  $R_{\text{AB}}$ -band magnitude between  $11.3^{+1.3}_{-1.4}$  and  $15.0^{+1.3}_{-1.4}$ . GRB 080207 fulfills the criterion of V09 as well as of J04 (Table 5.2). It entered the golden dark burst sample.

## GRB 080218B

GRB 080218B triggered *Swift*/BAT at 23:57:47 UT and had a duration of  $T_{90} = 6.2 \pm 1.2$  s (Schady et al. 2008b). *Swift* slewed immediately to the burst and XRT found a bright, uncatalogued X-ray source that could be localized with an uncertainty of  $r = 3''.0$ . UVOT started observing 551 seconds after the BAT trigger using the *white* filter. No afterglow candidate was found down to a  $3\sigma$  limiting magnitude of 20.6 (Schady et al. 2008a). Several limiting magnitudes based on ground-based observations were then reported:  $CR > 16$ , starting 60 s after the trigger (unfiltered, 0.4-m Watcher telescope, South Africa, French et al. 2008);  $I > 21$  and  $J > 18.7$  at 3.1 hr after the burst (1.3-m SMARTS telescope equipped with ANDICAM at CTIO, Cobb 2008a);  $H > 13.7$  at 2 min and  $K > 12.6$  at 8 min after the trigger (60-cm REM telescope on La Silla, Covino et al. 2008a);  $B > 22.1, V > 22.7, R > 22.9, I > 22.6$  at about 1 hr and  $J > 20.6, H > 20.1, K_s > 19.4$  at about 3 hr after the trigger using VLT/FORS2 and NTT/SOFI (Vreeswijk et al. 2008). Finally, no transient radio source was detected in the XRT error circle 2 weeks after the burst (Australia Telescope Compact Array, ATCA; Moin et al. 2008). Most important, GROND did not detect the afterglow down to deep limits in all seven bands in spite of a rapid response time (Table C.3).

GROND obtained an afterglow upper limit of  $r' > 24.7$  at 11520 s (mid-time) after the onset of the burst

(Rossi et al. 2008a), corresponding to  $r' > 24.3$  after correction for Galactic extinction. Using the observed spectral slope  $\beta_{\text{OX}} < 0.18$ , this corresponds to an upper limit of  $R_{\text{AB}} > 24.3$ . The observed X-ray flux predicts a non-extinguished  $R$ -band magnitude between  $15.1 \pm 1.6$  and  $18.9 \pm 1.6$ . GRB 080218B fulfills the criterion of V09 as well as of J04 (Table 5.2). It entered the golden dark burst sample.

### GRB 080602

*Swift*/BAT triggered on the burst at 01:30:28 UT (Beardmore et al. 2008a).  $T_{90}$  was  $74 \pm 7$  seconds (Beardmore et al. 2008e). The burst was also detected by *Konus-Wind*, observations of this satellite allowed the peak energy to be constrained to be larger than 226 keV (Golenetskii et al. 2008). *Swift*/XRT found a bright, uncatalogued X-ray source resulting in a  $5''.8$  error circle. Evidence for substantial X-ray absorption in excess of the Galactic value was found. *Swift*/UVOT started observing 123 s after the trigger but no afterglow candidate was detected. The XRT error circle was finally reduced to just  $1''.7$  and  $1''.8$ , respectively (Beardmore et al. 2008c,d). The only optical follow-up observation was reported by Malesani et al. (2008b) about 3.4 hr after the trigger using the NOT telescope on La Palma. No afterglow candidate was found down to  $R > 22.3$  (Malesani et al. 2008c).

UVOT obtained an upper limit of  $\nu > 20.3$  at 504 s (mid-time) after the onset of the burst (Beardmore et al. 2008e), corresponding to  $\nu > 20.2$  after correction for Galactic extinction. Using the observed spectral slope of  $\beta_{\text{OX}} < 0.05$ , this corresponds to an upper limit of  $R_{\text{AB}} > 20.2$ . Following Rol et al. (2005), the observed X-ray flux and spectral slope predicts a non-extinguished  $R_{\text{AB}}$ -band magnitude between  $13.0^{+0.9}_{-1.0}$  and  $16.7^{+0.9}_{-1.0}$ . GRB 080602 fulfills the J04 as well as the V09 criterion (Table 5.2). However, because the X-ray light curve is rather flat instead of decaying during the time when the optical upper limit was obtained, the burst does not enter the golden dark sample. Unfortunately no X-ray data is available contemporary to the deep NOT observations.

### GRB 080727A

*Swift*/BAT triggered on the burst at 05:57:39 UT with a duration ( $T_{90}$ ) of  $4.9 \pm 1.0$  s. About 109 seconds later *Swift*/XRT began observing the field (Immler et al. 2008), unveiling a light curve with constant decay and evolving spectral index (see the XRT repository, Evans et al. 2007, 2009). UVOT started observing at 113 seconds, no afterglow was found (Landsman & Immler 2008). Also UKIRT on Mauna Kea did not detect the afterglow down to  $K > 19.8$  at 0.63 hr after the trigger (Levan & Wiersema 2008). FORS1 on ESO/Paranal observed the field at 17.5 hr and did not detect the afterglow down to the very deep upper limit of  $R > 26$  (Malesani et al. 2008a).

Using the observed spectral slope  $\beta_{\text{OX}} < 0.85$ , the UKIRT upper limit corresponds to an upper limit of  $R_{\text{AB}} > 22.8$ . Following Rol et al. (2005), the observed X-ray flux and spectral slope at the time when the optical upper limit was obtained predicts a non-extinguished  $R_{\text{AB}}$ -band magnitude between  $17.9^{+1.3}_{-1.9}$  and  $21.7^{+1.3}_{-1.9}$ . The burst lies at the boundary region where it can fulfill or not the criterion of V09 ( $\Delta_{\text{min}} = -0.05$ ; Table 5.2). Unfortunately no X-ray data is available during the time of the deep VLT observations.

### GRB 080915A

GRB 080915A triggered *Swift*/BAT at 00:02:49 UT (Oates et al. 2008a). It was a long burst with a duration of  $T_{90} = (15 - 350 \text{ keV}) = 14 \pm 5$  s (Ukwatta et al. 2008a). Unfortunately, due to an observing constraint, *Swift* could not slew to the burst during the first hour after the event, therefore XRT and UVOT could start observing only 3.9 ks after the trigger. Starting at this time *Swift*/UVOT did not detect the optical afterglow (Oates et al. 2008b). ROTSE-IIIc, located at Mt. Gamsberg, Namibia, responded to GRB 080915A automatically and took unfiltered images starting 52 s after the GRB trigger (cloudy conditions, full Moon). No afterglow candidate was found in the BAT error circle down to about  $CR > 14$  (Rujopakarn et al. 2008). The robotic 60-cm REM telescope on La Silla started observing 2 min after the trigger. No afterglow candidates fainter than the 2MASS limits were seen in  $J, H, K$  (Covino et al. 2008b). Beginning 4.9 ks after the trigger *Swift*/XRT and *Swift*/UVOT started observing. XRT found a faint, fading X-ray source with an error circle of  $r = 6''.5$  (Evans & Oates 2008). Only upper limits could be reported for the UVOT bands (Breeveld & Oates 2008). Deep ground-based observations with ANDICAM on the SMARTS 1.3-m telescope at CTIO provided only upper limits of  $I > 21.9$  and  $J > 20.1$  (mid-exposure time of 1.9 hr after the burst; Cobb 2008b).

Deep prompt follow-up observations of the field were performed with GROND to search for the afterglow (Rossi et al. 2008b). They started already 4.9 min after the trigger and lasted for 130 minutes. No evidence



for a variable source was found when splitting these observations into two data sets (Table C.3). Second-epoch observations were performed with GROND in the following night. Again, no afterglow candidate was found. Using the GROND upper limit of  $r'_{AB} > 22.2$  at 6840 s (mid-time; Rossi et al. 2008b), and  $\beta_{OX} < 0.62$  (Table 5.2), this corresponds to an upper limit of  $R_{AB} > 22.0$ . Following Rol et al. (2005), I can use the observed X-ray flux as well as X-ray slope to predict the non-extinguished  $R_{AB}$ -band magnitude. However in this case due to the small number statistics I can only give an upper limit of  $R_{AB} < 21.4$ . The burst fulfills the criterion of V09, but not the one of J04 (Table 5.2). Also, the X-ray light curve is faint and very uncertain. Therefore, this burst is not included in the golden dark burst sample.

## GRB 081012

*Swift*/BAT triggered on the burst at 13:10:23 UT.  $T_{90}$  (15-350 keV) was  $29 \pm 4$  sec. The burst was also seen by Fermi/GBM, the peak energy was  $320 \pm 80$  keV (Bissaldi 2008). The XRT began observing the field 49 minutes after the BAT trigger, an X-ray afterglow was found (Kennea & Stroh 2008), the error circle is just  $1''.8$  in size (Evans et al. 2008). UVOT started observing 3 min after the XRT; no afterglow candidate was detected (Kuin & Stroh 2008). Deep ground-based follow-up observations were performed using ROTSE IIIa (with the first image 39 s after the burst), the 2.5-m NOT telescope (de Ugarte Postigo & Malesani 2008).

GROND obtained an upper limit on any optical afterglow of  $r'_{AB} > 23.6$  at  $\sim 70$  ks (mid-time) after the onset of the burst (Filgas et al. 2008; Table C.3), corresponding to  $r' = 23.5$  after correction for Galactic extinction. Using the observed spectral slope of  $\beta_{OX} < 0.83$ , this corresponds to an upper limit of  $R_{AB} > 23.4$ . Among all available optical upper limits, this observation provides the tightest constraint on the SED of the afterglow (Table 5.2). Based on these data the burst does not fulfill both the J04 and the V09 criterion (Table 5.2).

## GRB 081105

The burst triggered *Konus-Wind*, *Swift*, *AGILE*, *Suzaku* and *INTEGRAL* at 13:26:12 UT. It was localized via IPN only. The burst had a single peak, about 10 seconds long (Cummings et al. 2008). *Swift*/XRT and UVOT started observing the field about 16 hr later. An X-ray afterglow candidate was detected with an original uncertainty of  $4''.8$  (Beardmore & Cummings 2008) and later confirmed (Beardmore et al. 2008b). Observations with UVOT could only provide upper limits (Curran et al. 2008).

GROND obtained an afterglow upper limit of  $r' > 23.0$  at  $\sim 46$  ks (mid-time) after the burst (Clemens et al. 2008; Table C.3), corresponding to  $r' > 22.9$  after correction for Galactic extinction. Using  $\beta_{OX} < 0.61$  this corresponds to an upper limit of  $R_{AB} > 22.8$ . This observation provides the tightest constraints on the SED. Based on these data, the burst does not fulfill the J04 as well as the V09 criterion (Table 5.2).

## GRB 081204

The burst was detected by the *INTEGRAL* satellite at 16:44:55 UT. It lasted for about  $T_{90} = 20$  s (Götz et al. 2008). *Swift* reacted to the Integral alert, and started observing the field about 2.7 hr after the burst, and found an uncatalogued X-ray source (Mangano et al. 2008a,b). *Swift*/UVOT started observing 3 hr after the trigger in the *white* filter but no source was detected. Berger & Rest (2008) suggested an  $r = 23.5 \pm 0.3$  afterglow candidate based on observations with the Magellan/Clay telescope about 9 hr after the trigger.

The field was also observed with GROND which also detect the afterglow candidate observed by Berger & Rest (2008), together with another object, without finding evidence of fading in either source (Updike et al. 2008). Both objects are discussed in this work as host candidates (see Sec. 5.2.1). Stacking the best GROND data, I obtained the revised upper limits reported in Table C.3, centered at a mid-time of 9.6 hr. The GROND upper limit of  $r' > 24.1$  corresponds to  $r' > 24.0$  after correction for Galactic extinction. Using the observed  $\beta_{OX} < 0.55$  this corresponds to an upper limit of  $R_{AB} > 23.9$ . Following Rol et al. (2005), I can use the observed X-ray flux as well as the X-ray slope to predict the non-extinguished  $R_{AB}$ -band magnitude. However in this case due to the small number statistics I can only give an upper limit of  $R_{AB} < 23$  in the worse case of a break between optical and X-ray bands. The burst fulfills the V09 criterion (Table 5.2), but due to the faint XRT light curve and the not well determined high X-ray spectral slope ( $\beta_X = 1.93^{+1.56}_{-0.77}$ ) this burst did not enter the golden dark burst sample.

Table C.1: *Redshift estimates of the galaxies found in the XRT error circles for different model assumptions on their photometric properties.*

#	GRB	Object	(4)	(5)	(6)	(7)	(8)	(9)
1	050717	A	0.5	0.4	1.2	0.9	3.2	1.8
		B	0.7	0.6	1.7	1.2	–	2.4
2	050922B	A	1.7	1.2	–	2.4	–	–
3	060211	A	0.7	0.6	1.7	1.2	–	2.4
		B	0.4	0.3	0.9	0.7	2.3	1.4
4	060805A	A	0.9	0.7	2.3	1.4	–	3.0
		B	0.5	0.4	1.1	0.8	3.1	1.8
5	060919	A	1.5	1.0	4.2	2.1	–	4.5
6	060923B	A	0.4	0.3	0.9	0.7	2.4	1.5
		B	star	–	–	–	–	–
		C	0.7	0.6	1.7	1.2	–	2.4
		D	1.2	0.9	3.3	1.8	1.5	3.9
7	061102	A	0.6	0.5	1.4	1.0	4.1	2.1
		B	0.5	0.5	1.3	1.0	3.8	2.0
8	070429A	A	0.9	0.7	2.2	1.4	–	2.9
		B	0.6	0.5	1.5	1.0	4.2	2.1
		C	0.6	0.5	1.6	1.1	4.7	2.3
9	070517A	A	1.0	0.8	2.7	1.6	–	3.4
10	080123	A	1.1	0.8	2.9	1.7	–	3.6
		B	1.2	0.9	3.3	1.8	1.5	3.9
		C	0.2	0.1	0.4	0.3	0.9	0.7
		D	0.4	0.4	1.1	0.8	2.9	1.7
11	080207	A	0.9	0.7	2.4	1.5	–	3.1
		B	1.7	1.1	–	2.4	–	–
12	080218B	A	1.5	1.1	4.4	2.2	–	4.7
		B	0.7	0.6	1.8	1.2	–	2.5
13	080602	A	0.4	0.3	0.8	0.7	2.2	1.4
		B	0.6	0.5	1.4	1.0	3.9	2.0
15	080915A	A	star	–	–	–	–	–
		B	0.2	0.2	0.4	0.4	1.0	0.7
		C	0.8	0.6	1.9	1.3	–	2.6
		D	0.7	0.6	1.8	1.2	–	2.5
		E	1.0	0.8	2.8	1.6	–	3.5
16	081012	A	0.9	0.7	2.4	1.5	–	3.1
17	081105	A	0.5	0.4	1.2	0.9	3.3	1.8
		B	0.6	0.5	1.6	1.1	4.7	2.3
18	081204	A	0.4	0.3	0.9	0.7	2.5	1.5
		B	0.4	0.4	1.1	0.8	2.9	1.7
		C	0.4	0.3	0.9	0.7	2.4	1.5
		D	0.6	0.5	1.5	1.0	4.3	2.2
		E	0.6	0.5	1.6	1.1	4.7	2.3
		F	1.1	0.8	3.1	1.7	–	3.7

Notes: Columns (4) to (9) give the redshift of the galaxy for different assumptions on its spectral slope  $\beta$  and absolute magnitude  $M_R$ : = (0.0,–18), (1.0,–18), (0.0,–20), (1.0,–20), (0.0,–22), (1.0,–22). In detail see Sect. 5.3.6.

Table C.2: Log of the late-time optical/NIR observations to search for a GRB host candidate.

#	GRB	Instrument	Filter	Date obs	Calib	FWHM	Exp. (s)
1	050717	GROND	$g'r'i'z'$	2007/07/24-26	SA114-750	1''0	8880
		GROND	$JHK_s$	2007/07/24-26	2MASS	1''4	7200
2	050922B	FORS2	$R_C$	2009/08/15	ESO ZP	0''7	2930
		ISAAC	$K_s$	2009/07/06	2MASS	0''7	1920
		NEWFIRM	$K_s$	2008/11/08	2MASS	1''2	1800
3	060211A	GROND	$g'r'i'z'$	2007/10/20-22	SA95-190	1''0	10360
		GROND	$JHK_s$	2007/10/20-22	2MASS	1''6	8400
		NEWFIRM	$J$	2009/01/17	2MASS	1''1	10200
		NEWFIRM	$K_s$	2009/01/17	2MASS	1''2	3600
4	060805A	GROND	$g'r'i'z'$	2008/05/05-07	SDSS	0''9	4440
		GROND	$JHK_s$	2008/05/05-07	2MASS	1''6	3600
5	060919	FORS1	$R_C$	2008/04/10	SA110-362	0''8	2930
		ISAAC	$K_s$	2008/05/18	2MASS	0''6	1920
6	060923B	FORS1	$R_C$	2008/04/05	NGC2437	0''8	2930
		ISAAC	$K_s$	2008/04/15	2MASS	0''5	1920
7	061102	FORS1	$R_C$	2008/04/06	NGC2437	0''7	2930
		ISAAC	$K_s$	2008/04/18	2MASS	0''7	1920
8	070429A	FORS1	$R_C$	2008/04/08	SA110-362	1''0	2930
		ISAAC	$K_s$	2008/05/18	2MASS	0''6	2400
9	070517A	FORS1	$R_C$	2008/04/10	SA110-362	0''6	2930
		ISAAC	$K_s$	2008/08/05	2MASS	0''5	1920
10	080123	FORS2	$R_C$	2009/05/22	NGC2818	0''6	2930
		ISAAC	$K_s$	2009/05/28	2MASS	0''8	1920
11	080207	VIMOS	$R_C$	2010/02/10	PG1047+3	0''8	2930
		ISAAC	$K_s$	2010/02/07	2MASS	0''6	1920
12	080218B	FORS2	$R_C$	2009/05/26	PG1047	0''5	2930
		ISAAC	$K$	2009/03/20	2MASS	0''5	1920
13	080602	GROND	$g'r'i'z'$	2009/11/24	SDSS	1''1	4440
		GROND	$JHK_s$	2009/11/24	2MASS	1''3	3600
		FORS2	$R_C$	2009/06/05	NGC7006	0''8	2930
		ISAAC	$K_s$	2009/07/06	2MASS	0''7	1920
14	080727A	FORS1	$R_C$	2008/07/27	E5-Stetson	0''8	2930
		ISAAC	$K_s$	2010/02/10	2MASS	0''6	1920
15	080915A	FORS1	$R_C$	2008/09/27	E7	1''4	968
		HAWK-I	$K_s$	2008/09/16	2MASS	0''6	840
16	081012	VIMOS	$R_C$	2009/10/21	SA98	0''8	2400
		ISAAC	$K_s$	2009/10/08	2MASS	0''4	1920
17	081105	VIMOS	$R_C$	2009/10/21	SA98	1''0	2400
		ISAAC	$K_s$	2009/09/14	2MASS	0''4	1920
18	081204	VIMOS	$R_C$	2009/10/21	SA98	1''0	2400
		ISAAC	$K_s$	2009/09/14	2MASS	0''5	1920
		SOFI	$J$	2010/11/01	2MASS	0''5	3600

Notes for individual targets: GRB 070517A: a candidate optical afterglow was found by Fox et al. (2007), and we identify it as the GRB afterglow based on our data. *Standard star fields*: The fields PG1047+3, E5, E7, NGC 2437, NGC 2818, and NGC 7006 are from the internet pages of P. Stetson <http://www3.cadc-ccda.hia-ihp.nrc-cnrc.gc.ca/community/STETSON/>. Landolt equatorial standards stars (SA) for the  $R_C$  band were obtained from the internet page of the Canada-France-Hawaii Telescope <http://www.cfht.hawaii.edu/ObsInfo/Standards/Landolt/>. SA standard star fields for GROND optical calibrations are downloaded from the SDSS archive server at <http://www.sdss.org/>. ZP stands for photometric zero point calibration. *Filters*: Observations with FORS2 were performed using the  $R_{\text{special}+76}$  filter. FORS1 and VIMOS used the  $R_{\text{Bessel}+36}$  filter. The FWHM column refers to the FWHM of the average stellar PSF.

Table C.3: Summary of the early-time upper limits based on observations with GROND (see Table 5.2).

#	GRB	$t$ [hr]	Filter	UL
11	080207	9.75	$g'$	24.0
		9.75	$r'$	23.6
		9.75	$i'$	23.1
		9.75	$z'$	22.3
		9.75	$J$	21.0
		9.75	$H$	19.7
		9.75	$K_s$	19.0
12	080218B	0.75	$g'$	21.4
		0.75	$r'$	21.5
		0.75	$i'$	20.6
		0.75	$z'$	20.6
		0.75	$J$	20.8
		0.75	$H$	18.5
		0.75	$K_s$	17.8
		3.2	$g'$	24.6
		3.2	$r'$	24.7
		3.2	$i'$	23.9
		3.2	$z'$	24.7
15	080915A	0.15	$g'$	22.0
		0.15	$r'$	22.2
		0.15	$i'$	21.8
		0.15	$z'$	21.7
		0.15	$J$	20.1
		0.15	$H$	18.9
		0.15	$K_s$	17.6
		0.92	$g'$	23.0
		0.92	$r'$	23.5
		0.92	$i'$	23.0
		0.92	$z'$	23.1
		0.92	$J$	21.2
		0.92	$H$	20.0
0.92	$K_s$	18.6		
16	081012	19.35	$g'$	23.2
		19.35	$r'$	23.5
		19.35	$i'$	22.8
		19.35	$z'$	22.8
		19.35	$J$	21.5
		19.35	$H$	20.4
		19.35	$K_s$	19.4
17	081105	12.84	$g'$	24.0
		12.84	$r'$	23.0
		12.84	$i'$	22.1
		12.84	$z'$	21.8
		12.84	$J$	20.7
		12.84	$H$	19.6
		12.84	$K_s$	18.2
18	081204	9.60	$g'$	24.2
		9.60	$r'$	24.1
		9.60	$i'$	23.2
		9.60	$z'$	22.4
		9.60	$J$	20.7
		9.60	$H$	19.4
		9.60	$K_s$	18.3

Notes: For early-time observations by other groups see, e.g., the web page of J. Greiner at [www.mpe.mpg.de/~jcg/grbgen.html](http://www.mpe.mpg.de/~jcg/grbgen.html) or GRBlog at <http://grblog.org/grblog.php>. In all cases the data given here supersede the values given in the corresponding GRB circulars: GCN 7279, GRB 080207 (Küpcü Yoldaş et al. 2008); GCN 7319, GRB 080218B (Rossi et al. 2008a); GCN 8268, GRB 080915A (Rossi et al. 2008b); GCN 8373, GRB 081012 (Filgas et al. 2008); GCN 8492, GRB 081105 (Clemens et al. 2008); GCN 8627, GRB 081204 (Updike et al. 2008).

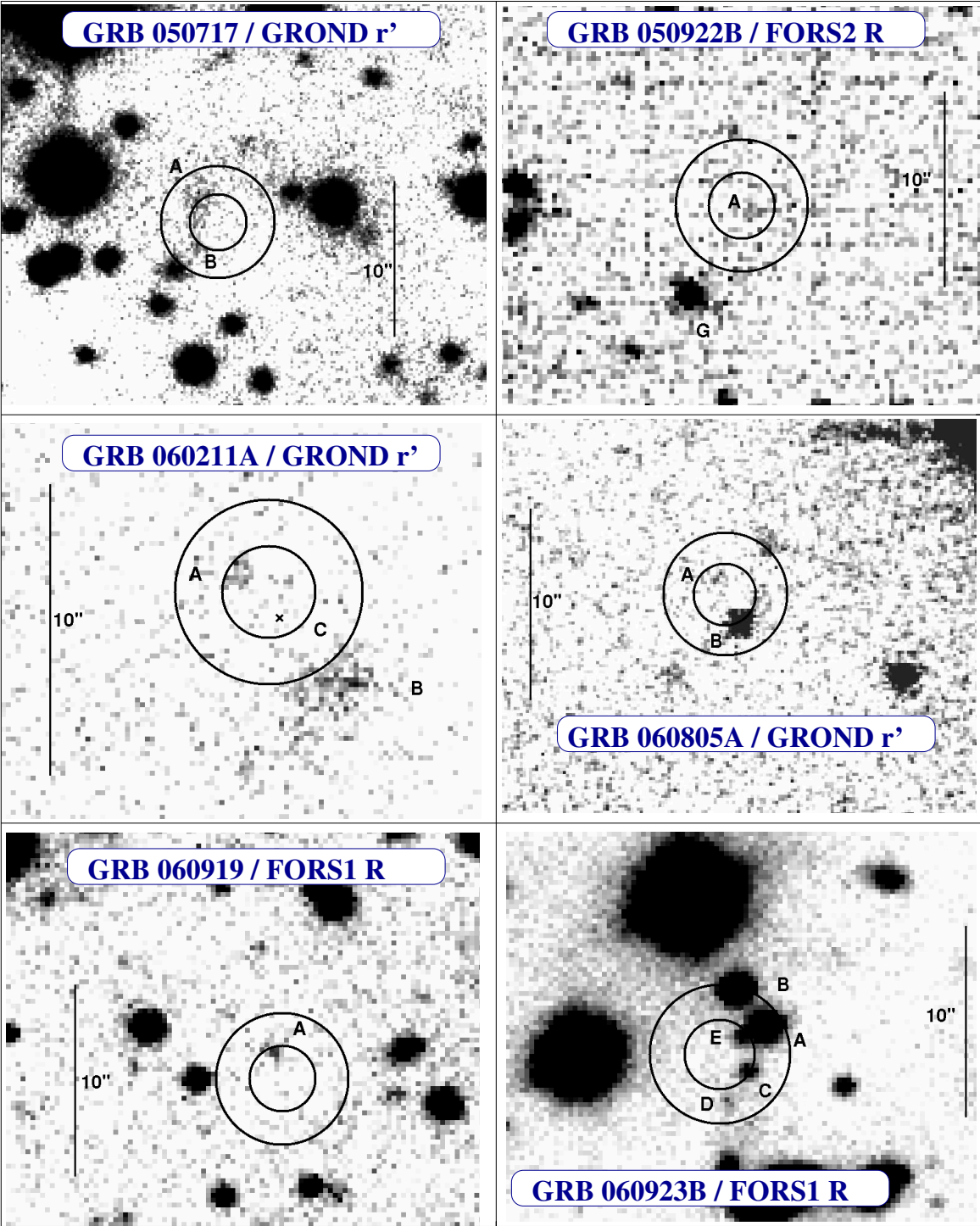
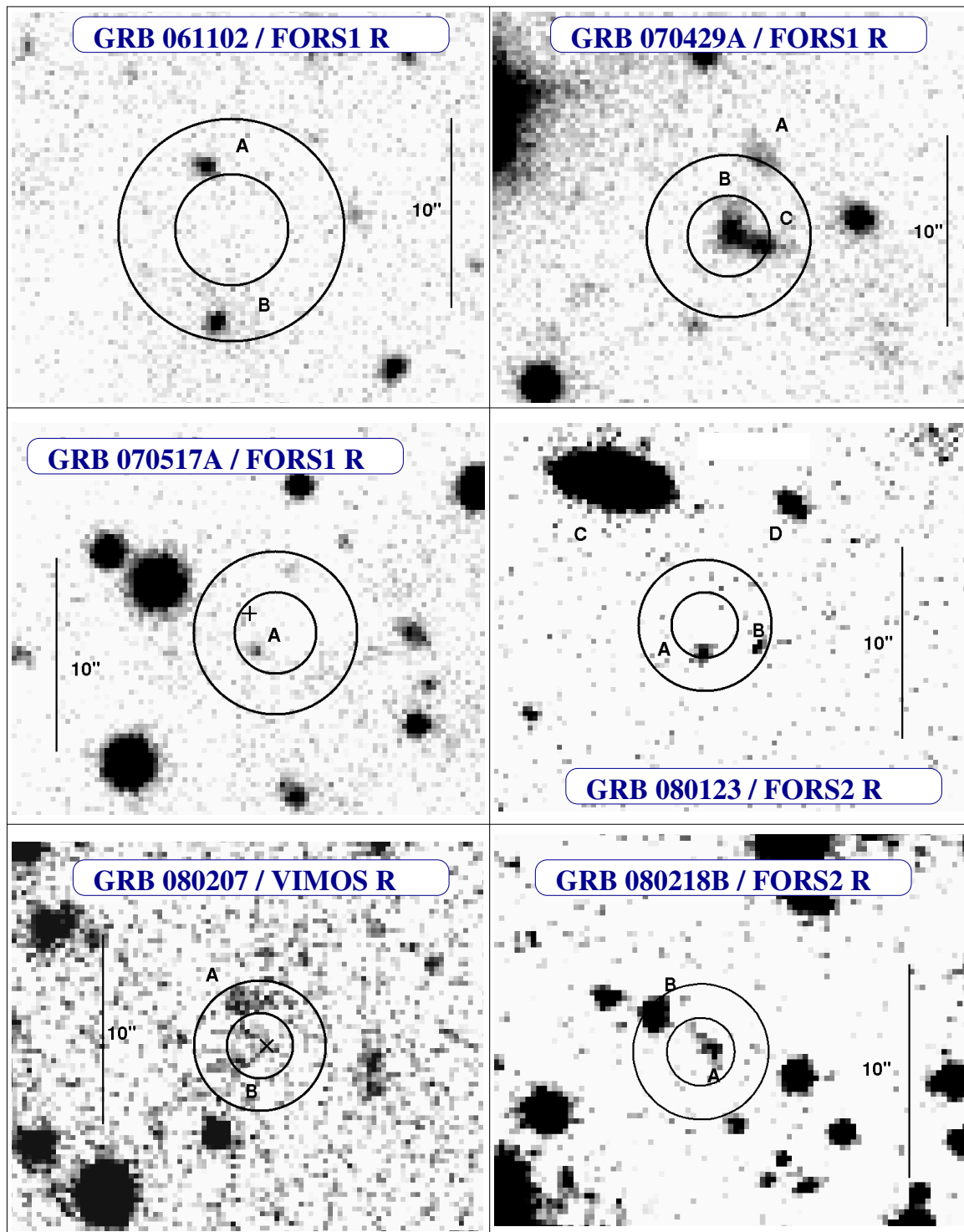


Figure C.2: Finding charts of dark GRBs fields. Host galaxy candidates are labeled.

Figure C.3: *Finding charts, continued.*

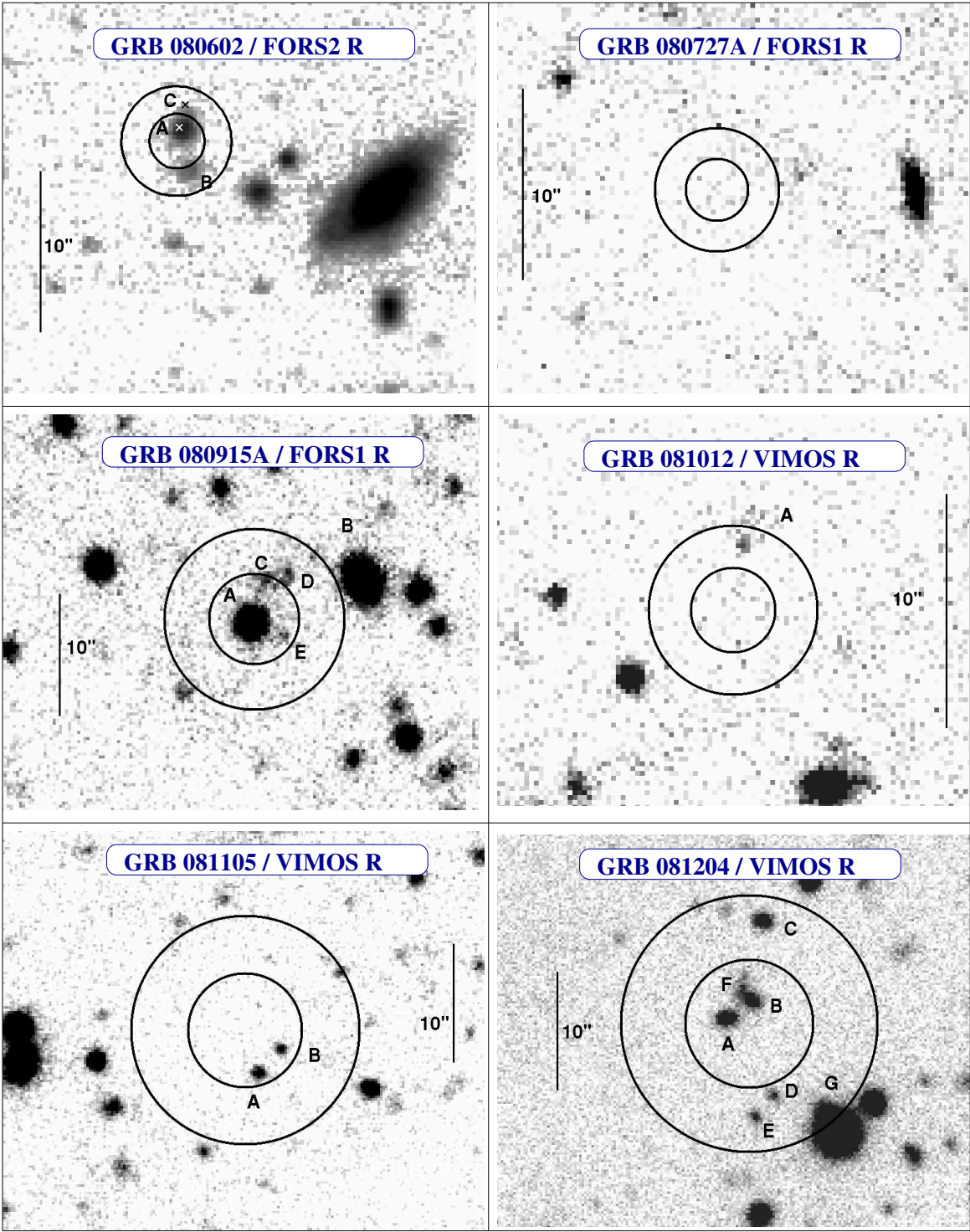


Figure C.4: Finding charts, continued.

## Additional references (Appendix only)

- Amati, L. 2006, *Mon. Not. R. Astron. Soc.*, 372, 233
- Andreev, M., Kurennya, A., & Pozanenko, A. 2008, *GCN Circ.*, 7333
- Barbier, L., Barthelmy, S., Cummings, J., et al. 2006a, *GCN Circ.*, 5403
- Barbier, L., Barthelmy, S. D., Cummings, J., et al. 2006b, *GCN Circ.*, 5595
- Barthelmy, S. D., Chincarini, G., Burrows, D. N., et al. 2005, *Nature*, 438, 994
- Barthelmy, S. D., Markwardt, C. B., Page, K. L., et al. 2007, *GCN Circ.*, 6355
- Beardmore, A. P., Barthelmy, S. D., Cummings, J. R., et al. 2008a, *GCN Circ.*, 7781
- Beardmore, A. P., Burrows, D. N., & Cummings, J. R. 2008b, *GCN Circ.*, 8522
- Beardmore, A. P. & Cummings, J. 2008, *GCN Circ.*, 8487
- Beardmore, A. P., Evans, P. A., Goad, M. R., & Osborne, J. P. 2008c, *GCN Circ.*, 7782
- Beardmore, A. P., Page, K. L., & Evans, P. A. 2008d, *GCN Circ.*, 7785
- Beardmore, A. P., Page, K. L., Evans, P. A., et al. 2008e, *GCN Report*, 145, 1
- Berger, E. & Lopez-Morales, M. 2005, *GCN Circ.*, 3639
- Berger, E., Lopez-Morales, M., & Osip, D. 2005, *GCN Circ.*, 3643
- Berger, E. & Rest, A. 2008, *GCN Circ.*, 8624
- Bissaldi, E. 2008, *GCN Circ.*, 8370
- Blustin, A., Hurkett, C., Smale, A., & Cominsky, L. 2005, *GCN Circ.*, 3638
- Breeveld, A. & Guidorzi, C. 2006, *GCN Circ.*, 5580
- Breeveld, A. & Oates, S. R. 2008, *GCN Circ.*, 8232
- Cannizzo, J., Barbier, L., Barthelmy, S. D., et al. 2007, *GCN Circ.*, 6362
- Castro-Tirado, A. J., Cunniffe, R., de Ugarte Postigo, A., et al. 2006, in Presented at the Society of Photo-Optical Instrumentation Engineers (SPIE) Conference, Vol. 6267, Society of Photo-Optical Instrumentation Engineers (SPIE) Conference Series
- Cenko, S. B. 2006, *GCN Circ.*, 5401
- Clemens, C., Rossi, A., Greiner, J., & McBreen, S. 2008, *GCN Circ.*, 8257, 1
- Cobb, B. E. 2008a, *GCN Circ.*, 7318
- Cobb, B. E. 2008b, *GCN Circ.*, 8248
- Covino, S., D'Avanzo, P., Antonelli, L. A., et al. 2008a, *GCN Circ.*, 7322
- Covino, S., D'Avanzo, P., Antonelli, L. A., et al. 2008b, *GCN Circ.*, 8233
- Cucchiara, A. & Fox, D. B. 2008, *GCN Circ.*, 7276
- Cucchiara, A. & Racusin, J. 2008, *GCN Circ.*, 7268
- Cummings, J., Barbier, L., Barthelmy, S., et al. 2005a, *GCN Circ.*, 3637
- Cummings, J., Barbier, L., Barthelmy, S., et al. 2005b, *GCN Circ.*, 4033
- Cummings, J., Barthelmy, S., Gehrels, N., et al. 2008, *GCN Circ.*, 8484
- Curran, P. A., Schady, P., & Cummings, J. 2008, *GCN Circ.*, 8488
- D'Avanzo, P., Antonelli, L. A., Covino, S., et al. 2008, *GCN Circ.*, 7269
- de Ugarte Postigo, A., Castro-Tirado, A. J., Jelinek, M., et al. 2007, *GCN Circ.*, 6361
- de Ugarte Postigo, A. & Malesani, D. 2008, *GCN Circ.*, 8366
- Evans, P. A., Beardmore, A. P., Page, K. L., et al. 2009, *Mon. Not. R. Astron. Soc.*, 397, 1177
- Evans, P. A., Beardmore, A. P., Page, K. L., et al. 2007, *Astron. & Astroph.*, 469, 379
- Evans, P. A., Goad, M. R., Osborne, J. P., & Beardmore, A. P. 2008, *GCN Circ.*, 8391
- Evans, P. A. & Oates, S. R. 2008, *GCN Circ.*, 8231
- Filgas, R., Kruehler, T., Greiner, J., et al. 2008, *GCN Circ.*, 8373
- Fox, D. B., Price, P. A., & Berger, E. 2007, *GCN Circ.*, 6420
- French, J., Jelinek, M., Kubanek, P., & de Ugarte Postigo, A. 2008, *GCN Circ.*, 7316
- Fugazza, D., D'Elia, V., D'Avanzo, P., Covino, S., & Tagliaferri, G. 2008, *GCN Circ.*, 7293
- Gilmore, A. C. 2007, *GCN Circ.*, 6412
- Godet, O., Page, K. L., Osborne, J. P., et al. 2005, *GCN Circ.*, 4031
- Golenetskii, S., Aptekar, R., Mazets, E., et al. 2005, *GCN Circ.*, 3640
- Golenetskii, S., Aptekar, R., Mazets, E., et al. 2008, *GCN Circ.*, 7784
- Gomboc, A., Guidorzi, C., Steele, I. A., et al. 2006, *GCN Circ.*, 4738
- Götz, D., Mereghetti, S., Paizis, A., et al. 2008, *GCN Circ.*, 8614
- Greiner, J., Bornemann, W., Clemens, C., et al. 2008, *Publ. Astron. Soc. Pacific*, 120, 405
- Guidorzi, C., Barthelmy, S. D., Evans, P. A., et al. 2006a, *GCN Circ.*, 5575
- Guidorzi, C., Romano, P., Moretti, A., & Vergani, S. 2006b, *GCN Circ.*, 5577
- Guziy, S., Jelinek, M., Gorosabel, J., et al. 2005, *GCN Circ.*, 4025
- Holland, S. & Cucchiara, A. 2006, *GCN Circ.*, 5603
- Holland, S. T. 2006, *GCN Circ.*, 5784
- Holland, S. T., Barthelmy, S. D., Chester, M. M., et al. 2006, *GCN Circ.*, 5776



- Hurkett, C., Beardmore, A., Godet, O., et al. 2006, GCN Circ., 4736  
Hurkett, C., Page, K., Burrows, D., et al. 2005a, GCN Circ., 3636  
Hurkett, C., Page, K., Kennea, J., et al. 2005b, GCN Circ., 3633  
Immler, S., Baumgartner, W. H., Gehrels, N., et al. 2008, GCN Circ., 8021  
Kennea, J. A., Burrows, D. N., Hurkett, C., Page, K., & Gehrels, N. 2005, GCN Circ., 3634  
Kennea, J. A. & Strohm, M. 2008, GCN Circ., 8364  
Khamitov, I., Kose, O., Yakut, K., et al. 2008, GCN Circ., 7270  
Klotz, A., Boer, M., & Atteia, J. L. 2006, GCN Circ., 5576  
Klotz, A., Boer, M., & Atteia, J. L. 2008, GCN Circ., 7267  
Kornienko, G., Rumyantsev, V., & Pozanenko, A. 2005, GCN Circ., 4047  
Krimm, H., Barbier, L., Barthelmy, S., et al. 2006a, GCN Circ., 4757  
Krimm, H. A., Hurkett, C., Pal'shin, V., et al. 2006b, ApJ, 648, 1117  
Kuin, N. P. M. & Strohm, M. C. 2008, GCN Circ., 8365  
Küpcü Yoldaş, A., Yoldaş, A., Greiner, J., et al. 2008, GCN Circ., 7279  
Landsman, W. B. & Immler, S. 2008, GCN Circ., 8027  
Leibler, C. N. & Berger, E. 2010, *Astroph. J.*, 725, 1202  
Levan, A. J. & Wiersema, K. 2008, GCN Circ., 8048  
Li, W. 2006, GCN Circ., 5400  
Lipunov, V., Kornilov, V., Kuvshinov, D., et al. 2006, GCN Circ., 4741  
Luckas, P., Trondal, O., & Schwartz, M. 2005, GCN Circ., 3642  
MacLeod, C., Kirschbrown, J., Haislip, J., et al. 2005, GCN Circ., 3652  
Malesani, D., Jakobsson, P., Levan, A. J., Rol, E., & Fynbo, J. P. U. 2008a, GCN Circ., 8039  
Malesani, D., Quirion, P., Fynbo, J. P. U., & Jakobsson, P. 2008b, GCN Circ., 7783  
Malesani, D., Quirion, P., Fynbo, J. P. U., & Jakobsson, P. 2008c, GCN Circ., 7783  
Mangano, V., Sbarufatti, B., La Parola, V., & Baumgartner, W. H. 2008a, GCN Circ., 8620  
Mangano, V., Sbarufatti, B., & Parola, V. L. 2008b, GCN Circ., 8616  
Marín, V. M., Sabater, J., Castro-Tirado, A. J., et al. 2008, GCN Circ., 7291  
Melandri, A., Gomboc, A., Smith, R. J., & Tanvir, N. 2006, GCN Circ., 5579  
Moin, A., Tingay, S., Phillips, C., et al. 2008, GCN Circ., 8466  
Muehleger, M., Duscha, S., Stefanescu, A., et al. 2006, GCN Circ., 5405  
Myers, J., D. 2009, Swift GRB Table and Lookup  
Norris, J., Barbier, L., Barthelmy, S., et al. 2005, GCN Circ., 4008  
Norris, J., Kutuyev, A., Ganguly, R., Canterna, R., & Pierce, M. 2006, GCN Circ., 4760  
Oates, S. R., Beardmore, A. P., Cummings, J. R., et al. 2008a, GCN Circ., 8227  
Oates, S. R., Ukwatta, T. N., Evans, P., & Breeveld, A. 2008b, GCN Report, 168, 1  
Pandey, S. B., Page, M. J., Ziaepour, H. Z., & Oates, S. R. 2006, GCN Circ., 5402  
Pasquale, M. D., Norris, J., Kennedy, T., Mason, K., & Gehrels, N. 2005, GCN Circ., 4028  
Price, P. A. 2007, GCN Circ., 6371  
Quimby, R. M., Rykoff, E. S., Yost, S. A., et al. 2006, *Astroph. J.*, 640, 402  
Racusin, J. L., Barthelmy, S. D., Baumgartner, W. H., et al. 2008, GCN Circ., 7264  
Rol, E. & Page, K. L. 2006, GCN Circ., 5406  
Rol, E., Wijers, R. A. M. J., Kouveliotou, C., Kaper, L., & Kaneko, Y. 2005, ApJ, 624, 868  
Rossi, A., Greiner, J., Küpcü Yoldaş, A., & Yoldaş, A. 2008a, GCN Circ., 7319  
Rossi, A., Kruehler, T., Greiner, J., et al. 2008b, GCN Circ., 8268  
Rujopakarn, W., Rykoff, E. S., Schaefer, B. E., Yuan, F., & Yost, S. A. 2006, GCN Circ., 4737  
Rujopakarn, W., Swan, H., & Guver, T. 2008, GCN Circ., 8228  
Rykoff, E. S., Schaefer, B. E., & Swan, H. 2007, GCN Circ., 6356  
Sato, G., Barbier, L., Barthelmy, S., et al. 2006a, GCN Circ., 4751  
Sato, G., Barbier, L., Barthelmy, S. D., et al. 2006b, GCN Circ., 5578  
Schady, P., Barthelmy, S. D., Baumgartner, W. H., et al. 2008a, GCN Circ., 7314  
Schady, P. & Cannizzo, J. 2007, GCN Circ., 6364  
Schady, P., Evans, P. A., & Krimm, H. 2008b, GCN Report, 117  
Schaefer, B. E., Quimby, R., Yost, S. A., & Rujopakarn, W. 2005, GCN Circ., 4010  
Sharapov, D., Ibrahimov, M., Pozanenko, A., & Rumyantsev, V. 2006, GCN Circ., 4927  
Sonoda, E., Maeno, S., Tokunaga, Y., & Yamauchi, M. 2005, GCN Circ., 4009  
Stamatikos, M., Barthelmy, S. D., Burrows, D. N., et al. 2006, GCN Circ., 5590  
Stamatikos, M., Barthelmy, S. D., Cummings, J., et al. 2008, GCN Circ., 7277  
Starling, R. L. C., Page, K. L., & Holland, S. T. 2006, GCN Circ., 5783  
Torii, K. 2005, GCN Circ., 4024  
Tueller, J., Barbier, L., Barthelmy, S. D., et al. 2006, GCN Circ., 5777  
Tueller, J., Barthelmy, S. D., Cummings, J., et al. 2008, GCN Circ., 7205

- Uehara, T., Ohno, M., Takahashi, T., et al. 2008, GCN Circ., 7223  
Ukwatta, T., Barthelmy, S. D., Baumgartner, W., et al. 2008a, GCN Circ., 8230  
Ukwatta, T. N., Baumgartner, W. H., Chester, M. M., et al. 2008b, GCN Circ., 7203  
Ukwatta, T. N., Tueller, J., Mangano, V., et al. 2008c, GCN Report, 111  
Updike, A. C., Milne, P. A., Williams, G. G., & Hartmann, D. H. 2008, GCN Circ., 7273  
Urata, Y., Kuwahara, M., Tashiro, M., et al. 2006, GCN Circ., 5204  
Vergani, S. D., Barthelmy, S. D., Beardmore, A. P., et al. 2007a, GCN Circ., 6411  
Vergani, S. D., Romano, P., Guidorzi, C., et al. 2007b, GCN Report, 56.2  
Vreeswijk, P., Fynbo, J., Milvang-Jensen, B., et al. 2008, GCN Circ., 7327  
Ziaeeppour, H. Z., Barthelmy, S. D., Cummings, J. R., et al. 2006, GCN Circ., 5398

# Acknowledgements

First of all, I want to express all my gratitude to Dr. habil. Sylvio Klose, the supervisor of my Ph.D. work. He has been always available for helping me to get the best out of my work. The support he gave me in all aspects, research and life, made this four years and half very fruitful. I will never be able to find all the words to thank him.

Many thanks also to Prof. Artie Hatzes for supporting this work at the University. Many thanks also to the BLANCEFLOR Boncompagni-Ludovisi, née Bildt foundation and the Thüringer Landessternwarte Tautenburg, which gave me the necessary financial support after the expiration of my DFG contract.

I want to thank all the observatory staff, in particular the members, and friends of mine, of the GRB group: Ana, Alex, Steve, Sebastian. It has been a pleasure to collaborate with them.

I thank the GROND collaboration, and especially Dr. habil. Jochen Greiner, who allowed me to stay 10 months on La Silla (Chile) during my PhD, for operating the most advanced imager in the world. And thanks to all the GROND team, in particular to Thomas Krühler, for always being very helpful and available.

A special thank to Eliana Palazzi, whose support and suggestions were always helpful. I thank also Laura Arnold and Eliza Gonsalves for helping analyzing the data.

Thanks to all friends I met in my stay in Tautenburg and in Jena: Alessio, Dania, Davide, Felice, Gianluca, Gionata, Massimiliano, Maria, Max, Rebeca, Patrizia, Vito and Teresa. I will never forget the wonderful moments we had together.

I want to thank also my parents and my brother for supporting me to finally reach this important goal. A special thanks to my father for always being interested and curious about my research.

A special and big Thank to Anna for always supporting me in this big effort, cheering me during the bad moments, and sharing many things during the last years.

And to all other friends of mine, everywhere in the world, thanks.

## Ehrenwörtliche Erklärung

Ich erkläre hiermit ehrenwörtlich, dass ich die vorliegende Arbeit selbständig, ohne unzulässige Hilfe Dritter und ohne Benutzung anderer als der angegebenen Hilfsmittel und Literatur angefertigt habe. Die aus anderen Quellen direkt oder indirekt übernommenen Daten und Konzepte sind unter Angabe der Quelle gekennzeichnet.

Bei der Auswahl und Auswertung folgenden Materials haben mir die nachstehend aufgeführten Personen in der jeweils beschriebenen Weise unentgeltlich geholfen:

1. Dr. habil. Sylvio Klose: Betreuung der vorliegenden Arbeit.
2. Dr. David Alexander Kann half bei der Erstellung und Analyse der optischen Lichtkurven und der Gestaltung der zugehörigen Abbildungen.
3. Dr. Patrizia Ferrero half bei der Photometrie für einige GRB-Muttergalaxien.
4. Dipl.-Phys. Steve Schulze half bei der Analyse der *Swift*/XRT Röntgendaten und bei der Erstellung der zugehörigen Abbildungen.
5. Dr. Arne Rau half bei Analyse der Fermi/GBM-Daten.

Weitere Personen waren an der inhaltlich-materiellen Erstellung der vorliegenden Arbeit nicht beteiligt. Insbesondere habe ich hierfür nicht die entgeltliche Hilfe von Vermittlungs bzw. Beratungsdiensten (Promotionsberater oder andere Personen) in Anspruch genommen. Niemand hat von mir unmittelbar oder mittelbar geldwerte Leistungen für Arbeiten erhalten, die in Zusammenhang mit dem Inhalt der vorgelegten Dissertation stehen.

Die Arbeit wurde bisher weder im In- noch im Ausland in gleicher oder ähnlicher Form einer anderen Prüfungsbehörde vorgelegt.

Die geltende Promotionsordnung der Physikalisch-Astronomischen Fakultät ist mir bekannt.

Ich versichere ehrenwörtlich, dass ich nach bestem Wissen die reine Wahrheit gesagt und nichts verschwiegen habe.

Jena, den 2. Mai 2012

Andrea Rossi

# Lebenslauf

## Zur Person:

Name: Rossi  
Vorname: Andrea  
Geburtsdatum: 28.03.1977  
Geburtsort: Cividale del Friuli (Italien)

## Werdegang:

- |                       |                                                                                                                                                                                                                 |
|-----------------------|-----------------------------------------------------------------------------------------------------------------------------------------------------------------------------------------------------------------|
| seit Apr. 2012        | Post-Doc an der Thüringer Landessternwarte Tautenburg                                                                                                                                                           |
| Feb. 2007 - Mär. 2012 | Doktorand an der Thüringer Landessternwarte Tautenburg<br>Betreuer: Dr. habil. Sylvio Klose<br>Titel: Combining X-ray and optical/NIR data to study GRBs and their host galaxies                                |
| Aug. - Okt. 2006      | Ausländischer Sommer-Student am Large Binocular Telescope (LBT), Arizona, U.S.A.                                                                                                                                |
| Okt. 1996 - Sep. 2005 | Studium der Physik an der Universität Trieste (Italien)<br>Betreuer: Prof. Guido Barbiellini<br>Titel: Proprietá d'ambiente delle galassie ospiti dei Gamma Ray Burst<br>Abschluß: Dottore Magistrale in Fisica |
| Sep. 1991 - Jul. 1996 | Liceo Scientifico "L. Magrini" - Gemona del Friuli (Italien)<br>Abschluß: Maturitá Scientifica (Hochschulzugangsberechtigung)                                                                                   |
| Sep. 1988 - Jun. 1991 | Scuola Media "Gen A. Cantore" - Gemona del Friuli (Italien)                                                                                                                                                     |
| Sep. 1987 - Jun. 1988 | Scuola Elementare "D. Alighieri" - Gemona del Friuli (Italien)                                                                                                                                                  |
| Sep. 1983 - Jun. 1987 | Scuola Elementare "G. Marchetti" - Gemona del Friuli (Italien)                                                                                                                                                  |

Jena, den 2. Mai 2012

Andrea Rossi

## Publications in International Refereed Journals

1. **Rossi, A.**, Klose, S., Ferrero, P., Greiner, J., Arnold, L.A., Gonsalves, E.E., Hartmann, D.H., Utdike, A.C., Kann, D.A., Krühler, T., Palazzi, E., Savaglio, S., Schulze, S., Afonso, P.M.J., Amati, L., Castro-Tirado, A.J., Clemens, C., Filgas, R., Gorosabel, J., Hunt, L., Küpcü-Yoldaş, A., Masetti, N., Nardini, M., Nicuesa Guelbenzu, A., Olivares E., F., Pian, E., Rau, A., Schady, P., Schmidl, S., Yoldaş, A. and de Ugarte Postigo, A. (2011). *A deep search for the host galaxies of GRBs with non-detected optical afterglows*. *Astron. & Astroph.*, submitted, revised.
2. Krühler, T., Greiner, J., Schady, P., Savaglio, S., Afonso, P.M.J., Clemens, C., Elliott, J., Filgas, R., Gruber, D., Kann, D.A., Klose, S., Küpcü-Yoldaş, A., McBreen, S., Olivares E., F., Pierini, D., Rau, A., **Rossi, A.**, Nardini, M., Nicuesa Guelbenzu, A., Sudilovsky, V., and Utdike, A.C. (2011). The SEDs and Host Galaxies of the dustiest GRB afterglows. *Astron. & Astroph.*, submitted, revised. *ArXiv e-prints*: astro-ph: 1108.0674.
3. Clemens, C., Greiner, J., Krühler, T., Pierini, D., Savaglio, S., Klose, S., Afonso, P.M.J., Filgas, R., Olivares, F.E., Rau, A., Schady, P., **Rossi, A.**, Küpcü Yoldaş, A., Utdike, A.C., and Yoldaş, A. (2011). *GRB 071028B, a burst behind large amounts of dust in an unabsorbed galaxy*. *Astron. & Astroph.*, 529:A110.
4. Pierini, D., Šuhada, R., Fassbender, R., Nastasi, A., Böhringer, H., Salvato, M., Pratt, G.W., Lerchster, M., Rosati, P., Santos, J. S. de Hoon, A., Kohnert, J., Lamer, G., Mohr, J.J., Mühlegger, M., Quintana, H., Schwöpe, A.D., Biffi, G., Chon, G., Giodini, S., Koppenhoefer, J., Montalto, M., Verdugo, M., Ziparo, F., Afonso, P.M.J., Clemens, C., Greiner, J., Krühler, T., Küpcü Yoldaş, A., Olivares E., F., **Rossi, A.**, and Yoldaş, A. (2011). *First simultaneous optical/near-infrared imaging of an X-ray selected, high-redshift cluster of galaxies with GROND*. *Astron. & Astroph.*, submitted.
5. Hunt, L., Palazzi, E., **Rossi, A.**, Savaglio, S., Cresci, G., Klose, S., Michałowski, M., and Pian, E. (2011). The Extremely Red Host Galaxy of GRB 080207. *Astroph. J.*, 736:L36.
6. Nardini, M., Greiner, J., Krühler, T., Filgas, R., Klose, S., Afonso, P., Clemens, C., Guelbenzu, A.N., Olivares E., F., Rau, A., **Rossi, A.**, Utdike, A., Küpcü Yoldaş, A., Yoldaş, A., Burlon, D., Elliott, J., and Kann, D.A. (2011). On the nature of the extremely fast optical rebrightening of the afterglow of GRB 081029. *Astron. & Astroph.*, 531:A39.
7. Nicuesa Guelbenzu, A., Klose, S., **Rossi, A.**, Kann, D.A., Krühler, T., Greiner, J., Rau, A., Olivares E., F., Afonso, P.M.J., Filgas, R., Küpcü Yoldaş, A., McBreen, S., Nardini, M., Schady, P., Schmidl, S., Utdike, A.C., and Yoldaş, A. (2011). GRB 090426: Discovery of a jet break in a short burst afterglow. *Astron. & Astroph.*, 531:L6.
8. **Rossi, A.**, Schulze, S., Klose, S., Kann, D.A., Rau, A., Krimm, H.A., Jóhannesson, G., Panaitescu, A., Yuan, F., Ferrero, P., Krühler, T., Greiner, J., Schady, P., Pandey, S.B., Amati, L., Afonso, P.M.J., Akerlof, C.W., Arnold, L.A., Clemens, C., Filgas, R., Hartmann, D.H., Küpcü Yoldaş, A., McBreen, S., McKay, T.A., Nicuesa Guelbenzu, A., Olivares, F.E., Pacieras, B., Rykoff, E.S., Szokoly, G., Utdike, A.C., and Yoldaş, A. (2011). *The Swift/Fermi GRB 080928 from 1 eV to 150 keV*. *Astron. & Astroph.*, 529:A142.
9. Filgas, R., Krühler, T., Greiner, J., Rau, A., Palazzi, E., Klose, S., Schady, P., **Rossi, A.**, Afonso, P.M.J., Antonelli, L.A., Clemens, C., Covino, S., D'Avanzo, P., Küpcü Yoldaş, A., Nardini, M., Nicuesa Guelbenzu, A., Olivares, F., Utdike, E.A.C., and Yoldaş, A. (2011). *The two-component jet of GRB 080413B*. *Astron. & Astroph.*, 526:A113.
10. Greiner, J., Krühler, T., Klose, S., Afonso, P., Clemens, C., Filgas, R., Hartmann, D.H., Küpcü Yoldaş, A., Nardini, M., Olivares E., F., Rau, A., **Rossi, A.**, Schady, P., and Utdike, A. (2011). *The nature of "dark" gamma-ray bursts*. *Astron. & Astroph.*, 526:A30.
11. Krühler, T., Schady, P., Greiner, J., Afonso, P., Bottacini, E., Clemens, C., Filgas, R., Klose, S., Koch, T.S., Küpcü-Yoldaş, A., Oates, S.R., Olivares E., F., Page, M.J., McBreen, S., Nardini, M., Nicuesa Guelbenzu, A., Rau, A., Roming, P.W.A., **Rossi, A.**, Utdike, A., and Yoldaş, A. (2011). *Photometric redshifts for gamma-ray burst afterglows from GROND and Swift/UVOT*. *Astron. & Astroph.*, 526:A153.

12. Schulze, S., Klose, S., Björnsson, G., Jakobsson, P., Kann, D.A., **Rossi, A.**, Krühler, T., Greiner, J., and Ferrero, P. (2011). *The circumburst density profile around GRB progenitors: a statistical study.* *Astron. & Astroph.*, 526:A23.
13. Gorosabel, J., de Ugarte Postigo, A., Castro-Tirado, A.J., Agudo, I., Jelínek, M., Leon, S., Augusteijn, T., Fynbo, J.P.U., Hjorth, J., Michałowski, M.J., Xu, D., Ferrero, P., Kann, D.A., Klose, S., **Rossi, A.**, Madrid, J.P., Llorente, A., Bremer, M., and Winters, J. (2010). *Simultaneous polarization monitoring of supernovae SN 2008D/XT 080109 and SN 2007uy: isolating geometry from dust.* *Astron. & Astroph.*, 522:A14.
14. Kann, D.A., Klose, S., Zhang, B., Malesani, D., Nakar, E., Pozanenko, A., Wilson, A.C., Butler, N.R., Jakobsson, P., Schulze, S., Andreev, M., Antonelli, L.A., Bikmaev, I.F., Biryukov, V., Böttcher, M., Burenin, R.A., Castro Cerón, J.M., Castro-Tirado, A.J., Chincarini, G., Cobb, B.E., Covino, S., D'Avanzo, P., D'Elia, V., Della Valle, M., de Ugarte Postigo, A., Efimov, Y., Ferrero, P., Fugazza, D., Fynbo, J.P.U., Gålfalk, M., Grundahl, F., Gorosabel, J., Gupta, S., Guziy, S., Hafizov, B., Hjorth, J., Holhjem, K., Ibrahimov, M., Im, M., Israel, G.L., Jelínek, M., Jensen, B.L., Karimov, R., Khamitov, I.M., Kiziloğlu, Ü., Klunko, E., Kubánek, P., Kutyrev, A.S., Laursen, P., Levan, A.J., Mannucci, F., Martin, C.M., Mescheryakov, A., Mirabal, N., Norris, J.P., Ovaldsen, J., Paraficz, D., Pavlenko, E., Piranomonte, S., **Rossi, A.**, Rumyantsev, V., Salinas, R., Sergeev, A., Sharapov, D., Sollerman, J., Stecklum, B., Stella, L., Tagliaferri, G., Tanvir, N.R., Telting, J., Testa, V., Utdike, A.C., Volnova, A., Watson, D., Wiersema, K., and Xu, D. (2010). *The Afterglows of Swift-era Gamma-ray Bursts. I. Comparing pre-Swift and Swift-era Long/Soft (Type II) GRB Optical Afterglows.* *Astroph. J.*, 720:1513.
15. McBreen, S., Krühler, T., Rau, A., Greiner, J., Kann, D.A., Savaglio, S., Afonso, P., Clemens, C., Filgas, R., Klose, S., Küpcü Yoldaş, A., Olivares E., F., **Rossi, A.**, Szokoly, G.P., Utdike, A., and Yoldaş, A. (2010). *Optical and near-infrared follow-up observations of four Fermi/LAT GRBs: redshifts, afterglows, energetics, and host galaxies.* *Astron. & Astroph.*, 516:A71.
16. Rau, A., Savaglio, S., Krühler, T., Afonso, P., Greiner, J., Klose, S., Schady, P., McBreen, S., Filgas, R., Olivares E., F., **Rossi, A.**, and Utdike, A. (2010). *A Very Metal-poor Damped Lyman- $\alpha$  System Revealed Through the Most Energetic GRB 090926A.* *Astroph. J.*, 720:862.
17. Antonelli, L.A., D'Avanzo, P., Perna, R., Amati, L., Covino, S., Cutini, S., D'Elia, V., Gallozzi, S., Grazian, A., Palazzi, E., Piranomonte, S., **Rossi, A.**, Spiro, S., Stella, L., Testa, V., Chincarini, G., di Paola, A., Fiore, F., Fugazza, D., Giallongo, E., Maiorano, E., Masetti, N., Pedichini, F., Salvaterra, R., Tagliaferri, G., and Vergani, S. (2009). *GRB 090426: the farthest short gamma-ray burst?* *Astron. & Astroph.*, 507:L45.
18. Greiner, J., Clemens, C., Krühler, T., von Kienlin, A., Rau, A., Sari, R., Fox, D.B., Kawai, N., Afonso, P., Ajello, M., Berger, E., Cenko, S.B., Cucchiara, A., Filgas, R., Klose, S., Küpcü Yoldaş, A., Lichti, G.G., Löw, S., McBreen, S., Nagayama, T., **Rossi, A.**, Sato, S., Szokoly, G., Yoldaş, A., and Zhang, X. (2009). *The redshift and afterglow of the extremely energetic gamma-ray burst GRB 080916C.* *Astron. & Astroph.*, 498:89.
19. Greiner, J., Krühler, T., Fynbo, J.P.U., **Rossi, A.**, Schwarz, R., Klose, S., Savaglio, S., Tanvir, N.R., McBreen, S., Totani, T., Zhang, B.B., Wu, X.F., Watson, D., Barthelmy, S.D., Beardmore, A.P., Ferrero, P., Gehrels, N., Kann, D.A., Kawai, N., Yoldaş, A.K., Mészáros, P., Milvang-Jensen, B., Oates, S.R., Pierini, D., Schady, P., Toma, K., Vreeswijk, P.M., Yoldaş, A., Zhang, B., Afonso, P., Aoki, K., Burrows, D.N., Clemens, C., Filgas, R., Haiman, Z., Hartmann, D.H., Hasinger, G., Hjorth, J., Jehin, E., Levan, A.J., Liang, E.W., Malesani, D., Pyo, T., Schulze, S., Szokoly, G., Terada, K., and Wiersema, K. (2009). *GRB 080913 at Redshift 6.7.* *Astroph. J.*, 693:1610.
20. Krühler, T., Greiner, J., Afonso, P., Burlon, D., Clemens, C., Filgas, R., Kann, D.A., Klose, S., Küpcü Yoldaş, A., McBreen, S., Olivares, F., Rau, A., **Rossi, A.**, Schulze, S., Szokoly, G.P., Utdike, A., and Yoldaş, A. (2009). *The bright optical/NIR afterglow of the faint GRB 080710 - evidence of a jet viewed off-axis.* *Astron. & Astroph.*, 508:593.
21. Krühler, T., Greiner, J., McBreen, S., Klose, S., **Rossi, A.**, Afonso, P., Clemens, C., Filgas, R., Yoldaş, A.K., Szokoly, G.P., and Yoldaş, A. (2009). *Correlated Optical and X-Ray Flares in the Afterglow of XRF 071031.* *Astroph. J.*, 697:758.

22. Giuliani, A., Mereghetti, S., Fornari, F., Del Monte, E., Feroci, M., Marisaldi, M., Esposito, P., Perotti, F., Tavani, M., Argan, A., Barbiellini, G., Boffelli, F., Bulgarelli, A., Caraveo, P., Cattaneo, P.W., Chen, A.W., Costa, E., D'Ammando, F., Di Cocco, G., Donnarumma, I., Evangelista, Y., Fiorini, M., Fuschino, F., Galli, M., Gianotti, F., Labanti, C., Lapshov, I., Lazzarotto, F., Lipari, P., Longo, F., Morselli, A., Pacciani, L., Pellizzoni, A., Piano, G., Picozza, P., Prest, M., Pucella, G., Rapisarda, M., Rappoldi, A., Soffitta, P., Trifoglio, M., Trois, A., Vallazza, E., Vercellone, S., Zanello, D., Salotti, L., Cutini, S., Pittori, C., Preger, B., Santolamazza, P., Verrecchia, F., Gehrels, N., Page, K., Burrows, D., **Rossi, A.**, Hurley, K., Mitrofanov, I., and Boynton, W. (2008). *AGILE detection of delayed gamma-ray emission from GRB 080514B*. *Astron. & Astroph.*, 491:L25.
23. **Rossi, A.**, de Ugarte Postigo, A., Ferrero, P., Kann, D.A., Klose, S., Schulze, S., Greiner, J., Schady, P., Filgas, R., Gonsalves, E.E., Küpcü Yoldaş, A., Krühler, T., Szokoly, G., Yoldaş, A., Afonso, P.M.J., Clemens, C., Bloom, J.S., Perley, D.A., Fynbo, J.P.U., Castro-Tirado, A.J., Gorosabel, J., Kubánek, P., Updike, A.C., Hartmann, D.H., Giuliani, A., Holland, S.T., Hanlon, L., Bremer, M., French, J., Melady, G., and García-Hernández, D.A. (2008). *A photometric redshift of  $z = 1.8_{-0.3}^{+0.4}$  for the AGILE GRB 080514B*. *Astron. & Astroph.*, 491:L29.

## Publications in non-refereed Conference Proceedings

1. Schulze, S., Klose, S., Björnsson, G., Jakobsson, P., Kann, D. A., **Rossi, A.**, Krühler, T., Greiner, J., Ferrero, P., *The circumburst density profile around GRB progenitors*, 2011 in Gamma Ray Bursts 2010: Proceedings of the Annapolis Conference, AIP Conference Proceedings, submitted; Conference held on November 1-4, 2010, Annapolis (Maryland);
2. **Rossi, A.**, Klose, S., Ferrero, P., Kann, D. A., Schulze, S., de Ugarte Postigo, A., Greiner, J., & Schady, P., *GRB 080514B: the first high-energy AGILE burst with optical/NIR afterglow*, 2009, in GAMMA-RAY BURST: Sixth Huntsville Symposium. AIP Conference Proceedings, Volume 1133, pp. 58-60. Conference held on October 10-24, 2008, Huntsville (Alabama);
3. Gorosabel, J., de Ugarte Postigo, A., Castro-Tirado, A. J., Jelínek, M., Larionov, V., Guziy, S., Augusteijn, T., Fynbo, J. P. U. Hjorth, J., Malesani, D., Xu, D., Ferrero, P., Kann, D. A., Klose, S., **Rossi, A.**, Llorente, A., Madrid, J. P., *Optical linear polarization in the case of two supernovae associated to XRFs: XRF060218/SN2006aj and XRF080109/SN2008D*, 2009, in Astronomical Polarimetry 2008: Science from Small to Large Telescopes, ASP Conference Series, Vol. 4\*\*, pp XX-XX, submitted; Conference held on July 6-11, 2008, Fairmont Le Manoir Richelieu, La Malbaie (Quebec, Canada);
4. **Rossi, A.**, Kann, D. A., Schulze, S., Ferrero, P., Filgas, R., Klose, S., Clemens, C., Küpcü Yoldaş, A., Krühler, T., Yoldaş, A., Greiner, J., *Dark bursts in the Swift era*, 2008, in GAMMA-RAY BURSTS 2007: Proceedings of the Santa Fe Conference, AIP Conference Proceedings, Volume 1000, pp. 327-330. Conference held on November 5-9, 2007, Santa Fe (New Mexico);
5. Ferrero, P., Kann, D. A., Klose, S., Greiner, J., Rykoff, E. S. (on behalf of the ROTSE collaboration), Mikuž, H., Dintinjana, B., Skvarč, J., Malesani, D., Schulze, S., Filgas, R., **Rossi, A.**, *A rapid response to GRB 070411*, 2008, in GAMMA-RAY BURSTS 2007: Proceedings of the Santa Fe Conference, AIP Conference Proceedings, Volume 1000, pp. 257-260. Conference held on November 5-9, 2007, Santa Fe (New Mexico);

## GCN Circulars

1. Filgas, R., **Rossi, A.**, Kann, A. D., Rau, A., & Greiner, J. 2011, GCN Circ., 12096;
2. Afonso, P., **Rossi, A.**, Klose, S., & Greiner, J. 2011, GCN Circ., 11949;
3. Olivares E., F., **Rossi, A.**, Greiner, J. 2010, GCN Circ., 11478;
4. Olivares E., F., **Rossi, A.**, Greiner, J., Elliott, J., Kann, D. A. 2010, GCN Circ., 11471;
5. Nardini, M., Kruehler, T., Klose, S., **Rossi, A.**, & Greiner, J. 2010, GCN Circ., 11337;
6. Afonso, P., Nicuesa, A., **Rossi, A.**, Klose, S., Kruehler, T., Yoldas, A., & Greiner, J. 2010, GCN Circ., 10815;
7. Schady, P., Olivares, F., **Rossi, A.**, & Greiner, J. 2010, GCN Circ., 10734;
8. Nicuesa, A., Kruehler, T., **Rossi, A.**, & Greiner, J. 2010, GCN Circ., 10383;



9. Updike, A., **Rossi, A.**, & Greiner, J. 2009, GCN Circ., 10271;
10. Updike, A., **Rossi, A.**, Rau, A., Greiner, J., Afonso, P., & Yoldas, A. 2009, GCN Circ., 10195;
11. **Rossi, A.**, Rau, A., Afonso, P., & Greiner, J. 2009, GCN Circ., 10008;
12. **Rossi, A.**, Olivares, F., Kruehler, T., & Greiner, J. 2009, GCN Circ., 9480 ;
13. **Rossi, A.**, Olivares, F., & Greiner, J. 2009, GCN Circ., 9458 ;
14. **Rossi, A.**, Olivares, F., & Greiner, J. 2009, GCN Circ., 9456 ;
15. **Rossi, A.**, Kruehler, T., & Greiner, J. 2009, GCN Circ., 9420;
16. **Rossi, A.**, Kruehler, T., Greiner, J., & Yoldas, A. 2009, GCN Circ., 9408;
17. **Rossi, A.**, Afonso, P., & Greiner, J. 2009, GCN Circ., 9395;
18. **Rossi, A.**, Afonso, P., & Greiner, J. 2009, GCN Circ., 9382;
19. **Rossi, A.**, Kruehler, T., Greiner, J., & Olivares, F. 2009, GCN Circ., 8850;
20. **Rossi, A.**, & Greiner, J. 2009, GCN Circ., 8849;
21. Olivares, F., **Rossi, A.**, Kupcu Yoldas, A., Greiner, J., Yoldas, A., & Copete, A. 2009, GCN Circ., 8826;
22. **Rossi, A.**, Olivares, F., Kupcu Yoldas, A., Greiner, J., & Yoldas, A. 2009, GCN Circ., 8820 ;
23. Olivares, F., **Rossi, A.**, Greiner, J., Yoldas, A., & Kupcu Yoldas, A. 2009, GCN Circ., 8812 ;
24. Filgas, R., Kruehler, T., Greiner, J., Clemens, C., Yoldas, A., **Rossi, A.**, Kupcu Yoldas, A., & Szokoly, G. 2008, GCN Circ., 8373;
25. **Rossi, A.**, Clemens, C., Greiner, J., Yoldas, A., Kruehler, T., Filgas, R., Yoldas, A. K., & Szokoly, G. 2008, GCN Circ., 8296 ;
26. Clemens, C., **Rossi, A.**, Greiner, J., McBreen, S., Kruehler, T., Yoldas, A., Yoldas, A. K., & Szokoly, G. 2008, GCN Circ., 8273;
27. Clemens, C., **Rossi, A.**, Greiner, J., McBreen, S., Kruehler, T., Yoldas, A., Yoldas, A. K., & Szokoly, G. 2008, GCN Circ., 8272;
28. **Rossi, A.**, Kruehler, T., Greiner, J., Yoldas, A., Clemens, C., Filgas, R., Yoldas, A. K., & Szokoly, G. 2008, GCN Circ., 8268;
29. **Rossi, A.**, Kruehler, T., Greiner, J., Yoldas, A., Clemens, C., Filgas, R., Yoldas, A. K., & Szokoly, G. 2008, GCN Circ., 8266;
30. Clemens, C., **Rossi, A.**, Greiner, J., & McBreen, S. 2008, GCN Circ., 8257;
31. Fynbo, J. P. U., Greiner, J., Kruehler, T., **Rossi, A.**, Vreeswijk, P., & Malesani, D. 2008, GCN Circ., 8225;
32. Greiner, J., Kruehler, T., & **Rossi, A.** 2008, GCN Circ., 8223;
33. **Rossi, A.**, Greiner, J., Kruehler, T., Yoldas, A., Klose, S., & Yoldas, A. K. 2008, GCN Circ., 8218;
34. Schulze, S., Kann, D. A., **Rossi, A.**, Gonsalves, E., Hoegner, C., & Stecklum, B. 2008, GCN Circ., 7972;
35. Gonsalves, E., Schulze, S., **Rossi, A.**, Klose, S., Stecklum, B., & Ludwig, F. 2008, GCN Circ., 7922;
36. **Rossi, A.**, Gonsalves, E., Schulze, S., Klose, S., Filgas, R., & Ludwig, F. 2008, GCN Circ., 7917;
37. **Rossi, A.**, Filgas, R., Kruehler, T., Greiner, J., Klose, S., Kupcu-Yoldas, A., Yoldas, A., & Szokoly, G. 2008, GCN Circ., 7756;
38. Filgas, R., Kupcu-Yoldas, A., Greiner, J., **Rossi, A.**, Klose, S., Yoldas, A., Kruehler, T., & Szokoly, G. 2008, GCN Circ., 7747;
39. Filgas, R., Kupcu-Yoldas, A., Greiner, J., **Rossi, A.**, Klose, S., Yoldas, A., Kruehler, T., & Szokoly, G. 2008, GCN Circ., 7741;
40. Filgas, R., Kupcu-Yoldas, A., Greiner, J., **Rossi, A.**, Klose, S., Yoldas, A., Kruehler, T., & Szokoly, G. 2008, GCN Circ., 7740;
41. **Rossi, A.**, Kupcu-Yoldas, A., Greiner, J., Klose, S., Filgas, R., Yoldas, A., Kruehler, T., & Szokoly, G. 2008, GCN Circ., 7724;

42. **Rossi, A.**, Kupcu-Yoldas, A., Greiner, J., Klose, S., Filgas, R., Yoldas, A., Kruehler, T., & Szokoly, G. 2008, GCN Circ., 7722;
43. **Rossi, A.**, Greiner, J., Kuepcue Yoldas, A., & Yoldas, A. 2008, GCN Circ., 7319;
44. Kuepcue Yoldas, A., Yoldas, A., Greiner, J., Kruehler, T., & **Rossi, A.** 2008, GCN Circ., 7303;
45. Primak, N., Szokoly, G., Greiner, J., Clemens, C., Kruehler, T., Kuepcue-Yoldas, A., Yoldas, A., Klose, S., **Rossi, A.**, Carrier, F. 2007, GCN Circ., 6590.